US Army Corps
of Engineers
Construction Engineering
Research Laboratories

USACERL Technical Manuscript 99/18
December 1998

Non-Ductile Behavior of Reinforced Concrete Frames With Masonry Infill Panels Subjected to In-Plane Loading

by
Ghassan Al-Chaar

Lessons learned from earthquakes in the last 50 years have spurred changes in building seismic code requirements. As these requirements became more stringent, structural evaluation of old structures became necessary to determine their seismic vulnerability.

This study addresses a popular type of building in high seismic zones that has lateral load-resisting systems constructed from reinforced concrete (R/C) frames with masonry infill panels. The R/C frames in old structures do not have the ductile detailing required for modern construction in high and medium seismic zones. Masonry infill panels were also not recognized as integral structural members and were exempt from old and current building code specifications. It is obvious that the masonry infill panels in a structural frame not only add significant strength and stiffness but also influence the dynamic behavior of the entire building.

An experimental program was carried out to evaluate this structural system. Five single-story half-scale laboratory models with different numbers of bays were constructed. The five models represent: a single-bay bare frame, single-bay with concrete masonry unit (CMU) infill, single-bay with brick infill, double-bay with CMU infill, and triple-bay with brick infill. These models were fully instrumented and tested under lateral in-plane loading to failure. Prior to cracking, the infill redistributes the stresses in the frame, resulting in more displacement and stresses in the windward column than in others. After cracking, diagonal struts were developed in the infill, resulting in increasing the overall strength of the infilled frame.

Non-linear finite element analyses were conducted on the experimental models. Load-deflection curves for finite element analysis (FEA) reasonably predicted experimental behavior of specimens in terms of deflection. Ultimate failure load corresponding to each specimen was predicted with accuracy.

Finally, a new idealized analytical model was proposed to determine the capacity evaluation of this structural system. This model characterizes the strength and stiffness behavior of multi-bay frames with infilled masonry. Post-yield behavior, residual strength, and the effects of bay multiplicity on structural behavior are also presented.

The contents of this report are not to be used for advertising, publication, or promotional purposes. Citation of trade names does not constitute an official endorsement or approval of the use of such commercial products. The findings of this report are not to be construed as an official Department of the Army position, unless so designated by other authorized documents.

DESTROY THIS REPORT WHEN IT IS NO LONGER NEEDED

DO NOT RETURN IT TO THE ORIGINATOR

USER EVALUATION OF REPORT

REFERENCE: USACERL Technical Manuscript 99/18, *Non-Ductile Behavior of Reinforced Concrete Frames With Masonry Infill Panels Subjected to In-Plane Loading*

Please take a few minutes to answer the questions below, tear out this sheet, and return it to USACERL. As user of this report, your customer comments will provide USACERL with information essential for improving future reports.

1. Does this report satisfy a need? (Comment on purpose, related project, or other area of interest for which report will be used.)

_____

_____

_____

2. How, specifically, is the report being used? (Information source, design data or procedure, management procedure, source of ideas, etc.)

_____

_____

3. Has the information in this report led to any quantitative savings as far as manhours/contract dollars saved, operating costs avoided, efficiencies achieved, etc.? If so, please elaborate.

_____

_____

4. What is your evaluation of this report in the following areas?

   a. Presentation: _____

   b. Completeness: _____

   c. Easy to Understand: _____

   d. Easy to Implement: _____

   e. Adequate Reference Material: _____

   f. Relates to Area of Interest: _____

   g. Did the report meet your expectations? _____

   h. Does the report raise unanswered questions? _____

i. General Comments. (Indicate what you think should be changed to make this report and future reports of this type more responsive to your needs, more usable, improve readability, etc.)

_____

_____

_____

_____

_____

_____

5. If you would like to be contacted by the personnel who prepared this report to raise specific questions or discuss the topic, please fill in the following information.

Name: _____

Telephone Number: _____

Organization Address: _____

_____

_____

6. Please mail the completed form to:

Department of the Army
CONSTRUCTION ENGINEERING RESEARCH LABORATORIES
ATTN: CECER-TR-I
P.O. Box 9005
Champaign, IL 61826-9005

REPORT DOCUMENTATION PAGE

Form Approved
OMB No. 0704-0188

1. AGENCY USE ONLY *(Leave Blank)*	2. REPORT DATE	3. REPORT TYPE AND DATES COVERED
	December 1998	Final

4. TITLE AND SUBTITLE
Non-Ductile Behavior of Reinforced Concrete Frames With Masonry Infill Panels Subjected to In-Plane Loading

5. FUNDING NUMBERS

6. AUTHOR(S)
Ghassan Al-Chaar

7. PERFORMING ORGANIZATION NAME(S) AND ADDRESS(ES)
U.S. Army Construction Engineering Research Laboratories (USACERL)
P.O. Box 9005
Champaign, IL 61826-9005

8. PERFORMING ORGANIZATION REPORT NUMBER
TM 99/18

9. SPONSORING / MONITORING AGENCY NAME(S) AND ADDRESS(ES)
U.S. Army Corps of Engineers (USACE)
ATTN: CEMP-ET
20 Massachusetts Avenue, NW.
Washington, DC 20314-1000

10. SPONSORING / MONITORING AGENCY REPORT NUMBER

11. SUPPLEMENTARY NOTES
Copies are available from the National Technical Information Service, 5285 Port Royal Road, Springfield, VA 22161.

12a. DISTRIBUTION / AVAILABILITY STATEMENT
Approved for public release; distribution is unlimited.

12b. DISTRIBUTION CODE

13. ABSTRACT (Maximum 200 words)

Lessons learned from earthquakes in the last 50 years have spurred changes in building seismic code requirements, making it necessary to determine the seismic vulnerability of old military structures.

This study addresses a popular type of building in high seismic zones that has lateral load-resisting systems constructed from reinforced concrete (R/C) frames with masonry infill panels. An experimental program was carried out to evaluate this structural system. Five single-story half-scale laboratory models with different numbers of bays were constructed. The five models represent: a single-bay bare frame, single-bay with concrete masonry unit (CMU) infill, single-bay with brick infill, double-bay with CMU infill, and triple-bay with brick infill. These models were fully instrumented and tested under lateral in-plane loading to failure.

Non-linear finite element analyses were carried out on the experimental models. Load-deflection curves for finite element analysis (FEA) reasonably predicted experimental behavior of specimens in terms of deflection. Ultimate failure load corresponding to each specimen was predicted with accuracy.

Finally, a new idealized analytical model was proposed to determine the capacity evaluation of this structural system. Post-yield behavior, residual strength, and the effects of bay multiplicity on structural behavior are also presented.

14. SUBJECT TERMS
reinforced concrete
seismic vulnerability
masonry
structural reliability
structural engineering

15. NUMBER OF PAGES
276

16. PRICE CODE

17. SECURITY CLASSIFICATION OF REPORT	18. SECURITY CLASSIFICATION OF THIS PAGE	19. SECURITY CLASSIFICATION OF ABSTRACT	20. LIMITATION OF ABSTRACT
Unclassified	Unclassified	Unclassified	SAR

Foreword

This study was conducted for the U.S. Army Corps of Engineers (USACE) under the Seismic Evaluation and Rehabilitation Program led by Dr. John R. Hayes and managed by Larry Windingland, Division Chief of the Engineering Division (FL-E) of the Facilities Technology Laboratory (FL), U.S. Army Construction Engineering Research Laboratories (USACERL). The technical monitors were Charles Gutberlet and Fidel Rodriguez (CEMP-ET). Dr. Michael J. O'Connor is Director of USACERL.

This manuscript was submitted in partial fulfillment of the requirements for the degree of Doctor of Philosophy in Civil Engineering in the Graduate College of the University of Illinois at Chicago. Dr. Mohsen A. Issa was the University of Illinois advisor for this thesis. Appreciation is extended to the graduate advisory committee: Professors Chien H. Wu, Alexander Chudnovsky, Ahmed Shabana, and Krishna Reddy. Thanks are also due to Dr. Mahmoud A. Issa for his assistance in the nonlinear finite element analysis.

Special thanks go to the USACERL Seismic and Structural Engineering Group: John Hayes, Steve Sweeney, Pamalee Brady, and James Wilcoski, and to James Gambill and William Gordon who assisted in carrying out the tests, and Sean Marzano and Jason Petti for assisting in acquiring the data. Thanks also to Gordon Cohen and Linda Wheatley of the Technical Information Team for their editorial comments.

TABLE OF CONTENTS

TABLE OF CONTENTS (Continued)

TABLE OF CONTENTS (Continued)

LIST OF TABLES

LIST OF TABLES (Continued)

LIST OF FIGURES

LIST OF FIGURES (Continued)

LIST OF FIGURES (Continued)

LIST OF FIGURES (Continued)

LIST OF FIGURES (Continued)

LIST OF FIGURES (Continued)

LIST OF FIGURES (Continued)

LIST OF FIGURES (Continued)

LIST OF FIGURES (Continued)

CHAPTER 1

INTRODUCTION

1.1 Background

Structural systems constructed of reinforced concrete (R/C) frame with masonry infill panels are classified as Type 10 in the common building types described in the National Earthquake Hazard Reduction Program (NEHRP) handbook "Seismic Evaluation of Existing Building," FEMA-178/June 1992 [19]. In this document, building types are classified based on the vertical structural elements of their lateral force-resisting systems.

Current building codes do not address the design and evaluation of reinforced concrete frames with masonry infill panels. Thus, engineers are often faced with a lack of procedures and guidelines to accurately determine the capacity of these systems. These systems are highly represented in the property inventory of federal structures, but they are not sufficiently understood.

Since the 1950s, reinforced concrete frames with masonry infill panels have become popular in high seismic zones because they are economical. Masonry infill panels were not recognized as integral structural members, therefore, masonry infill was exempt from building code specifications. Furthermore, the masonry and reinforced concrete codes did not address the complex composite behavior of these systems. The fact is that the behavior of a panel and the behavior of its reinforced concrete frame cannot be superimposed to calculate the combined behavior.

It is evident that a masonry panel standing alone has a very high in-plane stiffness and low ductility, while an open reinforced concrete frame is relatively ductile but has a low

stiffness. A masonry panel enclosed in an R/C frame produces a desirable structural system that reflects the strength features of the two components. Such a system can resist high in-plane load within acceptable limits of deflection.

The masonry infill panels in a structural frame were not only recognized to add significant strength and stiffness but also to influence the dynamic behavior of the entire building. The damping of a structure is highly influenced by the strength and stiffness degradation of the structural system under dynamic loads. The gradual breaking down of the bonded mortar will absorb a significant amount of energy, reducing the stresses on the structure. Also, the natural frequency of the structure decreases with increasing damage, altering the overall dynamic behavior of the structure.

In dealing with the capacity evaluation of existing Type 10 buildings, we need to identify the structures that were built during the 1950s and 1960s. Such structures do not have the ductile detailing required for modern construction in high and medium seismic zones. Therefore, they pose a severe life hazard. Researchers have been interested in retrofitting schemes to ensure that these buildings are brought up to current seismic code requirements.

In the effort to deal with the huge inventory of military dormitory-type buildings that are located in high seismic zones, the US Army Construction Engineering Research Laboratories (USACERL) initiated a research project to understand the structural behavior of this type of structure. A series of push over laboratory tests were carried out following a three-year dynamic testing program on a series of infilled frame specimens.

As infilled reinforced concrete frame structures gain more recognition as a credible structural system, the stochastic nature of masonry's physical properties will challenge researchers to predict the behavior as the structure enters the inelastic region.

A literature survey has revealed that although there have been a large number of static, pseudo-static, and a few dynamic tests on the behavior of R/C frames with masonry infill, standard guidelines for evaluating infill systems have yet to be established.

Currently available guidelines for the evaluation of structures with infilled frame structural systems are simplistic and are thought to produce overly conservative results. The relative strength and stiffness between the infill and frame, the lateral load history, the infill aspect ratio, the vertical load and its distribution, along with the effects that adjacent infilled bays have on structural performance, are among the factors not sufficiently understood. The many complexities inherent to infilled frame systems are best studied with the aid of experimental tests. Models that represent single-bay, one-story, infilled R/C frames were tested and analytical models have been established to describe their behavior. This research presents further work characterizing the behavior of single-story multiple- bay frames with non-ductile details.

1.2 Objectives and Scope

The study aims to idealization of the complicated subsystems of non-ductile reinforced concrete infill frames. The goal is to analyze these systems using conventional static and dynamic methods, but with a greater level of accuracy than currently exists. The objectives of this research are:

1) To study the behavior of non-ductile concrete frames infilled with masonry and to characterize the strength and stiffness behavior of masonry infilled frames responding to in-plane lateral loading. Post-yield behavior, residual strength, and the effects of bay multiplicity on structural behavior will also be presented.

2) To investigate the applicability of proposed analytical models by other researchers on non-ductile reinforced concrete frames infilled with a brick or concrete masonry unit (CMU). The experimental results will provide the information needed to validate old analytical models, or to develop new analytical models to characterize strength and stiffness behavior of masonry infill in non-ductile reinforced concrete frames.

1.3 Approach

The first step of the program was to review all current complementary efforts aimed toward finding an accurate quantitative procedure to evaluate existing structures of a similar type. Specific areas requiring further study were then identified. Five laboratory physical models of single-story structures with different numbers of bays were constructed and tested under in-plane monotonic loading. Descriptions of these models are given in Chapter 3. The experimental data was then compared to nine analytical models proposed by other researchers. Finally, an analytical model that characterizes the strength and stiffness behavior of multi-bay frames with infilled masonry was presented.

1.4 Structure of this Dissertation

Chapter 2 presents a literature review in chronological order of the most relevant publications pertaining to R/C frames with masonry infill subjected to in-plane loading. Due to some similarity in the philosophies of studying infilled R/C concrete frames and infilled steel frames, the literature search covered infilled steel frames. Chapter 3 presents the experimental program to include modeling, instrumentation, test setup, and mechanical material properties of models' materials.

Chapter 4 presents nine proposed analytical models by researchers. These models were developed for particular parameters. In some cases models were generalized for the lack of better procedures. The controlled parameter of the laboratory specimens were fed to these proposed simplified analytical procedures and compared to each other. The variation in results to determine stiffness and strength was clearly concluded in this chapter.

Chapter 5 describes the finite element modeling procedure developed for the tested models to predict the stress level and distribution for infilled R/C frame structural systems. The finite element modeling included linear and non-linear analysis.

In Chapter 6, the experimental test results were presented to include detailed descriptions of the modes of failure, strength, and stiffness measured for each model. In Chapter 7, these results were compared with analytical results presented in Chapter 4 and with the finite element results presented in Chapter 5.

Chapter 8 presents a new, simplified analytical procedure to be used on non-ductile R/C frames infilled with masonry. This procedure is based on identifying the modes of failure and running numerical analysis to suit the expected modes of failure. Finally, Chapter 9 presents further research needs related to R/C frames infilled with masonry structural systems and the conclusion of this dissertation.

Appendix A shows the supportive figures for the experimental analysis presented in Chapter 6. Appendix B contained calculations about the proposed analytical method presented in this thesis applied to experimental models.

CHAPTER 2

LITERATURE REVIEW

2.1 Introduction

This literature search categorized three groups of articles. The first group is summarized in Table I in chronological order. Significant articles related to the analytical and experimental work performed since 1956 were reviewed. Although investigations of steel frames infilled with masonry shall not be considered directly applicable to reinforced concrete frames infilled with masonry, such studies were considered in this chapter because of some similarity in the philosophies used to study the behaviors of both systems. The second category of literature includes articles based on field observation during earthquakes, as shown in Table II. The third group is related to using finite element methods to study the behavior of particular models.

2.2 Chronological Literature Review of Analytical and Experimental Studies

Polyakov (1956) first proposed the concept of the equivalent strut from in-plane loading tests on a three-story, three-bay steel frame with infill specimen [42]. From observations of the cracking patterns the system behaved more as a diagonally braced frame with compression struts only. It was reported in this study that stresses from the frame to the infill were only transmitted in the compression zone of the infill-to-frame interface. Also, deformations were concentrated at the ends of the compression diagonals whereas deformations diminished towards the ends of the tension diagonals. It was observed in this study that the wall did not behave as a homogenous shear wall, for the largest deformations did not occur in the upper windward and lower leeward panels, as it would be expected if the wall behaved as a homogenous shear wall. Instead, a

distribution analogous to a diagonally braced system was observed. Polyakov developed some equations to predict the contribution of each panel to the lateral load resistance. Apparently, the equations were good only for the top story of infill panels in the nine-bay structural system tested.

Benjamin and Williams (1958) tested three types of one-story and one-bay specimens under in-plane lateral loads and some approximate relationships were generated to predict the behavior of walls [8]. The types of specimens tested included brick masonry without enclosing frames, brick masonry infilled in reinforced concrete frames, and brick masonry infilled in steel frames. The model scales varied from 0.34 to 1.0 and the aspect ratio of the walls varied from 0.9 to 3.0 (length to height). While predictions of behavior were proposed in this paper, Benjamin and Williams limited their validity to very specific conditions that match those in the study. Predictions of behavior based on their work should only be considered approximate, and errors of as much as 50% in ultimate load and rigidity are common. It was reported in this study that the aspect ratio has an important influence on ultimate strength and rigidity. The greater the aspect ratio, the greater the strength. Plain brick masonry wall panels were found to have significant strengths when properly confined by a frame. Brick size was unimportant within the limits tested, and the frame had no important influence so long as it was strong enough to produce a failure in the infill first. Also, it was concluded from experiments that the variations in column concrete area and reinforcement steel area also had little effect. As for scaling, it was reported that masonry brick could be studied through the use of scaled-down models without significant misrepresentation of behavior. However, it is obvious that the higher the scaling factors the higher the error.

Holmes in 1961 considered a single-bay infilled specimen subjected to an in-plane force that produces a compressive resultant in the infill [23]. He determined the horizontal force causing failure by considering the forces in the frame and the infill separately, and by evaluating the shortening of the equivalent strut, assuming width of the equivalent strut equals one-third of the diagonal length of the infill panel. Holmes suggested a mathematical procedure for calculating ultimate (racking) load and side-sway deflection of an infilled steel frame. In 1963, Holmes tested reinforced concrete frames with masonry infill and developed semi-empirical equations to predict ultimate loads [24].

Smith (1962) conducted laboratory tests on infill panels constructed of mortar only. All tests were performed on a small scale of about 1:20 [49]. The frames were rectangular steel sections of unspecified dimensions. Smith evaluated the lateral stiffness for infill panels not bonded to the enclosing frame. Loading was performed to simulate a lateral load being applied to one corner of the panel. The corners of the panel in contact with the frame appeared to delineate a region of compression within the panel that laterally stiffened the frame. This observation by Smith is the basis for the equivalent strut method. Through theory and experiment, Smith sought to predict the lateral stiffness of the infilled frame by modeling masonry panels as compression struts. It was found that for an infill surrounded by a frame, the stiffer the frame, the longer was the length of contact between the panel and frame, and the longer the contact length, the wider the effective width of the equivalent diagonal strut. Smith's further investigations tested mortar panels with different aspect ratios. The stresses in the panels were analyzed using a theory-of-elasticity method with Airy's stress function in a finite difference approximation [4]. Smith's method attempts to evaluate the in-plane stiffness of infill frames. The stiffness for a panel was

then modeled as an equivalent strut with an effective width that was dependent on the panel's aspect ratio.

In 1966 Smith expanded upon his earlier investigation [50]. The length of contact between the infill and the surrounding frame was further studied, and a λ parameter was developed to determine this contact length. The parameter λ was then used to determine the width of the equivalent strut and the relative stiffness between the frame and infill. The evaluation of the theory was tested through several small-scale specimens. These specimens consisted of steel frames and micro-concrete infills of one and two stories. The behavior of the frames with respect to the infills was found to be very similar, with separation taking place between the frame and infill in the tensile corners. The stiffnesses were consistently overestimated for the stiffer frames, especially in the frames on the first story. Stiffnesses on the second story were better predicted but the author attributes that to coincidence. He states that any attempt to introduce another variable for story level in this simple method would not be justified. The two reported modes of failure were diagonal cracking and crushing. Diagonal cracking typically occurred first, and the loads could be increased until the infill began to be crushed. Crushing, or compressive failure of the infill, typically produced collapse in the system and defined the ultimate load carrying capacity of the system. Theoretical relationships were created to relate the stiffness parameter to diagonal cracking load and the crushing load of the infills. For stiff frames, diagonal cracking occurred first, followed by crushing. In flexible frames, crushing occurred first without diagonal cracking taking place. Crushing failures did not occur suddenly, but developed with rapid increases in deflections, demonstrating significant nonlinear behavior.

In 1968, Fedorkiw and Sozen worked on developing an analytical model for infilled frames [20]. They attempted to explain a unified behavior in their model rather than action of the separate entities. A discrete physical model was developed for the analysis of reinforced concrete frames with masonry filler. The entire analytical procedure was programmed and gives crack formation and load-deflection response up to the ultimate load. The use of a discrete model analysis transforms the problem of a plate subjected to in-plane forces into a system with a finite number of degrees of freedom. The model representing the filler consists of a lumped spring-mass system that is arranged to reproduce deformations and stresses in a plane solid. All solutions were obtained for in-plane static loading and assumed conditions of plane stress in the filler panel. Failure criteria were introduced to determine the formation of cracking in frame and filler, and these criteria further restricted the procedure to structures composed of tension-weak materials such as concrete and masonry.

Two one-bay infilled specimens were modeled. The first was one story and the second was five stories in height. Equal loads were applied at the quarter points of the beams at each level. The effects on behavior of different relative stiffness between frame and filler were investigated by varying the filler modulus and the amount of frame reinforcement. The single-story structure was investigated for the effect of variation in filler modulus, and the five-story structure was studied for variations in frame stiffness. In general, the effect of introducing a filler into a single-story structure served to reduce the level of flexural behavior of the frame and to increase the axial force in the columns. Except for the very low values of filler modulus, the resisting moment in the frame was mainly provided by the axial load component. This study demonstrated that a discrete physical model analysis may be successfully employed in determining load-deflection response and crack formation in reinforced concrete frames with

masonry fillers. Procedures were developed for modifying the components of the model to reproduce the effect of cracking in the frame and filler of an actual structure. The model is intended for the analysis of structures that are composed of tension-weak materials such as concrete and masonry. Tests with laboratory specimens have indicated that analytical studies may overlook such effects as residual stresses due to shrinkage and to cracking that was not caused by the application of external load.

Later in 1968, Fiorato, Sozen, and Gamble studied the resisting mechanisms of reinforced concrete multi-story frames with filler walls [21]. Five specimens (one-eighth scale) were constructed. Each specimen had one bay and five stories. The total height of each specimen was 90 inches. Four of the specimens had masonry filler walls and were compared to one specimen that had only the concrete frame. Two bounding limits were used to estimate the cracking load of the frames with filler walls. The upper limit assumes that the system acts as a cantilever beam. The assumptions are that strain distribution is linear and that the modulus of elasticity is equal in the wall and the frame. The lower limit is determined by assuming that the specimen acts as a frame without filler walls; this is referred to as "frame action." For frame action, the maximum moments occur at the bases of the first-story columns. It was observed that at the lower bound, frame action was closer to the experimental cracking load than the cantilever beam action prediction.

In 1968, Yorulmaz and Sozen studied the behavior of single-story reinforced concrete frames with varying amounts of steel and with brick filler walls [56]. The authors reported that frames without infill failed in flexure, developing a simple four-hinge mechanism, whereas frames with filler walls first showed cracks in the wall. After the wall cracked, the load was transmitted to the frame and varying failures occurred depending on the strength of the frame.

Another finding related to the amount of reinforcement used in the frames was that low amounts of reinforcement caused extension hinges in the beam and compression column to develop. Final failure occurred in extension hinges or as a pure shear failure in the tension column. High amounts of reinforcement caused a pure shear failure in the tension column.

Smith and Carter (1969) developed a method of analysis for infilled frames based on the equivalent strut concept [51]. Infills and frames were not assumed to be constructed integrally, nor were they deliberately bonded together. The lateral stiffness of the infilled frames was calculated based on an effective width of the equivalent strut deduced from strains in stress analysis. Lateral strength of infilled frames was based on the weakest of the various modes of failure of the frame and infill. Possible failure modes identified were tensile failure of windward columns, and shear failure of the columns and beams and their connections. The forces in the frames were compared to the tensile load calculated in the windward column and shearing components of the load in the equivalent pin-jointed diagonal struts, with the respective strengths of the columns, beams, and connections.

Fiorato, Sozen, and Gamble (1970) studied the interaction of reinforced concrete frames with masonry filler walls [22]. They investigated the response of masonry-infilled reinforced concrete frames subjected to static lateral loads. A total of 27 tests were carried out using one-eighth scale models of reinforced concrete frames. Eight one-story, one-bay infilled frame; 12 five-story one-bay infilled frame; and 6 two-story three-bay infilled frames were tested. One five-story one-bay frame was tested with no filler walls. In addition to height (number of stories) and width (number of bays), the controlled variables were the amount, quality, and arrangement of the frame reinforcement, vertical loads on the columns, and wall openings. It was concluded that reinforced concrete frames with filler walls subjected to lateral load do not behave as frames

at any other loading stage. The critical stage in the response of the frame-wall system was the development of a shearing crack, which ideally forms along a single joint separating the wall into two parts. The frame did contribute significantly to the capacity of the structures after cracking of the wall. Before the initiation of the shearing cracks, the load-deflection characteristics of the frame-wall systems could be estimated by the same methods used for the reinforced concrete beams. Following the initiation of shearing cracks, the load-deflection characteristics of the frame-wall systems could be calculated using a knee-braced frame concept based on the development of a system of columns braced by segments of the cracked wall. Transverse reinforcement in the columns of the frame would increase the ductility and, in some cases, the strength of the system.

Mainstone's (1971) work represents a further refinement of the equivalent-strut method developed by Holmes and Smith [35]. Mainstone claims that his investigation was distinguished from Smith's by the full range of behavior displayed by individual panels in tall frames. However, the aspect ratio of the frames was not directly taken into account in Mainstone's formulation, as it was in Smith and Carter's analysis. The experimental or empirical approach versus a purely rigorous analytical approach was emphasized. The behavior of an infilled frame system was presented to fall between two extremes under initial loading where the infill perfectly fits within the bounding frame. In such a case, the entire infill is stressed with uniform shear throughout. Conversely, the infill and frame may only interact within a small region of the compression corners forming a narrow diagonal compression strut. Upon subsequent loading, compression struts with a characteristic width will form. Depending upon the weaknesses inherent in the infill and the relative infill-to-frame stiffness, corner crushing or diagonal cracking of the infill may precipitate.

The study concluded that the stiffness of the infills relative to the columns was found to be the most important parameter. Tests also confirmed that there was a wide range of possible behavior, even between nominally identical specimens. For design purposes, only a fairly simple method for predicting the increases in stiffness and strength due to the presence of infills seemed to be justified. The equivalent-strut method was found superior to the interaction equation because the full range of behavior was better fitted to it. The equivalent-strut method could also be used to evaluate stiffness, as well as strength before and after ultimate strength. The composite elastic stiffness of the infilled frame will usually be larger than that of the infill alone. Composite strengths up to first crack may also be conservatively taken as those of the infills alone because the load carried by the frame at the deflection that produces the first crack is usually relatively small.

Mallick and Garg (1971) discussed the effects of the location of openings in the infill on lateral stiffness and ultimate load [36]. They recommended suitable positions for window and door openings. In their study, the effects of openings in the infill and shear connectors between the frame and the infill were investigated. Openings at either end of a loaded corner without shear connectors reduce the stiffness by 75%, and they reduce the stiffness by 85 to 90% compared to infilled frames without openings. The stiffness is reduced by 60 to 70% for infilled frames with shear connectors and openings, versus one without openings. A central opening within the infilled panel reduced stiffness by 25 to 50% as compared to the frames without openings. Doors are best placed in the center of the lower half, and windows are best placed at mid-height of the left or right side, toward the vertical edge as possible.

Yettram and Hirst (1972) studied the collapse load for square concrete infill panels. The panels were loaded in compression along their diagonals over a contact length [55]. Elastic

theory was used until the first crack, consisting of the original stress field. Further cracks depended on the distribution of stresses in the new field. The stress field was determined by using the equivalent plane-framework method. A theoretical procedure was presented for simulating the tensile mode of failure for concrete infill panels when surrounded by skeletal frames.

Leuchars and Scrivener (1973) tested three specimens of reinforced and unreinforced masonry infill frames [31]. The load was applied laterally to the frame along the top of the single story. No gaps were observed between the frame and the infill in the initial uncracked mode. After boundary cracking, separation of frame and infill occurred along the interface, except at the compression corners. Diagonals acted as struts, with width depending on contact length, which in turn depended on the relative stiffness of the columns and infill along with the stress-strain relationship of the infill material. It was concluded in this study that the beam analogy for uncracked infill frames and Smith and Carter's diagonal strut method give adequate predictions for stiffness, but are not so accurate for predicting strength at failure of the infill.

Smolira's (1973) study sought to introduce a way to analyze infills in a force-displacement matrix that will yield an approximation more accurate than assuming a solid cantilever [52]. This analysis was based on linearly elastic principles. Smolira assumes that Hooke's law is applicable, that superposition is valid, and that the deformations are so small that the infill performs as an undamaged shear wall in reference to compatibility and equilibrium conditions. Parameters such as contact pressure, spaces, shear, and axial deformation are also addressed in formatting the matrix. The matrix is designed to analyze a tight infill and an infill with interface spaces. However, it is stated that the windward top and leeward bottom interface between the infill and frame remain in contact. The results from the force-displacement matrix

were then compared to obtained experimental results. Experimentation was carried out on six-story, single-bay, reinforced concrete frames, with and without brick infill. The frames underwent static in-plane loading at the top beam. Smolira concludes that comparing the experimental and analytical results is difficult because of the numerous variables encountered during the formulation of the matrix and the construction of the specimen. However, the analytical approximation is reasonable and more accurate than assuming a cantilever.

Lefter and Colville (1974) present a rational method to analyze the earthquake resistance of existing structures with unreinforced masonry exterior infill panels [30]. Both in-plane and out-of-plane loadings were considered in addition to dynamic loads. Lateral load resistance was evaluated for walls in both uncracked and cracked states. Design requirements for earthquake resistance were proposed, and out-of-plane behavior was discussed.

Klingner and Bertero (1976) performed experiments consisting of quasi-static tests on one-third scale models of the lower three stories of an eleven-story frame, three bays wide with infills in the outer two bays [28]. The infill frame system was engineered to effectively resist seismic loadings. The infills contained closely spaced reinforcement, and the frames had high rotational ductility. The infill thickness was limited so that its strength would not exceed the available column shear resistance. From the investigation, a simplified macro model was developed to evaluate infilled frame systems.

Barura and Mallick (1977) studied the behavior of mortar-infilled steel frames under lateral load. An analytical model taking into account axial deformations and slip at the interface was summarized for linear elastic behavior of a homogeneous and isotropic infill [6]. The proposed method of analysis made predictions on stresses in the infill, length of contact, stiffness, and strength.

Klingner and Bertero (1978) investigated the in-plane hysteretic behavior of masonry-infilled ductile reinforced concrete frames [27]. The experimental phase of the investigation consisted of quasi-static cyclic load tests on a series of scale 3½ story, 1½ bay models. The investigation was not only concerned with the behavior of infilled frames, but also bare frames. An analytical model was also proposed to further investigate the behavior of other types of infilled specimens. One of the primary concerns with the design of the test specimens was the energy dissipation capacity of the infilled frame. In order to prevent brittle frame behavior, the frame members were designed with high rotational ductility and shear resistance under cyclic loading reversals. It was concluded that the use of engineered infills for reinforced concrete frames (compared with bare R/C frames) greatly increases not only the lateral stiffness of the assemblage (by as much as 500%), but also the maximum lateral strength and energy dissipation capacity.

Riddington (1984) studied the influence of initial gaps on infilled frame behavior. In his investigation he sought to determine how the behavior of infilled frames is affected by the presence of initial gaps between the infill and frame [45]. The testing regimen included steel frames of different stiffness. Each was tested with no infill, an infill with no initial gaps, and an infill with initial gaps. The panels had square dimensions and were approximately full-scale. Static loads applied at 10 kN increments were applied up to the maximum load, with strain measurements and observations recorded at each increment. Riddington concluded that the presence of gaps is undesirable because of the reductions in stiffness. This problem is likely to occur when masonry infills are used with concrete beams and columns. Oftentimes, gaps are left in the masonry to allow for creep in the concrete members. If no gaps are provided, the creep of

a concrete column could cause a crushing failure in the compression corner of the mortar of the infills.

Dawe (1985) carried out an experimental investigation of the shear resistance of masonry panels in steel frames [12]. Six large-scale masonry-infilled steel frame specimens were tested. All were loaded to ultimate, and the results were compared to the theoretical analysis as determined by other investigators. Dawe concluded that masonry infill increases the strength of the rigid steel frame considerably. The steel frame in turn provides the system with ductility. The column-to-panel ties, horizontal joint reinforcement, or bond beams do not change the ultimate load but can affect the crack pattern. The column-to-panel ties or horizontal joint reinforcement do not affect the cracking load, but the presence of bond beams do cause the cracking load to be reached just before the ultimate load. Dawe compared his tests to analytical methods proposed by others. The Smith method predicted the correct mode of failure but was conservative. The initial stiffness, as predicted by the Smith and Carter method, was close to agreement with experimental results. The plastic collapse theory of Liauw and Kwan correctly predicted the failure mode, but at a higher load. When Wood's factor was applied to the Liauw and Kwan method, the predicted ultimate load was in close agreement with the experimental value. Later, Dawe and Yong investigated the behavior of masonry-infilled steel frames. Twelve single-story, single-bay, large-scale specimens were tested under monotonic loading. Parameters that were tested included mortar strength, panel-to-column ties, friction between panel and frame, panel openings, and airspace between roof beam and wall. A finite-element analysis was then performed and refined so as to model the overall behavior.

Dawe and Seah (1989) studied the behavior of masonry-infilled steel frames [13]. They studied the effects of column-to-panel integrity, joint reinforcement, bond beams, diagonal

reinforcement, poor quality mortar, gaps between panel and roof beams, and non-rigid frames. In this study, panel-to-column ties produced an increase in initial stiffness but did not provide any significant increase in major crack and ultimate load. The ties also tended to increase the off-diagonal tensile cracking. Bond beams increased the pre-cracking stiffness and initial major-crack load to near ultimate. Reinforcing the compression diagonal increased the first major crack and ultimate load only slightly. It was concluded that reducing the panel-to-frame interface bond and friction reduced major-crack and ultimate strength. Also, horizontal joint reinforcement restricted random cracking after the major diagonal cracking had occurred, but had no significant effect on the ultimate capacity. Poor mortar resulted in reductions in initial stiffness along with major crack and ultimate loads. A gap at the top of the infill caused a drastic reduction in cracking and ultimate load capacity.

Durrani and Luo (1994) used a finite-element analysis to identify the parameters having the most influence on the behavior of reinforced concrete frames with masonry infill [16]. Results from the analysis were used to further establish the equivalent-strut method developed by Smith and Mainstone. New equations were presented for calculating the equivalent-strut width for infill panels with and without openings. At the time of the report, test data on the interaction of masonry infills with concrete frames subjected to in-plane loadings were insufficient, and the analytical models were not fully developed.

Angel (1994) investigated the loss of out-of-plane strength of masonry-infilled reinforced concrete frames as a result of in-plane cracking [5]. Specimens were of approximately half-scale, single-bay, single-story, and infilled with either concrete block or clay brick. Testing parameters consisted of varying masonry unit and mortar types, and varying the height-to-thickness ratio of the infill panel. The specimens were first subjected to cyclic in-plane forces

causing a lateral drift equal to twice that of initial cracking. The cracked infills in the specimens were then exposed to a uniform load applied to the face. Analytical models and evaluation procedures were then developed based on the observed behavior. Angel concluded that the stiffness of frame/infill specimen decreased greatly once cracking of the infill occurred. Stiffness of the frame/infill specimen was directly proportional to the masonry compressive strength. In-plane stiffness can be best approximated using an equivalent strut with a width equal to 1/8 the diagonal dimension of the panel.

Saneinejad and Hobbs (1995) studied the inelastic design of infilled frames [48]. This study carried out on steel frames with infill and presents a more refined iteration of the equivalent-strut method by taking into account elastic-plastic behavior and the limited ductility of infill materials. Imperfections, including lack of infill-to-frame fit and shrinkage of the infill can also be included in the analysis. As with previous forms of the equivalent-strut method, predictions of both the strength and stiffness as well as the load to cause infill diagonal cracking, can be made.

Al-Chaar and Sweeney (1995) performed research on the strength of concrete frames with masonry infill subjected to dynamic loading [0]. The test specimens consisted of both weak frames with reinforcement details designed using the 1956 ACI code, and strong frames with reinforcement details designed using the 1991 ACI code. Frames were initially tested without infill, then frames were filled with masonry and tested again. The bare frames were tested, and, on average, strong frames were stiffer than the weak ones. When reinforced concrete frames were infilled with masonry and tested, the weak frame data were close to those expected. The strong frame was significantly weaker than expected. Nonlinear analytical analysis was performed and was compared to the experimental data. Maximum base shear was close to the

predicted value. Many simplified analytical methods were also examined, including Holmes, Smith, and Liauw and Kwan among others.

Mehrabi, Shing, Schullar, and Noland (1996) tested two types of reinforced concrete moment-resisting frames [38]. One was considered weak, designed only for lateral wind load. The other was considered strong, designed for seismic load. The strong frame was similar to the weak frame but contained heavier columns, more shear reinforcement, and stronger beam-to-column connection. It was concluded from this study that the strength of the infill could significantly improve the performance of a reinforced concrete frame. The specimens with strong frames and strong infills had much better load resistance and energy dissipation capabilities. The strong panels surrounded by weak frames were observed to have shear failure in the columns, although this was usually at a high drift.

Al-Chaar, Sweeney, and Brady (1996) investigated the behavior of R/C frames with masonry infill [1]. Two half-scale specimens were tested with brick masonry infill, but one had a strong frame and the other had a weak frame. A third specimen, identified as the large frame, contained low modulus concrete masonry units and was full-scale. The failure mechanism, load versus drift behavior, diagonal deformation, and joint rotation were all examined for each of the three different specimens. The strong frame failed due to diagonal tension cracking, and showed ductile behavior. The weak frame failed from diagonal cracking and hinging in the windward column, and although at lower load resistance, it also showed ductile behavior. The large frame failed from poor bonding between blocks and exhibited joint slippage between all courses. Overall, it was concluded that more research is needed in the area of infilled frames. However, it was considered safe to conclude that, if structurally designed, infilled frames give significant

strength, ductility, and energy dissipation increases with respect to plane frames. These increases are very desirable in seismic regions.

In 1996, Bennett suggested that the Smith and Carter (1969) equivalent strut be considered for seismic analysis of existing structures [9]. They added two important additional restrictions on the equivalent strut. First, for very stiff columns, the strut formation predicts significantly high contact lengths. It was suggested that the contact length be limited to 20% of the infill height, to avoid unreasonably high stiffness of the infill. Second, it is suggested that the cracked moment of inertia for beams and columns be taken as one-half of the gross moment of inertia.

The European Consortium of Earthquake Shaking Tables and Prenormative Research in Support of Eurocode 8, has performed research into the seismic response of infilled frames [18]. It was recognized in this study that strong infills that is considered non-structural, have often provided most of the earthquake and collapse resistance of relatively flexible and weak R/C frames. However, their behavior can be unpredictable, with the possibility of failing in a brittle fashion, which can contribute to the development of a soft story. Due to these and other questions about infills, two lines of thought have developed concerning their design and use. The first maintains that the behavior of infills is too uncertain when considered structurally, having more negative effects than positive. Thus, if infills are needed in a building, they should be engineered to be non-structural and isolated from the surrounding structural members. The other view contends that every part of a building should be used structurally to resist peak seismic events because it is more economical and efficient. Previous codes have adopted the former view, thus penalizing infilled structures. That past experimental work has concentrated on simple infilled frames (usually one-story and one-bay) under in-plane cyclic loading. The

overall behavior has not been well correlated to the basic material properties of the infill frame systems. Attempts at modeling have been of two types: (1) local models or micromodels often using nonlinear finite elements; (2) macromodels or global models based upon observed behavior without much supporting theory or explanation.

The micromodels or nonlinear finite-element analysis can provide realistic results provided individual masonry units and joints are modeled in detail and the interface between the infill panel and surrounding frame is modeled. With sufficient calibration with experiments, the micromodels can be used to develop simpler phenomenological macromodels. Also, they can be used in conjunction with out-of-plane behavior, but this approach has high computational demands.

The macromodels or global models using the equivalent diagonal strut require computational efficiency. This approach is most appropriate for assessing the nonlinear seismic response of a full structure. It is, more or less, based upon observed behavior without a clear understanding of the failure mechanisms due to their complexity. The recommended code provision adopts these points:

1) Regularly infilled R/C structures (i.e., not having many open bays, especially at lower stories) have, in general, a net beneficial contribution to seismic performance.
2) Beyond the design motion, infills participate in the response by supplying strength and a means of energy dissipation although they add very little to the stiffness of the system.
3) After the post-ultimate strength of the infilled frames is reached, the cracked infills cannot supply much stiffness, but being bounded by the frame they retain most of their strength through large deformations.

4) In low intensity ground motion, infills do not significantly increase the global lateral stiffness or the effective natural periods of the nonlinear response.
5) The overall seismic responses of regularly infilled frames and bare frames are not much different except that the infills resist a significant amount of story shear, and deformations and structural damages were less.
6) The beneficial aspects of infills are obtained when they can retain most of their strength under cyclic loading without sudden disintegration.

Mosalam, White, and Gergely (1997) studied the static response of infilled frames using quasi-static cyclic loading on quarter-scale specimens with semi-rigid connections in the steel frame [40]. The infill material consisted of unreinforced concrete masonry, with no shear connectors between the frame and infill. Deformation-controlled tests continuing beyond peak load were used to interpret results in terms of ductility. Load-deformation hysteretic behavior and failure modes were investigated for number of bays, material properties, and openings. Conclusions about the equivalent-strut method were made, and the hysteresis loop formulation was shown to have physical quantities that were meaningful to the tested specimen.

Mehrabi, Shing, Schuller, and Noland (1997) performed experimental and analytical tests of 14, half-scale, masonry-infilled, R/C frame specimens [39]. The experimental tests investigated the lateral in-plane strength, stiffness, and behavior of the infilled frames with respect to type of frame, type of masonry units, lateral load history, the panel aspect ratio, magnitude and distribution of vertical loads, and presence of adjacent infilled bays. The analytical investigation sought to develop simple analytical models as well as complex finite element models that accurately predict the strength and stiffness of the specimen. They analyzed five failure mechanisms using various models to determine an ultimate failure load.

Table I

Chronological Listing of Articles on Analytical Equivalent-Strut Experimentation

Year	Author(s)	Subject	Notes
1956	Polyakov	Interaction between masonry filler walls	First mention of equivalent strut
1958	Benjamin, Williams	The behavior of one-story brick shear walls	Studied testing parameters and used shear beam method
1960	Holmes	Steel frames with brickwork and concrete infill	Studied stiffness and strength using equivalent-strut method
1962	Holmes	Combined loading on infill frames	Studied equivalent strut on two stories with vertical loads
1962	Smith	Lateral stiffness of infilled frames	Studied stiffness using only equivalent-strut. Developed SS1 analytical method
1966	Smith	Behavior of square infilled frames	Introduced equivalent-strut and frame infill stiffness ratio
1968	Fedorkiw, Sozen	A lumped-parameter model to simulate the response of structures	Tested multi-story R/C frames as a shear beam.
1968	Fiorato, Sozen, Gamble	Behavior of five-story reinforced concrete frames.	Tested five-story R/C frames and studied the effect of reinforcement
1968	Yorulmaz, Sozen	Behavior of single-story R/C frames with filler walls	Tested fills with reinforcement
1969	Smith, Carter	A method of analysis for infilled frames	Studied equivalent strut and the effects of aspect ratios. Developed SS2 analytical method
1970	Fiorato, Sozen, Gamble	An investigation of the interaction of R/C frames with infill panels	Tested the effects of openings, frame reinforcement, and vertical loads
1971	Mainstone	On the strength and stiffness of infilled frames	Studied empirical stiffness and strength using equivalent-strut
1971	Mallick, Garg	Effect of openings on the lateral stiffness of infilled frames	Studied the effect of openings and shear connectors and used FEA comparison
1972	Yettram, Hirst	Collapse load of concrete infill panels	Tests on concrete infill panels
1973	Leuchars, Scrivener	Masonry infilled panels subjected to in-plane cyclic loading	Tested masonry-infilled R/C frames and used equivalent-strut idealization
1973	Smolira	Analysis of infilled shear walls	Used force-displacement matrix and introduced the concepts of double arching
1975	Lefter, Colville	Reinforcing existing buildings to resist earthquake forces	Shear beam method, design requirements

Table I (Continued)

Chronological Listing of Articles on Analytical Equivalent-Strut Experimentation

Year	Author(s)	Subject	Notes
1976	Klingner, Bertero	Infilled frames in earthquake resistant construction	Studied seismic resistant design of multi-bay multi-story using quasi-static tests
1977	Barua, Mallick	Behavior of mortar filled steel frames under lateral load	Studied slip between steel frame and infill, assuming elastic isotropic infill
1978	Klingner, Bertero	Earthquake resistance of infilled frames	Studied hysteresis seismic response
1985	Dawe	Experimental investigations of the shear resistance of system	Studied joint reinforcement, panel ties, and bond-beams and proposed evaluation methods
1985	Dawe, Yong	Investigation of factors influencing the behavior of masonry infilled R/C frames	Tested the effect of openings and gaps. Compared empirical data with finite element analysis
1988	Dawe, Schriver, and Sofocl	Masonry infilled steel frames subjected to dynamic loads	Dynamic study
1989	Thomas, Klingner	Behavior of infilled frames	Overview of infill frame analysis methods
1989	Dawe, Seah	Behavior of masonry infilled steel frames	Studied interface conditions, openings, frame rigidity, and bond beams
1994	Abrams, edt.	Proceedings from the NCEER workshop on seismic response	Contains several articles, Durrani and Lou
1994	Angel	Behavior of R/C frames with masonry infills	Test in-plane effects on out-of-plane response
1994	Durrani and Lou	Seismic retrofit of flat-slab buildings with masonry infills	Used Mainstone's equivalent-strut method and studied the effect of openings using finite element analysis
1995	Saneinjad, Hobbs	Inelastic design of infilled frames	Studied stiffness, strength, and lack of fit. Used equivalent-strut idealization
1995	Shing, Mehrabi	Influence of masonry infill on lateral resistance of masonry infilled frame	Carried out push-over test and studied modes of failure
1996	FEMA, NHERP	Commentary on the guidelines for the seismic rehabilitation	Adopted Mainstone's method and presented acceptance criteria for strength and stiffness
1996	ECOEST/PRE C8	Experimental and numerical investigations on the seismic behavior of structures	Compared analytical methods and emphasized the importance of macro-modeling

Table I (Continued)

Chronological Listing of Articles on Analytical Equivalent-Strut Experimentation

Year	Author(s)	Subject	Notes
1996	Mehrabi, et al.,	Experimental evaluation of masonry infilled RC frames	Tested infilled-frame
1996	Al-Chaar, Sweeney, Brady	Push over laboratory testing of URM infills	Overview of analysis methods
1997	Mosalam, et al.,	Static response of infilled frames using quasi-cyclic loading	Used quasi-static tests on 1 and 2 bays. Studied the effect of openings
1997	Mehrabi, et al.,	Performance of masonry infilled RC frames under in-plane loads	Tested half scale and used finite element analysis and analytical studies. Presented failure mechanisms

2.3 Finite Element Analysis View

In 1977, Riddington, and Smith used an elastic finite element model to simulate reinforced concrete frames with unreinforced masonry infills [46]. The models allowed for movement between the infill and frame boundaries using an iterative technique. Several different parameters were evaluated which included: (1) Single bays with various boundary conditions, length-to-height ratios, frame stiffnesses, and beam-to-column stiffnesses, (2) Three-story square infills with different boundary conditions, and (3) Square triple-bay specimens with different applications of lateral load. No tests were performed to examine the validity of the finite element models. It was concluded that stresses at the center of infills were found to be dependent upon the aspect ratio of the bay. The stiffness of the frame and the friction between infill and frame had little effect on the stresses. Stresses at the compression corners of the infills increased with increasing flexibility of the frames. As the length of contact in the corners diminishes with increased flame flexibility that results in a thinner equivalent width. Changes in the beam stiffnesses had little effect on the overall behavior of the infill frames. With the

method used, lateral deflections could not be accurately determined, but conservative values could be obtained by performing a frame analysis with a pin-connected equivalent strut with a diameter equal to one tenth of the infill length.

King and Pandey (1978) used the finite element method with modified friction elements to represent the lateral in-plane behavior of infilled masonry frames is investigated in this paper [26]. The models represented square infilled panels with steel frames enclosing them. The limitation of replacing a masonry infill by an equivalent strut in a frame analysis was also discussed. Several values for the shear stiffness at the infill-frame interface were used, and the shear strength had negligible affect on the behavior of the model beyond initial loading. Further models were made with openings and were compared to experimental tests. Experiments were performed on two-story, three-bay frames with infill panel dimensions of 150 mm by 150 mm. The authors claim that the equivalent strut method is satisfactory in most cases where infilled frames are subjected to lateral loads, except when shear connectors are used or larger openings exist. It is also claimed from their studies, that in a practical sense, diagonal struts from corner to corner cannot be used to analyze a building frame under all loading conditions. The location and length of contact between the infill and frame was found to vary depending on the vertical and lateral loading conditions.

Dhanasekar, and Page (1986) investigated the application of a finite element analysis of the behavior of masonry infilled frames subjected to in-plane loading [16]. A large number of biaxial tests of half-scale solid-clay brick masonry panels were performed in order to develop a material model for brick masonry including the mortar joints. Using the observed elastic and inelastic stress-strain relationships in conjunction with the observed failure mode, an iterative non-linear finite element model was constructed to predict the behavior of infill panels. Half-

scale tests were carried out on various panel and frame geometry with varying panel stiffnesses to verify the finite element model. It was concluded that the modulus of elasticity of the infill masonry significantly influences the load-deflection characteristics of the composite frame, and to lesser extent can influence its ultimate strength. The influence of variations in Poisson's ratio is insignificant. For a push-over test (where the bulk of the masonry is in a stress state of biaxial tension-compression), the influence of the inelastic deformation characteristics of the masonry found insignificant. Elastic-brittle material characteristics were found to satisfactorily reproduce the behavior in this case. Variations in masonry compressive strength did not influence the capacity of infilled frames when failure occurs by shearing down the panel diagonal. If failure had occurs by corner crushing, the ultimate strength would be influenced by changes in compressive strength. A progressive increase in masonry compressive strength for panels that had failed by corner crushing would eventually cause the mode of failure to change to one of diagonal shearing. The tensile and shear bond strengths of the masonry critically influenced the load-deflection behavior, the ultimate load, and in extreme cases, the mode of failure of the infilled frame. Realistic methods of analysis of infilled frames must therefore consider these parameters as well as the relative frame-wall stiffness and frame geometry.

El Haddad (1991) studied the uses of a finite element analysis to evaluate the effects of cracking in the concrete frame and separation of the infill and frame [17]. The presented model did not attempt to find the ultimate strength of infilled frames, but sought to identify over-stressed areas caused by cracking and separation, which could lead to subsequent deterioration. The model took into consideration the effects of crack size and location, infill frame relative stiffness, geometry of the frame and frame infill contact length. Bending moments in frame members and horizontal deflections were evaluated for the different crack and infill/frame

parameters. Frame members were divided into standard uncracked and complex cracked beam elements. The masonry infills were modeled as plane stress four node bilinear elements. It was reported from this study that bending moments and deflection at the frame joints decreased as the infill frame relative stiffness factor increased. Bending moment at cracked corner of the frame decreased as the crack depth increased. This effect was more pronounced as the infill frame relative stiffness decreased. Bending moment at uncracked section of the frame increased as crack size increased at other cracked section. This effect is more pronounced as the infill frame relative stiffness decreased. The horizontal deflection of the frame increased as crack size increased and as the infill frame relative stiffness decreased. In filler walls, magnitude and location of the uniform principal stresses had been affected by crack size, column infill contact length, and infill frame relative stiffness. As the column infill contact length increased, bending moments and deflection in frame were shown to decrease. Use of appropriate filler material and good construction techniques reduces the damage due to separation and cracking phenomena.

Lotfi and Shing (1991) evaluated the applicability of representing masonry infills by smeared crack finite element models [33]. In past studies the models were found to work very well for flexure-dominated behavior, but have not been able to capture the brittle shear behavior of unreinforced panels. Smeared crack elements were not able to represent the brittle failure behavior of masonry, unreinforced masonry in particular. Spurious shear strength develops in the element when discrete cracks form. These cracks were modeled by continuous displacement approximation functions where any shear distortion related to a crack opening was associated with diagonal compression strains that provide shear resistance after cracking. The restraint associated with the crack formation therefore generates spurious shear resistance instead of

compressive resistance only. One possible solution would be to model the crack formation discretely instead of continuously.

In 1994, Lotfi and Shing explained how the lateral in-plane behavior of masonry infilled frames was predicted using the finite element method with interface and smeared crack elements [34]. The models were capable of simulating the initiation and propagation of fractures caused by both normal and shear stresses. By simulating previous tests on infilled panel frames, the models were found to accurately predict the shear capacity and dilatancy (expansion of material associated with crack formation) of the infills. Due to the composite nature of unreinforced masonry with mortar joints between masonry units, an infill's behavior is both heterogeneous and anisotropic. At a basic level, infills can be modeled with basic linear elements assuming a homogeneous material response. Otherwise, the bricks and mortar joints can be discretely modeled with continuum elements (i.e., smeared crack elements). A constitutive model was developed for the formulation of the interface elements.

Reinhorn, Madan, Valles, and Reichmann, (1995) used theoretical/analytical macro-modeling as the primary mode for non-linear analysis by a computer program of buildings with masonry infills [44]. Simulation and experimentation were used for a three story steel frame with clay brick infill. There appeared to be only one central bay for the specimen that was subjected to cyclic lateral loading using an actuator. Of the three specimens, two had different ferrocement overlays and one had no infill. The hysteresis loops and force versus story drift curves resulted from the experiment and simulation, were then compared. A dynamic analysis was performed on models that were made to one-third scale of a three story building, with three bays and with or without one or two-wythe masonry infill panels. When the number of wythes were increased, the shear force in the columns remained about the same, and the deformation of

the columns was reduced. The amount of deformation was found to decrease 76% for single panels and 88% for double panels. However, the overall shear force increased with an increase in the number of panels, thus leading to an overall increase in stiffness. They concluded from this information that the connections in frames with infill, such as from the masonry to the beam and from the column to the beam, are very important. It was also found that when shear infill panels were used there was a reduction of hysteretic energy dissipation in the columns, which would lessen structural damage. They deduced that damage is worse when there is no infill used compared to frames with masonry infill. From this they surmise that only cosmetic repairs may be necessary following an earthquake. When subjected to dynamic loads, the frames without infill acted as moment resistant frames and the frames with infill behaved as braced frames. From this they reasoned that the braced frame effect was more desirable because the lateral loads were resisted by a sort of truss mechanism similar to a tie-strut, because of the compression in the panel and tension in the columns. Because this analysis was an application of macro modeling, there was no study of the effects on the infilled masonry or where frame and infill meet. Macro modeling was used to assess the overall structural damage and distribution of damage.

Mehrabi and Shing (1997) tested fourteen one-half-scale reinforced concrete frames infilled with concrete masonry units at the University of Colorado at Boulder [37]. Results from these tests were used to calibrate a finite element model. In this study, a cohesive dilatant interface model was developed to simulate the behavior of mortar joints between masonry units as well as the behavior of the frame-to-panel interface. A smeared crack finite element formulation has been used to model concrete in the reinforced concrete frame and masonry units in the infill panels. Experimental studies showed that for the fourteen one-half-scale models,

infill panels increased the strength and stiffness of a reinforced concrete frame by a substantial amount. In an infilled frame, significant nonlinear behavior usually started with the cracking of the infill. A smeared crack finite element formulation developed by Lotfi and Shing (1991) was used in this study to model concrete in the frame and masonry units in the infill panels. To model the behavior of mortar joints some new considerations were taken into account. These have not been known to be included in other similar models. These factors include the compressive hardening behavior of interfaces, the reversal of shear dilatancy in the case of cyclic loading, and the normal contraction of interface under shear sliding. Numerical results have shown that the models can capture the failure mechanisms of the frame specimens. The maximum lateral resistance of the specimens was estimated fairly well. Also, it observed that bond-slip behavior has an important influence on the response of a bare frame, but not on the behavior of the infilled frames.

2.4 Field Observations on Infilled Masonry after Sizable Earthquakes

Despeyroux's (1982) observations of structural damage were taken from the El Asnam earthquake of 1980 [14]. This earthquake exceeded the intensity usually taken into account by codes and it had a large vertical component. The author claims that the infills were generally extremely stiff and would not allow the columns to be deformed beyond their elastic flexural limit. Shear failures at the top of the columns were therefore observed where the stiff infills created large shear forces in the columns. The leeward columns also had reduced shear strengths as they were in tension. This failure mode is typical and expected in R/C frames with stiff infills. Langenbach's (1992) article reviewed the issues concerning masonry in the Loma Prieta earthquake of 1989. Few buildings with infilled-frame construction sustained significant

structural damage during the earthquake, but the 1988 Uniform Building Code (UBC) formulated stiff requirements for the rehabilitation of such structures. The cost of rehabilitation for infilled-frame buildings has proven unreasonable and, in some cases, dangerous. The 1988 UBC was intended for new building construction and was not compatible with rehabilitation. According to the code, masonry walls were to be treated entirely as dead load offering little or no structural resistance. Most retrofit efforts sought to place the entire structural capacity onto the concrete or steel frame members. The main problem with masonry is not the apparent structural degradation caused by cracks, but endangering safety from broken material. Two benefits are obtained from cracking masonry under seismic loading: (1) the building becomes less stiff with progressive cracking and its resonance frequency changes, and (2) the cracking of masonry aids in damping without significantly diminishing the vertical load-carrying capacity. The masonry also helps support concrete or steel members as their structural capacity deteriorates. In this process, the infill panels form diagonal struts that resist lateral loads in compression rather than in shear. The author concludes that the UBC needs reworking to fit older buildings and that cracked masonry does not represent failure.

NEHRP 274, document 1998, proposed strength and stiffness acceptance criteria [41]. The elastic in-plane stiffness of a solid unreinforced masonry infill panel were represented by an equivalent diagonal compression strut. The stiffness of cracked unreinforced masonry infill panels can be represented by equivalent struts, provided that the nonlinear behavior of the cracked masonry has been evaluated from a detailed analysis. Stiffnesses for existing and new infills can be assumed to be the same. Transfer of story shear through a confined masonry infill panel is considered a deformation-controlled action. The expected infill shear strength is equal to the net mortared and grouted area times the shear strength of the masonry. The shear strength

of existing masonry was calculated based on in-plane shear tests, where the shear strength of newly constructed infill panels were presented with recommended limits. This document recommended strength requirements for columns and beams adjacent to infill panels.

Table II

Chronological Listing of Articles on Observations and Studies from Earthquakes

Year	Author(s)	Subject	Notes
1982	Despeyroux	The El Asnam earthquake of October 10, 1980	Infills stiffness for proper column behavior
1992	Langenbach	Earthquakes: a new look at cracked masonry	Problems with rehabilitation and retrofit of unreinforced masonry
1996	Bennett, et al.,	Evaluations and analysis of the performance of masonry-infilled R/C frames	Presented positive and negative aspects of modeling and suggested using the SS2 idealization method.

2.5 Highlights of Literature Review

2.5.1 General Observations

- Polyakov introduced the equivalent-strut method.
- Holmes based the strength and stiffness of the equivalent strut on the thickness and modulus of the infill material, and the infill width was taken as 1/3 of diagonal length.
- Smith made the width of the equivalent strut a function of the relative infill and frame stiffness, and values of the width varied from 1/4 to 1/10 the diagonal length. Lack of consistency in results has been attributed to misrepresentation of boundary stress distributions.
- Mainstone expanded Smith's work by correlating the theoretical relationships with more realistic model tests.

- Benjamin and Williams observed that after the formation of the equivalent strut, the strength of the infill frame system depended on the capacity of the compression column under shear, axial, and moment loads produced by action of the infill.

2.5.2 Analytic Investigations

Two types of analytical investigations have been carried out. These simplified concepts include the equivalent strut and numerical methods (including finite element analysis and finite difference procedures). Numerical methods are often complex as they attempt to model the nonlinear behavior of the infills. At the time of this investigation, the results from numerical approaches have been disappointing.

2.5.3 Mechanical Characteristics of Materials

Bare frames, infilled frames with clay brick, and infilled frames with concrete masonry units were tested. From masonry prism tests, it was found that grouted masonry had a much more consistent behavior than ungrouted or partially grouted prisms. For this reason, grouted masonry was thought to be more suited for macroscopic models such as the equivalent strut.

2.5.4 Predictions of Infilled Frame Behavior

The equivalent-strut concept was used to develop macroscopic models because of the limitations and inconsistencies of microscopic modeling and the tendency of infilled-frame systems to behave as braced frames. It was used to predict initial stiffness and strength, as well as degrading stiffness and strength behavior. The proposed equivalent-strut models were not intended to take into account the non-ductile behavior of the infilled-frame. These models are

insensitive to the multiplicity of bays. Therefore, the developed models in their current forms are not applicable to our current investigation. Before applying these models to old structures, these models need to be verified and they may need to be modified or replaced.

2.5.5 Seismic Design Implications

Heavy non-structural elements should be avoided in building systems that could be subjected to earthquake motions. However, well-engineered infills can be used efficiently to help withstand seismic forces because of their contribution to stiffness and ability to dissipate energy.

CHAPTER 3

EXPERIMENTAL PROGRAM

3.1 Introduction

This chapter describes the experimental test program that was carried out at the United States Army Construction Engineering Research Laboratory (USACERL) to evaluate the performance of a structural system consisting of masonry infill in non-ductile reinforced concrete frames. All test specimens represent a single story of single, double, or triple bay construction. One bare frame and four frames fully infilled were tested to an increasing horizontal displacement of 5 to 6 inches. These tests were designed to study each specimen's load-deformation behavior with reference to elastic deformation (i.e., up to the appearance of the first crack), ultimate strength, and residual strength under significant drift. These parameters are elastic deformation that is limited by the appearance of the first crack in the model under consideration, ultimate strength, and residual strength under significant drift. Descriptions of the test specimens, test-setup, scaling concepts, data acquisition, instrumentation, and material properties are presented.

3.2 Test Specimens

This section describes five half-scale, non-ductile reinforced concrete frame specimens fully infilled with half-scale brick or CMU walls. The design of all concrete frames was based on a prototypical structure of a typical dormitory, Building 1211 at Castle Air Force Base. The building is a three-story reinforced concrete frame constructed in 1952. Longitudinal frames of

Building 1211 were the basis for the specimen models. The prototype structures were constructed in accordance with ACI 318-51. Features distinguishing them from newer structures are:

- larger spacing distances between stirrups and ties
- discontinuity in the bottom longitudinal reinforcement of the beam at the joints
- lower steel grade (40 ksi)
- lower concrete compressive strength
- less stringent code requirements on splice overlap and standard hooks

Each model had an overall height, from the bottom of the column to the top of the beam, of 60 inches. Typical bay width was 72 in. between column centerlines. Columns were 8 in. wide by 5 in. deep; a typical beam was 7.75 in. deep by 5 in. wide. Prototype and model parameters are shown in Table III.

Table III

Half-Scale Factor Parameters for Model and Prototype

Parameter	Prototype	Model
Bay width	160 in.	80 in.
Bay height	120 in.	60 in.
Column depth	16 in.	8 in.
Column width	10 in.	5 in.
Beam depth	15.5 in.	7.75 in.
Beam width	10 in.	5 in.
Column longitudinal reinforcement	4-#6 (ρ=0.0125)	4-#3 (ρ=0.0125)
Column ties	# 3 at 12 in. (ρ=0.0065)	(ρ=0.0065)
Beam longitudinal reinforcement	4-#6 top (ρ=0.012) 2-#6 bottom (ρ=0.006)	3-#3 top (ρ=0.012) 2-#3 bottom (ρ=0.0125)
Beam ties	9-#3 at 6 in. (ρ=0.013)	6 gage at 3 in. (ρ=0.013)

Half-scale brick and concrete masonry units were cut from full-scale units as shown in Figure 3.1. Their nominal dimensions are 3.75 in. for CMU and 2.25 in. for brick. A professional mason constructed the walls in a running bond pattern. Type N mortar was used in all cases. These frames had a slenderness ratio (h_{wall}/t_{wall}) of 13.9 for the CMU wall and 23.13 for the brick wall. The aspect ratios (h_{wall}/l_{wall}) were 1.38 for all walls.

3.3 Scaling the Tested Models Using π Buckingham Theorem

Push-over laboratory tests on full-scale assemblies of reinforced concrete frames infilled with masonry were not possible at the available testing facilities, and equipment did not meet the requirements for testing the assemblies under consideration. As a result, experimentation was carried out on scale models under controlled conditions during which the behavior of models can project their prototypes. This section defines scaling parameters for half-scale models.

In testing these models, it was desirable to load the specimens to nearly 10% of the drift ratio. The analysis of scale models loaded into the nonlinear region involved some level of error in the relevant scaling parameters. The behavior of the models in the nonlinear region are valid only where crack formation, crack growth, and bonding mechanism are scaled properly or their effects are minimized. Significant accumulated errors and the level of uncertainty from numerous parameters would be greater with smaller scale models. Thus, half-scale models were chosen to meet the facilities and equipment limitations, while minimizing errors.

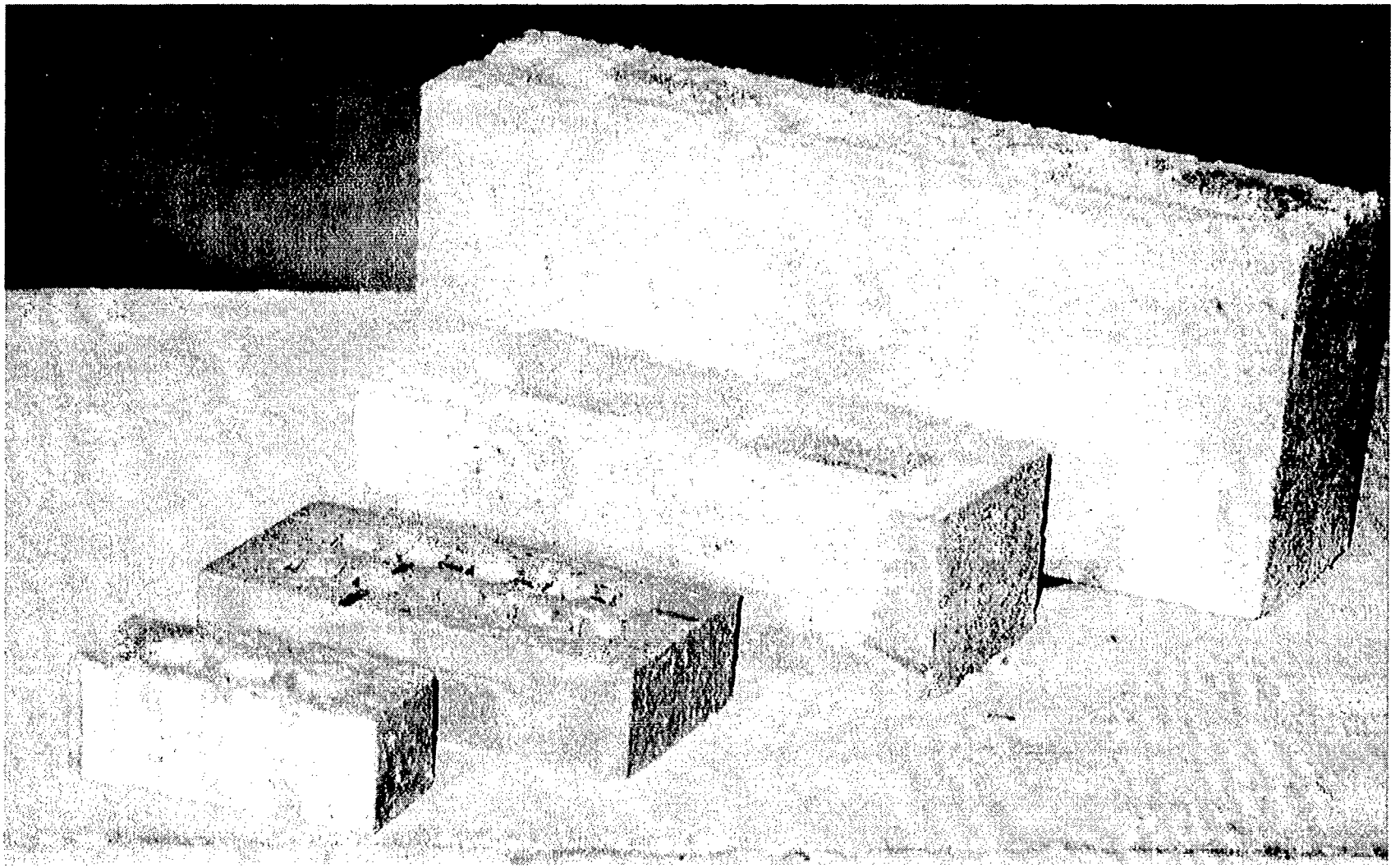

Figure 3.1 Description Of Half-Scale Bricks and CMU

To minimize the differences in behavior between the model and the prototype, the scaled specimens were constructed of the same materials as the prototype. A dimensional scaling factor of one-half was assigned between the models and the prototype. Other scaling parameters that satisfy scaling laws were calculated.

The basic equation relates five quantities, or describes the force in term of four variables:

$$F = \phi(E, M, h, t)$$

E (F / L2): the modulus of elasticity of the composite R/C frame infilled with masonry which is not constant over the loading region of interest

M (FT2 / L): mass assigned at the top of the story

h (L): any linear dimension

t (T): time is only a factor in stroke factor

F (F): force

In order to describe engineering quantities, the necessary fundamental independent units are:

F: force

L: length

T: time

In applying the required scaling laws to design a scale model, such that the test results from the model could be projected to describe the behavior of the prototype structure, it has been found that many different solutions can reasonably satisfy the scaling equations.

One concern related to the term E, is that it is not constant in the inelastic zone. However, it is assumed the change in E in the prototype equals the change in E in the models.

Since the models and the prototype use the same materials to retain the required similarity over the loading range, the assumption that E_m represents E_P in the nonlinear zone may also be accepted but with some small error.

Theoretically, the method employed to satisfy the mass ratio is to increase the mass by a factor of four. However, since the density of material cannot be increased, the mass ratio shall be increased by eight. In applying the results of the models to their prototypes, it is necessary that the effect of additional mass equals eight times the self-weight of the model under consideration. Consequently, it is reasonable to increase the shear resistance model by 20% of the normal stresses caused by the added mass.

Table IV is a summary of scaling used in modeling the specimens. Nevertheless, even though the models were intended to represent prototypes, they were treated as small size prototype specimens to prove theoretical concepts that describe their physical behaviors.

Table IV

Prototype/Mode, Scaling Ratio of Half-Scale Parameters that Satisfy Scaling Law

Scaling parameters	Prototype	USACERL Model	Remarks
Dimension ratio*	1	½	Assigned
Modulus of elasticity ratio	1	1	Same material
Mass ratio	1	4 8	Theoretically Actually, to account for density scaling
Time ratio	1	$2^{½}$	Calculated to satisfy scaling law
Force ratio	1	$1+\eta$*	Scaling law is satisfied

* η = 20% of stresses due to additional mass equals the eight times the tributary mass

The models also could be studied as full-scale small specimens, with the size effect of the tested specimens and the structures they represent accounted for analytically.

3.4 Test Setup

The five models shown in Figures 3.2 through 3.5 were constructed on stiff reinforced concrete base beams. The base beam of each model was bolted to the USACERL high bay strong floor. For models 2, 3, and 4, a pair of 50 kip hydraulic actuators was installed to horizontally extend from a steel reaction frame. The two actuators simultaneously loaded a steel I-beam placed transverse to their direction of loading. The beam transmitted the load to the end of the overhang beam of the specimen concentrically. Greased Teflon plates were installed between the steel I-beam and the specimen loading point to eliminate any shear effects that could result from friction between the two components.

For Models 1 and 5, a 50 kip and a 148 kip hydraulic actuator, respectively, were installed to horizontally extend from a reaction concrete structure. The actuator was positioned to load the end of the overhang beam of the specimens. Greased Teflon plates were installed between the steel I-beam and the specimen loading point to eliminate any shear effects resulting from friction between the models and the actuators. In Model 5, the loaded end of the beam was wrapped with overlay fiberglass composite material to reduce the concentration of the stress at the loaded end. Also, the specimen was braced laterally to eliminate out-of-plane movements. Teflon plates were installed at the loading end and at the support points of the steel braces.

In-plane monotonic loading, stroke-controlled push-over tests were carried out to understand the post-elastic behavior of each model configuration as it was subjected to

increasing drift ratios. The intention of each test was to continuously load the specimen under a stroke control condition of up to 10% drift ratio, approximately, at a rate of 1.66×10^{-3} in. per second.

The overall static push-over experimental program, summarized in Table V, consisted of five models statically tested under monotonic loading. Model 1 was a bare frame non-ductile reinforced concrete frame. Model 2 was a one-bay R/C frame with CMU infill wall. Model 3 was similar to Model 2 except it had a brick infill wall. Model 4 was a two-bay frame with CMU infill, and Model 5 was a three-bay frame with brick infill.

Table V

Push-Over Experimental Program for Masonry Infilled Reinforced Concrete Frames

Model	Frame	Infill	Date of Testing
1	One-bay RC frame	None	10/15/97
2	One-bay RC frame	CMU infill	2/4/97
3	One-bay RC frame	Brick infill	2/6/97
4	Two-bay RC frame	CMU infill	7/25/97
5	Three-bay RC frame	Brick infill	5/1/98

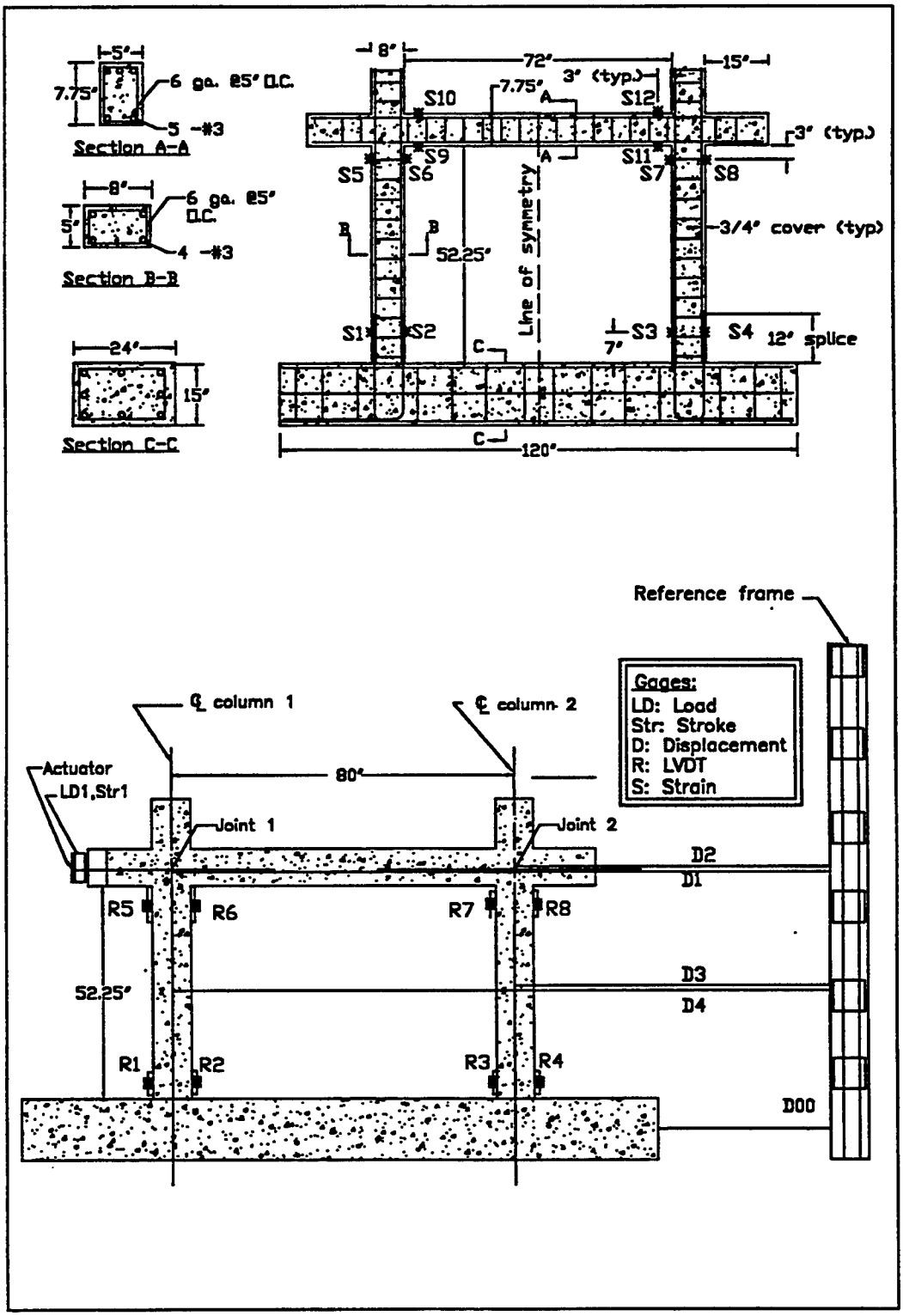

Figure 3.2 Reinforcement Details and Instrumentation Plan for the Bare Frame Specimen (Model 1)

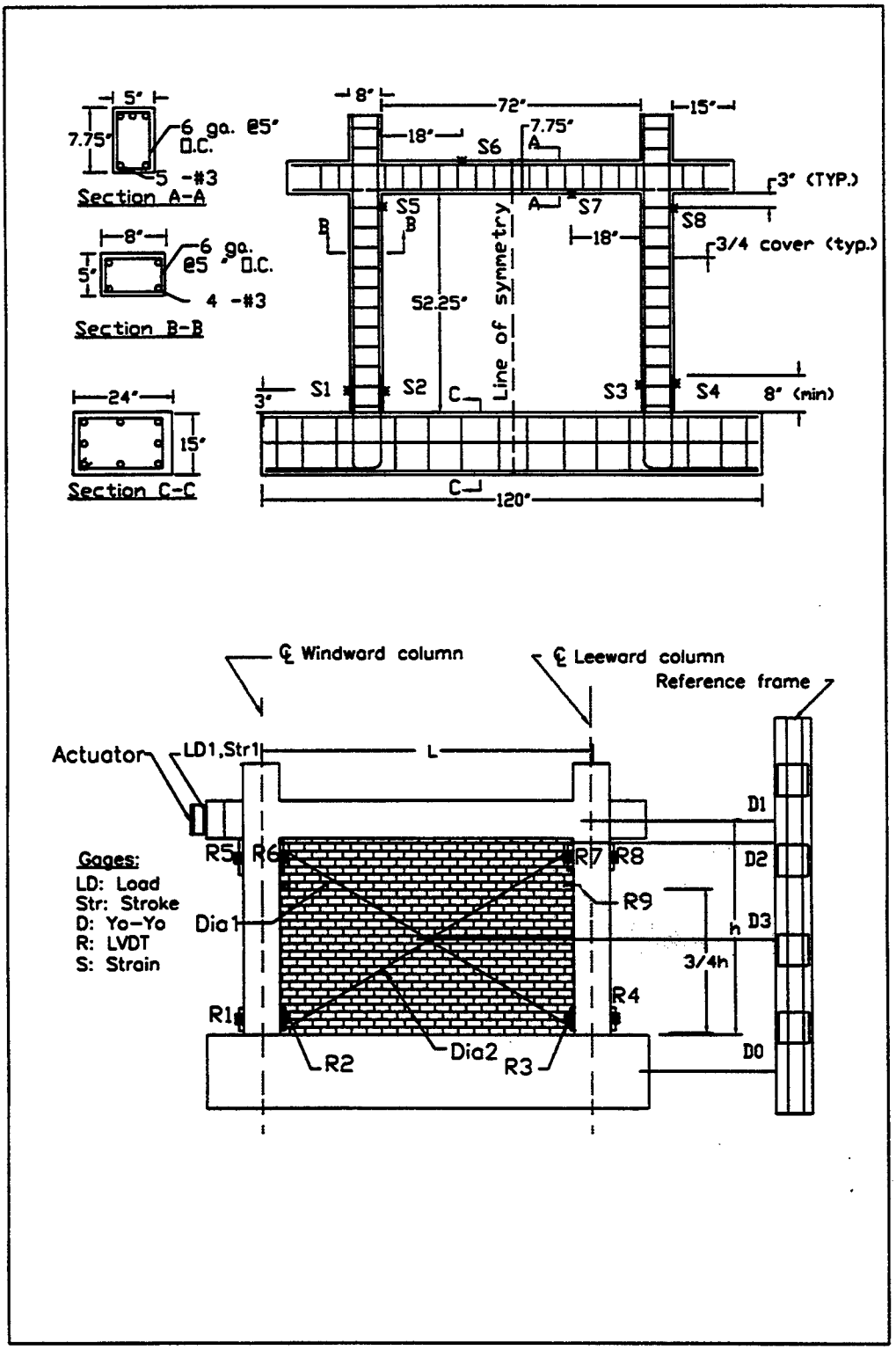

Figure 3.3 Reinforcement Details and Instrumentation Plan for the One-Bay Brick and CMU Infilled Specimens (Models 2 and 3)

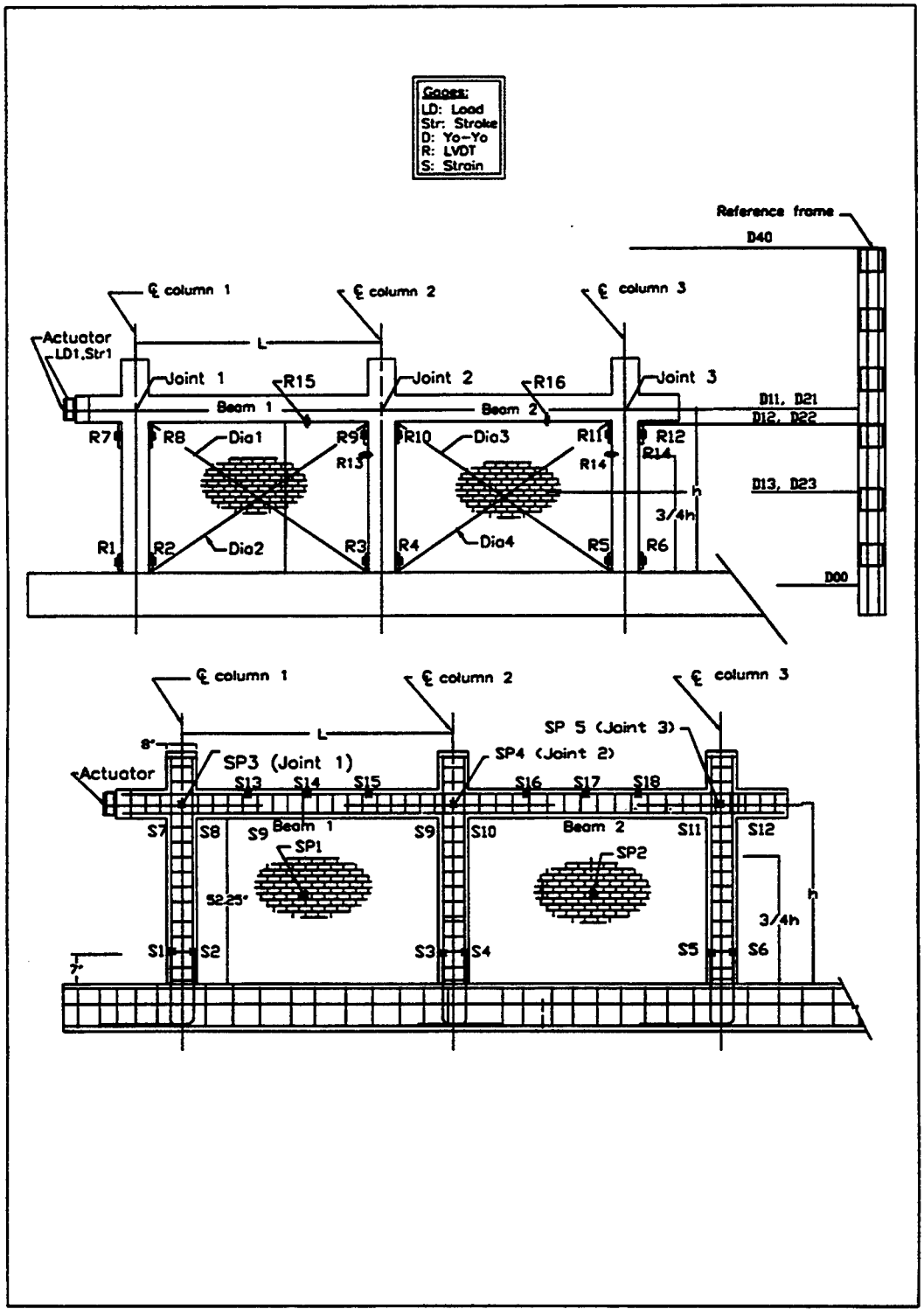

Figure 3.4 Reinforcement Details and Instrumentation Plan for the CMU Two-Bay Specimen (Model 4)

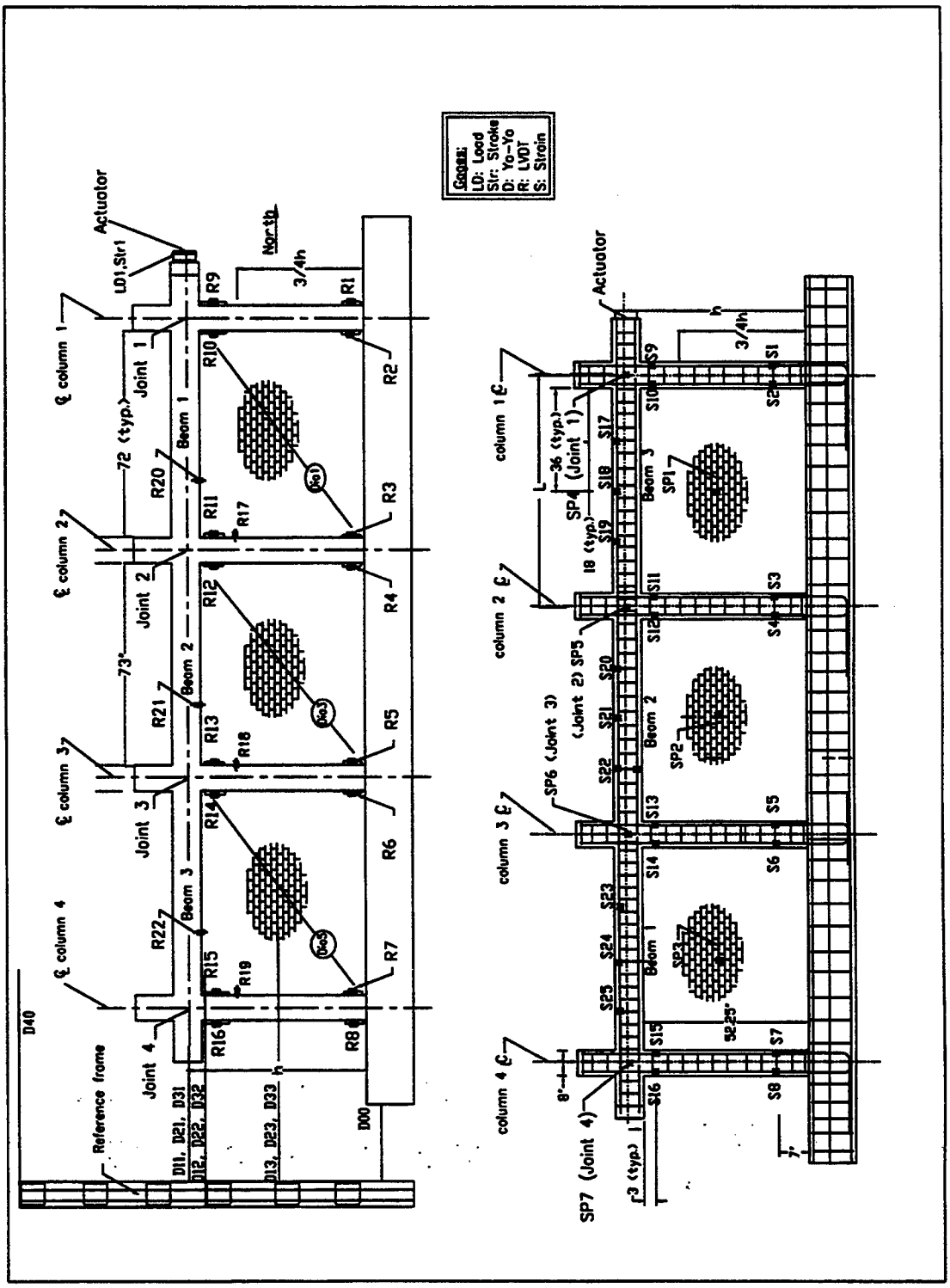

Figure 3.5 Reinforcement Details and Instrumentation Plan for the CMU Three-Bay Specimen (Model 5)

For each frame, a stroke of approximately 6 inches was imposed slowly over 15 minutes, while other dependent parameters were recorded in 2 second intervals. The load-displacement curves encompass four segments of the capacity curve: linear elastic, post-yield, post-failure, and residual capacity. Some of the major parameters acquired during the tests were loads, frame displacement, infill panel diagonal deformation, and frame joint rotation. Modes of failure were observed during the tests, indicated by crack propagation in the infill panels and the formation of cracks and hinges in the R/C frames.

3.5 Instrumentation and Data Acquisition

Three types of instrumentation were employed during the tests to measure the response of the test wall: electrical resistance strain gages, linear variable displacement transducers (LVDTs), and linear-resistive displacement transducers. The applied load and displacement of the hydraulic actuators were also measured. Tables VI, VII, VIII, and IX show the instrumentation plan for all models, and Figures 3.2, 3.3, 3.4, and 3.5 show the placement of the instrumentation for pushover tests.

3.5.1 Strain Gages

Electrical resistance strain gages were installed at several locations on the steel reinforcing longitudinal bars embedded in the concrete. The steel reinforcing bars were instrumented with Measurements Group Model CEA-06-125UN-350 electrical resistance strain gages with constantan grids and complete polyamide encapsulation. The sensing grid is 0.125 in. long by 0.100 in. wide. Each gage was connected to a Vishay Model 2120 signal conditioner to

provide power, balancing, and signal amplification. In this configuration, the strain gage formed one arm of the wheatstone bridge, and the remaining three arms were composed of precision resistors located in the signal conditioner.

3.5.2 Linear Variable Displacement Transducers (LVDTs)

The Schaevitz Model 200HR and RPS Model KB200 LVDTs were used to measure the relative displacement at various locations on the wall. The 200HR LVDTs have a range of ±0.2 in. They were used to measure the displacement across the concrete-masonry joint and rotation of the concrete column joint. The KB200 LVDTs have a range of ± 1.0 in. They were used to measure displacement diagonally across the face of the masonry infill. These transducers are AC-powered units that contain a set of transformer windings and a movable metal core. The core is attached to the measurement point, and when displacement occurs, the movement of the core changes the electrical coupling between the windings, which in turn changes the output signal. The LVDTs were connected to an Endevco Model 4478.1A signal conditioners, which provide AC power, signal amplification, AC-to-DC conversion, and electrical balancing.

Table VI

Instumentation Plan for Model 1, Bare R/C Frame
(Cast on 9/3/1997, Tested on 10/15/1997)

Chan. No.	Sensor No.	Scale Factor	Type	Gage Length (in)	Location	Remarks
1	L4	5000 lb/V	Load cell	N/A	West actuator	
2	S4	0.3 in/V	Stroke	N/A	West actuator	
3	R1	0.0199 in/V	LVDT	Along 3 in.	Bottom of windward column, outside face	
4	R2	0.02 in/V	LVDT	Along 3 in.	Bottom of windward column, inside face	
5	R3	0.02 in/V	LVDT	Along 3 in.	Bottom of leeward column, inside face	
6	R4	0.02 in/V	LVDT	Along 3 in.	Bottom of leeward column, outside face	
7	R5	0.02 in/V	LVDT	Along 3 in.	Top of windward column, outside face	
8	R6	0.02 in/V	LVDT	Along 3 in.	Top of windward column, inside face	
9	R7	0.02 in/V	LVDT	Along 3 in.	Top of leeward column, inside face	
10	R8	0.02 in/V	LVDT	Along 3 in.	Top of leeward column, outside face	
11	D00	1.9968 in/V	Displacement gage	N/A	Base beam	
12	D1	1.9901 in/V	Displacement gage	N/A	Joint 1	
13	D2	1.9893 in/V	Displacement gage	N/A	Joint 2	
14	D3	1.9602 in/V	Displacement gage	N/A	Center of the windward column	
15	D4	1.9602 in/V	Displacement gage	N/A	Center of the leeward column	
16	S1		Strain on rebar	0.125 in.	Bottom of windward column, outside face	7 in. from the base of the column
17	S2		Strain on rebar	0.125 in.	Bottom of windward column, inside longitudinal bar	7 in. from the base of the column
18	S3		Strain on rebar	0.125 in.	Bottom of leeward column, inside longitudinal bar	7 in. from the base of the column
19	S4		Strain on rebar	0.125 in.	Bottom of leeward column, outside longitudinal bar	7 in. from the base of the column
20	S5		Strain on rebar	0.125 in.	Top of windward column, outside face	3 in. from the bottom face of of the beam
21	S6		Strain on rebar	0.125 in.	Top of windward column, inside longitudinal bar	3 in. from the bottom face of of the beam
22	S7		Strain on rebar	0.125 in.	Top of leeward column, inside longitudinal bar	3 in. from the bottom face of of the beam
23	S8		Strain on rebar	0.125 in.	Top of leeward column, outside longitudinal bar	3 in. from the bottom face of of the beam

Table VI (Continued)

Instrumentation Plan for Model 1, Bare R/C Frame
(Cast on 9/3/1997, Tested on 10/15/1997)

Chan. No.	Sensor No.	Scale Factor	Type	Gage Length (in)	Location	Remarks
24	S9		Strain on rebar	0.125 in.	Windward end of the beam, bottom longitudinal bar	3 in. from the base of the column
25	S10		Strain on rebar	0.250 in.	Windward end of the beam, top longitudinal bar	3 in. from the base of the column
26	S11		Strain on rebar	0.250 in.	Leeward end of the beam, bottom longitudinal bar	
27	S12		Strain on rebar	0.250 in.	Leeward end of the beam, top longitudinal bar	
28	S13		Embedded strain	0.125 in.	Windward end of the beam, bottom longitudinal bar	3 in. from the base of the column
29	S14		Embedded strain	0.250 in.	Windward end of the beam, top longitudinal bar	3 in. from the base of the column
30	S15		Embedded strain	0.250 in.	Leeward end of the beam, bottom longitudinal bar	
31	S16		Embedded strain	0.250 in.	Leeward end of the beam, top longitudinal bar	

Table VII

Instrumentation Plan for Models 2 and 3, Single-Bay Infilled R/C Frames (Tested on 2/4/1997 for CMU and 2/6/1997 for Brick)

Chan. No.	Sensor No.	Scale Factor	Type	Gage Length (in)	Location	Remarks
1	L4	5000 lb/V	Load cell	N/A	West actuator	
2	S4	0.3 in/V	Stroke	N/A	West actuator	
3	L5	5000 lb/V	Load cell	N/A	East actuator	
4	S5	0.3 in/V	Stroke	N/A	East actuator	
5	R1	0.0199 in/V	LVDT	Along 3 in.	Bottom of windward column, outside face	
6	R2	0.02 in/V	LVDT	Along 3 in.	Bottom of windward column, inside face	
7	R3	0.02 in/V	LVDT	Along 3 in.	Bottom of leeward column, inside face	
8	R4	0.02 in/V	LVDT	Along 3 in.	Bottom of leeward column, outside face	
9	R5	0.02 in/V	LVDT	Along 3 in.	Top of windward column, outside face	
10	R6	0.02 in/V	LVDT	Along 3 in.	Top of windward column, inside face	
11	R7	0.02 in/V	LVDT	Along 3 in.	Top of leeward column, inside face	
12	R8	0.02 in/V	LVDT	Along 3 in.	Top of leeward column, outside face	
13	R9	0.02 in/V	LVDT		3/4 height of infill and leeward column	To measure gap b/ infill and column
14	Dia 1	0.099 in/V	LVDT	Along 77 in.	Infill, diagonal from upper windward to lower leeward corners	
15	Dia 2	0.1 in/V	LVDT	N/A 77 in.	Infill, diagonal from lower windward to upper leeward corners	
16	D0	1.9968 in/V	Displacement gage	N/A	Base beam	
17	D1	1.9901 in/V	Displacement gage	N/A	Center of top beam	
18	D2	1.9893 in/V	Displacement gage	N/A	Top of the infill	
19	D3	1.9602 in/V	Displacement gage	N/A	Center of the infill	
20	D4	2.0560 in/V	Displacement gage	N/A	Top center of the reaction frame	
21	ST1	0.0005 (brick) 0.001(CMU)	Strain	0.125 in	Bottom of windward column, outside face	7 in. from the base of the column
22	ST2	0.0005 (brick) 0.001(CMU)	Strain	0.125 in.	Bottom of windward column, inside longitudinal bar	7 in. from the base of the column
23	ST3	0.0005 (brick) 0.001(CMU)	Strain	0.125 in.	Bottom of leeward column, inside longitudinal bar	7 in. from the base of the column

Table VII (Continued)

Instrumentation Plan for Models 2 and 3, Single-Bay Infilled R/C Frames (Tested on 2/4/1997 for CMU and 2/6/1997 for Brick)

Chan. No.	Sensor No.	Scale Factor	Type	Gage Length (in)	Location	Remarks
24	ST4	0.0005 (brick) 0.001(CMU)	Strain	0.125 in.	Bottom of leeward column, outside longitudinal bar	7 in. from the base of the column
25	ST5	0.0005 (brick) 0.001(CMU)	Strain	0.125 in.	Top of windward column, outside face	3 in. from the bottom face of of the beam
26	ST6	0.0005 (brick) 0.001(CMU)	Strain	0.125 in.	Top of windward column, inside longitudinal bar	3 in. from the bottom face of of the beam
27	ST7	0.0005 (brick) 0.001(CMU)	Strain	0.125 in.	Top of leeward column, inside longitudinal bar	3 in. from the bottom face of of the beam
28	ST8	0.0005 (brick) 0.001(CMU)	Strain	0.125 in.	Top of leeward column, outside longitudinal bar	3 in. from the bottom face of of the beam
29	ST9	0.0005 (brick) 0.0006(CMU)	Embedded strain	30 mm	Bottom of windward column, outside face	3 in. from the base of the column
30	ST10	0.0005 (brick) 0.0006(CMU)	Embedded strain	30 mm	Bottom of leeward column, inside longitudinal bar	3 in. from the base of the column ***Not working for "brick" test***
31	ST11	0.0005	Rosette vertical	30 mm	Center of the infill, vertical rosette	Only for "brick" test
32	ST12	0.0005	Rosette diagonal	30 mm	Center of the infill, diagonal rosette	Only for "brick" test
33	ST13	0.0005	Rosette horizontal	30 mm	Center of the infill, horizontal rosette	Only for "brick" test

Table VIII

Instrumentation Plan for Model 4 Two-Bay CMU Infilled R/C Frame (Tested 7/25/1997)

Chan. No.	Sensor No.	Scale Factor	Type	Gage Length (in)	Location	Remarks
1	L1	5000 lb/V	Load cell	N/A	West actuator	
2	Str1	0.3 in/V	Stroke	N/A	West actuator	
3	L2	5000 lb/V	Load cell	N/A	East actuator	
4	Str2	0.3 in/V	Stroke	N/A	East actuator	
			LVDT for Rotation			
5	R1	0.0199 in/V	LVDT	Along 3 in.	Bottom of column 1 (windward), windward face	
6	R2	0.02 in/V	LVDT	Along 3 in.	Bottom of column 1 (windward), leeward face	
7	R3	0.02 in/V	LVDT	Along 3 in.	Bottom of column 2, windward face	
8	R4	0.02 in/V	LVDT	Along 3 in.	Bottom of column 2, leeward face	
9	R5	0.0199 in/V	LVDT	Along 3 in.	Bottom of column 3, windward face	
10	R6	0.02 in/V	LVDT	Along 3 in.	Bottom of column 3, leeward face	
11	R7	0.0199 in/V	LVDT	Along 3 in.	Top of column 1 (windward), windward face	
12	R8	0.02 in/V	LVDT	Along 3 in.	Top of column 1 (windward), leeward face	
13	R9	0.02 in/V	LVDT	Along 3 in.	Top of column 2, windward face	
14	R10	0.02 in/V	LVDT	Along 3 in.	Top of column 2, leeward face	
15	R11	0.0199 in/V	LVDT	Along 3 in.	Top of column 3, windward face	
16	R12	0.02 in/V	LVDT	Along 3 in.	Top of column 3, leeward face	
			LVDT for Gap Width			
17	R13	0.02 in/V	LVDT		Column 1 at 3/4 height of infill	To measure gap b/ infill and column
18	R14	0.02 in/V	LVDT		Column 2 at 3/4 height of infill	To measure gap b/ infill and column
19	R15	0.02 in/V	LVDT		Beam 1 at 3/4 the infill width from column 1	To measure gap b/ infill and beam
20	R16	0.02 in/V	LVDT		Beam 2 at 3/4 the infill width from column 2	To measure gap b/ infill and beam

Table VIII (Continued)

Instrumentation Plan for Model 4 Two-Bay CMU Infilled R/C Frame (Tested 7/25/1997)

Diagonal LVDT

Chan. No.	Sensor No.	Scale Factor	Type	Gage Length (in)	Location	Remarks
21	Dia 1	0.099 in/V	LVDT	Along 77 in.	Infill 1, diagonal from upper windward to lower leeward corners	
22	Dia 2	0.1 in/V	LVDT	N/A 77 in.	Infill 1, diagonal from lower windward to upper leeward corners	
23	Dia 3	0.099 in/V	LVDT	Along 77 in.	Infill 2, diagonal from upper windward to lower leeward corners	
24	Dia 4	0.1 in/V	LVDT	N/A 77 in.	Infill 2, diagonal from lower windward to upper leeward corners	

Displacement Gages

25	D00	1.9968 in/V	Displacement gage	N/A	Base beam	
26	D11	1.9901 in/V	Displacement gage	N/A	Center of top beam 1	
27	D12	1.9893 in/V	Displacement gage	N/A	Top of the infill 1	
28	D13	1.9602 in/V	Displacement gage	N/A	Center of the infill 1	
29	D21	1.9901 in/V	Displacement gage	N/A	Center of top beam 2	
30	D22	1.9893 in/V	Displacement gage	N/A	Top of the infill 2	
31	D23	1.9602 in/V	Displacement gage	N/A	Center of the infill 2	

Column Reinforcement Strain Gauges

33	S1	0.0005	Strain	0.125 in.	Bottom of column 1 (windward), windward reinforcement bar	7 in. from the base of the column
34	S2	0.0005	Strain	0.125 in.	Bottom of column 1 (windward), leeward reinforcement bar	7 in. from the base of the column
35	S3	0.0005	Strain	0.125 in.	Bottom of column 2, windward reinforcement bar	7 in. from the base of the column
36	S4	0.0005	Strain	0.125 in.	Bottom of column 2, leeward reinforcement bar	7 in. from the base of the column
37	S5	0.0005	Strain	0.125 in.	Bottom of column 3, windward reinforcement bar	3 in. from the bottom face of of the beam
38	S6	0.0005	Strain	0.125 in.	Bottom of column 3, leeward reinforcement bar	3 in. from the bottom face of of the beam
39	S7	0.0005	Strain	0.125 in.	Top of column 1 (windward), windward reinforcement bar	7 in. from the base of the column
40	S8	0.0005	Strain	0.125 in.	Top of column 1 (windward), leeward reinforcement bar	7 in. from the base of the column
41	S9	0.0005	Strain	0.125 in.	Top of column 2, windward reinforcement bar	7 in. from the base of the column
42	S10	0.0005	Strain	0.125 in.	Top of column 2, leeward reinforcement bar	7 in. from the base of the column
43	S11	0.0005	Strain	0.125 in.	Top of column 3, windward reinforcement bar	3 in. from the bottom face of of the beam
44	S12	0.0005	Strain	0.125 in.	Top of column 3, leeward reinforcement bar	3 in. from the bottom face of of the beam

Table VIII (Continued)

Instrumentation Plan for Model 4 Two-Bay CMU Infilled R/C Frame (Tested 7/25/1997)

Beam Reinforcement Strain Gages

Chan. No.	Sensor No.	Scale Factor	Type	Gage Length (in)	Location	Remarks
45	S13	0.0005	Strain	0.125 in.	Beam 1 at 1/4 of the infill width from column 1, top reinf. bar.	
46	S14	0.0005	Strain	0.125 in.	Beam 1 at 1/2 of the infill width from column 1, top reinf. bar.	
47	S15	0.0005	Strain	0.125 in.	Beam 1 at 3/4 of the infill width from column 1, top reinf. bar.	
48	S16	0.0005	Strain	0.125 in.	Beam 2 at 1/4 of the infill width from column 2, top reinf. bar.	
49	S17	0.0005	Strain	0.125 in.	Beam 2 at 1/2 of the infill width from column 2, top reinf. bar.	
50	S18	0.0005	Strain	0.125 in.	Beam 2 at 3/4 of the infill width from column 2, top reinf. bar.	

Infill Rosette Strain Gages

51	SP1V	0.0005	Strain Rosette, vert.	30 mm	Center of the infill, vertical Rosette	
52	SP1D	0.0005	Strain Rosette, dia	30 mm	Center of the infill, diagonal Rosette	
53	SP1H	0.0005	Strain Rosette horiz.	30 mm	Center of the infill, horizontal Rosette	
54	SP2V	0.0005	Strain Rosette, vert.	30 mm	Center of the infill, vertical Rosette	
55	SP2D	0.0005	Strain Rosette, dia	30 mm	Center of the infill, diagonal Rosette	
56	SP2H	0.0005	Strain Rosette horiz.	30 mm	Center of the infill, horizontal Rosette	

Joint Rosette Strain Gages

57	SP3V	0.0005	Strain Rosette, vert.	30 mm	Center of joint 1, vertical rosette	
58	SP3D	0.0005	Strain Rosette, dia	30 mm	Center of joint 1, diagonal rosette	
59	SP3H	0.0005	Strain Rosette horiz.	30 mm	Center of joint 1, horizontal rosette	
60	SP4V	0.0005	Strain Rosette, vert.	30 mm	Center of joint 2, vertical rosette	
61	SP4D	0.0005	Strain Rosette, dia	30 mm	Center of joint 2, diagonal rosette	
62	SP4H	0.0005	Strain Rosette horiz.	30 mm	Center of joint 2, horizontal rosette	
63	SP5V	0.0005	Strain Rosette, vert.	30 mm	Center of joint 3, vertical rosette	
64	SP5D	0.0005	Strain Rosette, dia	30 mm	Center of joint 3, diagonal rosette	
65	SP5H	0.0005	Strain Rosette horiz.	30 mm	Center of joint 3, horizontal rosette	

Table IX

Instrumentation Plan for Model 5, Three-Bay Brick Infilled R/C Frame (Tested on 4/27/1998)

Chan. No.	Sensor No.	Scale Factor	Type	Gage Length (in.)	Location	Remarks
73	L4	N/A	Load cell	N/A		
74	S4	N/A	Stroke	N/A		
			LVDTs for Rotation			
1	R1	0.0200 in/V	LVDT	Along 3 in.	Bottom of column 1 (windward), windward face	
2	R2	0.0198	LVDT	Along 3 in.	Bottom of column 1 (windward), leeward face	
3	R3	0.0199	LVDT	Along 3 in.	Bottom of column 2, windward face	
4	R4	0.0199	LVDT	Along 3 in.	Bottom of column 2, leeward face	
5	R5	0.0200	LVDT	Along 3 in.	Bottom of column 3, windward face	
6	R6	0.0200	LVDT	Along 3 in.	Bottom of column 3, leeward face	
7	R7	0.0199	LVDT	Along 3 in.	Bottom of column 4, windward face	
8	R8	0.0199	LVDT	Along 3 in.	Bottom of column 4, leeward face	
9	R9	0.0248	LVDT	Along 3 in.	Top of column 1 (windward), windward face	
10	R10	0.0244	LVDT	Along 3 in.	Top of column 1 (windward), leeward face	
11	R11	0.0247	LVDT	Along 3 in.	Top of column 2, windward face	
12	R12	0.0253	LVDT	Along 3 in.	Top of column 2, leeward face	
13	R13	0.0250	LVDT	Along 3 in.	Top of column 3, windward face	
14	R14	0.0245	LVDT	Along 3 in.	Top of column 3, leeward face	
15	R15	0.0244	LVDT	Along 3 in.	Top of column 4, windward face	
16	R16	0.0245	LVDT	Along 3 in.	Top of column 4, leeward face	
			LVDT for Gap Width			
17	R17	0.0248 in/V	LVDT		Column 2 at 3/4 height of infill	To measure gap b/ infill and column (R18 was not used)
18	R19	0.0243	LVDT		Column 4 at 3/4 height of infill	To measure gap b/ infill and column
19	R20	0.0246	LVDT		Beam 1 at 3/4 the infill width from column 1	To measure gap b/ infill and beam
20	R21	0.0244	LVDT		Beam 2 at 3/4 the infill width from column 2	To measure gap b/ infill and beam
21	R22	0.0248	LVDT		Beam 3 at 3/4 the infill width from column 3	To measure gap b/ infill and beam

Table IX (Continued)

Instrumentation Plan for Model 5, Three-Bay Brick Infilled R/C Frame (Tested on 4/27/1998)

Diagonal LVDT

Chan. No.	Sensor No.	Scale Factor	Type	Gage Length (in.)	Location	Remarks
22	Dia 1	-0.0998 in/V	LVDT	Along 77 in.	Infill, diagonal from upper windward to lower leeward corners, infill 1	Dia2 was not used
23	Dia 3	-0.0998	LVDT	Along 77 in.	Infill, diagonal from upper windward to lower leeward corners, infill 2	Dia2 was not used
24	Dia 5	-0.0995	LVDT	Along 77 in.	Infill, diagonal from upper windward to lower leeward corners, infill 3	Dia2 was not used

Displacement Gages

25	D00	0.9956 in/V	Displacement gage	N/A	Base beam	
26	D11	2.0090	Displacement gage	N/A	Center of top beam 1	
27	D12	1.9655	Displacement gage	N/A	Top of the infill 1	
28	D13	0.9993	Displacement gage	N/A	Center of the infill 1	
29	D21	2.0499	Displacement gage	N/A	Center of top beam 2	
30	D22	2.0014	Displacement gage	N/A	Top of the infill 2	
31	D23	0.9949	Displacement gage	N/A	Center of the infill 2	
32	D31	1.9772	Displacement gage	N/A	Center of top beam 3	
33	D32	1.9848	Displacement gage	N/A	Top of the infill 3	
34	D33	2.0050	Displacement gage	N/A	Center of the infill 3	
35	D40	0.9944	Displacement gage	N/A	Top center of the reaction frame	

Column Reinforcement Strain Gages

43	S8	0.0005	Strain	0.125 in.	Bottom of column 1, windward reinforcement bar	7 in. from the base of the column
42	S7	0.0005	Strain	0.125 in.	Bottom of column 1, leeward reinforcement bar	7 in. from the base of the column
41	S6	0.0005	Strain	0.125 in.	Bottom of column 2, windward reinforcement bar	7 in. from the base of the column
40	S5	0.0005	Strain	0.125 in.	Bottom of column 2, leeward reinforcement bar	7 in. from the base of the column
39	S4	0.0005	Strain	0.125 in.	Bottom of column 3, windward reinforcement bar	7 in. from the base of the column
38	S3	0.0005	Strain	0.125 in.	Bottom of column 3, leeward reinforcement bar	7 in. from the base of the column
37	S2	0.0005	Strain	0.125 in.	Bottom of column 4 (leeward), windward reinforcement bar	7 in. from the base of the column
36	S1	0.0005	Strain	0.125 in.	Bottom of column 4 (leeward), leeward reinforcement bar	7 in. from the base of the column

Table IX (Continued)

Instrumentation Plan for Model 5, Three-Bay Brick Infilled R/C Frame (Tested on 4/27/1998)

Column Reinforcement Strain Gages

Chan. No.	Sensor No.	Scale Factor	Type	Gage Length (in.)	Location	Remarks
51	S16	0.0005	Strain	0.125 in.	Top of column 1, windward reinforcement bar	3 in. from the bottom face of of the beam
50	S15	0.0005	Strain	0.125 in.	Top of column 1, leeward reinforcement bar	3 in. from the bottom face of of the beam
49	S14	0.0005	Strain	0.125 in.	Top of column 2, windward reinforcement bar	3 in. from the bottom face of of the beam
48	S13	0.0005	Strain	0.125 in.	Top of column 2, leeward reinforcement bar	3 in. from the bottom face of of the beam
47	S12	0.0005	Strain	0.125 in.	Top of column 3, windward reinforcement bar	3 in. from the bottom face of of the beam
45	S10	0.0005	Strain	0.125 in.	Top of column 4 (leeward), leeward reinforcement bar	3 in. from the bottom face of of the beam (S11 is bad Gage)
44	S9	0.0005	Strain	0.125 in.	Top of column 4 (leeward), leeward reinforcement bar	3 in. from the bottom face of of the beam

Beam Reinforcemet Strain Gages

60	S25	0.0005	Strain	0.125 in.	beam 1 at 1/4 the infill width from column 2, top reinf. bar	
59	S24	0.0005	Strain	0.125 in.	Beam 1 at 1/2 the infill width from column 1, top reinf. bar	
58	S23	0.0005	Strain	0.125 in.	Beam 1 at 3/4 the infill width from column 1, top reinf. bar	
57	S22	0.0005	Strain	0.125 in.	Beam 2 at 1/4 of the infill width from column 2, top reinf. bar.	
56	S21	0.0005	Strain	0.125 in.	Beam 2 at 1/2 of the infill width from column 2, top reinf. bar.	
55	S20	0.0005	Strain	0.125 in.	Beam 2 at 3/4 of the infill width from column 2, top reinf. bar.	S19 is a bad gage
53	S18	0.0005	Strain	0.125 in.	Beam 3 at 1/2 of the infill width from column 3, top reinf. bar.	
52	S17	0.0005	Strain	0.125 in.	Beam 3 at 3/4 of the infill width from column 3, top reinf. bar.	

Infill Rosette Strain Gages

67	SP3V	0.0005	Strain Rosette, vert.	30 mm	Center of infill 1, vertical rosette windward infill	
68	SP3D	0.0005	Strain Rosette, dia.	30 mm	Center of infill 1, diagonal rosette windward infill	
69	SP3H	0.0005	Strain Rosette horiz.	30 mm	Center of infill 1, horizontal rosette windward infill	
64	SP2V	0.0005	Strain Rosette, vert.	30 mm	Center of infill 2, vertical rosette	
65	SP2D	0.0005	Strain Rosette, dia	30 mm	Center of infill 2, diagonal rosette	
66	SP2H	0.0005	Strain Rosette horiz.	30 mm	Center of infill 2, horizontal rosette	

Table IX (Continued)

Instrumentation Plan for Model 5, Three-Bay Brick Infilled R/C Frame
(Tested on 4/27/1998)

Infill Rosette Strain Gages (Cont.)

Chan. No.	Sensor No.	Scale Factor	Type	Gage Length (in.)	Location	Remarks
61	SP1V	0.0005	Strain Rosette, vert.	30 mm	Center of infill 3, vertical rosette leeward infill	
62	SP1D	0.0005	Strain Rosette, dia	30 mm	Center of infill 3, diagonal rosette leeward infill	
63	SP1H	0.0005	Strain Rosette horiz.	30 mm	Center of infill 3, horizontal rosette leeward infill	

Embedded Strain Gages

70	Se1	0.0005	Strain	30 mm	Beam 3 at 1/4 of the infill width from column 3, top reinf. bar.	
71	Se2	0.0005	Strain	30 mm	Beam 2 at 1/4 of the infill width from column 2, top reinf. bar.	

3.5.3 Absolute Displacement Transducers

Celesco Model PT101-10 and PT101-60A variable resistance displacement transducers were used to measure the absolute displacement at various locations on the test wall. These units employ a spring-loaded precision rotary potentiometer with a flexible steel cable wrapped around the potentiometer shaft. The other end of the cable is attached to the point where the displacement is to be measured. When displacement occurs, the cable motion rotates the shaft of the potentiometer, causing a change in resistance. These transducers were mounted on a steel reference frame affixed to the load floor, but independent of the test wall or the loading fixture. The transducer sensing elements were attached to the wall using standard steel extension wires. These transducers were connected to Endevco Model 4471.3 signal conditioners, which provide DC power and electrical balancing but no amplification.

3.5.4 Data Acquisition and Test Control

Figure 3.6 is a functional block diagram of the instrumentation, data acquisition, and test control systems. All of the transducer output signals were connected to a Hewlett Packard Model 3052A data logging system. The system was controlled by a personal computer through an instrument controller interface buss. The record channels were scanned at a predetermined sampling rate, and the data were recorded as ASCII text files on the personal computer.

The loading system consisted of two CGS/Lawerence Model 307-50 electro-hydraulic actuators controlled by closed-loop servo controllers and a function generator. The actuators were operated in a displacement control mode. In this mode, the function generator supplies a

slowly changing command signal to the controllers. The controllers send a drive signal to each of the actuators, which causes them to move until the displacement measured by LVDTs located inside each actuator is equal to the command signal. The actuators also include load transducers that measure the applied load.

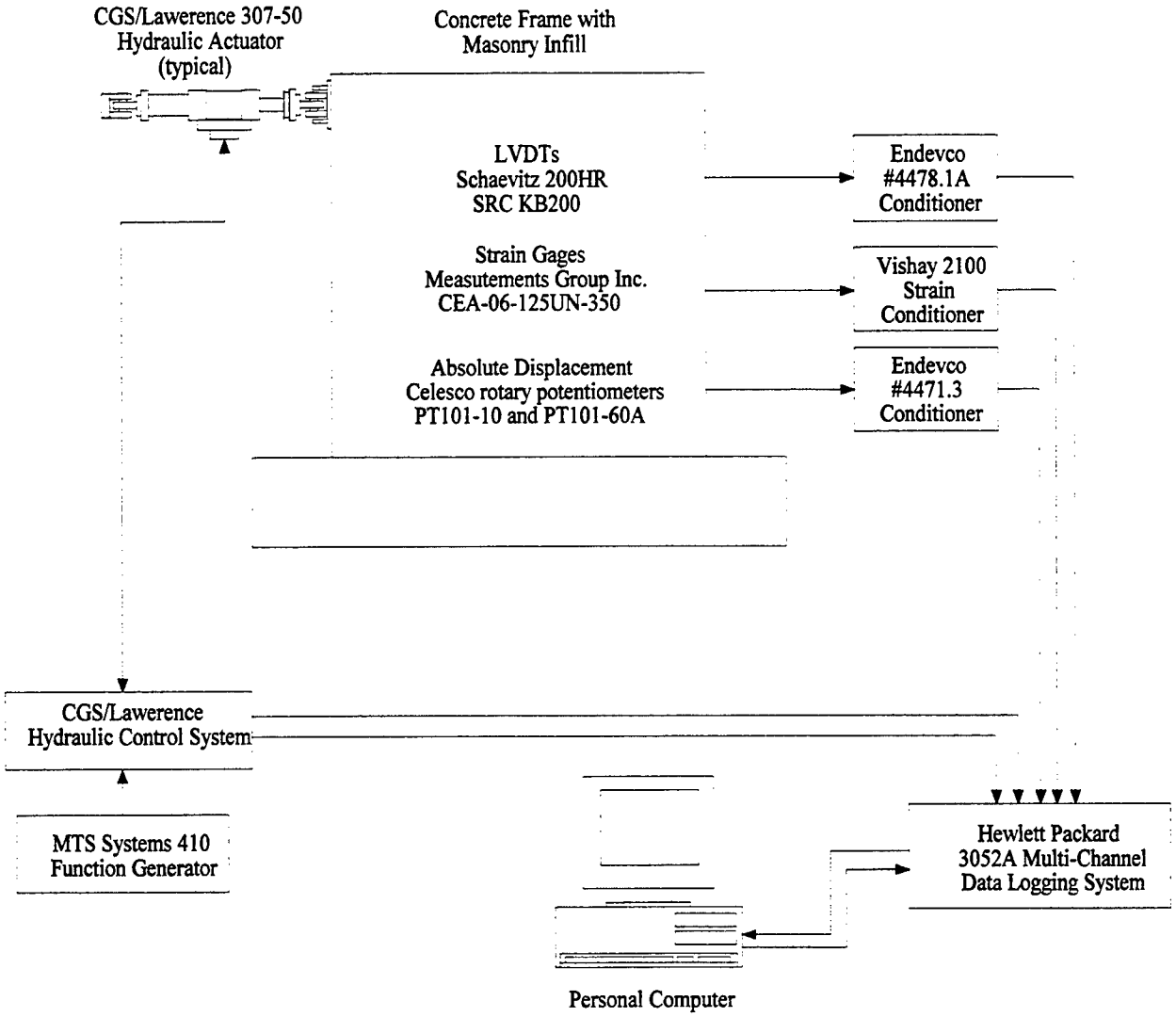

Figure 3.6 Functional Block Diagram of Instrumentation, Data Acquisition, and Test Control Systems

3.6 Material Test Report

3.6.1 Concrete Tests

Concrete tests were performed for each batch of concrete poured. Both of the single-bay frames were poured using the same batch of concrete, and each of the triple-bay frames was poured with separate batches of concrete. All of the cylinders and beams were made according to ASTM specifications and were cured with moistened burlap and plastic placed over the top.

3.6.1.1 Compressive Strength Test

Compressive tests were performed according to the ASTM C39-94. The cylinders for the single-bay frames were tested on the 52nd day of curing, which was within five days of the lateral load tests. The average from this batch of concrete was taken from tests on six cylinders. Compression tests for the concrete pours of the triple-bay specimen were performed on approximately the 28th and 33rd day of curing, and on the day the specimen was tested. The average strength from three cylinders was taken for each series of tests. The cone and cone-and-split failure patterns were typical of most of the cylinders tested. A summary of concrete compressive strength is shown in Table X.

3.6.1.2 Compressive Strain at Failure

Standard compression tests were performed on one cylinder from each batch of concrete with strain gages attached to the cylinder surfaces. The stress-strain curves are shown in Figure 3.7. Two 2 in. strain gages were attached to the outside surfaces at the mid-height of the cylinder

sides. One gage was positioned to measure strain about the circumference and the other to measure axial strain. The compression strains at failure were taken from the axial strain gages only, and data about the circumference were not used as they were not directly applicable. A summary of strain at failure is shown in Table XI.

Table X

Concrete Compressive Strength

Batch	Age at Time of Testing (days)	Average Compressive Strength (psi)
Single-bay bare frame	49	5548
Single-bay infilled frames	52	6195
Double-bay frames with CMU infill	33	5478
Double-bay frames with CMU infill	132	5701
Triple-bay frames with brick infill	28	4943
Triple-bay frames with brick infill	332	5585

Table XI

Concrete Compressive Strain at Failure

Batch	Age at Time of Testing (days)	Poisson's Ratio	Modulus of Elasticity (Ksi)	Compressive Strain at Failure
Single-bay frames	129	0.217	4621	0.0026
Double-bay frames with CMU infill	33	0.195	4303	0.0034
Triple-bay frames with brick infill	28	0.208	4165	0.0028

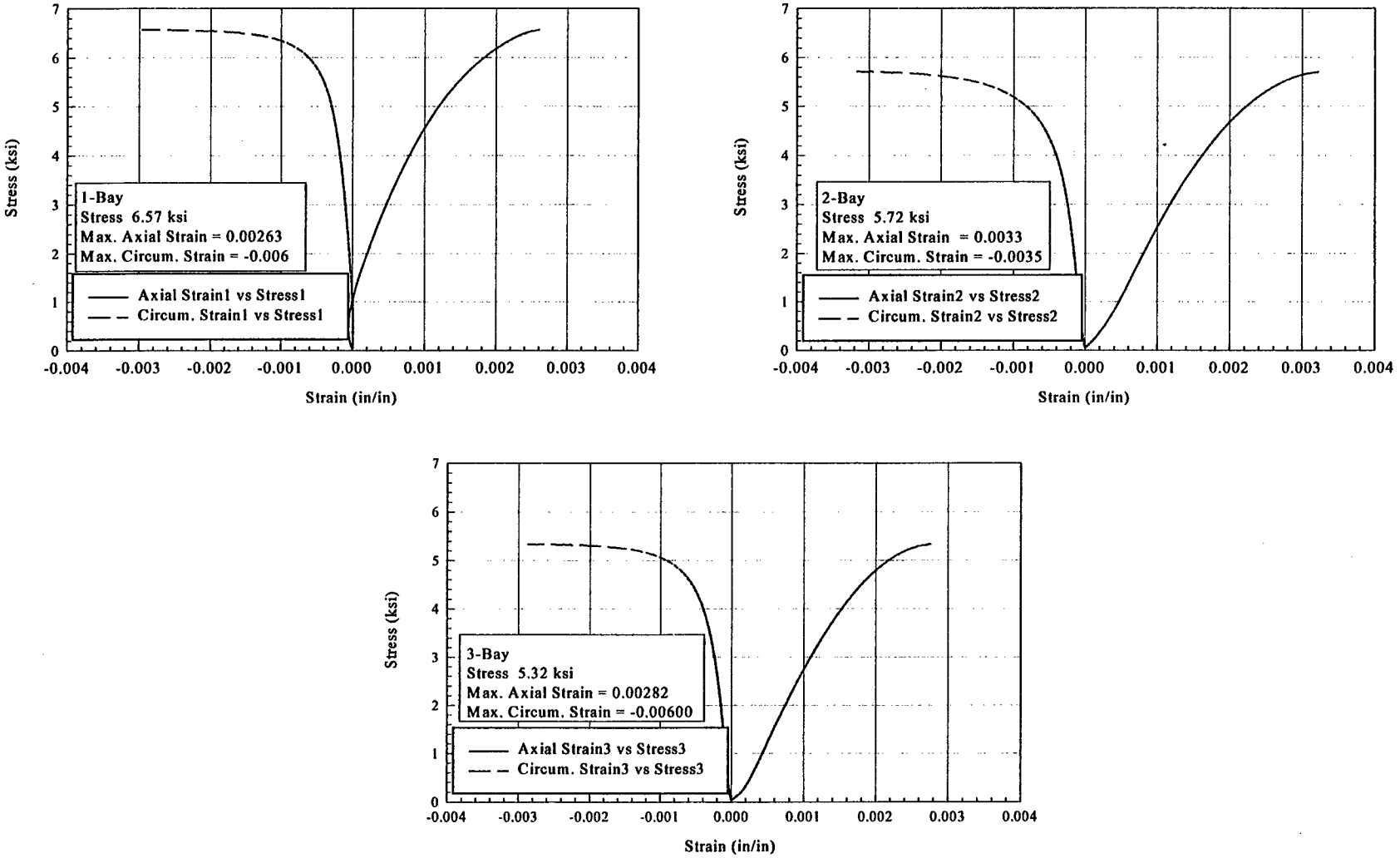

Figure 3.7 Concrete Cylinder Test – 1-Bay (upper left), 2-Bay (upper right), 3-Bay (lower)

3.6.1.3 Split Cylinder Test

Split cylinder tests were performed according to the ASTM C496-96. The average from three cylinders was used for each series

of tests. The typical splitting failure pattern was observed for all of the specimens tested. A summary of the split cylinder test results is shown in Table XII.

Table XII

Split Cylinder Test.

Batch	Age at Time of Testing (days)	Average Splitting Tensile Strength (psi)
Single-bay frames	130	492
Double-bay frames With CMU infill	34	421
Triple-bay frames With brick infill	29	398

3.6.1.4 Flexural Strength

The flexural strength for each batch of concrete was determined from third-point bend tests performed on simple beams according to the ASTM C78-94. All specimens tested failed within the center third of the beams. A summary of concrete flexural strength results is shown in Table XIII.

Table XIII

Flexural Strength of Concrete.

Batch	Age at Time of Testing (days)	Average Rupture Strength (psi)
Single-Bay Frames	130	1187
Double-Bay Frames With CMU infills	34	648
Triple-Bay Frames With brick infills	29	735

3.6.2 Masonry Tests

3.6.2.1 Compressive Strength of Concrete Masonry Units and Brick

The compressive strength tests of the CMU and clay brick were performed according to the ASTM C140 and the ASTM C67, respectively. Since the CMU and bricks contained hollow sections, compressive strengths were calculated both for the gross and net cross sections. The net cross-sectional areas were taken from averages of the specimens tested. Due to difficulties in the capping procedures some of the test specimens were unevenly loaded, which caused their compressive strengths to be significantly lower. These low values were disregarded, thus averaging the compressive strengths. A summary of the CMU and clay brick units' compressive strength is shown in Table XIV.

Table XIV

Compressive Strength of Concrete Masonry Units and Brick

Masonry Type	Gross Compressive Strength (psi)	Net Compressive Strength (psi)
Concrete masonry units, single and double-bay infills	1872	2505
Clay brick, single-bay infills	11,743	14,791
Clay brick, triple-bay infills	12,368	15,202

3.6.2.2 Compressive Strength of Mortar

The compressive strength tests of mortar cubes were performed according to ASTM C109. Several different batches of mortar were used in laying the masonry, and Figure 3.8 shows approximately where each batch was used in the triple-bay infills. A summary of the mortar compressive strength tests is shown in Table XV.

Table XV

Mortar Compressive Strength

Batch, (infills)		Age at Time of Testing (days)	Compressive Strength (psi)
Single-bay frames with CMU infill		31	962
Single-bay frames with brick infill		29	1058
Double-bay frames with CMU infill	1 and 2	33	1248
Triple-bay frames with brick infill	1	30	1438
	2	31	1619
	3	32	1539
	Average*	- -	1532

* Average values were used for the analytical models

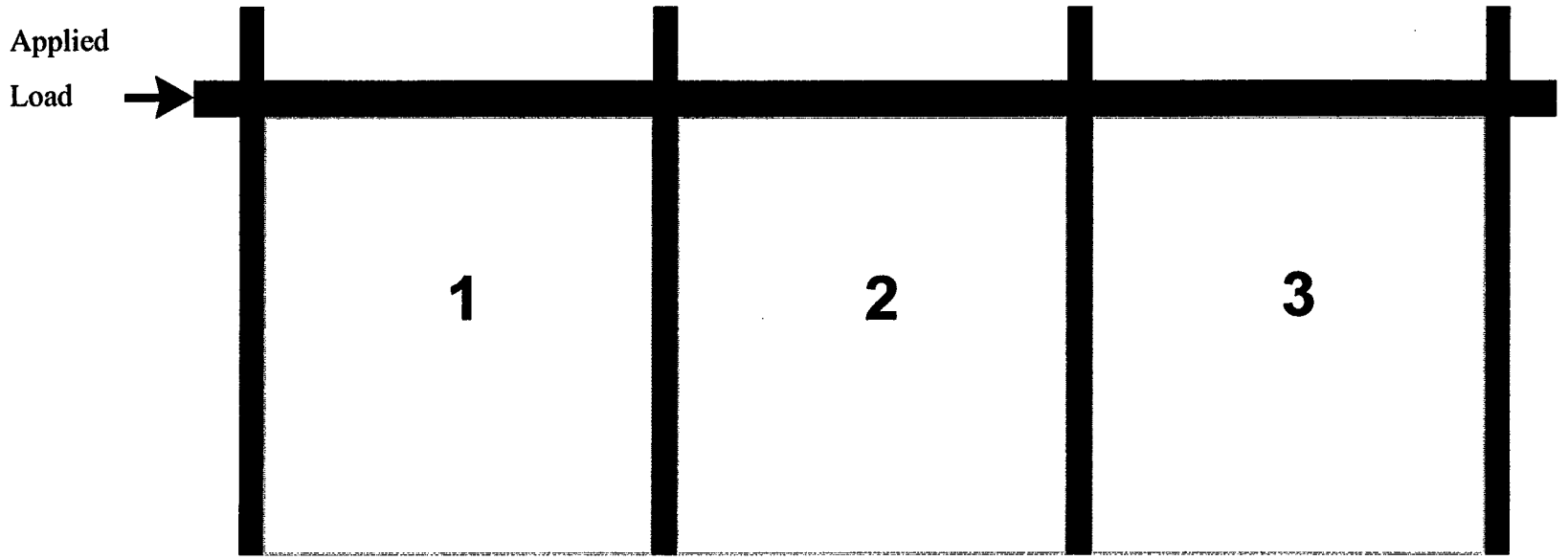

Figure 3.8 Infill Labels with Respect to the Applied Load

3.6.2.3 Compressive Strength of Masonry Prisms

Prism samples were constructed as shown in Figure 3.9. Compressive strength tests for prism samples were performed according to ASTM E447-84. Due to problems in capping as noted previously, not all of the prisms were uniformly loaded. The affected data were not used. Three prisms were tested for each of the single-bay infills. The same dimensions used in the compressive tests on the brick and masonry units were used to calculate the gross and net compressive strengths of the prisms. The nature of failures in the concrete masonry prisms varied greatly with splits or cone shapes within the units, or with crushing of the mortar. The mortar between the clay bricks typically initiated failure, turning into a powder like substance upon crushing. A summary of prism test results is shown in Table XVI.

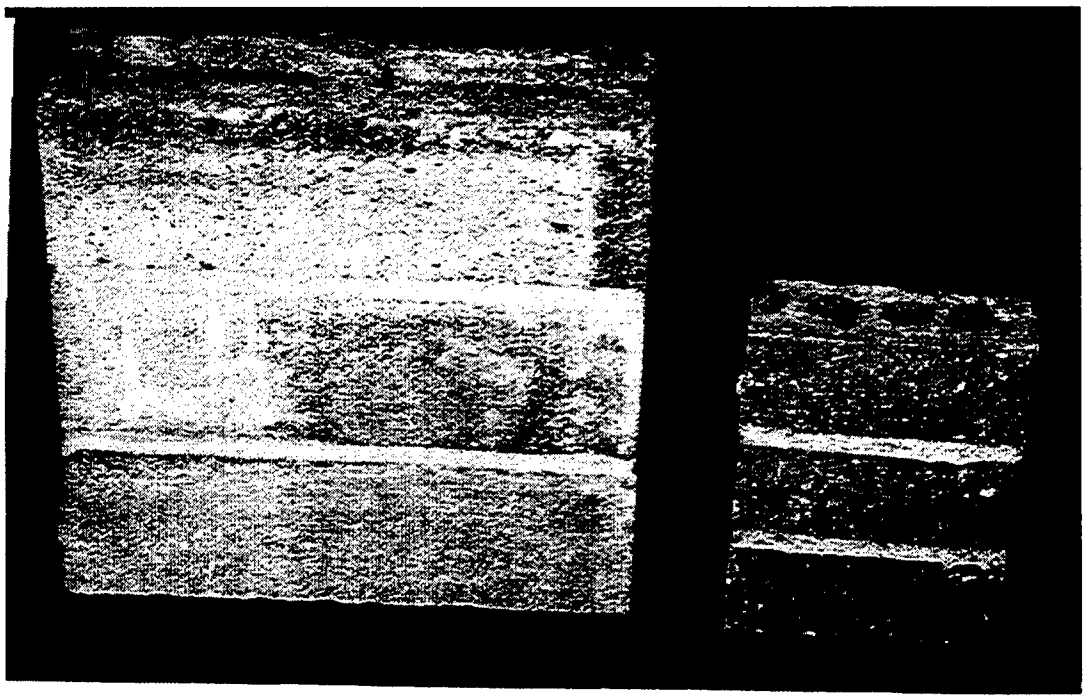

Figure 3.9 Typical Prism Samples

Table XVI

Prism Test Results

Prism Type	Age at Time of Testing (days)	Gross Compressive Strength (psi)	Net Compressive Strength (psi)
Concrete masonry prisms, single-bay infill	26	2409	3224
Clay brick prisms, single-bay infill	25	2697	3387
Concrete masonry prisms, double-bay infill	29	1525	2041
Clay brick prisms, triple-bay infill	31	3555	4369

3.5.2.4 Raking Test

Diagonal tension testing of the CMU masonry sample was conducted per ATTM E 519-81 on 24 in. x 24 in. sample. Shear stress of 0.225 ksi was calculated based on an effective thickness of 2.71 in. and net area 65.04 in^2 and load of failure 20.71 kips as obtained from the laboratory test.

3.6.3 Steel Reinforcement Tests

Steel reinforcement #3 Grade 40 bars were tested according to ASTM A615-95b both by the steel supplier and USACERL. The steel satisfied the chemical requirements, the minimum yield and tensile strengths, and the minimum percent elongation. Tests were performed to confirm the information given by the steel supplier and to find the elastic modulus of the steel. Tests were conducted on five bars according to ASTM A615-95b and ASTM E8-95a using a 1

in. extensometer to measure strains. Since a sharply defined yield point was not apparent, a 0.02% offset was used to determine the yield strength. The values obtained by USACERL were used to evaluate the performance of the infill frames. A summary of the steel properties is listed in Table XVII. Stress vs. strain curves for bar reinforcements are shown in Figure 3.10.

Table XVII

Steel bars properties.

Test of #3 Steel Reinforcement	Elastic Modulus (ksi)	Yield Strength (ksi)	Tensile Strength (ksi)
Certified material test report from steel supplier	29,000	63.6*	90
Tests performed by USA-CERL	28,300 ± 2,900	49.1 ± 0.5	79.0 ± 0.1

* Before annealing process used to reduce the strength.

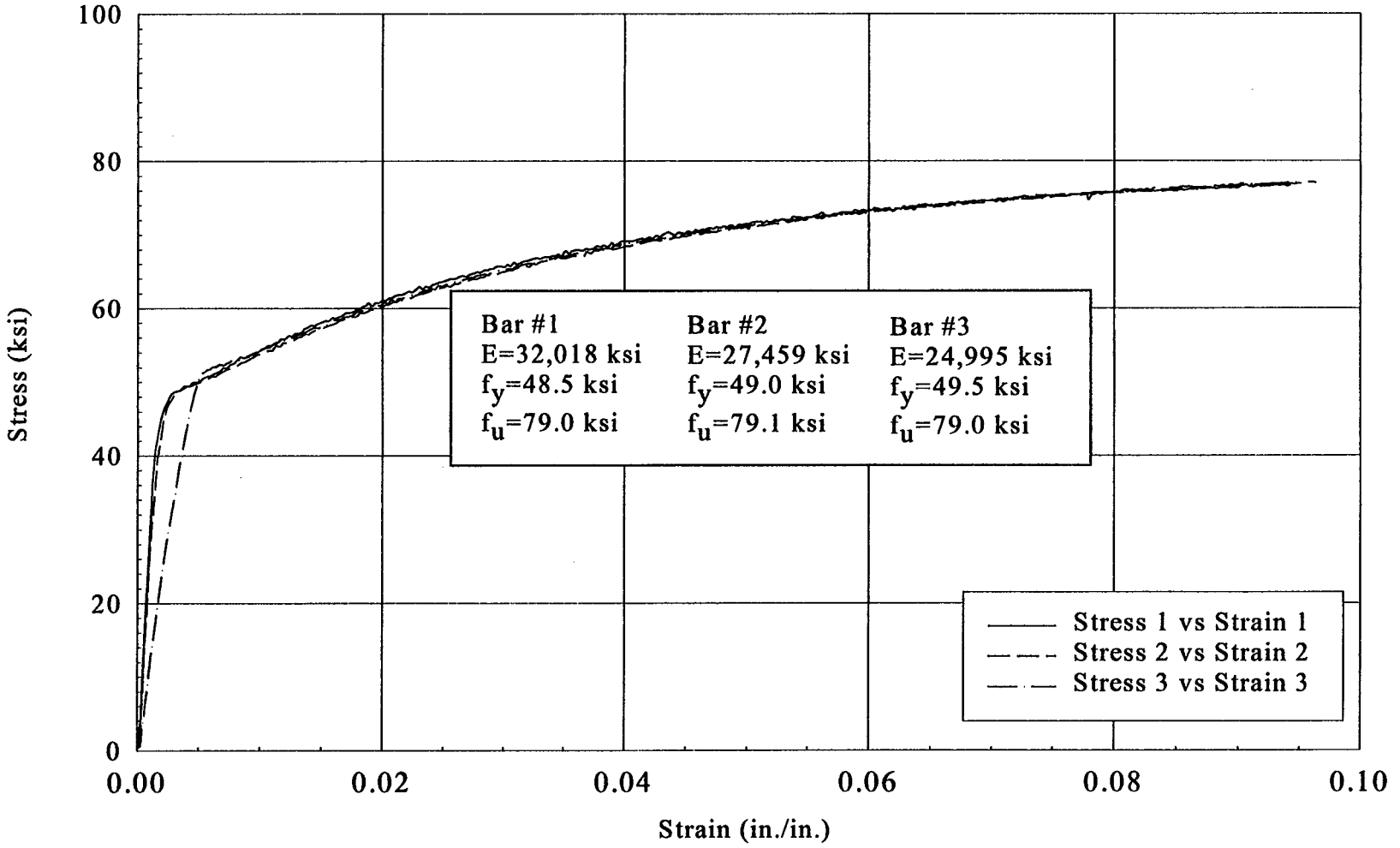

Figure 3.10 Stress vs. Strain - Tensile Test of #3 Bar Reinforcement

CHAPTER 4

ANALYTICAL IDEALIZATION

4.1 Introduction

Over the past 50 years, the following simplified analytical methods have been proposed by several researchers. These models were based on experimental study of structural frames of steel or concrete infilled with masonry brick or CMU. Each method was generated to satisfy specific variables and parameters, and may not to be applicable to the models under consideration. Their applicability to these models will be examined and presented in Chapter 7.

4.2 Holmes Method

Holmes (1961) considers the forces that cause failure in the frame and infill separately [23]. The horizontal load that causes failure is equal to the sum of the contributions from the frame and the infill, respectively:

$$H = \frac{24EI_c e'_c d}{h^3\left(1+\frac{I_c}{I_b}\cot\theta\right)\cos\theta} + Af_c\cos\alpha$$

where the contribution of the frame should be limited to $\frac{4M_p}{h}$, where M_p is the lesser of M_p^c and M_p^b.

The deflection at failure is equal to:

$$S_H = e'_c d\cos\theta$$

The lateral stiffness of the infilled frame is:

$$K = \frac{H}{S_H}$$

where:

H	=	height of steel frame
D	=	diagonal of steel frame
T	=	thickness of infill
E	=	modulus of elasticity of columns
I_b	=	moment of inertia of beams
I_c	=	moment of inertia of columns
F_c	=	compressive strength of infill
e'_c	=	strain in infill at failure
A	=	cross-sectional area of equivalent strut, *td/3*
θ	=	angle of the diagonal from horizontal
M_p^b	=	fully plastic moment of beam
M_p^c	=	fully plastic moment of column

4.3 Smith Method 1

Smith (1962) determined that once the effective width was determined, an equivalent area for the strut could be calculated by multiplying the thickness of the infill by the width [49]. The equivalent strut could then be used in a frame analysis, and the stiffness computed.

$$A_s = wt$$

The effective width w was determined empirically. With the aspect ratio, the value of w/d, which is the width over the diagonal length, can be obtained from a graph provided by Smith, or from the following equation:

$$\frac{w}{d} = -0.0914 \ln\left(\frac{l}{h'}\right) + 0.2314 \quad \text{from which } w \text{ can be solved}$$

where l and h' are the length and height of the infill, respectively.

The equivalent strut and frame properties are then used to determine the lateral stiffness of a single-story frame directly, without analysis. Factors in calculating the lateral stiffness include the angle of the diagonal to the horizontal, the effective width of the diagonal, the elastic modulus of the infill and frame, the thickness of the infill, the height of the column, the length of the beam, and the cross-sectional areas and second moments of frame members. The lateral stiffness is defined as:

$$K = \frac{A + B + C}{C(A + B)}$$

where:

$$A = \frac{h \tan^2 \theta}{A_c E_f}$$

is the strain energy from tension in the windward column,

$$B = \frac{d}{A_s E_i \cos^2 \theta}$$

is the strain energy from compression of the equivalent strut, and

$$C = \frac{h^3 (3 I_b h + 2 I_c L)}{12 E_f I_c (6 I_b h + I_c L)}$$

is the strain energy from bending of the frame.

The variables in the above equations are defined as:

h' = height of infill

h = height of columns

θ = angle of diagonal from horizontal

A_c = cross sectional area of column

d = diagonal length of infill panel

A_s = equivalent strut area of infill panel

E_I = elastic modulus of infill material

E_f = elastic modulus of frame material

I_c = moment of inertia of column

I_b = moment of inertia of beam

l = length of infill

4.4 Smith Method 2

In this investigation, the length of contact between the infill and the surrounding frame is studied and a parameter is developed to determine this contact length [10, 50, 51]. The parameter is then used to determine the width of the equivalent strut. The parameter λ developed is a measure of the relative stiffness between the frame and infill. The parameter λh is calculated as:

$$\lambda h = h \sqrt[4]{\frac{E_c t \sin 2\theta}{4EIh'}}$$

where:

λ = relative stiffness parameter of infill and frame; a higher value of λh denotes a more flexible frame

h = height of frame, column center-to-center (inch)

E_c = Young's modulus of infill (ksi)

E = Young's modulus of frame (ksi)

I = moment of inertia of columns (in^4)

t = infill thickness (inch)

h' = height of infill (inch)

θ = angle of diagonal from horizontal

The aspect ratio and λh can be used to determine the value for w/d, for which w can be solved for. The value for w/d can also be determined by the following equation for an aspect ratio of 1.38.

$$\frac{w}{d} = 0.0005\lambda h^2 - 0.0143\lambda h + 0.2534 \qquad \text{if} \quad \lambda h \le 13.0$$

$$\text{otherwise} \qquad \frac{w}{d} = -0.0013\lambda h + 0.167$$

Smith uses a relationship based on a *beam on elastic foundation* formulation to derive the following relationship for the contact length between the frame and the infill:

$$\alpha = \frac{\pi}{2\lambda}$$

where:

α = length of contact between the frame and infill

4.5 Mainstone Method

Mainstone's (1971) analysis defined three different areas of each test [35]. Equations for the stiffness prior to cracking, the first cracking strength, and the crushing strength of the infill were developed. The relative stiffness of the infills to the columns was found to be most significant, and was evaluated as:

$$\lambda_h h = h \sqrt[4]{\frac{E' t \sin 2\theta}{4EI_h h'}} \qquad \text{(Smith's Equation)}$$

where:

$\lambda_h h$ = relative stiffness parameter of infill and columns

E' = Young's modulus of infill calculated as $400f'c\ MN/m^2$

h = height of frame

h' = height of infill

EI_h = flexural rigidities of columns

θ = angle of the diagonal from horizontal

t = thickness of infill

Several plots were made of the ratio of equivalent strut widths versus the relative stiffness parameters. From these plots, the width of the equivalent struts could be related to the relative stiffness parameter as Smith had done. Equations related to brickwork for values of $\lambda_h h$ from 4 to 5 are:

$$w'_{eK}/_{w'} = 0.175(\lambda_h h)^{-0.4} \quad \text{stiffness prior to cracking}$$

$$w'_{et}/_{w'} = 0.17(\lambda_h h)^{-0.4} \quad \text{crushing strength of infill}$$

$$w'_{ec}/_{w'} = 0.56(\lambda_h h)^{-0.875} \quad \text{first cracking strength of infill}$$

for values of larger than 5, the plots were approximated as:

$$w'_{eK}/_{w'} = 0.16(\lambda_h h)^{-0.3} \quad \text{stiffness prior to cracking}$$

$$w'_{et}/_{w'} = 0.15(\lambda_h h)^{-0.3} \quad \text{crushing strength of infill}$$

$$w'_{ec}/_{w'} = 0.52(\lambda_h h)^{-0.8} \quad \text{first cracking strength of infill}$$

where:

suffix K = mean stiffness prior to cracking

suffix c = crushing strength of infill

suffix t = first cracking strength of infill

w' = characteristic width of infill, equal to $d'\sin 2\theta$

d' = the diagonal length of infill

In using the equivalent-strut analogy, better estimates of the strength and stiffness were obtained than when using the interaction equation. However, the relationships between the relative stiffnesses and equivalent-strut width were solely dependent on the specimens tested, so it is not surprising that the estimate and the test values were always similar. The lateral crushing strength or cracking strength can be determined with the following relationships:

$$H = H_F + H_I$$

where:

$$H_I = R'_c \cos\theta$$

or

$$H_I = R'_t \cos\theta$$

depending on crushing or cracking, respectively,

where:

$$R'_c = w'_{ec} f'_c t$$

or

$$R'_t = w'_{et} f'_c t$$

depending on crushing or cracking, respectively.

where:

H_I = nominal horizontal racking strength of infill

H_F = nominal horizontal racking strength of frame, obtained from conventional methods

R'_c = nominal diagonal crushing load of infill

R'_t = nominal diagonal cracking load of infill

The effective widths of the diagonal strut for the different failure modes were determined as a ratio to the characteristic width w':

$$w'_{eK}/w' = K'_R/E't\sin 2\theta$$

from which the stiffness before cracking, K'_R, can be solved for.

4.6 Lefter and Colville Method

The equation for lateral stiffness is fairly straightforward in itself, but obtaining the variables requires additional calculations [30]. The transformed moment of inertia and transformed area of the wall must be calculated. This is accomplished by taking the ratio of the elastic moduli of the frame and infill. The ratio is used to obtain the wall thickness as equivalent concrete, or the column thickness as equivalent infill, depending on the ratio calculated. Inertia and area calculations are then made with the equivalent dimensions.

The lateral in-plane stiffnesses of masonry-infilled concrete frames in an uncracked condition were computed by:

$$K = \frac{1}{\frac{h^3}{12EI_t} + \frac{1.2h_w}{A_w G_w}}$$

where:

h = distance to mid-height of beam
h_w = height of infill wall
E = modulus of elasticity of concrete
I_t = transformed moment of inertia of the frame-wall system
A_w = transformed area of wall
G_w = modulus of rigidity of wall material

4.7 Liauw and Kwan Method

Liauw and Kwan (1982) used a nonlinear finite element analysis along with plastic theory to arrive at their equation [32]. Their analysis gives the possibility of three different failure modes. The modes are (1) corner crushing with failure in the columns, (2) corner crushing with failure in the beams, and (3) diagonal crushing (see Figure 4.1). The in-plane strength for each failure mode is as follows:

Mode 1:
$$H_u = \sigma_c th \sqrt{\frac{2(M_{pj} + M_{pc})}{\sigma_c th^2}}$$

Mode 2:
$$H_u = \frac{\sigma_c th}{\tan\theta} \sqrt{\frac{2(M_{pj} + M_{pb})}{\sigma_c th^2}}$$

Mode 3:
$$H_u = \frac{4M_{pj}}{h} + \frac{\sigma_c th}{6}$$

where:

H	=	Story height
T	=	Infill thickness
M_{pb}	=	Plastic moment of beam
M_{pc}	=	Plastic moment of column
M_{pj}	=	the smaller of M_{pb} and M_{pc}
σ_c	=	Crushing strength of panel

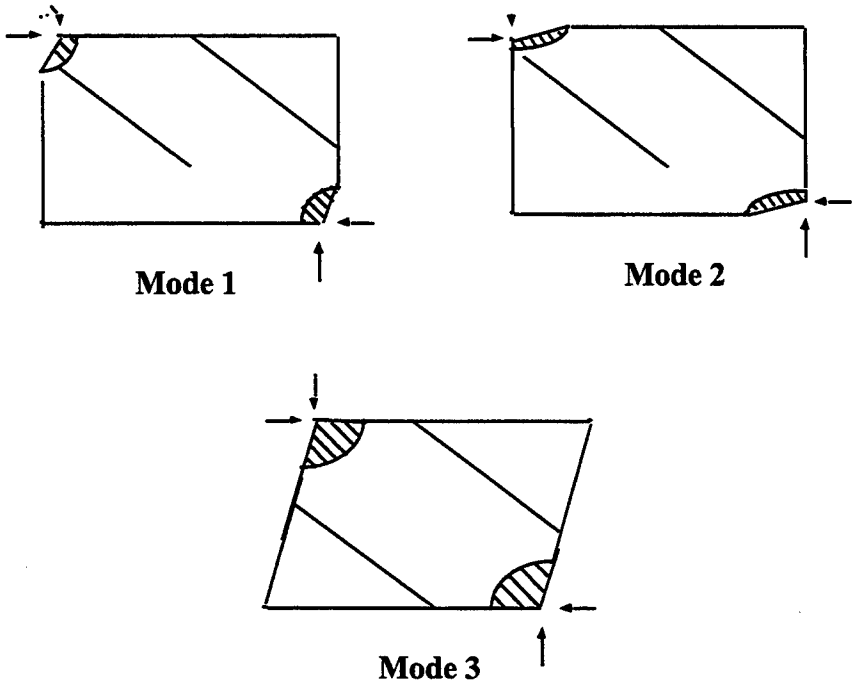

Figure 4.1 Modes of Failure for Infilled Frame (Liauw and Kwan, 1982)

4.8 Dawe and Seah Method

The Dawe and Seah (1989) method is a version of the equivalent strut method developed by Stafford Smith [13]. Their approach gives the effective width of the equivalent strut to be:

$$W_{ef} = a_c \cos\theta + a_b \sin\theta$$

where a_c and a_b are the effective contact lengths of the infill and column or the beam:

$$a_c = \frac{\pi}{1.5\lambda_h}$$

$$a_b = \frac{\pi}{1.5\lambda_t}$$

the length parameters are calculated as:

$$\lambda_h = \sqrt[4]{\frac{E_w H_{in} \sin 2\theta}{4E_c I_c t_w}}$$

$$\lambda_t = \sqrt[4]{\frac{E_w L_{in} \sin 2\theta}{4 E_b I_b t_w}}$$

where:

H_{in}, L_{in} = clear infill panel height and length, respectively

E_b, E_c, E_w = elastic modulus of beam, column, and infill, respectively

I_b, I_c = beam and column moment of inertia, respectively

θ = angle of the diagonal from horizontal

t_w = thickness of infill

Area of the diagonal strut is expressed as:

$$A_{strut} = W_{ef} t_w$$

4.9 Durrani and Luo Method

Durrani and Luo (1994) have tried to fit empirical data to the results of a finite element analysis [16]. The effective width, w_e, of the equivalent strut can be expressed in terms of the effective width factor:

$$\gamma = \frac{w_e}{w_d} = \frac{w_e}{d \sin 2\theta}$$

From finite element analysis, the effective width factor, γ, equals:

$$\gamma = 0.32\sqrt{\sin 2\theta}\left(\frac{H^4 E_i t}{m E_c I_c b}\right)^{-0.1}$$

where m equals:

$$m = 6\left(1 + \frac{6\arctan\left(\frac{E_b I_b H}{E_c I_c L}\right)}{\pi}\right)$$

and where:

w_e = effective width of equivalent diagonal strut

w_d = net width of infill diagonal panel

t = thickness of infill

d = diagonal length of infill

θ = slope of diagonal

m = ratio of beam-to-column stiffness, which varies from 6 for very flexible beams to 24 for very stiff beams

E_i = modulus of infill

E_c = modulus of column material

E_b = modulus of beam material

I_c = moment of inertia of column

I_b = moment of inertia of beam

H = story height

b = height of infill panel

L = length of beam between centerlines of columns

The area of the diagonal strut is expressed as:

$$A_{strut} = w_e t$$

4.10 ECOEST/PREC 8

The *European Consortium of Earthquake Shaking Tables - Prenormative Research in Support of Eurocode 8* (ECOEST/PREC 8, 1996) reviews other methods for calculating the seismic response of infilled frames [18]. It compares results from the various methods and how they compare to test data. It also introduces some simple equations for determining the lateral stiffness, cracking strength, and ultimate strength. Lateral stiffness of the infilled frame is given as:

$$K = \frac{G_w A_w}{h_{in}}$$

with the horizontal cross-sectional area of the infill equaling:

$$A_w = L_w t_w$$

Infill cracking strength:

$$H_c = \tau_{cr} A_w$$

Infill ultimate strength:

$$H_u = 1.3\tau_{cr} A_w$$

where:

G_w = masonry shear modulus (diagonal compression test)
L_w = length of infill
t_w = thickness of infill
h_{in} = height of infill
τ_{cr} = diagonal compressive strength of a panel wallet diagonally loaded at the corners

4.11 NEHRP 274 Document

In this method the elastic in-place stiffness of a solid unreinforced masonry infill panel is represented by an equivalent diagonal compression strut of width, a:

$$a = 0.175(\lambda_1 h_{col})^{-0.4} r_{\text{inf}}$$

where:

$$\lambda_1 = \left[\frac{E_m t_{\text{inf}} \sin 2\theta}{4E_{fe} I_{col} h_{\text{inf}}}\right]^{1/4}$$

and:

h_{col} = column height between centerlines of beams (inch)

h_{inf} = height of infill panel (inch)

E_{fe} = expected modulus of elasticity of frame material (psi)

E_{me} = expected modulus of elasticity of infill material (psi)

I_{col} = moment of inertia of column (in^4)

L_{inf} = length of infill panel (inch)

r_{inf} = diagonal length of infill panel (inch)

t_{inf} = thickness of infill panel and equivalent strut (inch)

θ = angle whose tangent is infill height-to-length aspect ratio (rad)

Shear strength acceptance criteria were proposed as follows:

$$Q_{CE} = V_{ine} = A_{ni} f_{vie}$$

where:

V_{ine} = expected infill shear strength

A_{ni} = area of net mortared/grouted section across infill panel (in^2)

f_{vie} = expected shear strength of masonry

Shear strength of existing masonry is expressed as:

$$v_{me} = \frac{0.75\left(0.75v_{te} + \frac{P_{CE}}{A_n}\right)}{1.5}$$

where:

P_{CE} = expected gravity compressive force applied to a wall or pier component stress considering load combinations given in Equations 3-13 and 3-14 of the NEHRP Guideline for the Seismic Rehabilitation of Buildings [41]

A_n = area of net mortared/grouted section (in^2)

v_{te} = average bed-joint shear strength (psi)

The factor of 0.75 on v_{te} may be waived for single wythe masonry or if the collar joint is known to be absent or in poor condition. Values of mortar shear strength shall not exceed 100 psi for the determination of v_{me} as calculated above.

Average bed-joint shear strength, v_{te}, is determined from individual shear strength test values, v_{to}, in accordance with:

$$v_{to} = \frac{V_{test}}{A_b} - P_{D+L}$$

where:

V_{test} = load at first movement of masonry unit

A_b = net mortared area of the bed joints above and below test brick (in^2)

P_{D+L} = estimated gravity stress at test location (psi)

When no tests are performed default values of shear strength for unreinforced masonry may be used as follows:

running bond masonry in good condition = 27 psi

running bond masonry in fair condition = 20 psi

running bond masonry in poor condition = 13 psi

These values may be used in fully grouted masonry other than running bond, and if not fully grouted are reduced by 60% of these values.

Shear strength of newly constructed infill panels, f_{vie}, shall not exceed:

$$2.0\sqrt{f_{me}}$$

masonry in running bond that is not grouted solid = 92 psi

masonry other than running bond with open end units grouted solid = 92 psi

masonry in running bond that is grouted solid = 150 psi

masonry other than running bond grouted solid without open end units = 37 psi

Column and beam members adjacent to a stiff masonry infill can cause the surrounding frame to take more stress than it can resist, which causes failure in the frame elements. The expected flexural and shear strengths of column members adjacent to an infill panel shall exceed forces resulting from one of the following conditions:

- the application of the horizontal component of the expected infill strut force applied at a distance, l_{ceff}, from the top or bottom of the infill panel equal to:

$$l_{ceff} = \frac{a}{\cos\theta}$$

- the shear force resulting from development of expected column flexural strengths at the top and bottom of a column with a reduced height equal to, l_{ceff}.

These same requirements apply to beams enclosing the infill also:

$$l_{beff} = \frac{a}{\sin\theta}$$

These requirements need not be checked if the expected masonry shear strength is less than 50 psi (NEHRP, 1996).

Table XVIII Width of Equivalent Diagonal Struts (inches)

Model	Holmes	SS1	SS2	Mainstone	Lefter & Colville	Liauw & Kwan	Dawe & Seah	Durrani	ECOEST
Applicability	Stiffness Estimated up to Infill Crushing	Nondescript General Stiffness	Stiffness at Onset of Panel Yielding	Stiffness Prior to Cracking	Stiffness	Ultimate Strength	Nondescript General Stiffness	Initial Stiffness	Stiffness & Ultimate Strength
One-bay with bricks	29.7	18.0	18.7	8.8	-	-	8.4	17.5	-
One-bay with CMU	29.7	18.0	18.3	8.3	-	-	9.8	16.6	-
Two-bay with CMU	29.7	18.0	18.6	8.7	-	-	10.9	17.3	-
Three-bay with bricks	29.7	18.0	18.4	8.4	-	-	8.0	16.8	-

Table XIX Strength of Each Model Based on Simplified Analytical Methods (kips)

Model	Holmes	SS1	SS2	Mainstone	Lefter & Colville	Liauw & Kwan	Dawe & Seah	Durrani	ECOEST
Applicability	Stiffness Estimated up to Infill Crushing	Nondescript General Stiffness	Stiffness at Onset of Panel Yielding	Stiffness Prior to Cracking	Stiffness	Ultimate Strength	Nondescript General Stiffness	Initial Stiffness	Stiffness & Ultimate Strength
One-bay with bricks	126.1	-	-	67.2	-	38	-	-	45
One-bay with CMU	214.7	-	-	100.6	-	50	-	-	57
Two-bay with CMU	137.7	-	-	71	-	40	-	-	52
Three-bay with bricks	181.2	-	-	87.5	-	46	-	-	69

Table XX Stiffness of Each Model Based on Simplified Analytical Methods (kips/inch)

Model	Holmes	SS1	SS2	Mainstone	Lefter & Colville	Liauw & Kwan	Dawe & Seah	Durrani	ECOEST
Applicability	Stiffness Estimated up to Infill Crushing	Nondescript General Stiffness	Stiffness at Onset of Panel Yielding	Stiffness Prior to Cracking	Stiffness	Ultimate Strength	Nondescript General Stiffness	Initial Stiffness	Stiffness & Ultimate Strength
One-bay with bricks	876	543	556*	322*	1817	-	313*	528*	2267
One-bay with CMU	1491	839	834*	457*	3081	-	520*	774*	3926
Two-bay with CMU	957	579	1268*	662*	1981	-	802*	1210*	2486
Three-bay with bricks	1258	727	2611*	1266*	2602	-	1219*	2392*	3298

* Designates that SAP 90 was used in obtaining stiffness values.

CHAPTER 5

FINITE ELEMENT ANALYSIS

5.1 Introduction

Reinforced concrete (R/C) frames may exist as either bare or infilled. The effect of infill materials on the overall structural behavior of these frames was investigated previously by many researchers. Until now, there is no clear analytical approach that can be used to analyze these structures. A typical R/C frame with masonry infill specimen consists of reinforcing steel, concrete, brick or CMU, and mortar. Subjecting these structures to in-plane loads result in a complex stress state that is often not fully understood. The objective of this chapter is to model single-story single, double, and triple bay infilled R/C frames by using the finite element analysis.

Finite element modeling of such structures is quite complex due to the highly brittle, heterogeneous and inelastic response of concrete, CMU, Brick, and mortar. In addition, crack initiation and trajectory, stress concentrations, as well as the interactive effects between concrete and the steel reinforcement makes the problem more complex. Tensile cracking in concrete occurs at a very low value of the tensile stress compared to the compressive stress. CMU, brick and mortar have also low values of tensile stress compared to their compressive strength. The reduction in stiffness of the infilled R/C frame is due to the formation of tensile cracks in the concrete and the infill. Tensile cracking is considered as the main cause to the nonlinear response of such structures. The value of tensile stress at the cracked surfaces abruptly goes to zero after crack formation. In concrete, forces are then transmitted across the cracks by the bridging of reinforcing steel and aggregate interlock, while in the infill forces are transmitted across cracks by internal friction.

Nonlinear finite element modeling procedures were developed for the modeling and analysis of all tested specimens, described in Chapter 3, to predict the stress level and stress distribution in the entire structure. The analysis was carried out to predict the ultimate load, as well as the load-deformation behavior of the member. Finite element modeling was performed by the commercial package called "ALGOR" [2]. This package enable modeling the behavior of the tested specimens based on material non-linearity. The results from the finite element analysis for each model were carefully analyzed to serve as a useful preliminary guide in evaluating the behavior of such structures. In addition, they provided needed information for locating critical sections where strain gages, extensometers, and LVDTs should be mounted on the test specimens.

5.2 Description of Element Types used

5.2.1 Concrete, CMU, Brick and Mortar

Three-dimensional isoparametric eight-node solid elements were used to model the Concrete, CMU, Brick and Mortar components in each specimen. This element type enabled the prediction of the stress level and stress distribution in the models. Figures 5.1 to 5.3 show the three-dimensional models for concrete, CMU and mortar, respectively, discretized by the solid elements. Figure 5.4 shows the wire mesh, the boundary conditions and the distribution of applied load for a single-bay CMU infilled frame.

5.2.2 Steel reinforcement

Three-dimensional truss elements were used in modeling the longitudinal and transverse steel reinforcements. A truss element has three degrees of freedom at each node, i.e., three

translations along the three global x, y and z directions, and only capable of transmitting compressive and tensile axial forces. Figures 5.5 shows the three-dimensional truss elements used to model reinforcing steel for a two-bay specimen.

5.3 Material Models

5.3.1 Material Model for concrete, CMU, Brick and Mortar

Nonlinear analysis with only material non-linearity was adopted to perform the finite element analysis for the concrete. A nonlinear curve model representing the behavior of the material was introduced to impose the non-linearity condition. In this model the instantaneous bulk and shear moduli are functions of the stress and strain invariant, and are defined by piece-wise linear functions of the current volume strain [2,7]. The specified material properties needed in the analysis for concrete, CMU, brick and mortar are presented in Tables XIII and XV and XVI, in Chapter 3.

5.3.2 Material Model for steel reinforcement

The nonlinear elastic behavior is defined by specifying the stress as a piece-wise linear function of the current infinitesimal strain. Thus, the total stress and the tangent modulus are directly defined in terms of the total strain. Both loading and unloading follow the user defined (specified) stress strain curve [2]. Table XVII shows the specified yield strength, yield strain, modulus of elasticity, and ultimate strength for the steel.

5.4 Models Analyzed

A total of six models were analyzed to determine the structural behavior of R/C frames with

masonry infill under lateral in-plane loading. Two out of the seven models, designated as B1O and B1F-CMU represent single-bay bare and CMU infilled, respectively. Another two models designated as B2O and B2F-CMU represent double-bay, bare and CMU infilled R/C frames, respectively. The remaining two models designated as B3O and B3F-BR represent triple-bay bare and brick infilled R/C frames, respectively.

5.5 Modeling Techniques

The nonlinear analysis for each specimen was performed through two different models. The first model was used for the uncracked structure. In the second model, cracks in concrete frame and the infill specimen were introduced at critical sections. Location of the critical sections was observed and detected from the FE results of the uncracked model. The results from the two different models for each specimen enabled the prediction of the overall structural behavior of each specimen.

All models have geometrical and loading symmetry. Thus to minimize the computer run time, it was possible to simulate the analysis on half of the specimen. The geometrical mesh generation was separately prepared for each material, and the boundary conditions were specified for each element type in a separate file. The first set of files was for the three-dimensional solid elements, and the second set of files was for the three-dimensional truss elements. Then, each file had to be decoded by a utility program, which translates the previously mentioned boundary condition files into finite element models. Type of element, analysis type, material properties and global boundary conditions are defined in the decoder by several options. Afterward, the two different sets of files were combined by a utility program to form an input file to be analyzed later by an appropriate finite element processor. The results from analyses were very important in terms

of understanding the structural behavior of these structures, and in locating critical sections for the strain gages, LVDTs and strain gauges.

5.6 Analysis of Results for Models

The resulting load-deflection curves are presented in Figures 5.6, 5.7, and 5.8. The deflection was taken at the centroid of left edge of the upper beam (s). The ultimate load for each model was taken where a change in direction in the load-deflection curve as shown in Figures 5.6, 5.7, and 5.8. Table 5.1 summarized the finite element results for each model under the applied in-plane lateral loading. The finite element results are discussed in detail in the following sections.

Table XXI

Load Capacity of Models Resulted from Finite Element Analysis

Model	Model Designation	Description	Ultimate Load (kips)	Corresponding displacement (in)	Stiffness (kips/in.)
I	B1O	Single-bay bare frame	7.0	0.370	18.9
II	B1F-CMU	Single-bay CMU infilled frame	20.5	0.050	410.0
III	B2O	Double-bay CMU bare frame	16.5	0.580	28.5
IV	B2F-CMU	Double-bay CMU infilled frame	67.0	0.047	1425.0
V	B3O	Triple-bay bare frame	21.5	0.800	26.9
VI	B3F-BR	Triple-bay Brick infilled frame	88.0	0.053	1660.0

5.6.1 Model I:

An ultimate load of 7.0 kips at a displacement of 0.37 in. was achieved when a change of direction was noticed in the load-deflection curve in Figures 5.6a, 5.7, and 5.8. The deflected model

is shown in Figure 5.9. The predicted longitudinal stress, σ_{zz}, distribution in the uncracked model is shown in Figure 5.10, while the maximum principal stress distribution in the uncracked model is shown in Figure 5.11. The predicted shear stress distribution in the uncracked model is shown in Figure 5.12. The stress distribution at the predicted ultimate load for steel reinforcement is shown in Figure 5.13. A close-up view of the concrete longitudinal stress distribution at the upper left beam is shown in Figure 5.14.

5.6.2 Model II:

An ultimate load of 20.5 kips at a displacement of 0.05 in. was achieved when a change of direction was noticed in the load-deflection curve in Figures 5.6a, 5.7, and 5.8. The deflected model is shown in Figure 5.15. The predicted longitudinal stress, σ_{zz}, distribution in the uncracked model is shown in Figure 5.16, while the maximum principal stress distribution in the uncracked model is shown in Figure 5.17. The predicted shear stress distribution in the uncracked model is shown in Figure 5.18. The stress distribution at the predicted ultimate load for steel reinforcement is shown in Figure 5.19.

In comparing Figure 5.15 with Figure 5.9, it is noticeable that the infill has a great influence on the overall structural behavior of the model. The predicted ultimate load for this model is about 2.9 that of the bare model. Also, the deflection at ultimate load was found to be about 13.5% of the bare model. Thus, having the infill increase significantly the ultimate load capacity and the overall stiffness of the model. For the bare frame model (I), the windward and the leeward columns seem to resist the load equally as shown in Figure 5.10, while the CMU infill in this model redistributed the stresses in the frame resulting in more displacement and stresses in the windward column than

that of the leeward, as illustrated in Figure 5.16. Having the CMU infill in the single-bay model increased the overall stiffness about 21.7 times.

5.6.4 Model III:

An ultimate load of 16.5 kips at a displacement of 0.58 in. was achieved when a change of direction was noticed in the load-deflection curve as shown in Figures 5.6b, 5.7 and 5.8. The deflected model is shown in Figure 5.20. The predicted longitudinal stress, σ_{zz}, distribution in the uncracked model is shown in Figure 5.21, while the maximum principal stress distribution in the uncracked model is shown in Figure 5.22. The predicted shear stress distribution in the uncracked model is shown in Figure 5.23. The stress distribution at the predicted ultimate load for steel reinforcement is shown in Figure 5.24.

5.6.5 Model IV:

An ultimate load of 67 kips at a displacement 0.047 in. was achieved when a change of direction was noticed in the load-deflection curve as shown in Figures 5.6b, 5.7 and 5.8. The deflected model is shown in Figure 5.25. The predicted longitudinal stress, σ_{zz}, distribution in the uncracked model is shown in Figure 5.26, while the maximum principal stress distribution in the uncracked model is shown in Figure 5.27. The predicted shear stress distribution in the uncracked model is shown in Figure 5.28. The stress distribution at the predicted ultimate load for steel reinforcement is shown in Figure 5.29

In comparing Figure 5.25 with Figure 5.20, it is noticeable that the infill has a significant influence on the overall structural behavior of the model. The predicted ultimate load for this model

was about 4.1 that of the bare model. Also, the deflection at ultimate load was found to be about 8.1 of the bare model III. Thus, having the infill increase significantly the ultimate load capacity and the overall stiffness of the model. Having the CMU infill in the double-bay model increased the overall stiffness about 50 times.

5.6.6 Model V:

An ultimate load of 21.5 kips at a displacement of 0.8 in. was achieved when a change of direction was noticed in the load-deflection curve as shown in Figures 5.6c, 5.7 and 5.8. The deflected model is shown in Figure 5.30. The predicted longitudinal stress, σ_{zz}, distribution in the uncracked model is shown in Figure 5.31, while the maximum principal stress distribution in the uncracked model is shown in Figure 5.32. The predicted shear stress distribution in the uncracked model is shown in Figure 5.33. The stress distribution at the predicted ultimate load for steel reinforcement is shown in Figure 5.34.

5.6.7 Model VI:

An ultimate load of 88 kips at a displacement of 0.053 in. was achieved when a change of direction was noticed in the load-deflection curve as shown in Figures 5.6c, 5.7, and 5.8. The deflected model is shown in Figure 5.35. The predicted longitudinal stress, σ_{zz}, distribution in the uncracked model is shown in Figure 5.36, while the maximum principal stress distribution in the uncracked model is shown in Figure 5.37. The predicted shear stress distribution of the infill in the uncracked model is shown in Figure 5.38. The stress distribution at the predicted ultimate load for steel reinforcement is shown in Figure 5.39

In comparing Figure 5.30 with Figure 5.25, it is noticeable that the infill has a great influence on the overall structural behavior of the model. The predicted ultimate load for this model is about 4.1 that of the bare model. Also, the deflection at ultimate load was found to be 6.6% of the bare model. Thus, having the infill increase significantly the ultimate load capacity and the overall stiffness of the model. Having the infill in the triple-bay brick model increased the overall stiffness about 61.7 times.

5.7 Comparison of Results for Different Models

The infill increases significantly the ultimate load capacity and the overall stiffness of the single-bay frames. The predicted ultimate load for all infilled models II, IV, and VI were 2.9, 4.1, and 4.1 times that of the bare frame models I, III, and V, respectively (Table 5.1). The deflections at ultimate loads for the infill models II, IV, and VI were found to be 13.5%, 8.1%, and 6.6% of their bare models I, III, and V, respectively. For the bare frame model (I), the windward and leeward columns seem to resist the load equally (Figure 5.8), while the CMU infill in this model redistributed the stresses in the frame resulting in more displacement and stresses in the windward column than that of the leeward (Figures 5.9, 5.10, 5.15 and 5.16).

Prior to cracking, the windward and leeward columns in the bare frame model (I) seem to resist the load equally (Figures 5.9 and 5.10). The CMU infill in model (II) redistributed the stresses in the frame resulting in more displacement and stresses in the windward column than that of the others (Figures 5.15 and 5.16). After cracking, the infilled frame behaved as a truss.

Similarly, prior to cracking, the windward and the leeward columns in the bare frame model (III) seem to resist the load equally (Figures 5.21 and 5.22). The CMU infill in model (IV) redistributed the stresses in the frame resulting in more displacement and stresses in the windward

column than that of the others (Figures 5.30 and 5.31). After cracking, the infilled frame behaved as a truss. Similar behavior was noticed for models V and IV.

The stiffness ratio of models II, IV, and VI relative to their bare frame models I, III, and V, are 21.7, 50.0, and 61.7, respectively. The higher value of stiffness ratio in the two-bay models agreed with the experimental results. By increasing the number of bays, the overall stiffness increases.

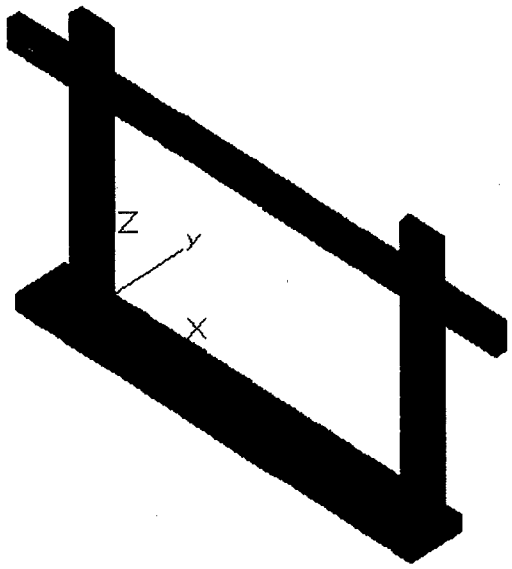

Figure 5.1 Three-dimensional concrete solid elements for single-bay

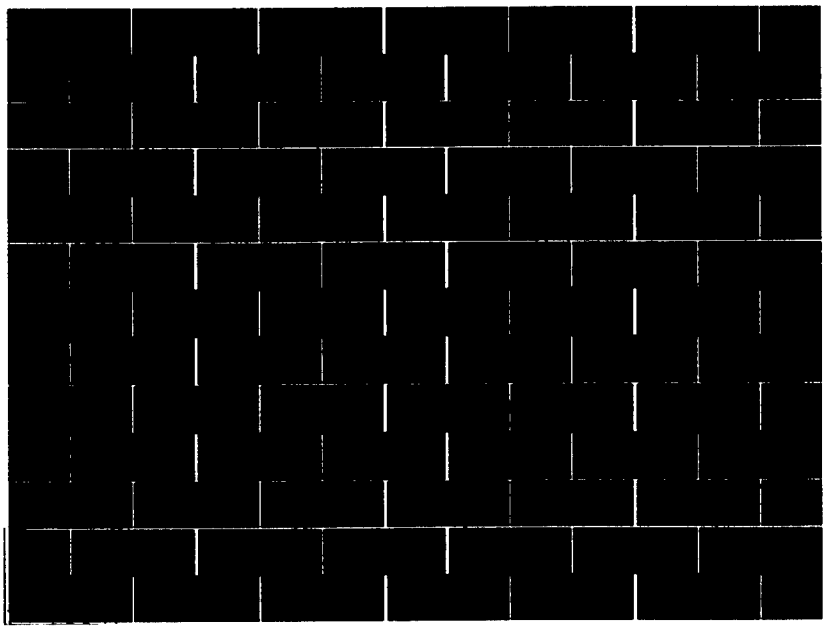

Figure 5.2 Three-dimensional concrete brick elements for single-bay CMU infill

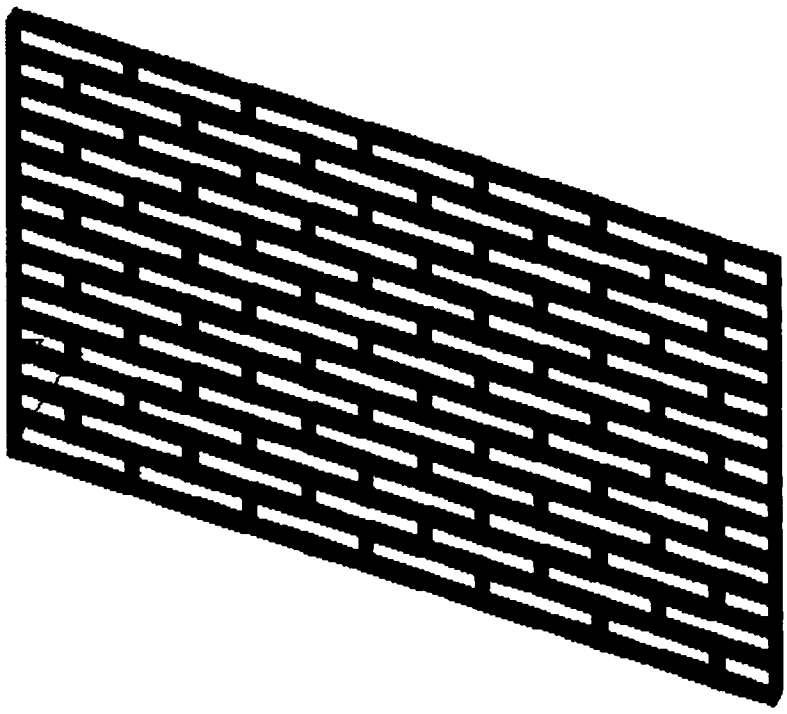

Figure 5.3 Three-dimensional concrete brick elements for single-bay CMU mortar

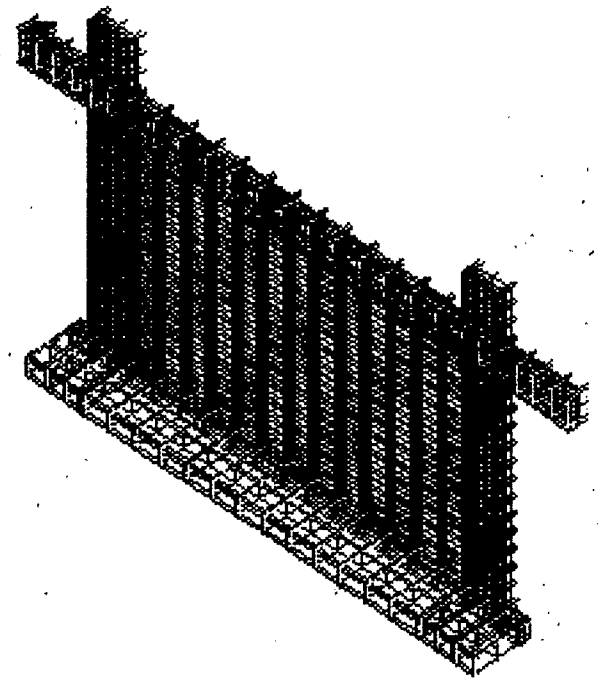

Figure 5.4 Mesh generation, boundary conditions, and applied loads for single-bay CMU infill frame

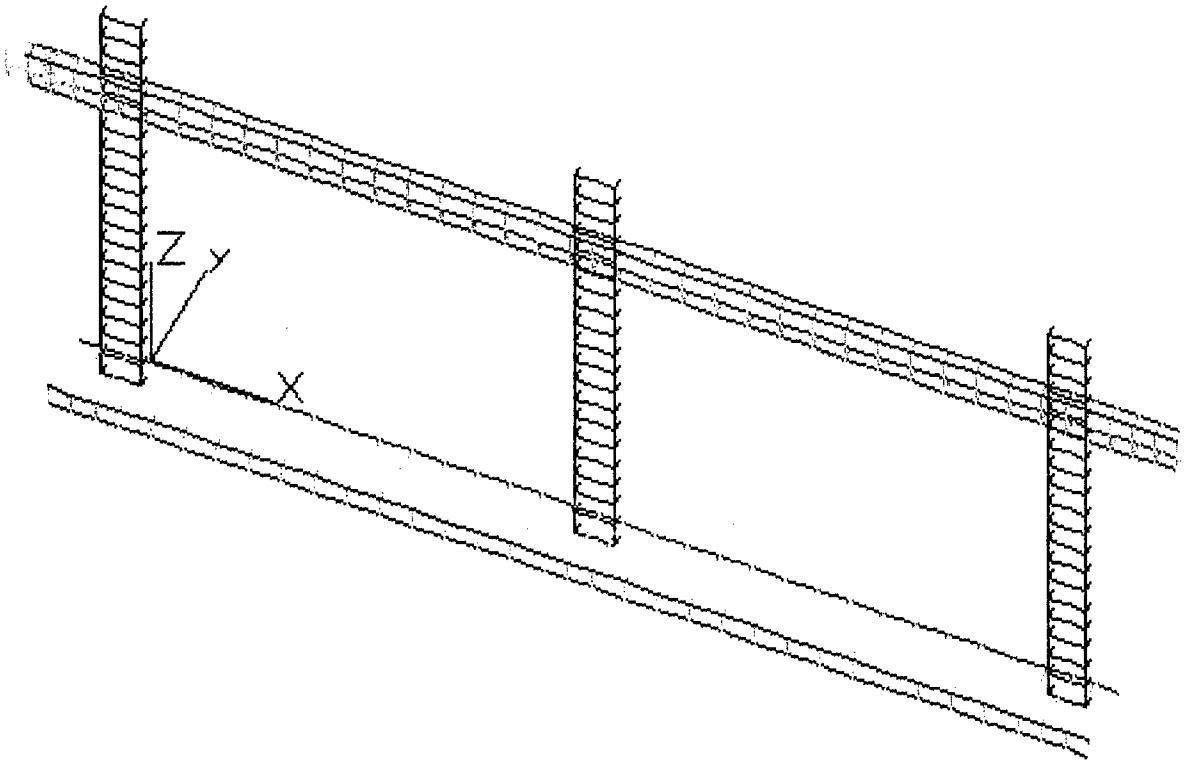

Figure 5.5 Three-dimensional steel truss elements for double-bay model

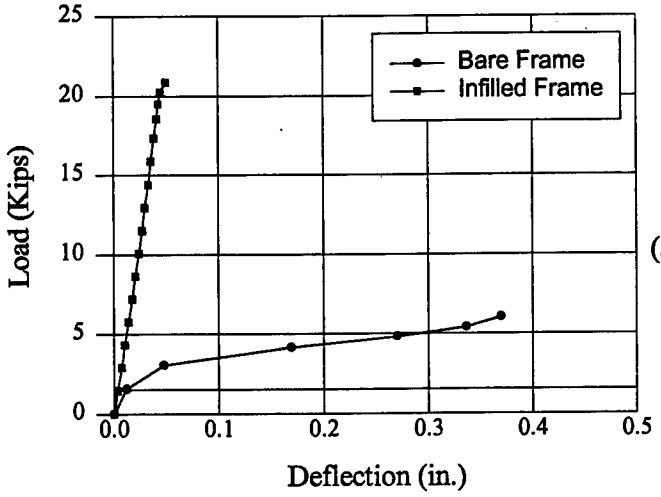

(a) Single Bay Models

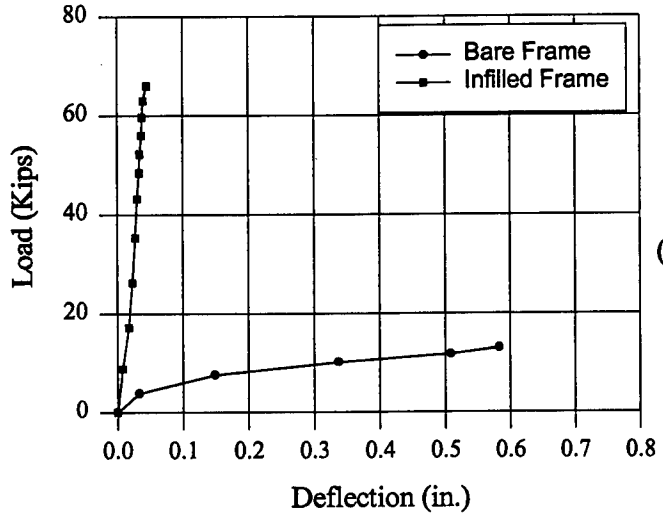

(b) Double Bay Models

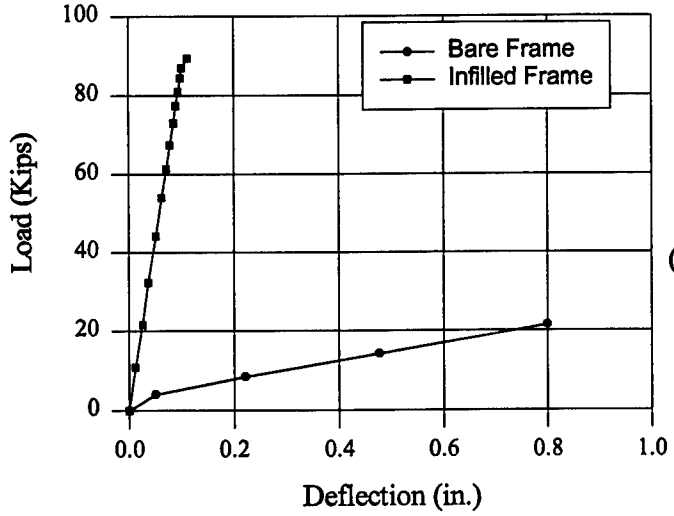

(c) Triple Bay Models

Figure 5.6 Load-Deflection Curves

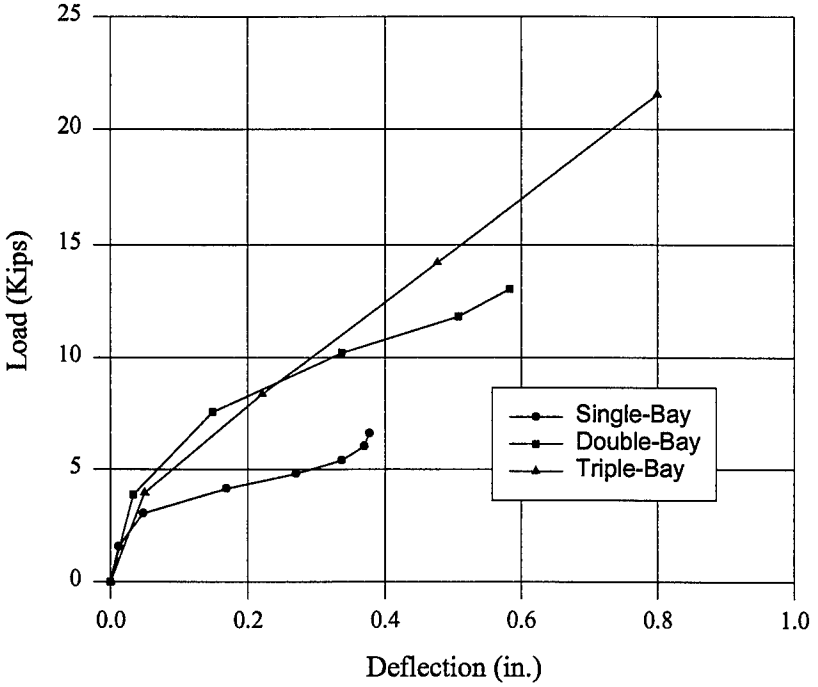

Figure 5.7 Load Deflection Curves for Bare Frame Models

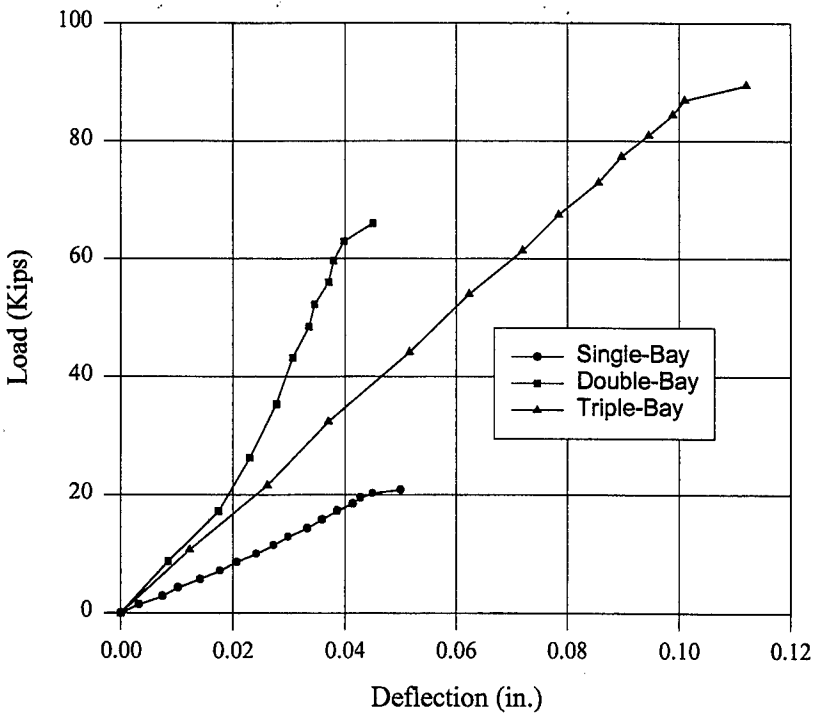

Figure 5.8 Load-Deflection Curves for Infilled Frame Models

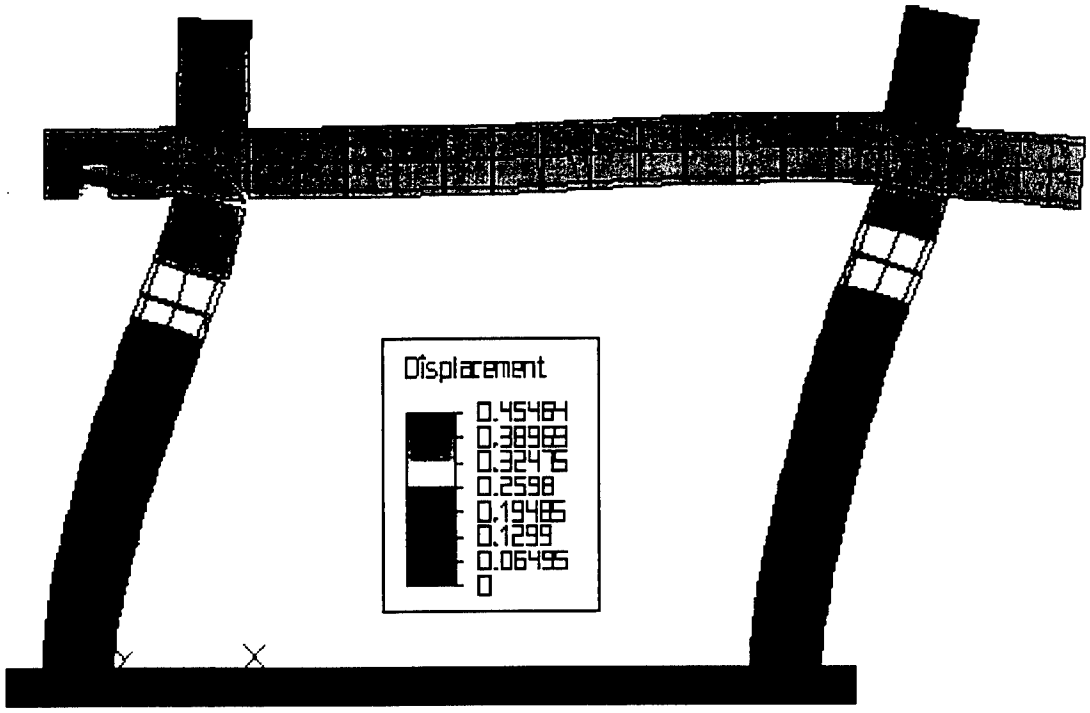

Figure 5.9 Deflection of Model I at ultimate loading

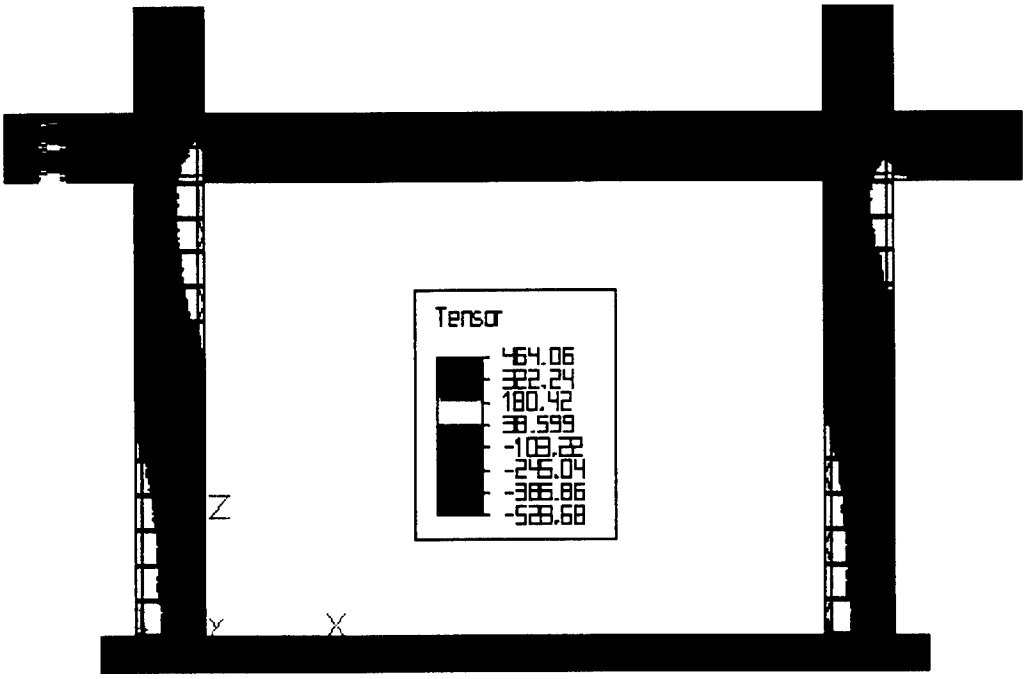

Figure 5.10 Longitudinal stress σ_{zz} for Model I

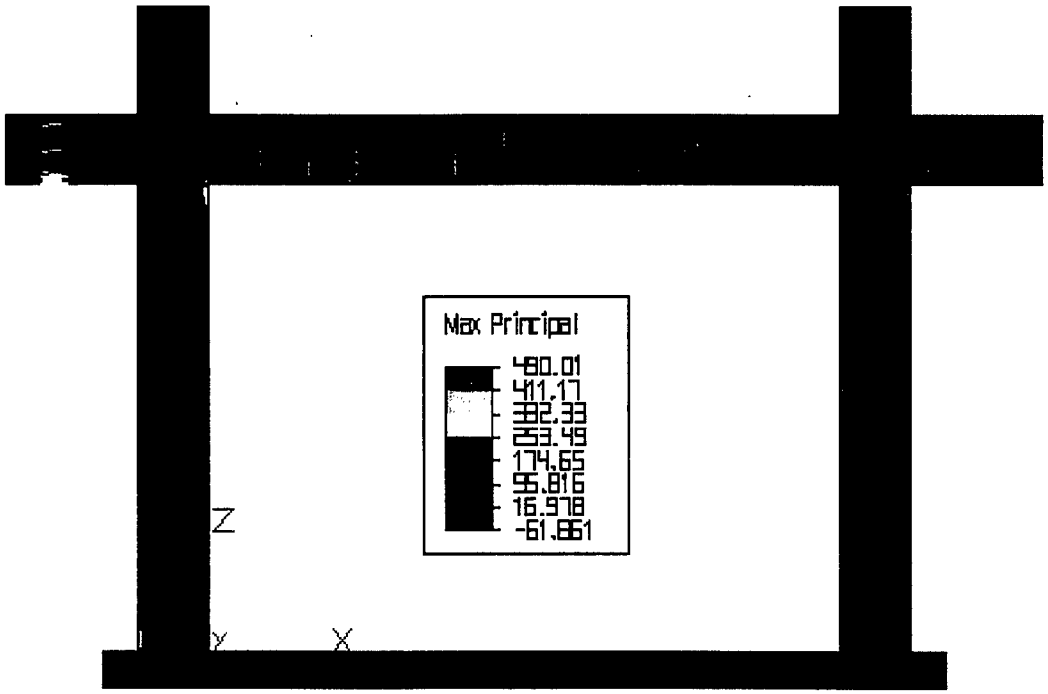

Figure 5.11 Maximum principal stress distribution for Model I at initial cracking

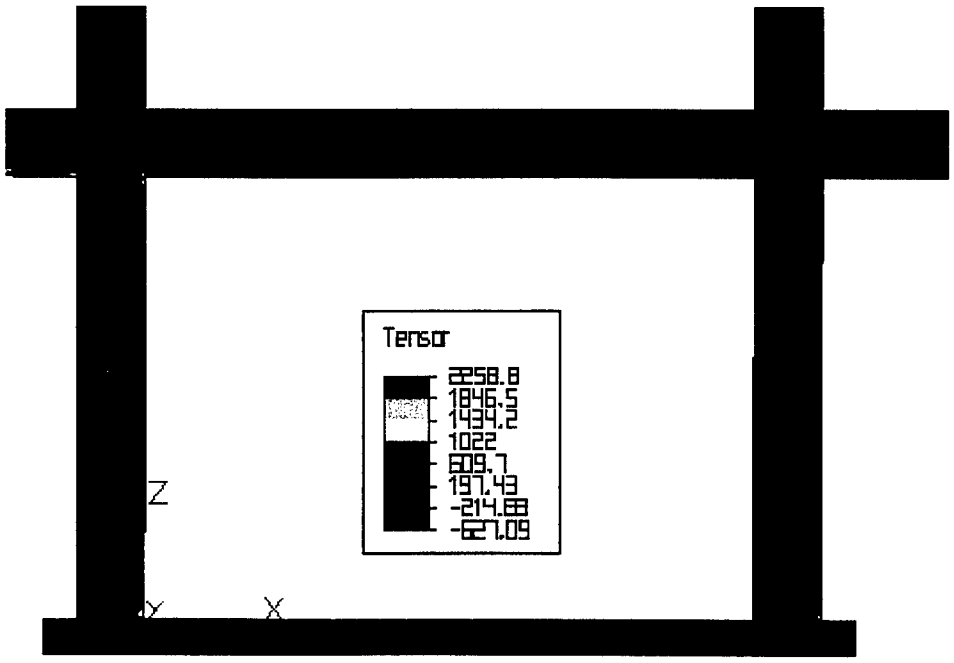

Figure 5.12 Shear stress distribution for Model I at initial cracking

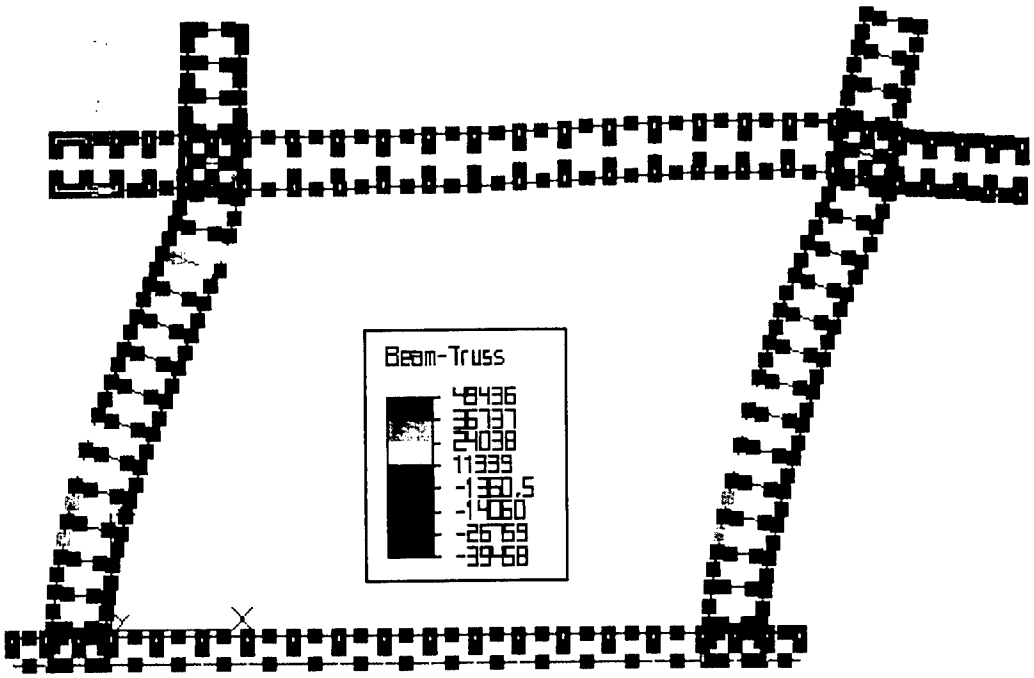

Figure 5.13 Stress distribution in steel for Model I at ultimate cracking

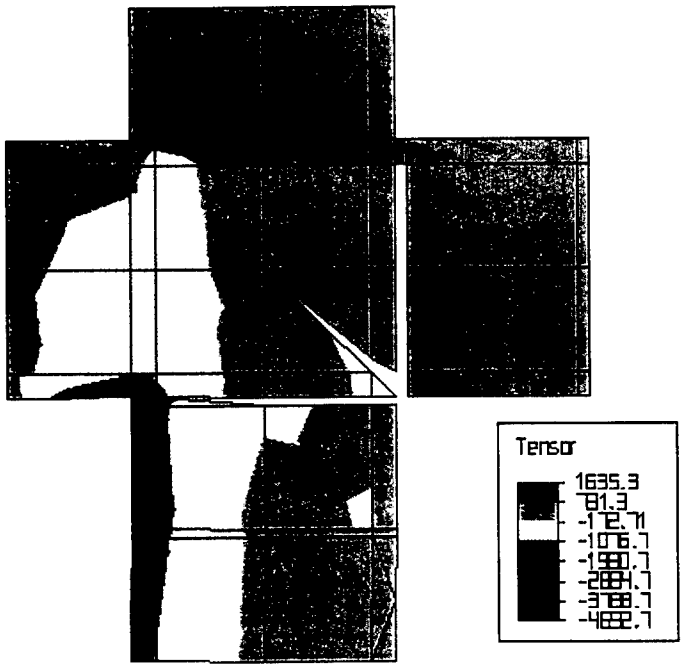

Figure 5.14 Close-up view of longitudinal stress distribution at the upper left beam to column connection for Model I.

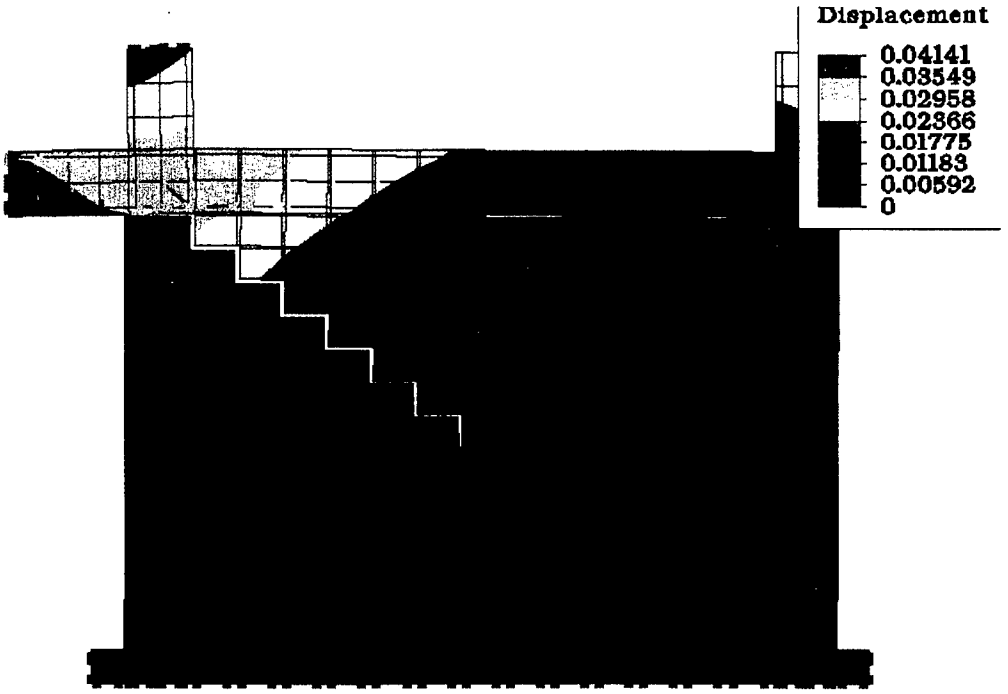

Figure 5.15 Deflection of Model II at ultimate loading

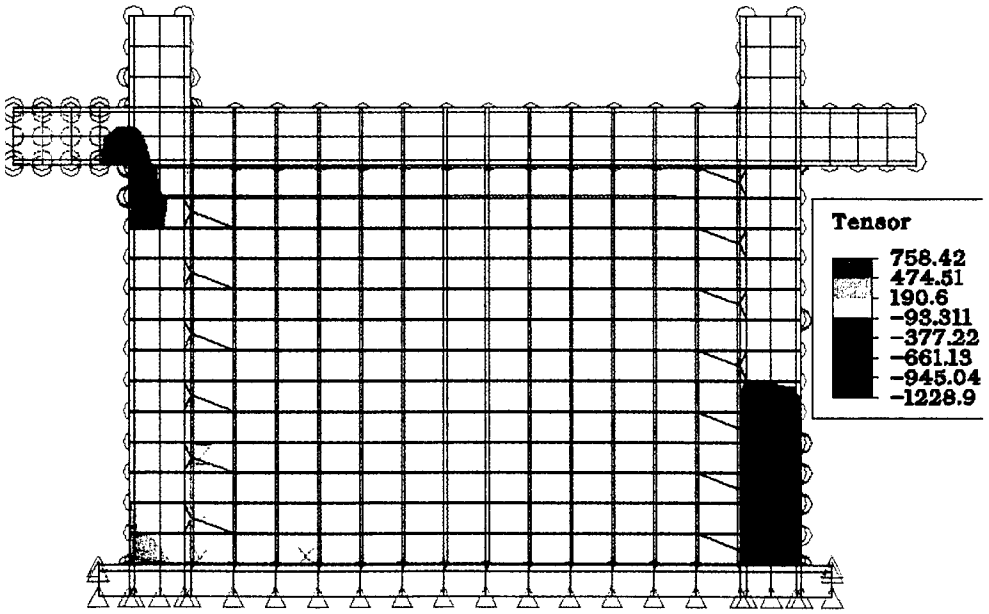

Figure 5.16 Longitudinal stress σ_{zz} for Model II

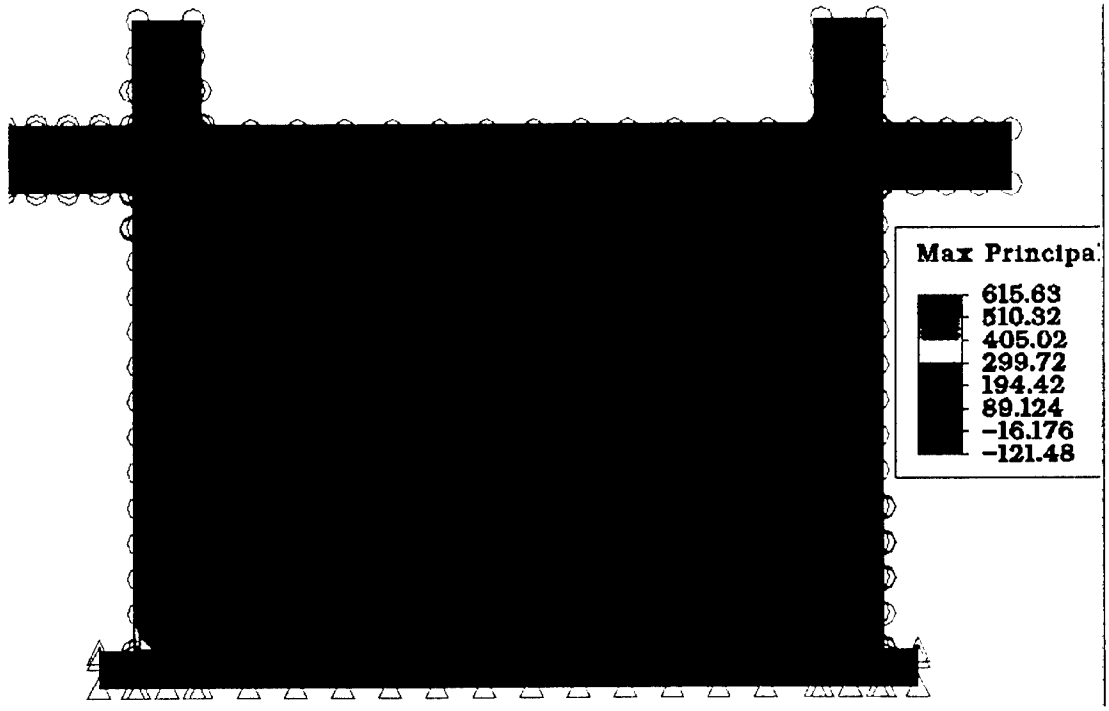

Figure 5.17 Maximum principal stress distribution for Model II at initial cracking

Figure 5.18 Shear stress distribution for Model II at initial cracking

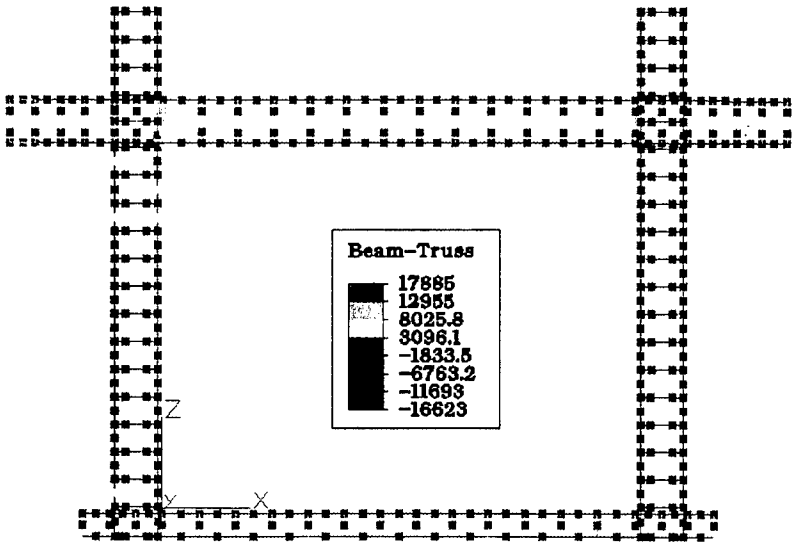

Figure 5.19 Stress distribution in steel for Model II at initial cracking

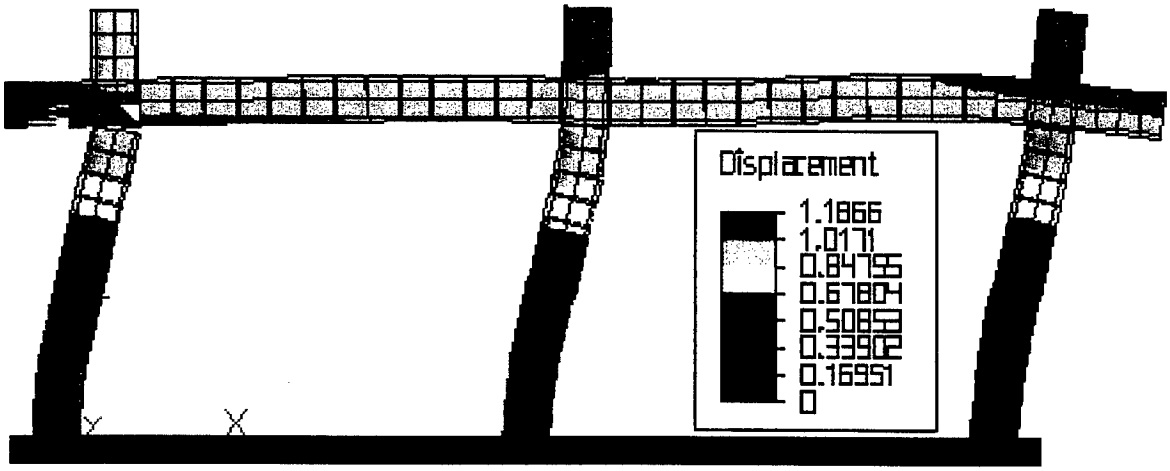

Figure 5.20 Deflection of Model III at ultimate loading

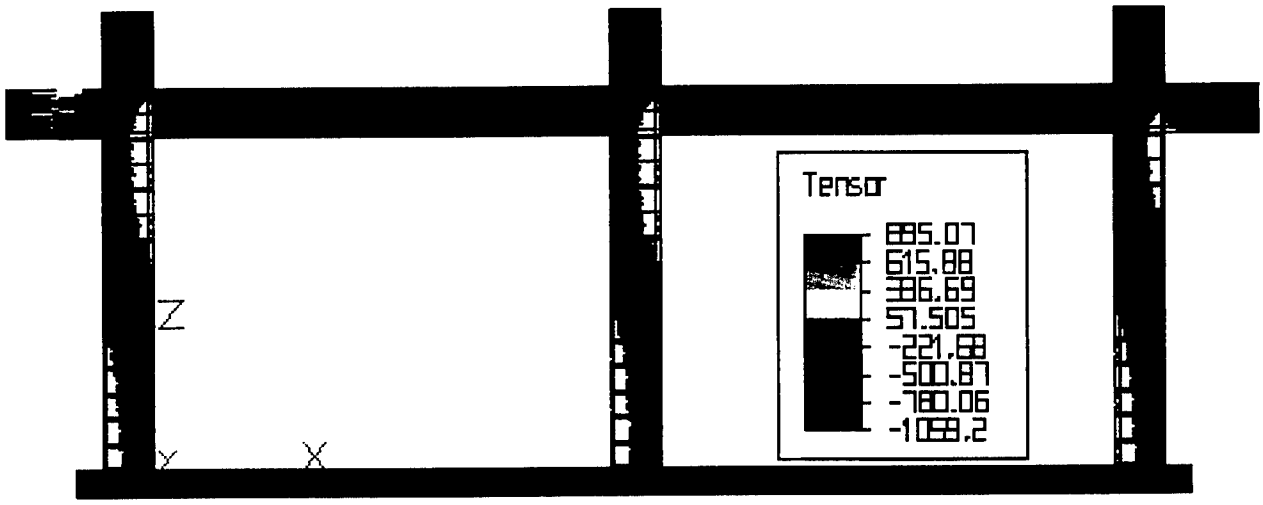

Figure 5.21 Longitudinal stress σ_{zz} for Model III

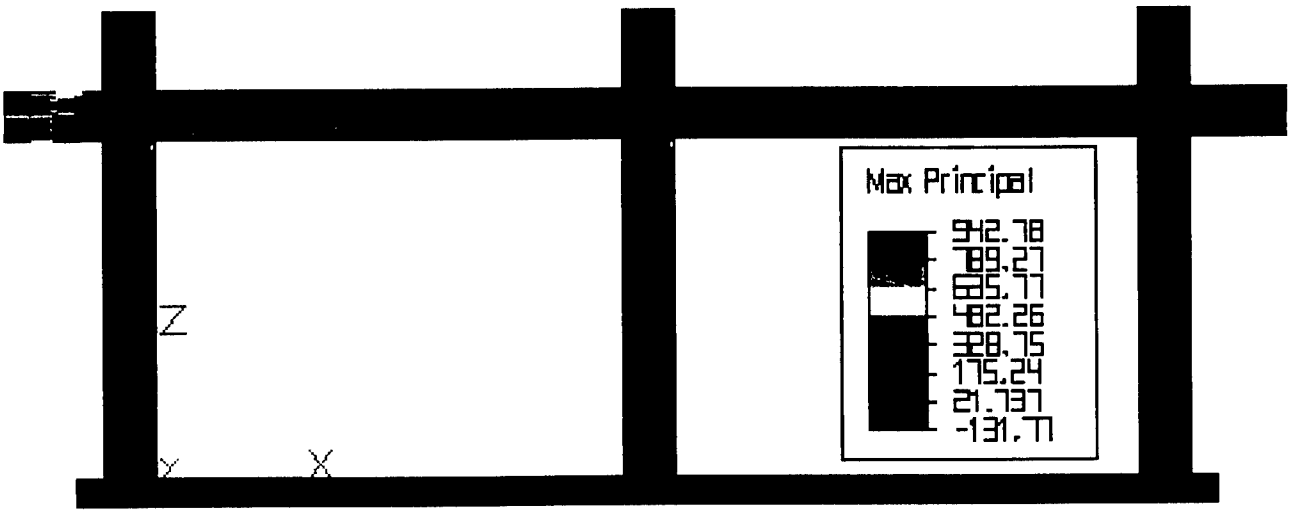

Figure 5.22 Maximum principal stress distribution for Model III at initial cracking

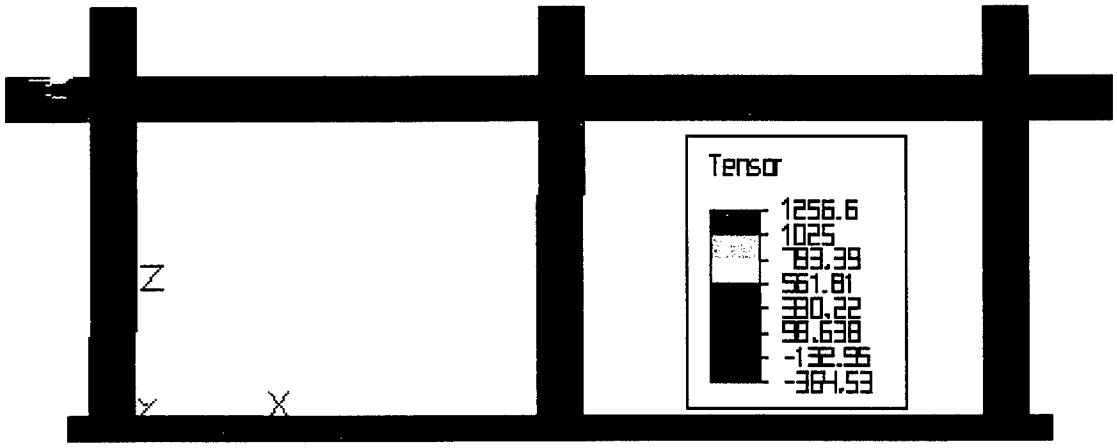

Figure 5.23 Shear stress distribution for Model III at initial cracking

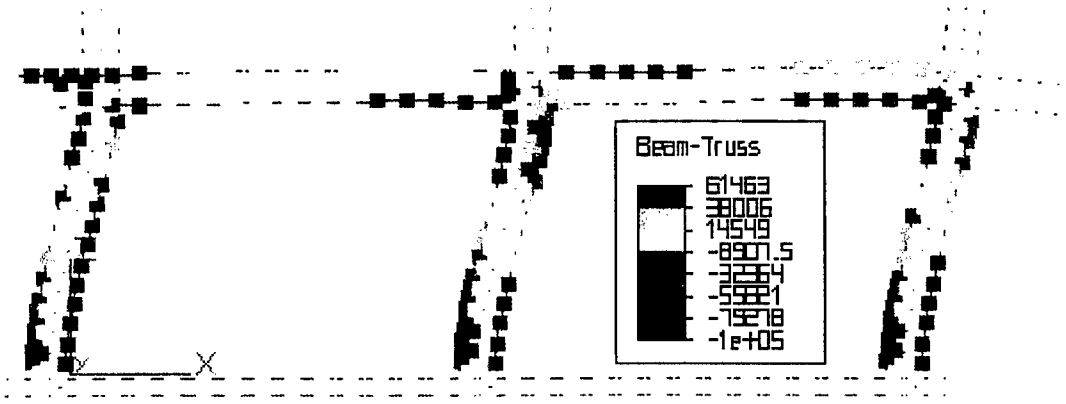

Figure 5.24 Stress distribution in steel for Model III at initial cracking

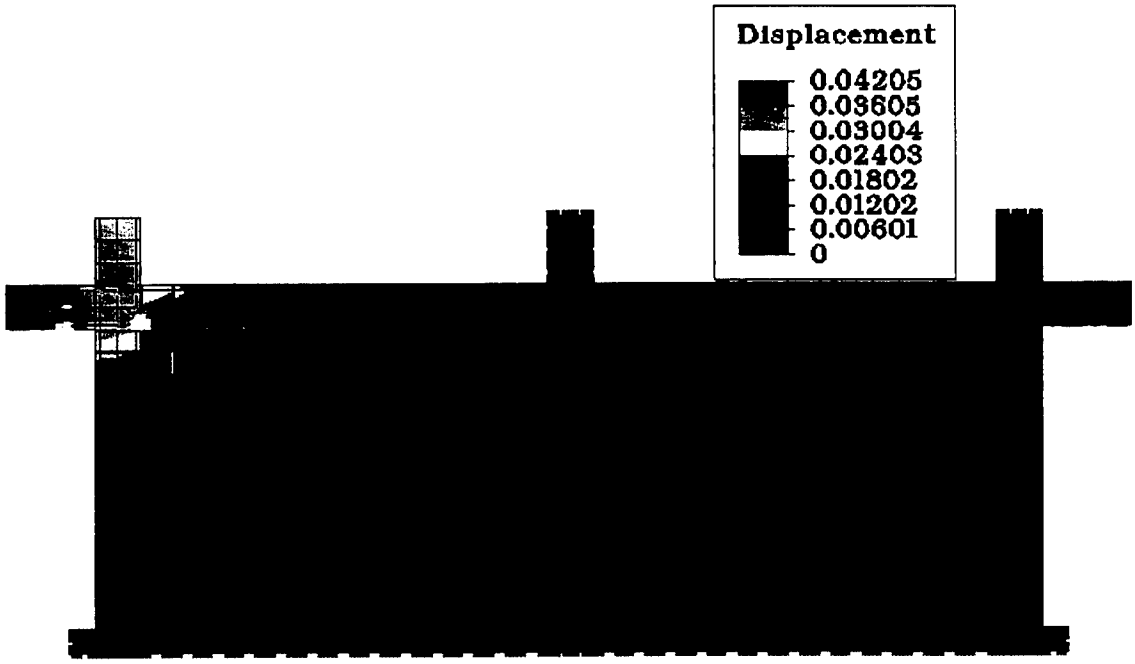

Figure 5.25 Deflection of Model IV at ultimate loading

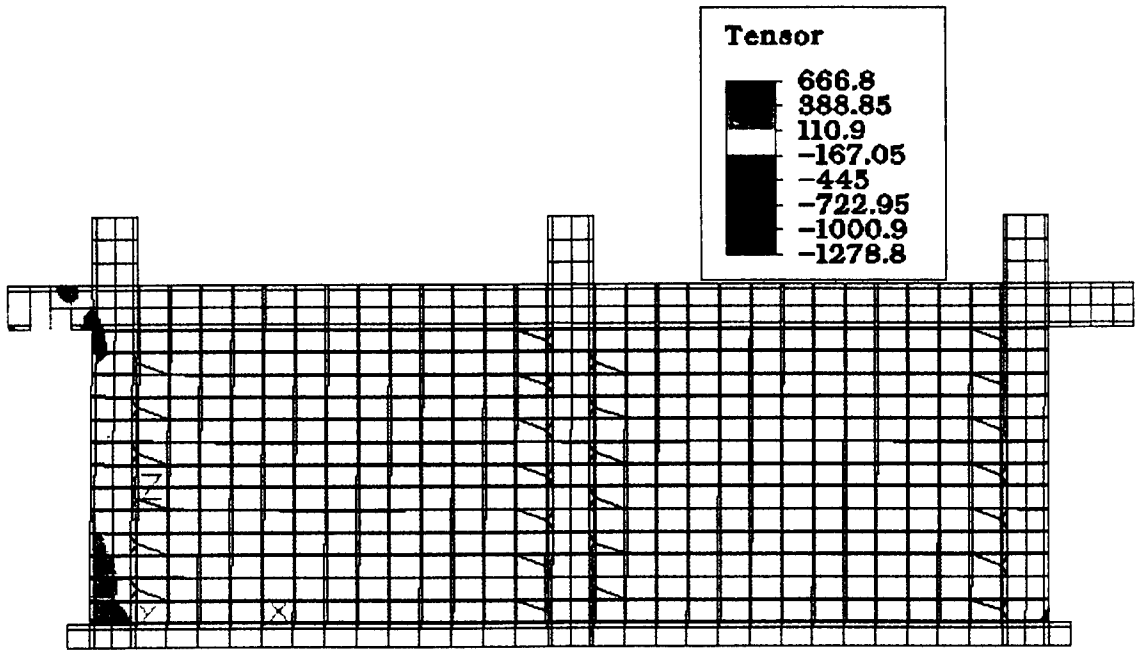

Figure 5.26 Longitudinal stress σ_{zz} for Model IV

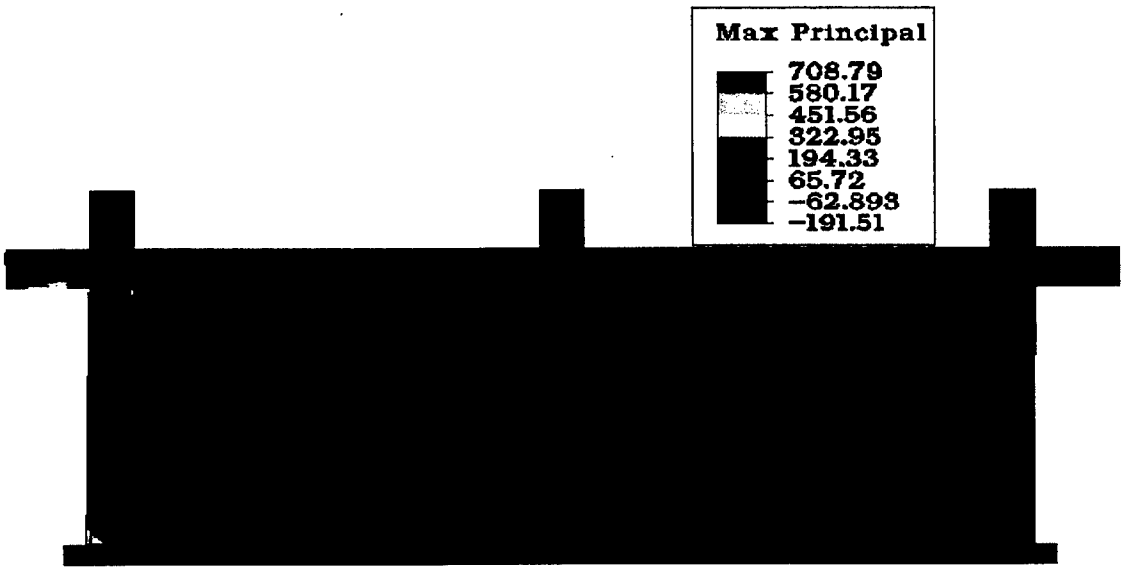

Figure 5.27 Maximum principal stress distribution for Model III at initial cracking

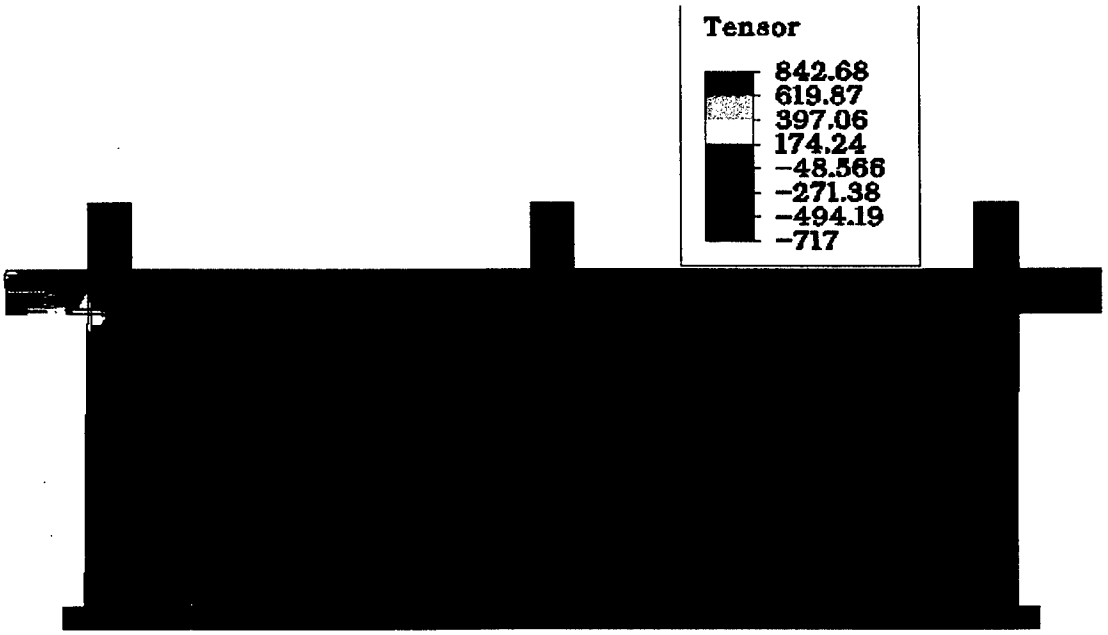

Figure 5.28 Shear stress distribution for Model IV at initial cracking

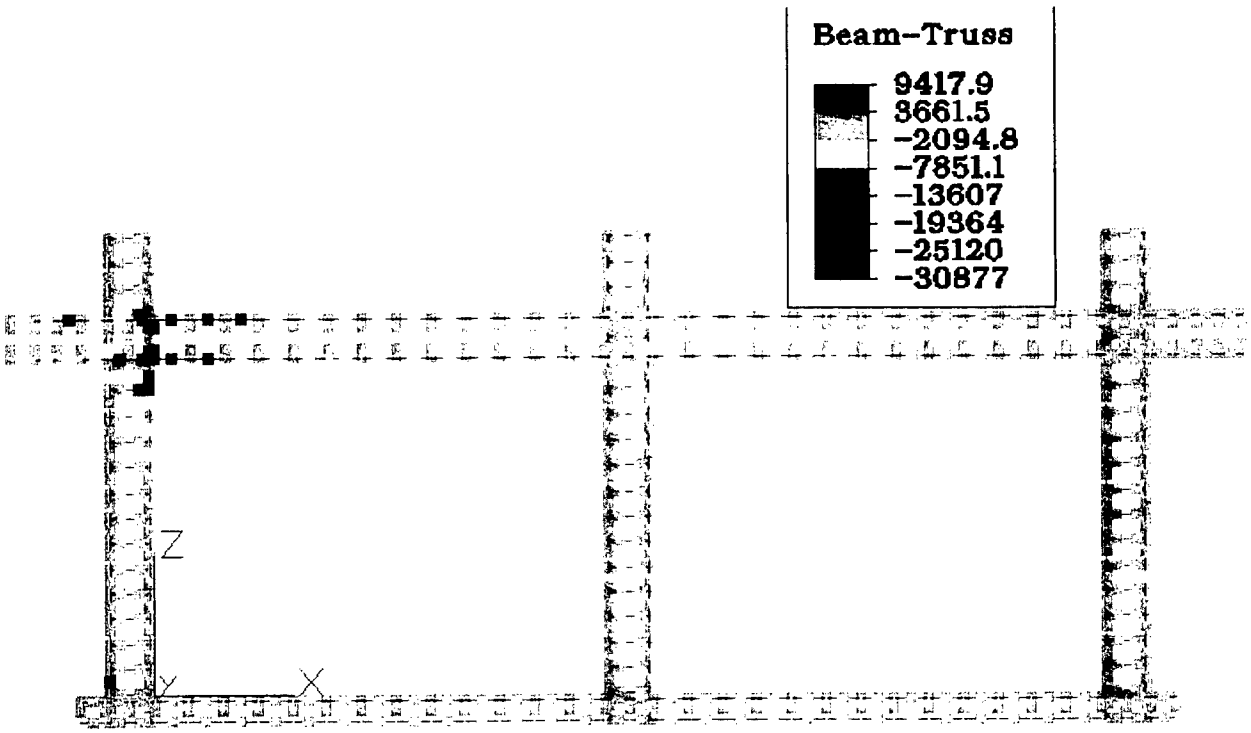

Figure 5.29 Stress distribution in steel for Model IV at initial cracking

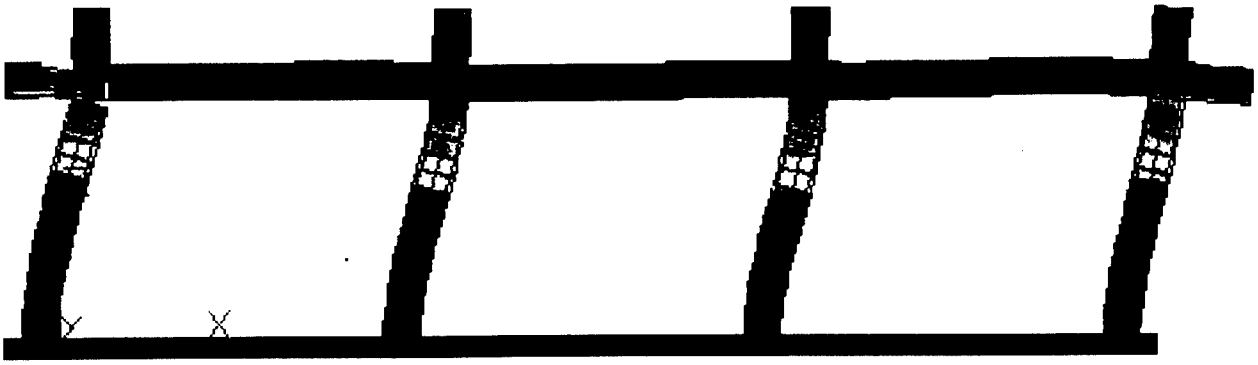

Figure 5.30 Deflection of Model V at ultimate loading

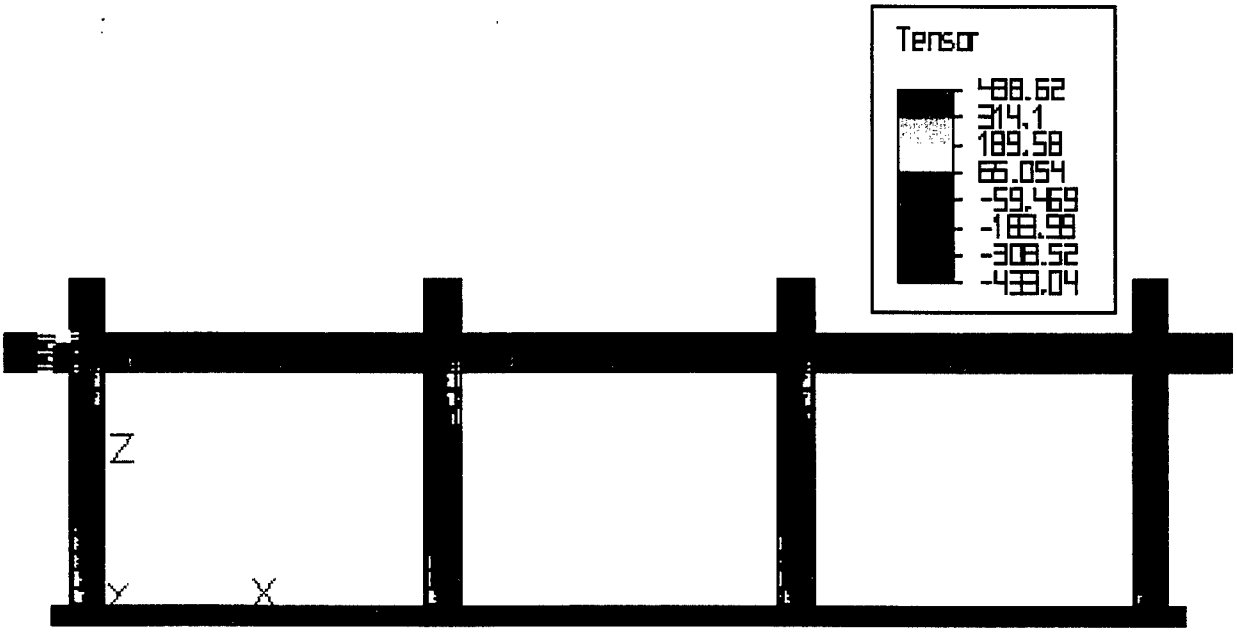

Figure 5.31 Longitudinal stress σ_{zz} for Model V

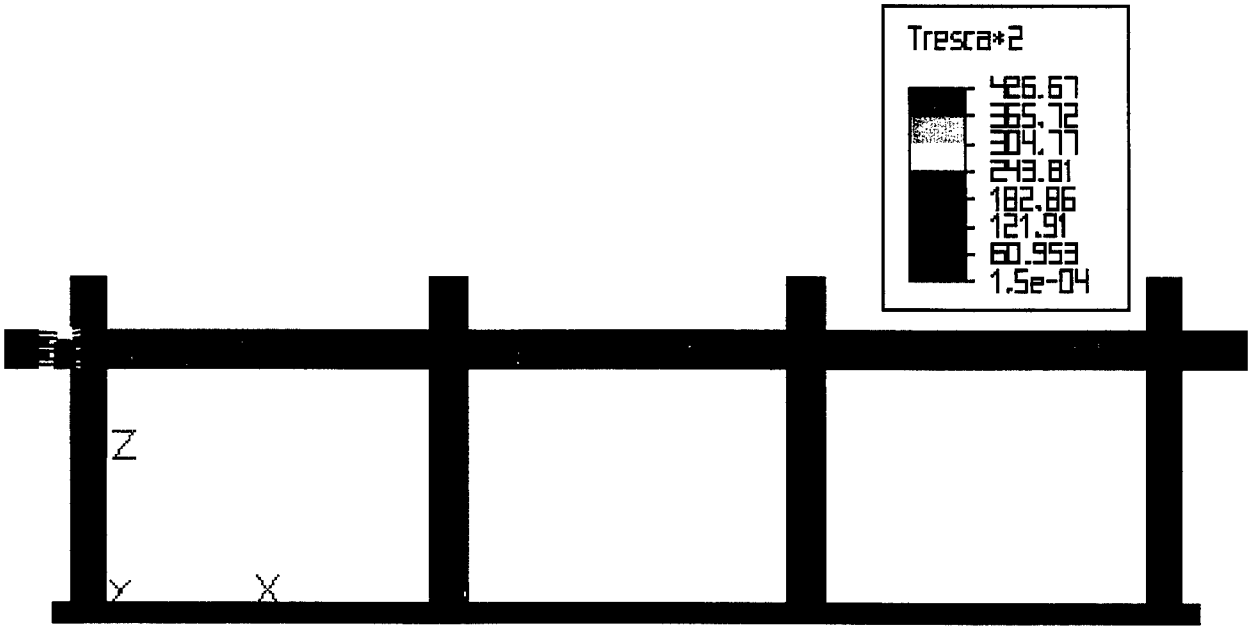

Figure 5.32 Maximum principal stress distribution for Model V at initial cracking

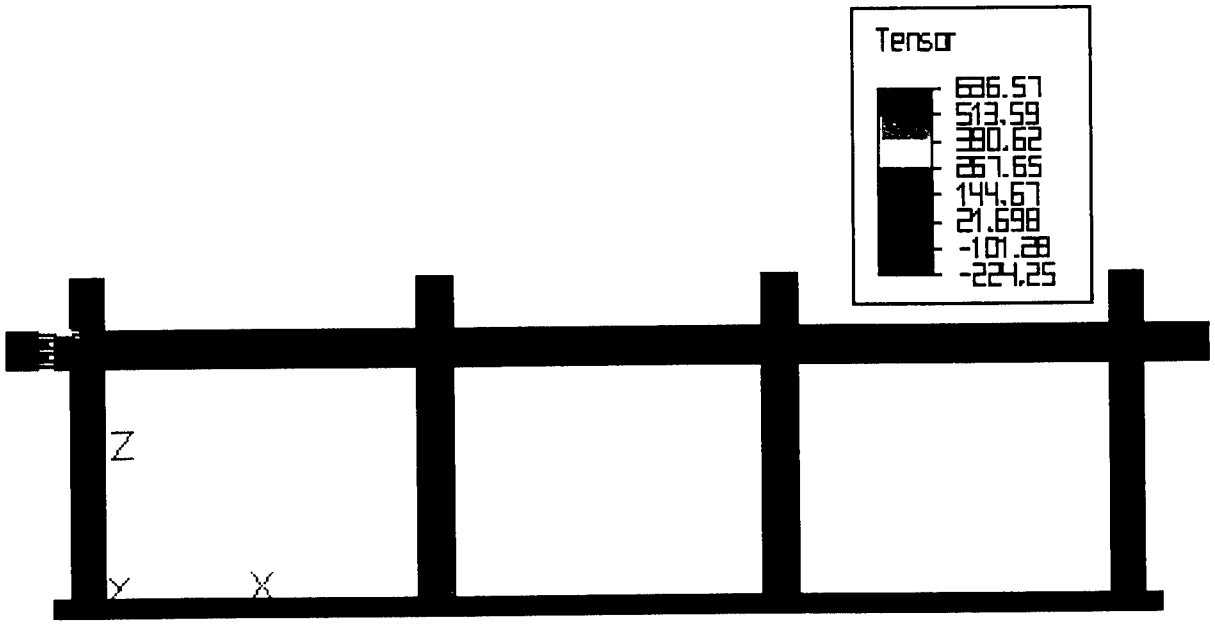

Figure 5.33 Shear stress distribution for Model V at initial cracking

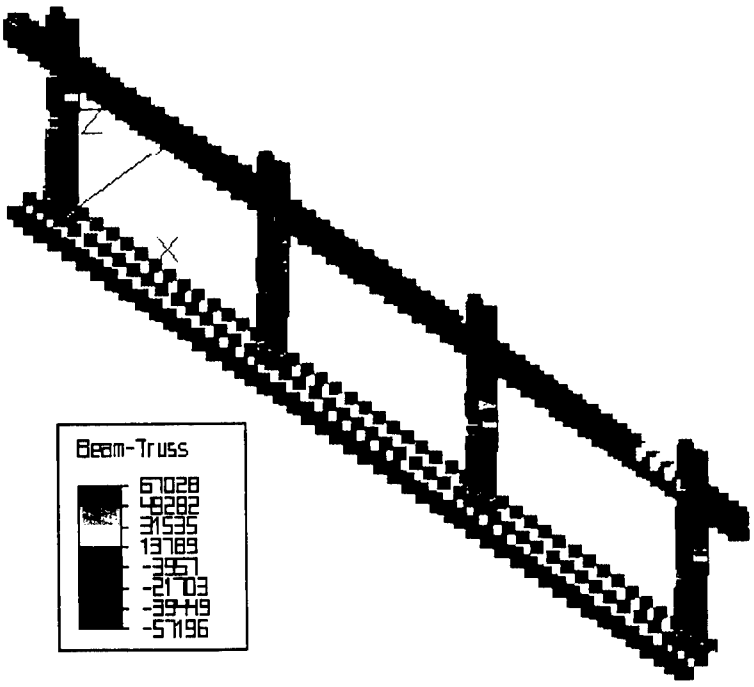

Figure 5.34 Stress distribution in steel for Model V at initial cracking

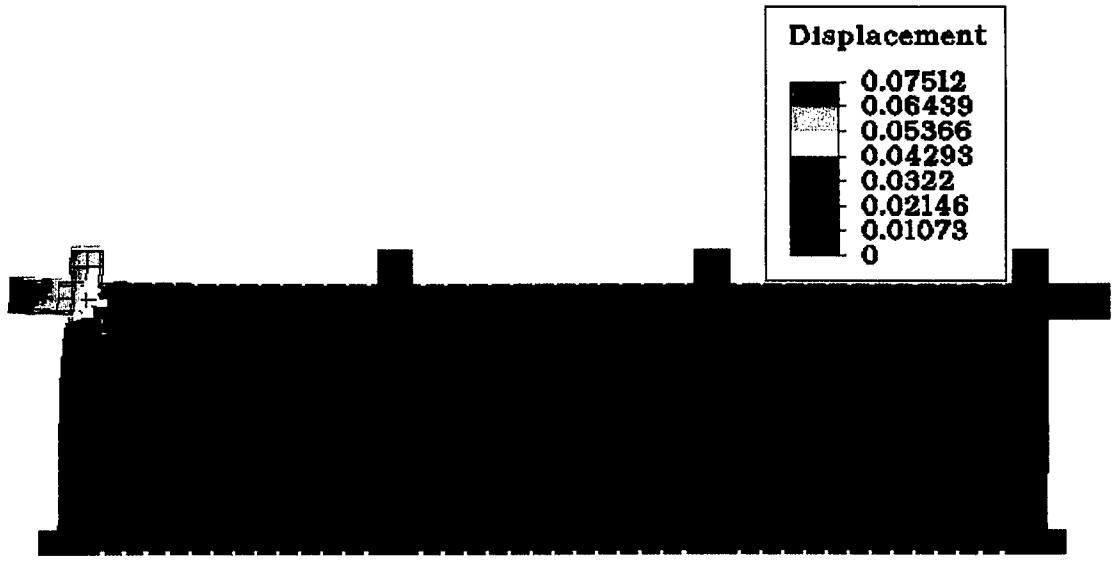

Figure 5.35 Deflection of Model VI at ultimate loading

Figure 5.36 Longitudinal stress σ_{zz} for Model VI

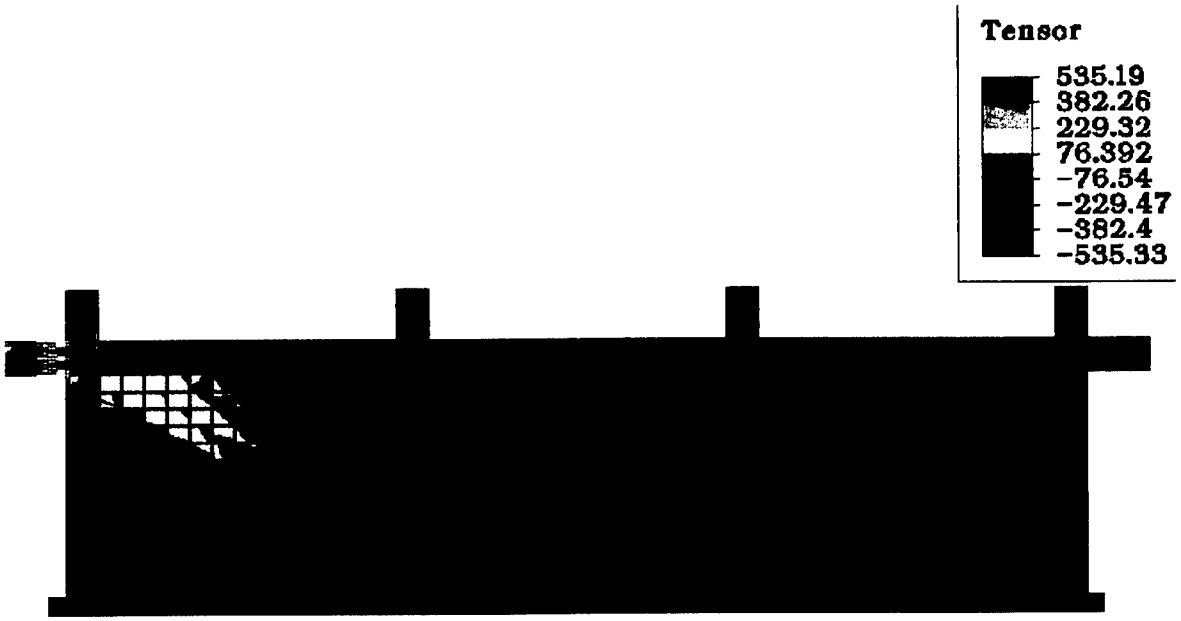

Figure 5.37 Maximum principal stress distribution for Model VI at initial cracking

Figure 5.38 Shear stress distribution for Model VI for CMU and Mortar at Ultimate

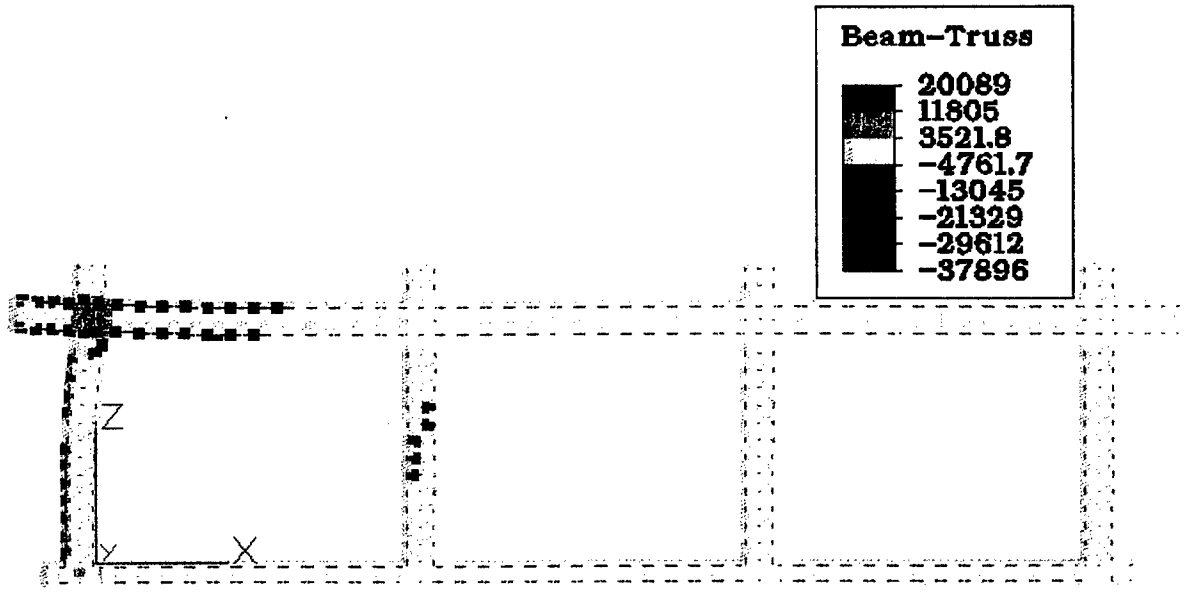

Figure 5.39 Stress distribution in steel for Model VI at initial cracks

CHAPTER 6

EXPERIMENTAL RESULTS

6.1 Introduction

In this chapter the failure mechanism of each specimen is presented. The intention of this research is to study the parameters that describe the structural behavior of the models. Parameters such as the yield strength of the models for its importance in the design of new structures, ultimate strength for its importance in the evaluation of existing structures, and residual strength for its importance for the safety of structures during earthquakes. The stiffness of each specimen is considered an important parameter for the serviceability of structures and their dynamic behaviors. Other parameters such as reinforcement strain and rotation at critical sections were also measured. Diagonal deformation of infills, gap widths at critical locations, and shear stresses (in some cases, taken at the center of the infill panels and center of joints) were all measured for each specimen. All these parameters are briefly presented and are considered the bases for identifying the behavior of this complex structural system.

6.2 Bare Frame (Model 1)

The bare frame Model 1 was tested and its failure mechanism is shown in Figure 6.1. The experimental and predicted load-deflection curves are shown in Figure 6.2, Initially the predicted load was higher than the experimental load. The predicted ultimate load for the bare frame is 5.1 kips.

The discontinuities in the bottom longitudinal reinforcement of the beam at the joint are considered to be weak links in Model 1. Cracks begin forming near the beam-column joints at

early loading. The formation of these cracks would be expected to result in stress release in the R/C frame, with a consequent redistribution of loads.

As shown in Figure 6.2, the elastic zone on the load-deflection curve was within 1 kip. The first crack visually appeared in the windward joint at 0.49 in. of lateral deformation (0.86% drift ratio). A small tension crack initiated near the top of the leeward column at 0.72 in. (1.28% drift ratio). These cracks were followed by one tension crack near the base of the windward column and a shear crack near the base of the leeward column. Both occurred at about 0.82 in. of lateral displacement (1.5 drift ratio). At a drift ratio of 5%, a sudden shear crack formed in the leeward column. Finally, at about 3.5 in. of deformation, (6.3% drift), a separation between the columns and the base beam were observed. The sequence of failure indicated the following:

1. The first crack was due to the lack of developmental length in the bottom longitudinal reinforcements. After this crack, the model behaved as a frame with a plastic hinge of a small rotational capacity, formed on the top of the windward column. The residual strength remained constant.
2. After the formation of the plastic hinge, the residual strength of the model stabilized at approximately 7.7 kips.
3. The sequence of crack formation did not result in any significant drop in the strength of the frame. The load distribution in the frame obviously changed as new cracks formed and the old cracks propagated, but the model was stable at constant strength.

The load-displacement curves at the windward joint, leeward joint, and mid-height of the columns are presented in Figure 6.3. The leeward column displaced less than the windward

column at joints and mid-height points. The difference in displacements increased beyond the formation of hinge shear cracks.

Analysis of the behavior of a single-bay, single-story bare frame subjected to in-plane loading revealed that most critical sections are, in descending order, top of the windward column, top of the leeward column, bottom of the windward column, and bottom of the leeward column. This is due to stresses from the elastic rotations at these sections.

In Figure A.1, the LVDT displacement remained linear and small within 6 kips of loading. The load-displacement curve patterns recorded on the bottom of the columns were similar. Both yielded smaller displacement on their leeward faces than on their windward faces in the nonlinear regions. The rotations of the joints were calculated from the LVDT displacements as shown in Figure 6.4. The least rotation is on the windward joints due to the formation of the hinge. The largest rotations were on the bases of columns. They were almost identical. The leeward joint rotated less than the column bases. It can be concluded that the magnitude of joint rotation in the nonlinear deformation zone reversed in order as compared to the magnitude of joint rotations in the elastic deformation zone. The tensile strain values recorded for the longitudinal bar reinforcement at a critical section near the joints were very small as presented in Figure A.2.

6.3 Single-Bay CMU Infilled Frame (Model 2)

The instrumented side of the single-bay frame infilled with CMU is shown in Figure 6.5. The cracks were surveyed on the other side at various stages of damage. A picture of the model before testing is shown in Figure 6.6. Figures 6.7 - 6.10 show the sequence of failures. The first crack observed was a sudden stair crack in the infill. It occurred at 0.4 in. of in-plane

deformation. At 0.75 in. of deformation, the first crack was followed by many cracks; specifically, a crack in the windward end of the beam, a horizontal crack in the infill three courses above the horizontal segment of the first crack, a shear crack in top of the windward column, and tension cracks above the mid-height of the windward column. As the top beam displaced one in., several tension cracks formed on the beam at two-thirds of the distance from the windward end of the beam. The beam started to curve up to form a hinge while a gap between the frame and the infill appeared on the upper windward corner of the infill. On the leeward column at 1.7 in., a shear crack formed on the bottom along with tension cracks. The crack continued to enlarge, and crushing of the CMU in the top windward corner was observed at 3.3 in. and 5.5 in. of deformation.

When the test stopped, the unsound infill was removed, as shown in Figure 6.11. The shear cracks and hinges are more pronounced in this figure. The sound infill that remained, referred to as the "survival zone," is shown in Figure 6.12. Finally, the unsound concrete was removed to reveal the most stressed section in the frames as shown in Figure 6.13.

This mode of failure is best described by the yield lines in the bound several plates, namely:

- the survival zone plate (most confined and protected)
- the upper corner of the leeward side of the infill
- the plate below the first stair crack and above the survival zone plates (most unstable)
- the remaining section

These plates distinctly tended to resist the deformation of the frame, weakening the shear resistance of the leeward column. As the strain continued to accumulate in the third plate, the strain limits were reached and crushing of the CMU occurred.

The load-displacement curves in Figure 6.14 show the measured displacements at the center of the beam, top of the infill, and center of the infill. As the first stair crack appeared, the displacement at the center of the infill did not change significantly because the center of the infill was below the crack.

It is clear in Figure 6.15 that the diagonal deformation curves, in tension and compression, within 2 in. of lateral deformation are almost mirror images of each other. The measured gap between the infill and the column at three-fourths of the column height was less than 0.04 in., as shown in Figure A.3.

The LVDTs recorded displacements are shown in Figure A.4. The highest LVDT displacement was measured in R4 and R6. The rotations calculated from the LVDT displacement are presented in Figure 6.16. The highest rotation occurred in the base of the leeward column. The smallest rotation was observed on the base of the windward column and on top of the leeward column.

The strain gages on the longitudinal reinforcement of the columns and beams exhibited consistent patterns with their corresponding rotations. Their magnitudes were below the yielding limits, but did not exhibit elastic behavior. The strains in the beams indicated that the top beam tended to deform in a double-curvature manner.

6.4 Single-Bay Brick Infilled Frame (Model 3)

Figure 6.17 is a snapshot of the instrumented model before testing. The model was loaded gradually, and the first crack appeared in the top of the leeward column. The first crack in the

infill initiated at 0.6 in. of deformation, as shown in Figure 6.18. This stair crack appeared almost along the diagonal of the infill. Parallel to the diagonal crack another stair crack appeared in the infill at a deformation of 1.2 in. Between the two stair cracks a diagonal strut formed was more pronounced toward the leeward bottom corner of the infill as shown in Figure 6.19. At about the same deformation level as the first stair crack, a shear crack and tension cracks formed in the middle of the leeward column, and a shear crack appeared in the leeward end of the beam. As the model was further loaded, a crack formed at 2 in. of deformation in the middle of the diagonal strut as if it had been split into two diagonal struts, as shown in Figure 6.20. Similarly, each of the two diagonal struts was split into two at 5.7 in. of deformation, as shown in Figure 6.21. Figure 6.22 shows the survival zone, a hinge in the middle of the windward column, a hinge in the windward end of the beam, the separation between the leeward column and the base beam due to failure in reinforcement development length, and a hinge in the beam at the top, two-thirds of the distance from leeward end of the beam, (which occurred at 2 in. of deformation).

This sequence of failures is different from those observed in Model 2, the single CMU infilled frame. In Model 3 there is the physical formation of an obvious diagonal strut, whereas in Model 2, yield lines formed distinct plates. These two different modes of failures to the fact that the brick model is characterized by high prism strength and low shear strength, whereas the CMU infill is characterized by lower prism strength and higher shear strength. It may be that the ratio of prism strength to the shear strength can serve as a new parameter to predict which mode of failure will prevail.

The load-displacement curve in Figure 6.23 shows the measured displacements at the center of the beam, top of the infill, and center of the infill. As the first stair crack appeared, the

displacement at the center of the infill did not change significantly because the cracks formed above the center of the infill.

It is clear in Figure 6.24 that the diagonal deformation curves in tension and compression, within 2 in. of lateral deformation, were almost mirror images of each other. A 0.12 in. gap width was measured between the leeward column and the infill, as shown in Figure A.6.

The LVDT recorded displacements are shown in Figure A.8. The highest displacement was measured in R6. As the hinge formed in the top of the leeward column, that joint had more freedom to rotate. The LVDT measured displacements at the bottom of the windward column were expected to be small, but a recording error in the base of the column could result in such small displacements. The displacements measured on the leeward column were consistent. The rotations calculated from the LVDT measured displacements are presented in Figure 6.25. The highest rotation occurred in the top of the windward column. The smallest rotation was observed at the base of the windward column due to the formation of a hinge in the middle of the windward column. The rotation magnitude at the top and bottom of the leeward column were very close, but their rotations were in opposite directions. The rotation directions at the tops of columns were consistent.

The strain gages on the longitudinal reinforcement of the columns exhibited a consistent pattern with their corresponding rotations. Their magnitudes were below the yielding limits, but did not exhibit elastic behavior. The strains in the beams indicate that the top beam tended to deform in double curvature manner (see Figure A.9).

To determine the stress at the center of the infill from strain measurements, 45 degree rosette strain gages were used. Using the basic relationship between stress and strain in Mohr's circle, the measured strains were used to calculate corresponding stresses. Each rosette strain

gage measured the strain in three directions 45 degrees apart: the horizontal (ε_a), the vertical (ε_c), and the diagonal (ε_b) as shown in Figure 6.26. The shear strength is calculated using the following equation [47]:

$$\tau_{max} = \frac{E}{2(1+\nu)}\sqrt{(\varepsilon_a + \varepsilon_c)^2 + [2\varepsilon_b - (\varepsilon_a + \varepsilon_c)]^2}$$

where,

E = modulus of elasticity of the brick masonry units

ν = Poisson's ratio of the brick masonry units

This equation was used to convert the recorded strain data into absolute shear stress values. The strain data measured in each channel are shown in Figure 6.26, while the load-shear stress curves are shown in Figure 6.27. The maximum value reached is about 285 psi. This value is much higher than the value obtained from a raking test due to the confinement of the R/C frame.

6.5 Double-Bay Brick Infilled Frame (Model 4)

Model 4, before testing, is shown in Figure 6.28. Figures 6.29 – 6.34 show the failure mechanism by the formation of two hinges on the top of the windward and center columns, semi-diagonal cracking in the infill, and shear cracking in the base of the leeward. After the formation of these cracks, the strength of the model is attributed to the rotational capacity of the two hinges and shear friction between the survival zone plate in the leeward infill and the plates formed above it. The sequence of failure was as follows:

1. Within 1.5 in. of deformation several cracks occurred, including the formation of four tension cracks on the upper two-thirds of the height of the windward column,

and the formation of three tension cracks on the upper two-thirds of the height of the center column.

2. At about 1.8 in. of deformation, a major shear crack formed on the top of the center column, a semi-diagonal crack formed in the leeward infill, a shear crack formed in the bottom of the leeward column, and separation between the infill and the frame at the top occurred near the corners. Thereafter, these corners started to crush.

3. At 2 in. of deformation, the yield lines on the leeward infill formed three plates above the survival zone plate. As the deformation continued, these plates struggled to stabilize in their confinement, while the upper corner of the windward infill continued to crush.

4. At higher deformation levels, the relative movement between the middle and top plates formed another hinge at 5.6 in. of deformation, and the cracks continued to widen while the crushed infill started to spall.

Inspection of Figure 6.35 reveal that top beam displacements were identical, while at the top of the leeward infill and center of both infill panels, displacement disengaged from the active deformed sections. The diagonal deformation reported in Figure 6.36 reflected the failure of the model where the upper corners of the windward infill had crushed and the load transferred directly to the leeward infill.

The LVDT measured displacements are given in Figure A.10. Their corresponding rotations are shown in Figure 6.37. Significant rotations were observed on the bottom of the windward column, top of the center column, and top of the leeward column. The measured strain on the longitudinal reinforcements agreed with rotation during early loading only, but later were not reliable (compare the curves in Figure A.11 and Figure 6.37). The gap widths between

infill panels and frame are shown in Figure 6.38. The largest gaps were measured in the leeward column and the windward beam at about 0.25 in. The strains measured in the rosette gages are given in Figures A.12 though Figure A.16. The corresponding shear stresses are presented in Figure 6.39. The windward joint exhibited the largest stress of all joints and the leeward infill exhibited the larger shear stress of both infill panels.

6.6 Triple-Bay Brick Infilled Frame (Model 5)

An overall view of Model 5 is shown in Figure 6.40. The failure of this specimen was dominated by shear. The modes of failure observed were the formation of four shear cracks in the four columns. Failure was also observed in a shear crack on top of the windward column, shear cracks on the leeward column, and two shear cracks on the center columns that almost lined up with windward and leeward shear cracks. The cracks in the infill formed a survival zone in each infill. The survival zone in the windward infill was the largest of the three and formed four small plated areas above it pushing on the top of the central columns. The survival zone in the center infill was shorter than the survival zone in the windward infill. The survival zone in the leeward infill was the shortest falling below a horizontal crack that propagated into a diagonal stair crack toward the bottom leeward corner of the leeward infill. Tension cracks appeared at three-fourths of the height of the windward column, one-third of the height of the leeward central column, and at the center of the beam. Also, one shear crack formed in the center of the center beam. All these failures were observed between 51 and 66 kips.

In this test, ultimate strength was adjusted to account for specimen damage from previous test trials. This adjustment in load was based on previous tests. The ultimate load was estimated to be the strength of the two-bay model plus the strength of the single-bay brick model

subtracting from the single-bay brick model the strength of a bare frame. This resulted in an 83 kips adjusted load that is only used in comparing the ultimate loads of all models. The remaining investigation was based on the unadjusted load recorded directly from the model. The author realized the difficulties of quantifying damage, but this adjustment of ultimate load represents a conservative estimate as compared with the other models.

Figures 6.41 through 6.46 show the sequence of failures at various levels of deformation. Figure 6.47 shows the load-displacement curves at the center of the three beams, the top center of each infill, and the center of each infill. The displacements at the center and windward beams were almost identical. The displacement of the leeward column did not follow the displacements of the other columns due to the formation of curvature in the beam. The displacements at the top of the infill very much followed the displacement in their beams, indicating no slippage had occurred between beams and infill panels. The displacement in the center of the infills stopped at about 0.12 in. (see Figure 6.47). This is because the displacements were measured at the centers of the infills in the survival zones.

The diagonal compression deformation of the infill panels and their load-displacement curves are shown in Figure 6.48. In the regions below ultimate strength on the load-displacement curves, the leeward infill displaced the least, whereas the center infill displaced the most. Beyond the ultimate strength points of the load-displacement curves, windward infill displaced the most while the leeward infill displaced the least due to formation of curvature in its beam.

The gaps between the beams and the infill was measured in three locations at three-quarters of the beam length from their perspective windward columns; their load-displacement curves are shown in Figure A.17. Gaps formed at about 25 kips, 35 kips, and 71 kips for the

windward beam, center beam, and leeward beam, respectively. Beyond ultimate strength, the leeward beam exhibited the highest gap width. Furthermore, the gaps between the windward infill and the windward center column, and the leeward infill and leeward column, were measured. As their load-displacement curves behaved, no displacements were measured before ultimate load. However, after ultimate load the windward gap reached about 0.3 in. while the other gaps reached about 0.02 in. only, as shown in Figure A.18.

The LVDT load-displacement curves in Figures A.19 and A.20 reveal that the measured displacement at the bases of columns across 3 in. sections increased in magnitude in a column order of 1, 2, 3, and 4, respectively. The displacements on each side occurred in opposite directions, which indicates that the neutral axis of each column fell inside it near the centerline. The LVDT measured displacement on top of the columns showed that column 4 barely recorded any significant displacement due to movement of the upper plate suppressing any rotation in the leeward joint of the model. From these LVDT measured displacements, rotations of joints were calculated, and their load-rotation curves are presented in Figures 6.49 and 6.50. Very small rotations were observed at the bottom of columns 1, 2, and 3, and at the top of column 4.

The strains measured on the longitudinal bar reinforcements were consistent with the calculated rotations. These measured strains were compared with the elastic strain of about 1700 μ in./in. (Fy / E = 49.1 ksi / 29000 ksi), and were found to exceed the yielding point at the joints when at high rotations. The generated curves were rough, and jerks were observed due to the failure nature of the complex system. The load-strain curves of the column and beam reinforcements are shown in Figures A.21 and A.22.

The rosette strain gages were placed on the center of the infill panels with one terminal in the vertical direction, one in the horizontal direction, and one diagonal at 45 degrees. The load-

strain curves for each channel were plotted as shown in Figures A.23 through A.28. The shear stresses were analyzed as described for Model 4. At about a 60 kips load, all infill panels experienced reduction in shear stresses, but at different shear stress levels of about 200 psi, 90 psi, and 130 psi for the windward, center, and leeward infill, respectively. It is obvious the survival zone in the windward infill received the highest stress build-up after a reduction in shear stresses. Shear stresses calculated from rosette gages are shown in Figure 6.51.

6.7 Experimental Initial Stiffness of Infilled Frames

6.7.1 Single-Bay Bare Frame, Single-Bay with Brick, Single-Bay with CMU, and Triple-Bay with Brick

For these specimens, the initial stiffnesses were calculated by dividing half the peak load by the deflection in the most central beam at half load:

$$K = \frac{P_{0.5\max}}{\delta_{0.5\max}}$$

The deflection $\delta_{0.5max}$ was estimated to be the value linearly interpolated from the load and deflection data of each test. The supporting data and summary of model stiffnesses are shown in Table XXII

6.7.2 Double-Bay with CMU

The method described above could not be used to determine the initial stiffness of the CMU-infilled double-bay specimen because of the significant sliding of the base beam during

the testing. The base beam was pushed across the floor approximately 0.8 in. by the actuator's applied loads. The sliding occurred in increments nearly all the way up to where the maximum load was reached for the specimen. Therefore, the sliding of the beam greatly affected the displacements measured by the yo-yo gages. The effects of the base beam sliding were accounted for simply by subtracting its displacement from the displacements of the various elements of the test specimen. The base beam tended to slide in increments where the applied loads would become sufficient to overcome the static friction of the beam on the floor. The beam would quickly slide and then come to a rest, during which time the load applied by the actuator would appreciably drop. During more advanced stages of loading, the load would not decrease all the way to zero. More than 50 such cyclical loadings were observed in the testing. This seems to be a plausible explanation since the actuator movement was set at a specified rate (i.e., displacement control was used).

During the time when the load was increasing to an amount large enough to overcome the friction between the base beam and floor, the test specimen was being loaded by the actuator as typically occurs during a proper test. Therefore, the stiffness of the specimen could be calculated for the range of loading up until the static friction was overcome. Stiffnesses were calculated during many of the recurring loadings as the test progressed, until a little more than half of the peak load was reached. Since these stiffnesses tended to vary, average stiffnesses were calculated for certain ranges of loading. Furthermore, the average stiffnesses were obtained from individual stiffnesses that were weighted by the amount of load applied in the cycle. Table XXIII shows the procedure. Based on these average stiffnesses, a deflection of 0.0439 in. was determined for a load equaling half the maximum load, and the initial stiffness of 814 kips/in was determined for the specimen.

Table XXII

Initial Stiffness of Infilled Frames Calculated from the Experimental Data

Load (kips)	Deflection (in)	Stiffness (kips/in)	Interpolated Stiffness (kips/in)
Single-Bay Bare Frame Infill			
3.81	0.1644	23	23
3.88	0.1681	23	
Single-Bay with Brick Infill			
9.71	0.0233	417	410
10.29	0.0256	403	
Single-Bay with CMU Infill			
9.36	0.0170	552	547
9.72	0.0182	534	
Three Bay with Brick Infill			
34.94	0.0394	887	923
35.75	0.0375	953	

Table XXIII

Double Bay Stiffness Calculation

Load 1	Load 2	One-Two	Stiffness	Weighted Ave.*	Avg. Stiffness	Max Load	Deflection **
-0.5	7.1	7.6	2046	15550			
-0.3	5.9	6.2	1248	7738			
0.6	7.3	6.7	975	6533			
1.2	8.8	7.6	1518	11537			
2.3	9.4	7.1	3424	24310			
3.0	10.3	7.3	1664	12147			
3.5	10.7	7.2	1657	11930			
2.6	11.6	9.0	2086	18774			
6.3	12.8	6.5	1048	6812			
8.5	14.5	6.0	2422	14532	1824	15	0.00822
14.3	19.4	5.1	827	4218			
16.7	21.1	4.4	1418	6239			
18.7	24.4	5.7	761	4338	973	23	0.00822
21.7	26.9	5.2	340	1768			
26.9	28.4	1.5	765	1148			
25.3	30.2	4.9	1105	5415			
30.7	32.5	1.8	793	1427			
31.0	35.6	4.6	372	1711			
26.8	37.2	10.4	929	9662			
34.9	38.5	3.6	652	2347	734	35.7	0.02746
35.7							0.04390
Stiffness = 814 kips/in.							

* Weighted by difference between Load 1 and Load 2.

6.8 Experimental Ultimate and Residual Strength of All Models

The ultimate and residual strengths of each model are listed in Table XXIV. The residual strength was defined as the minimum load beyond ultimate and within a 9% drift ratio. Load-displacement curves are presented in Figures 6.52 and 6.53.

Table XXIV

Summary of Ultimate and Minimum Residual Strengths of All Models

Model	Ultimate Strength (kips)	Minimum Residual Strength* (kips)	Percentage Residual Strength To Ultimate
Single-Bay Bare Frame Infill	7.7	5.9	76.6%
Single-Bay with Brick Infill	20.0	14.8	74.0%
Single-Bay with CMU Infill	18.9	13.5	71.4%
Double-Bay with CMU Infill	71.4	27.6	38.7%
Triple-Bay with Brick Infill	83.0	59.5	71.7%

* Within 9% drift ratio

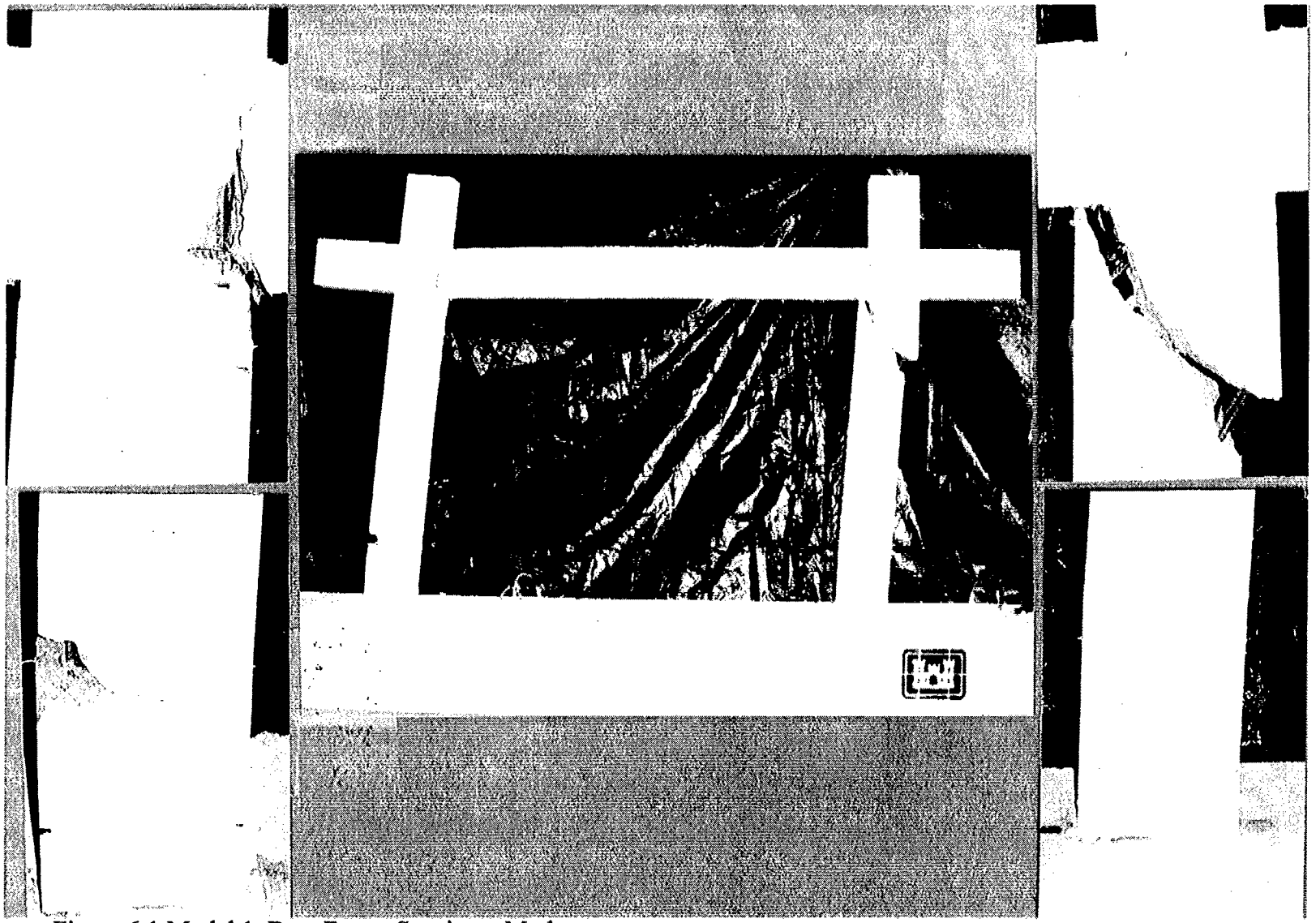

Figure 6.1 Model 1, Bare Frame Specimen Modes

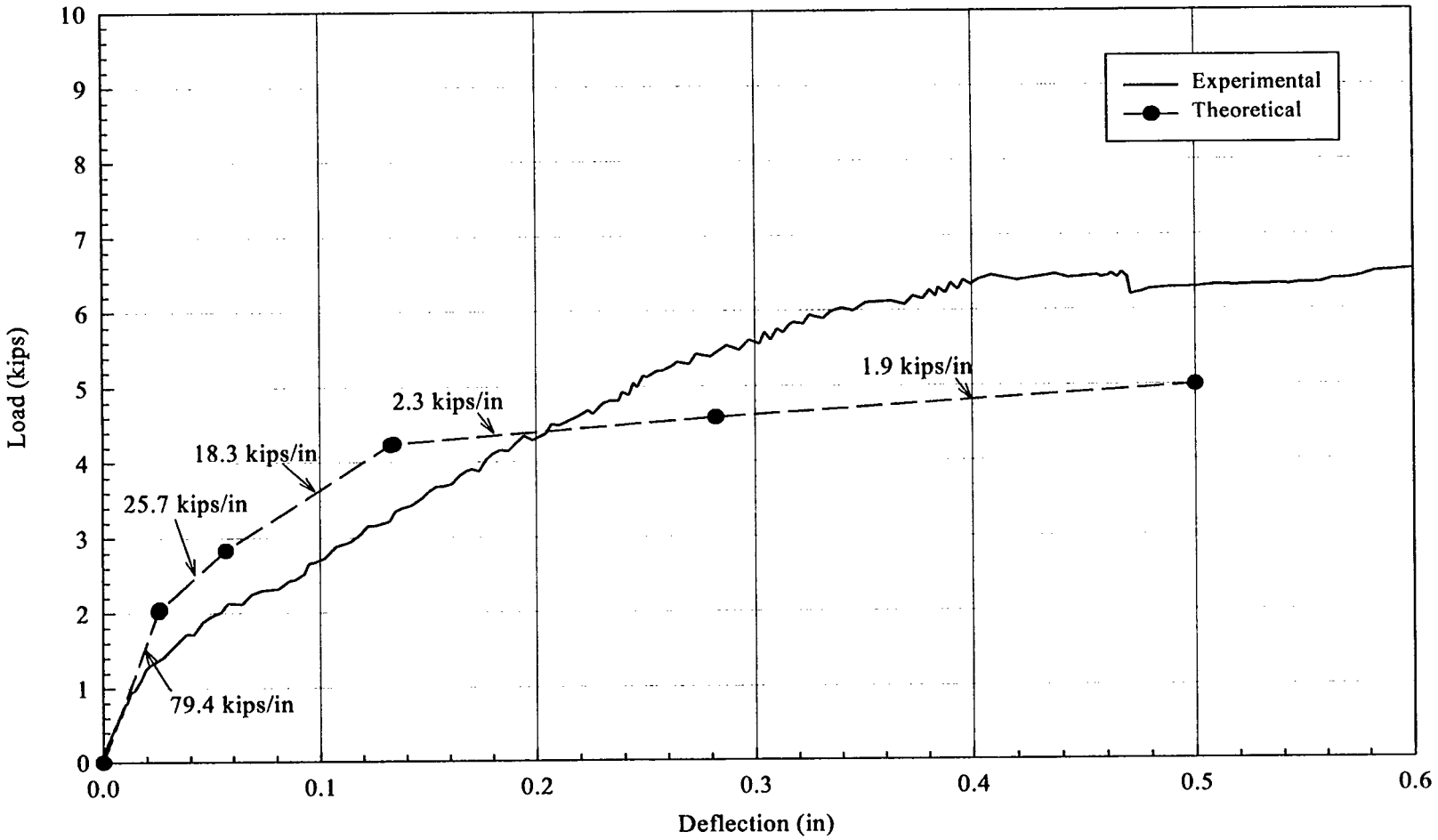

Figure 6.2 Model 1, Experimental and Theoretical Load-Deflection Curves for Bare Frame Specimen

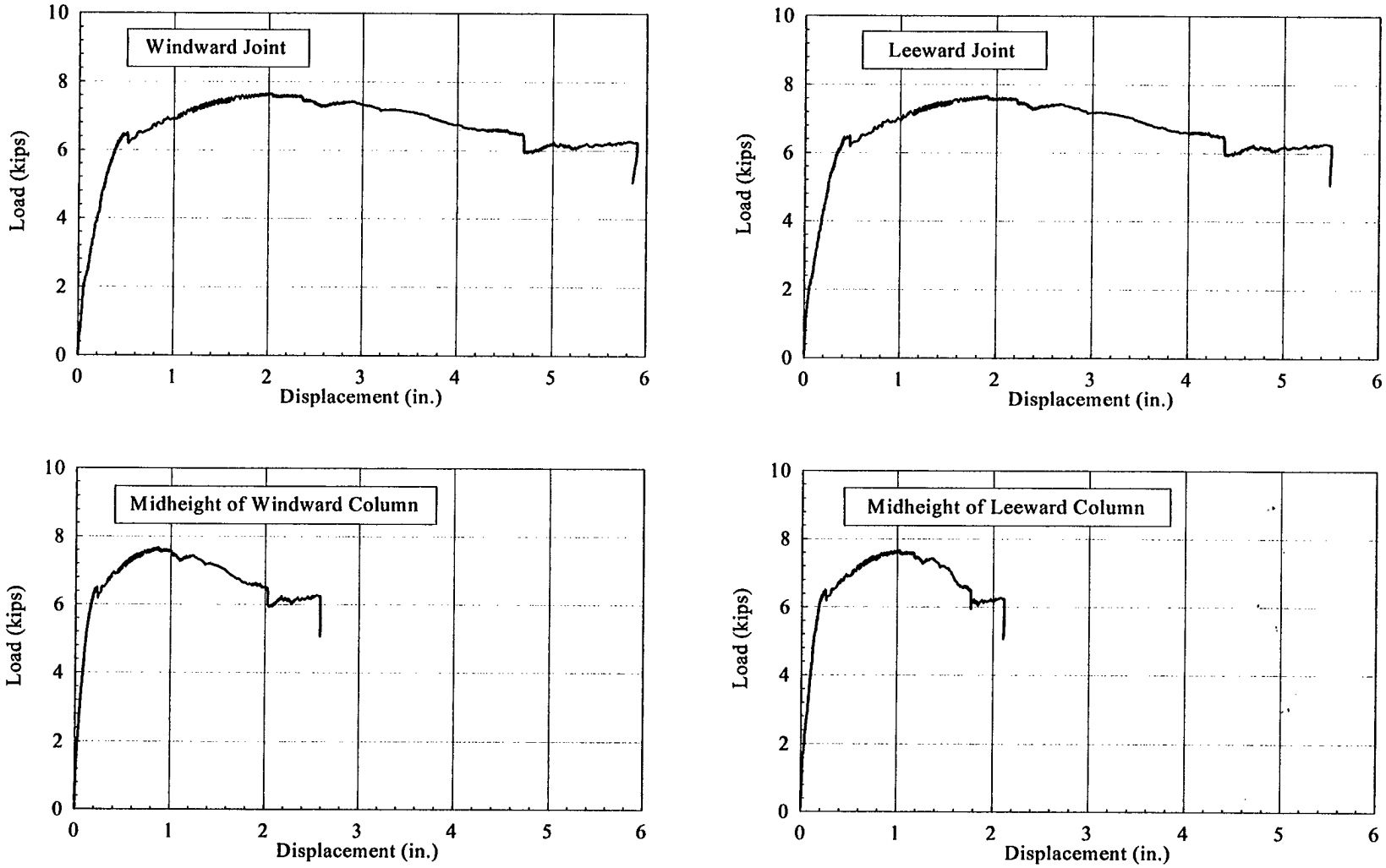

Figure 6.3 Model 1, Single-Bay Frame Specimen Lateral Displacement

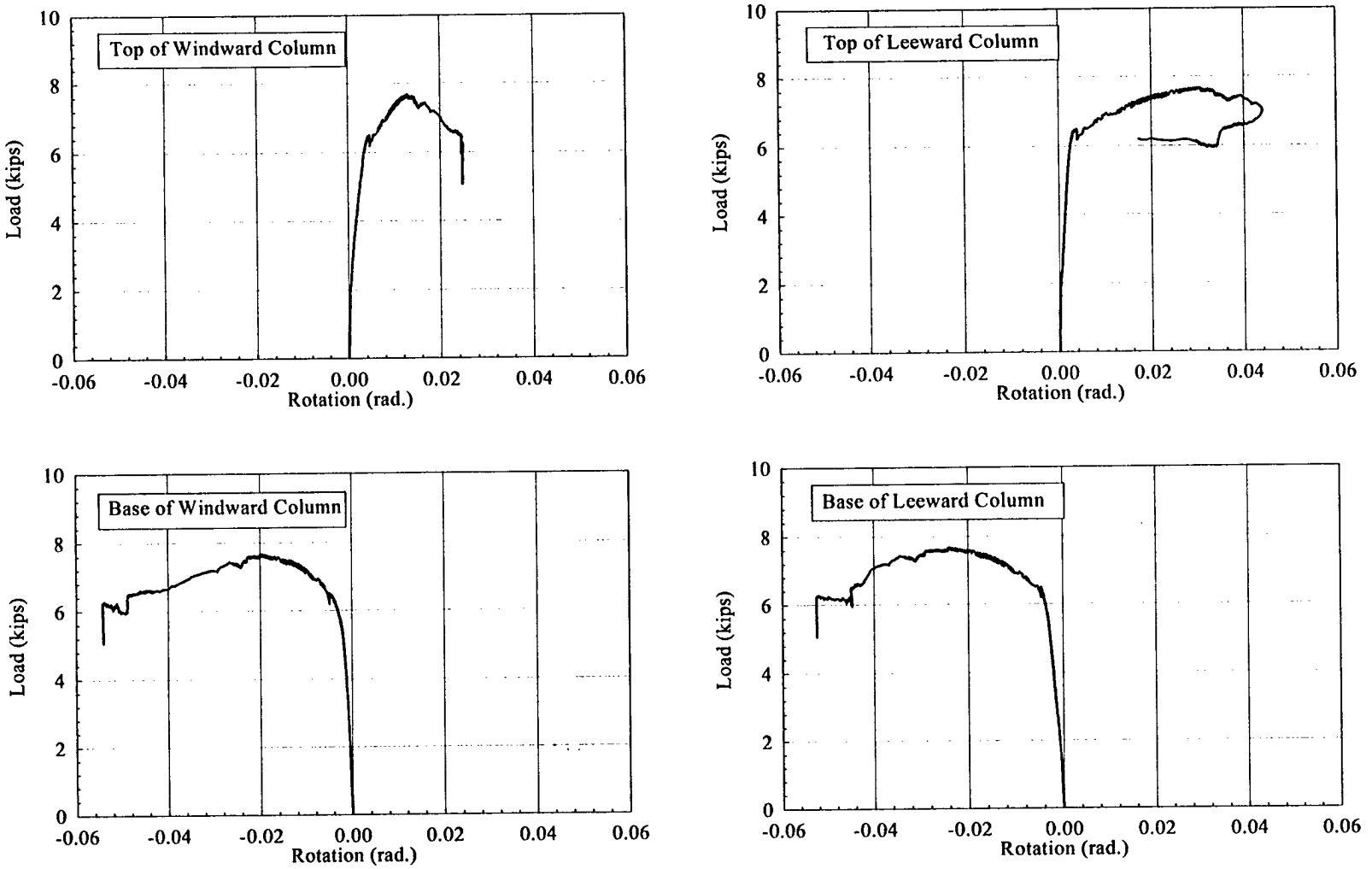

Figure 6.4 Model 1, Single-Bay Bare Frame Specimen Rotations

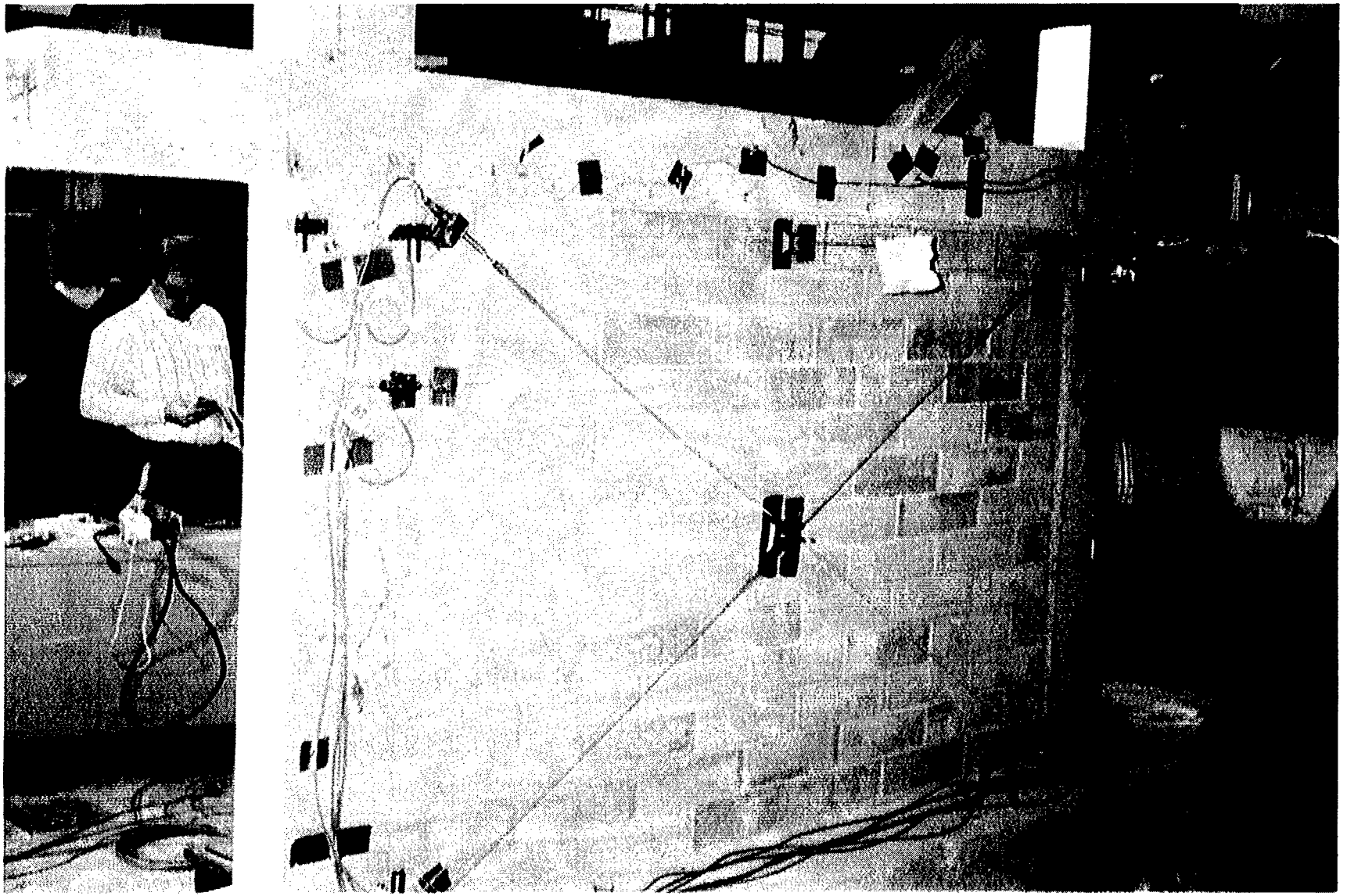

Figure 6.5 Model 2, Intrumentation of Single-Bay CMU-Infilled Frame

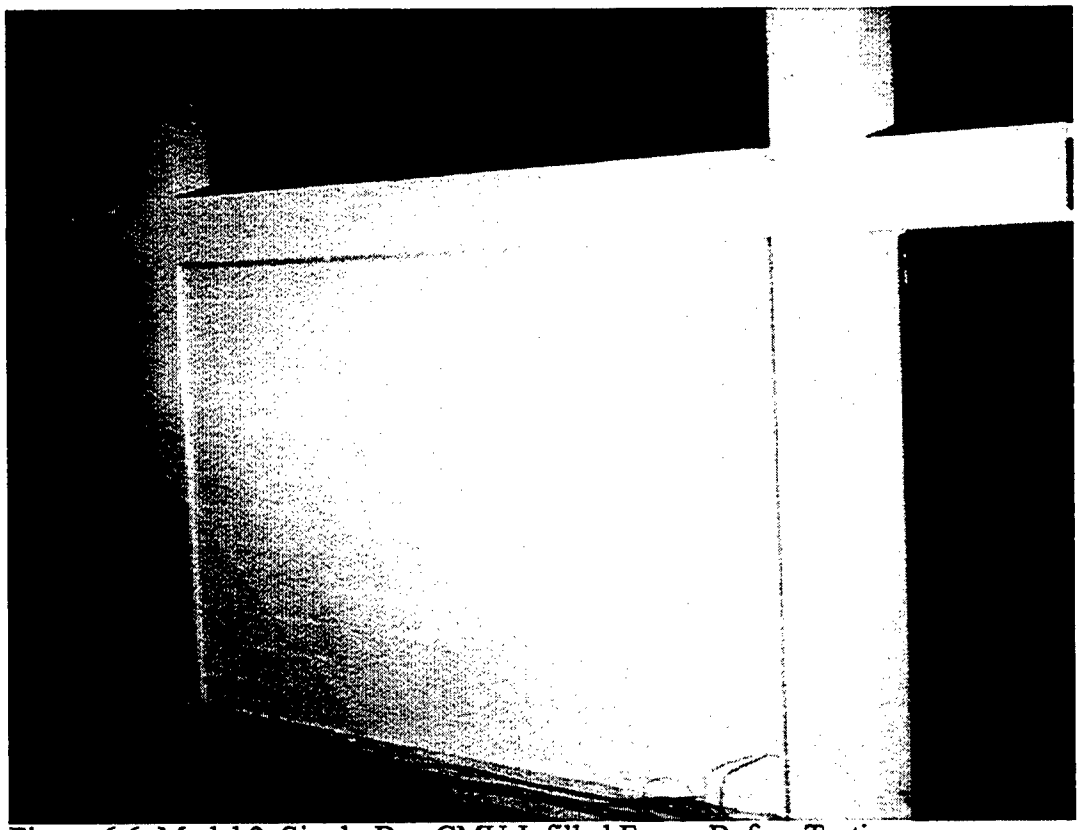

Figure 6.6 Model 2, Single-Bay CMU-Infilled Frame Before Testing

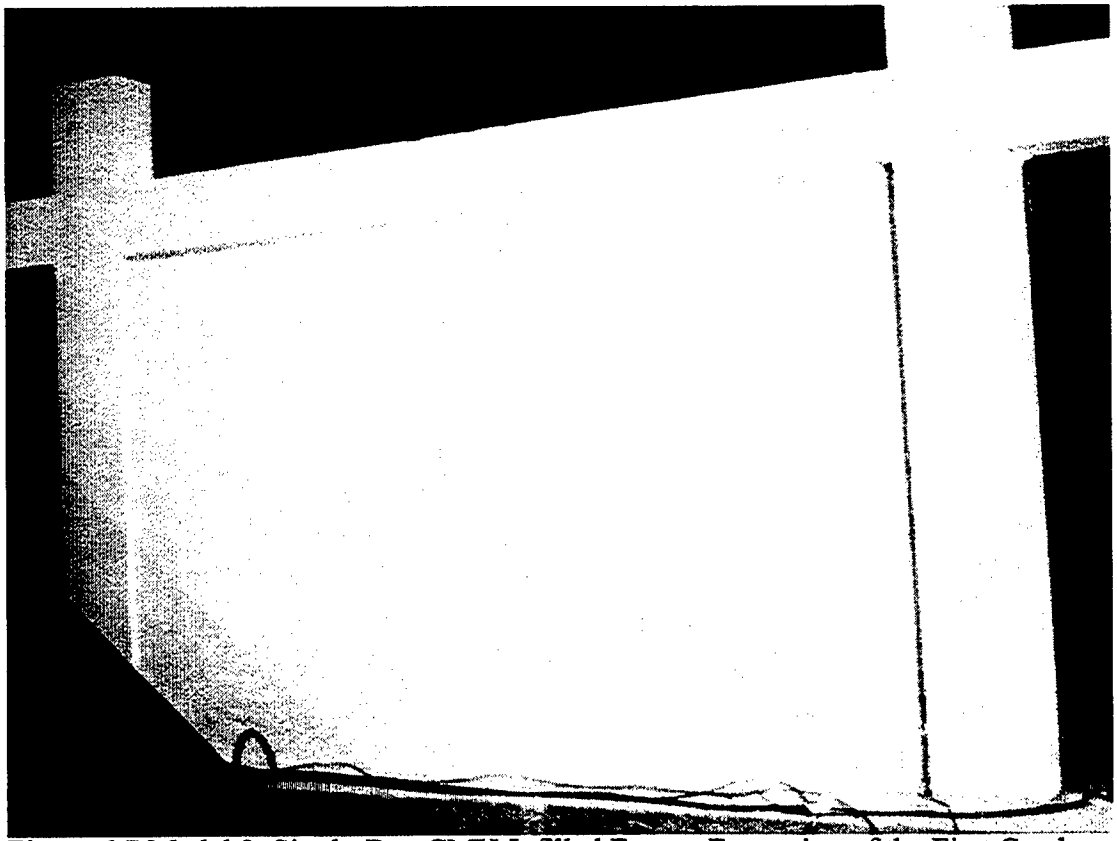

Figure 6.7 Model 2, Single-Bay CMU-Infilled Frame, Formation of the First Crack

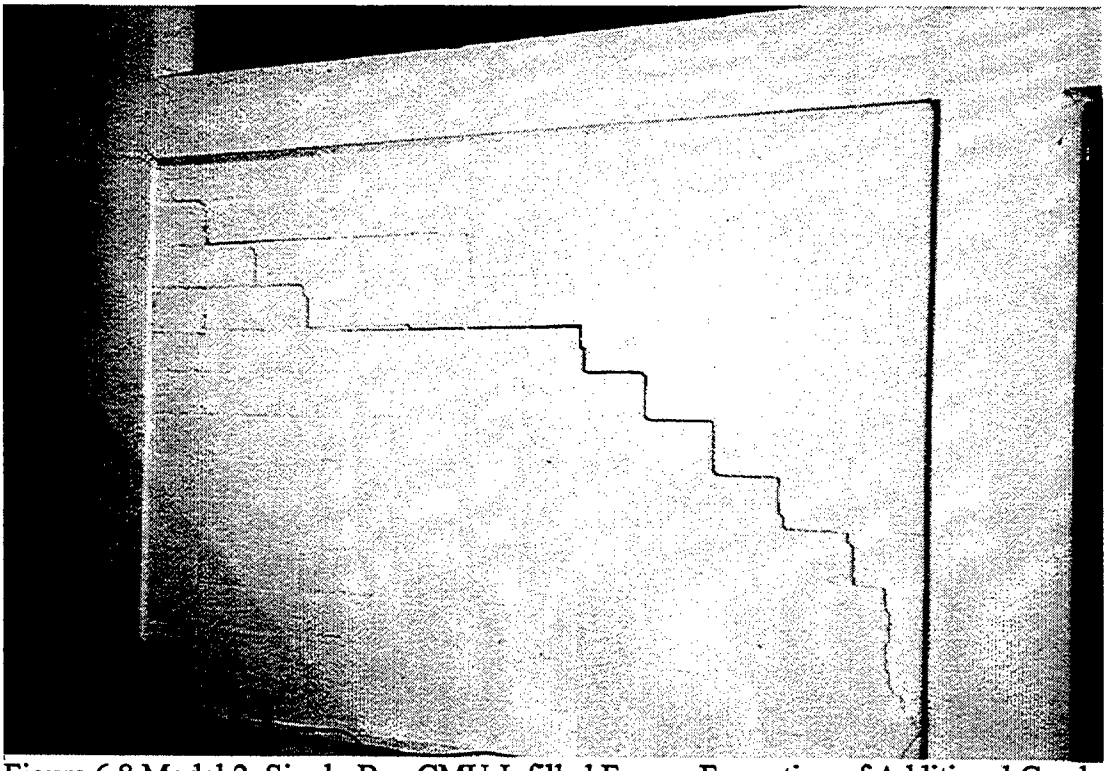

Figure 6.8 Model 2, Single-Bay CMU-Infilled Frame, Formation of Additional Cracks

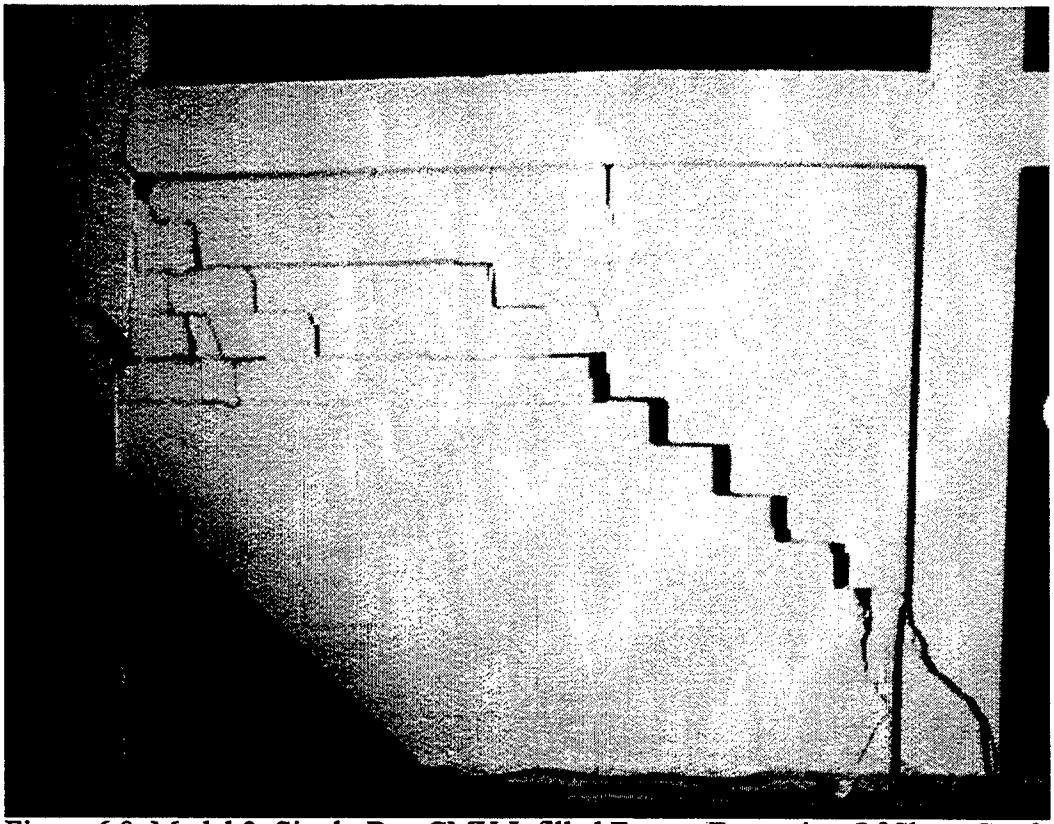

Figure 6.9 Model 2, Single-Bay CMU-Infilled Frame, Formation Of Shear Crack In The Leeward Column

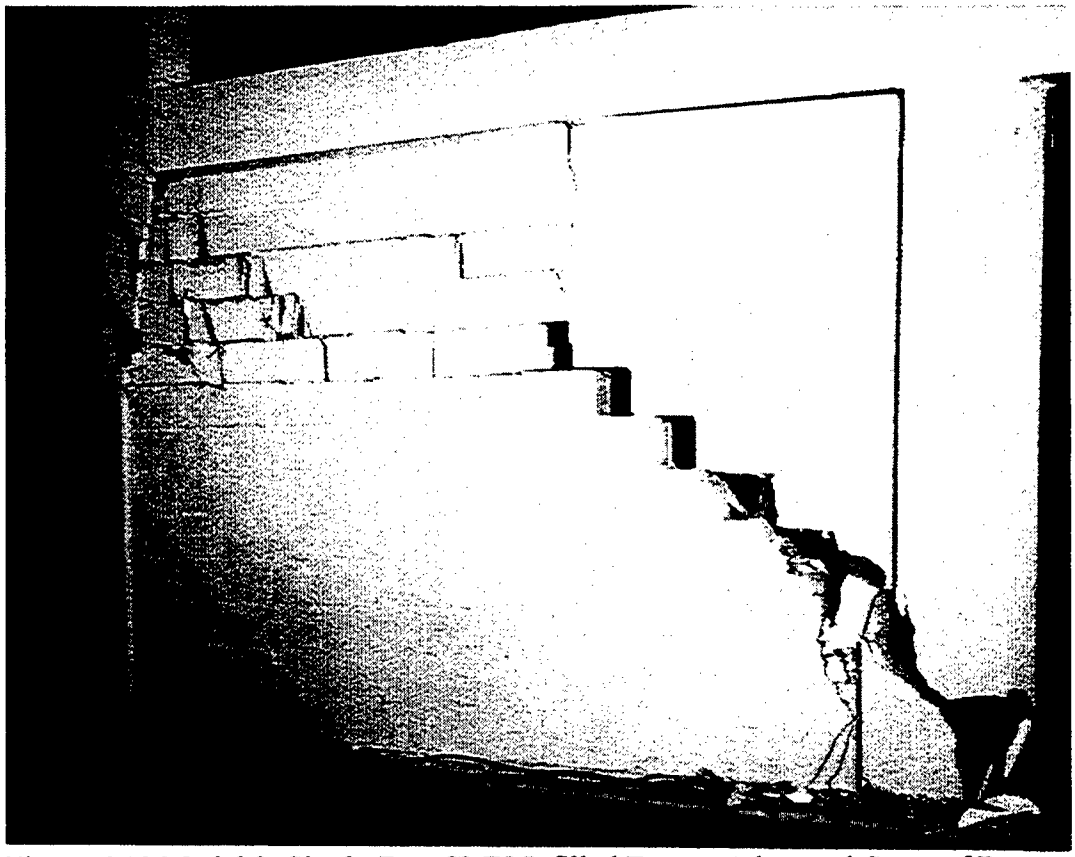

Figure 6.10 Model 2, Single-Bay CMU-Infilled Frame, Advanced-Stage of Damage

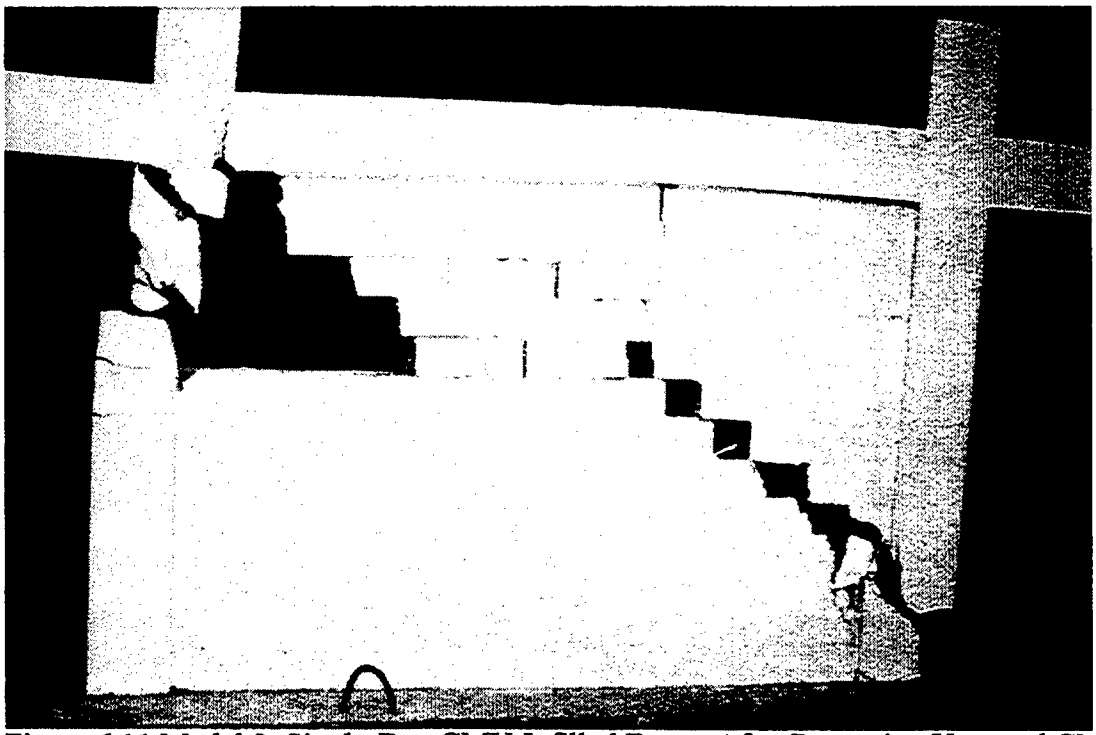

Figure 6.11 Model 2, Single-Bay CMU-Infilled Frame After Removing Unsound CMU Blocks From Crushed Corner

Figure 6.12 Model 2, Single-Bay CMU-Infilled Frame After Removing Unsound CMU Blocks Above the Survival Zone

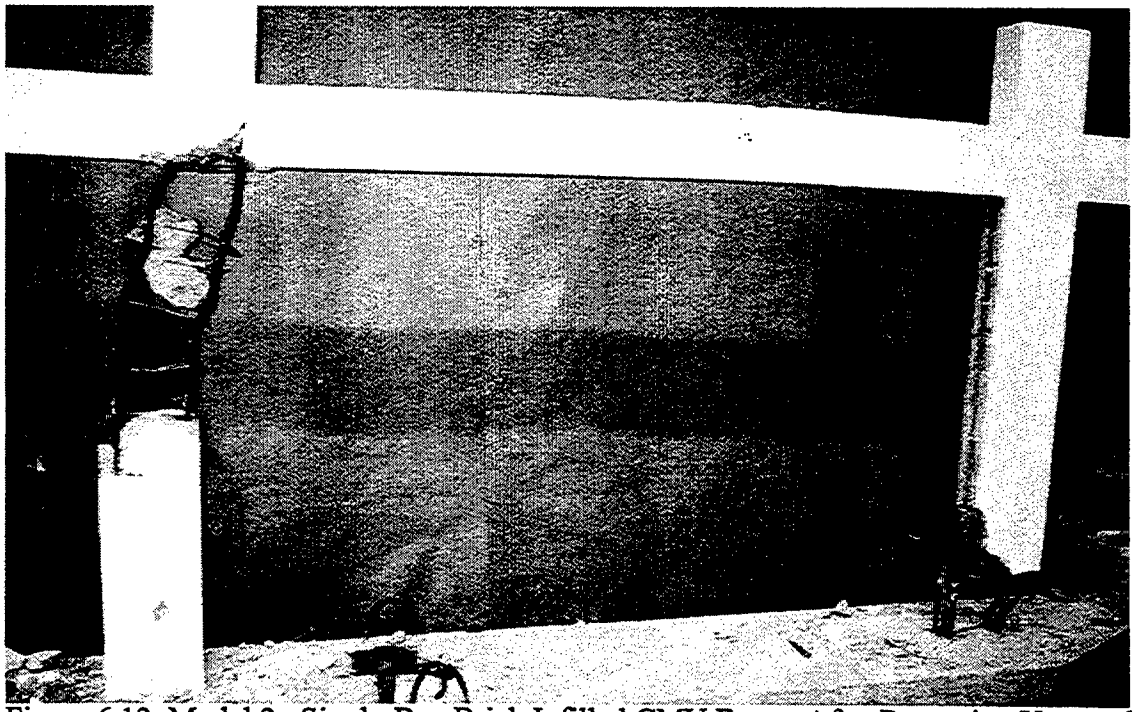

Figure 6.13 Model 2, Single-Bay Brick Infilled CMU Frame After Removing Unsound Concrete

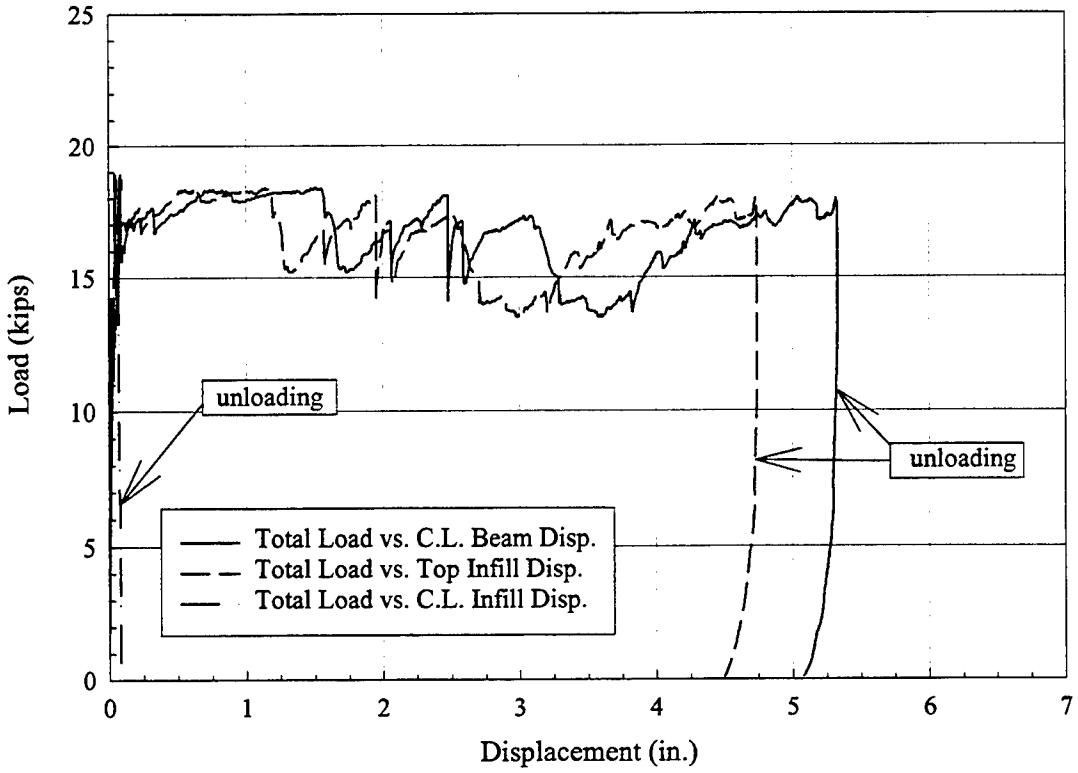

Figure 6.14 Model 2, Single-Bay CMU Infilled Specimen Lateral Displacement of Infill and Frame

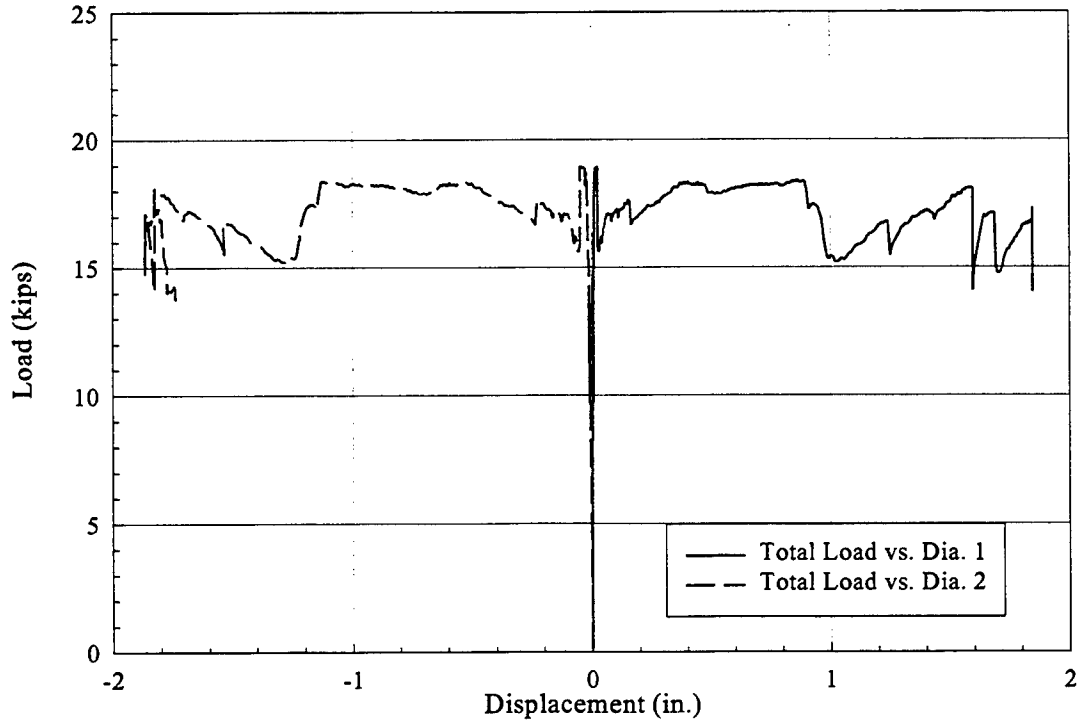

Figure 6.15 Model 2, Single-Bay CMU Infilled Specimen Displacements Across the Diagonals

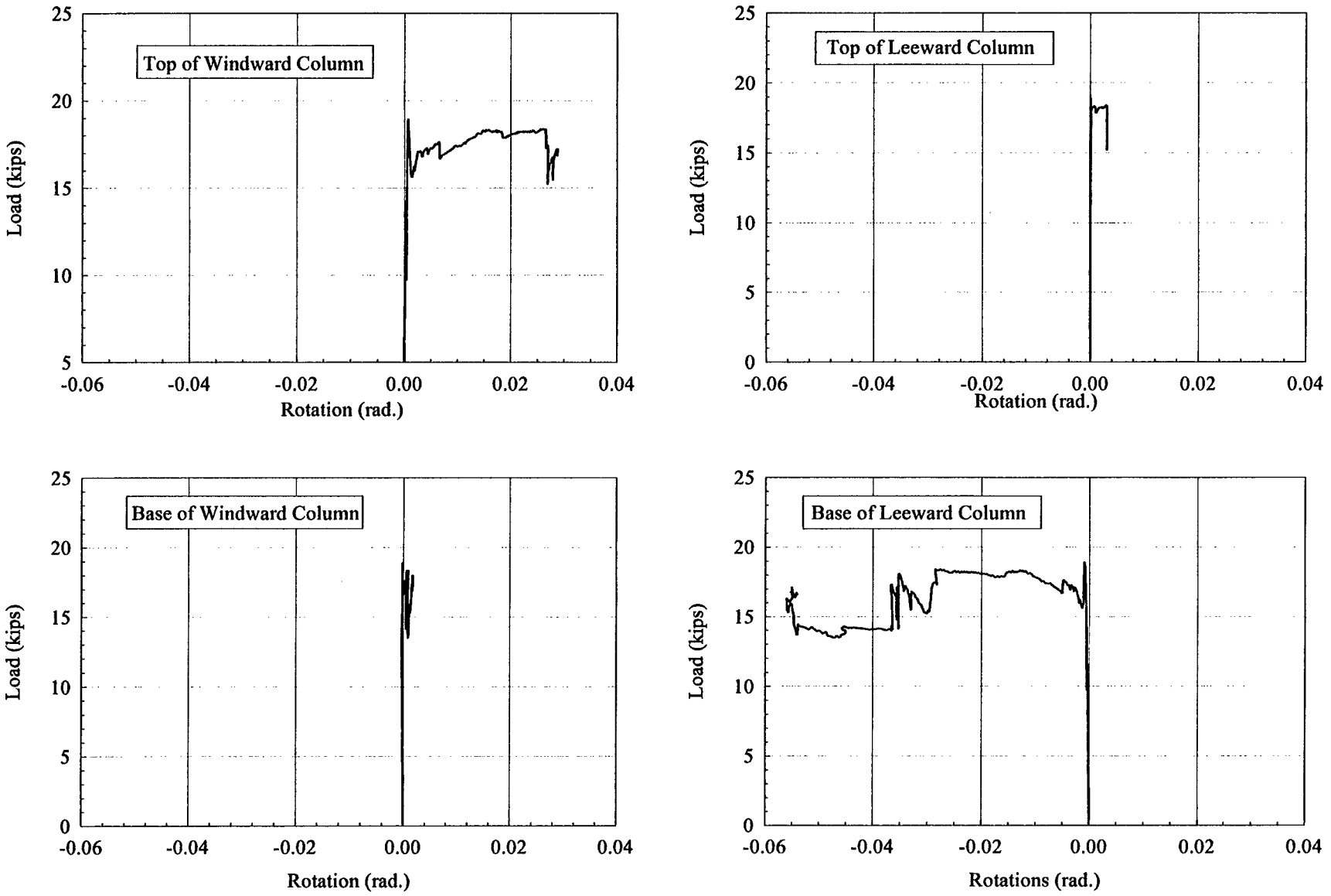

Figure 6.16 Model 2, Single-Bay CMU Infilled Specimen Rotations

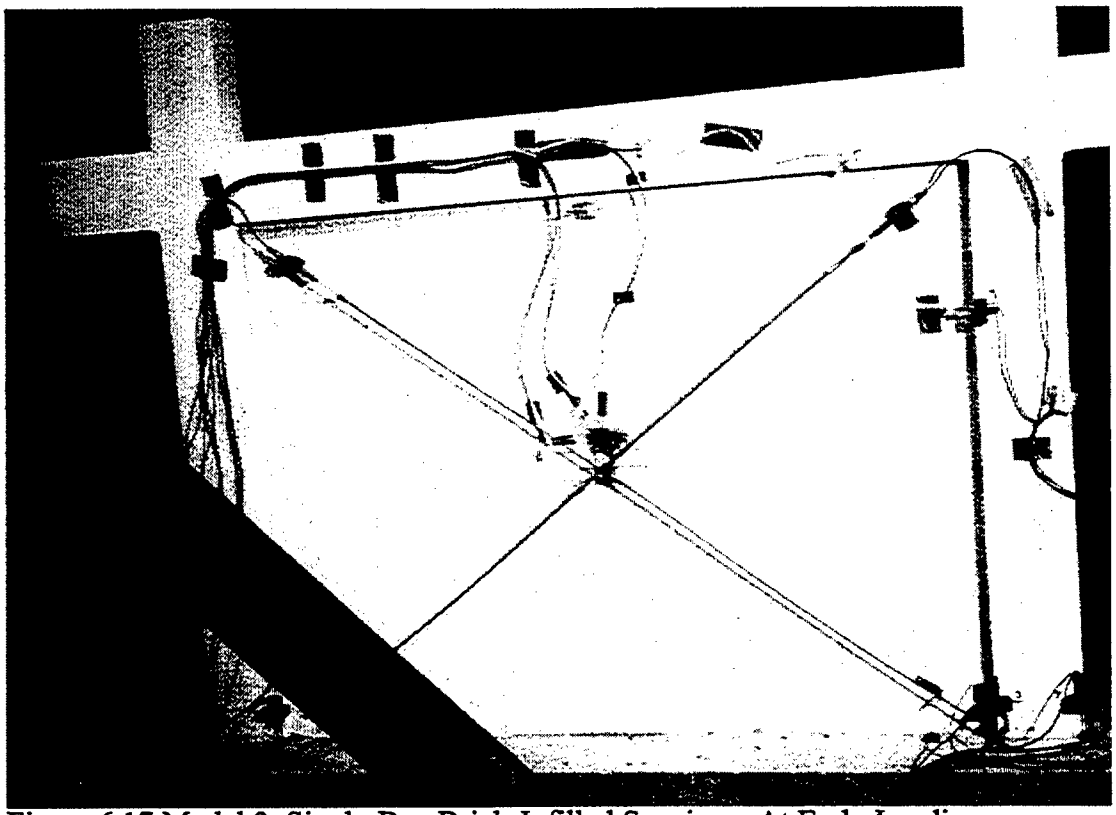

Figure 6.17 Model 3, Single-Bay Brick-Infilled Specimen At Early Loading

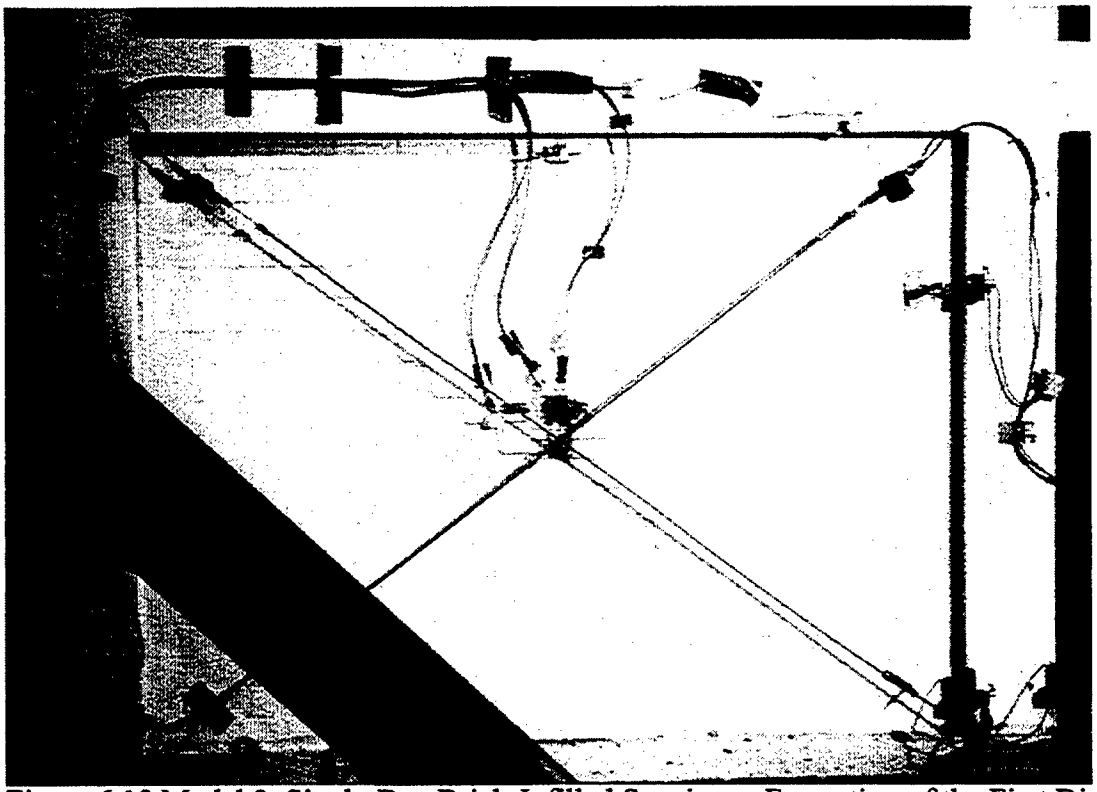

Figure 6.18 Model 3, Single-Bay Brick-Infilled Specimen, Formation of the First Diagonal Crack in the Infill

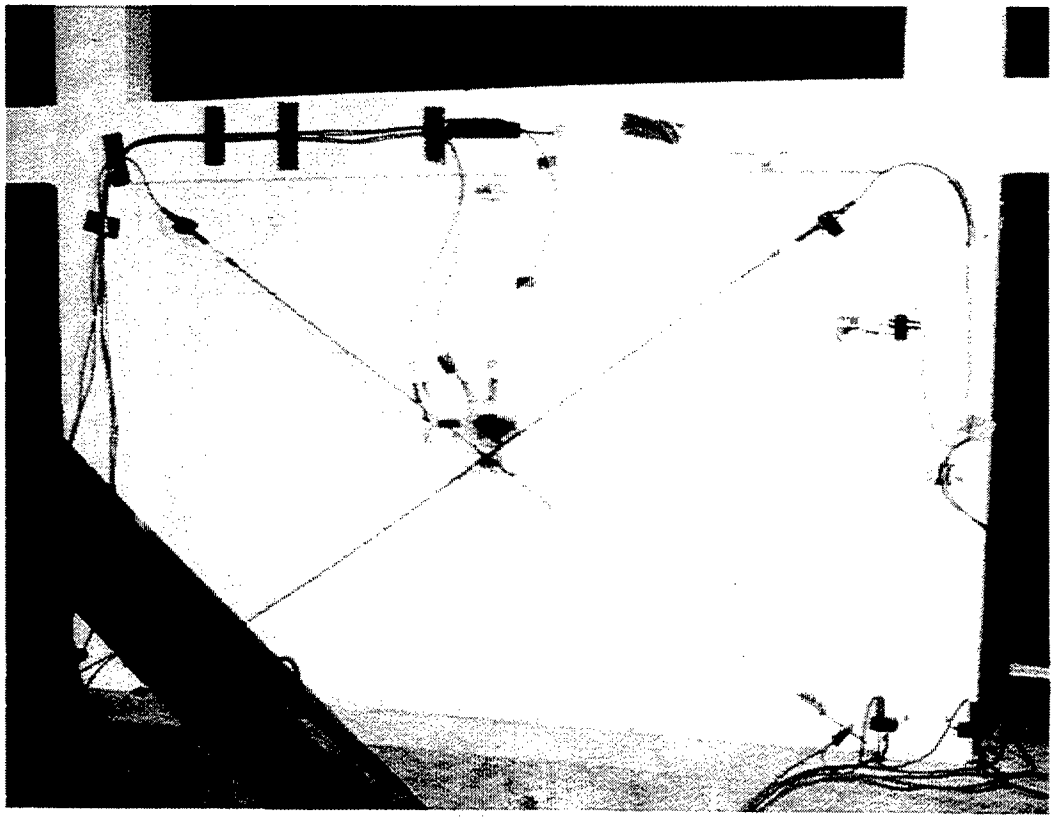

Figure 6.19 Model 3, Single-Bay Brick-Infilled Specimen, Formation of Diagonal Strut

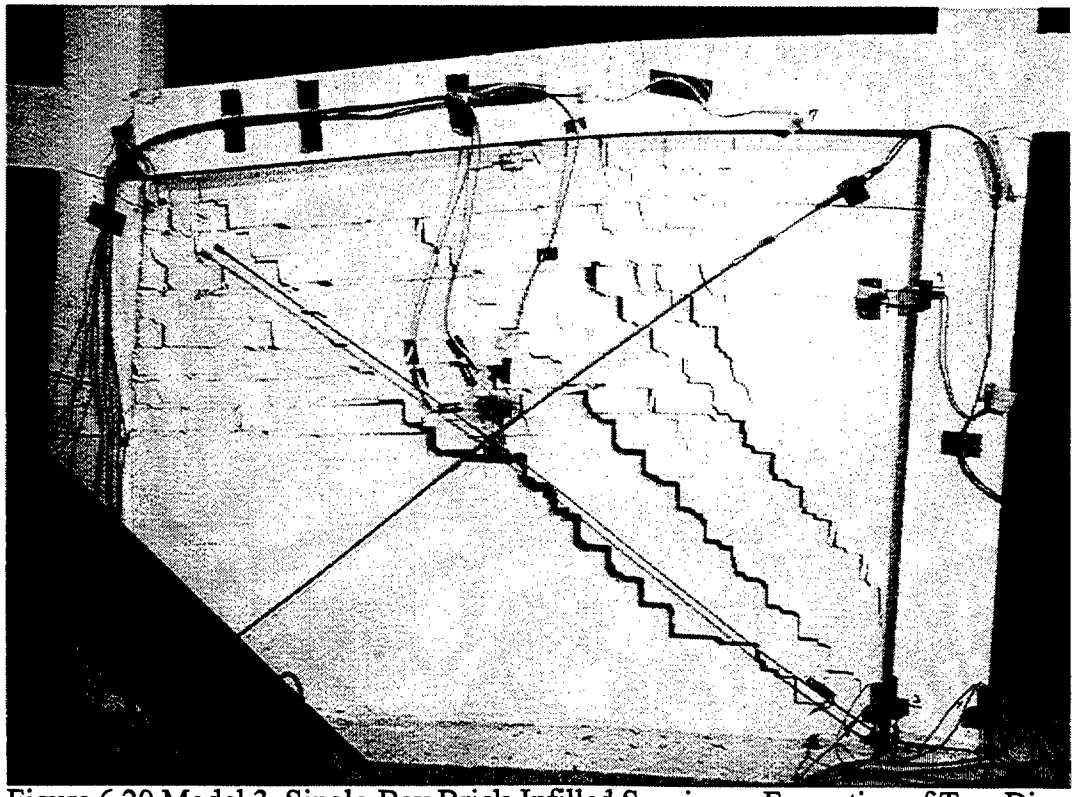

Figure 6.20 Model 3, Single-Bay Brick-Infilled Specimen, Formation of Two Diagonal Struts

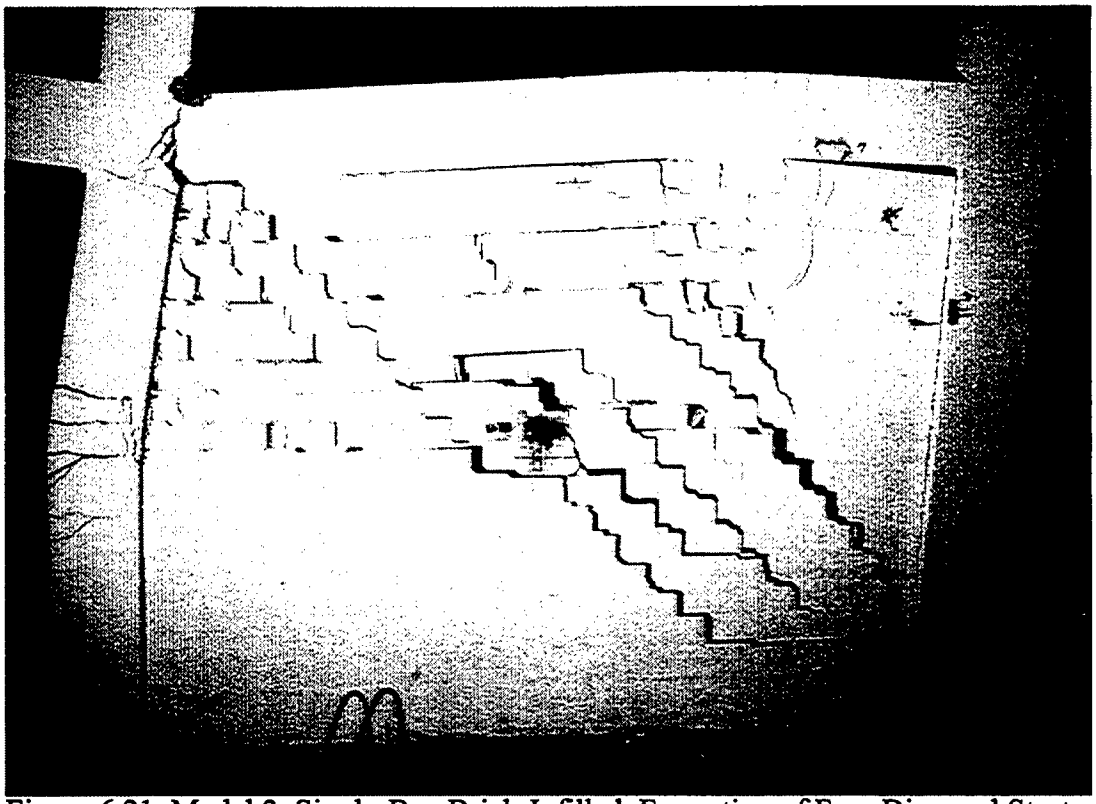

Figure 6.21 Model 3, Single-Bay Brick-Infilled, Formation of Four Diagonal Struts

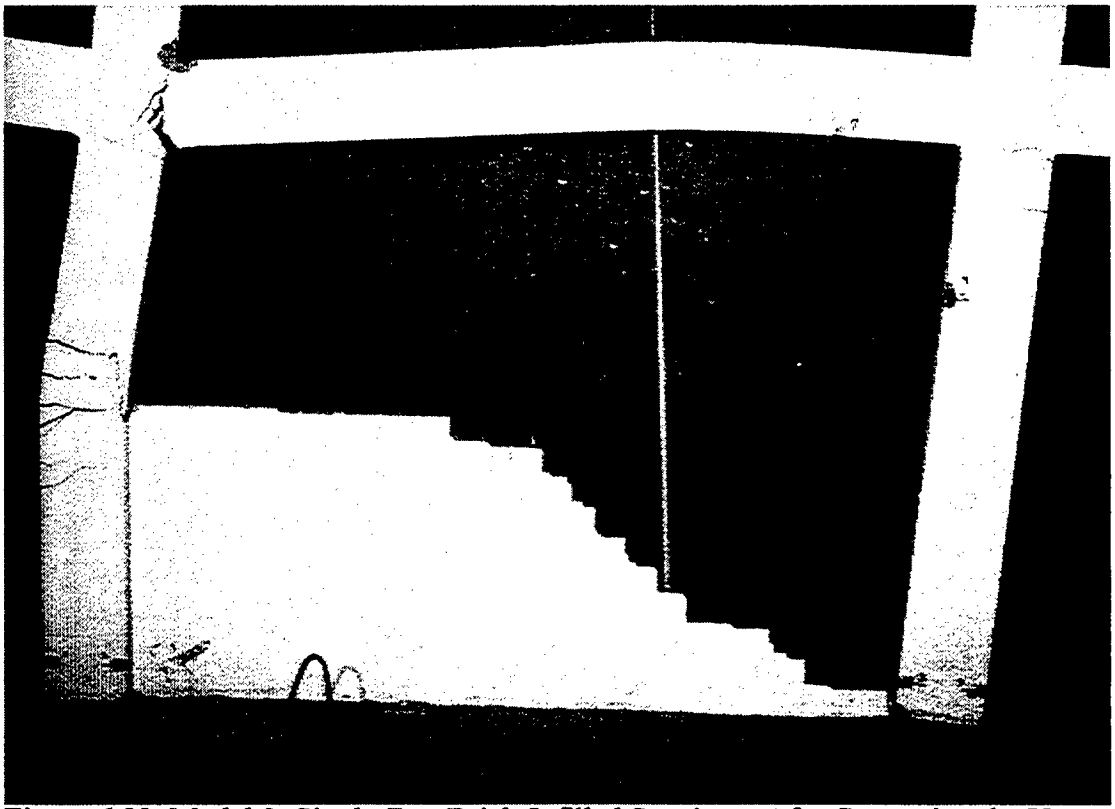

Figure 6.22 Model 3, Single-Bay Brick-Infilled Specimen After Removing the Unsound Brick

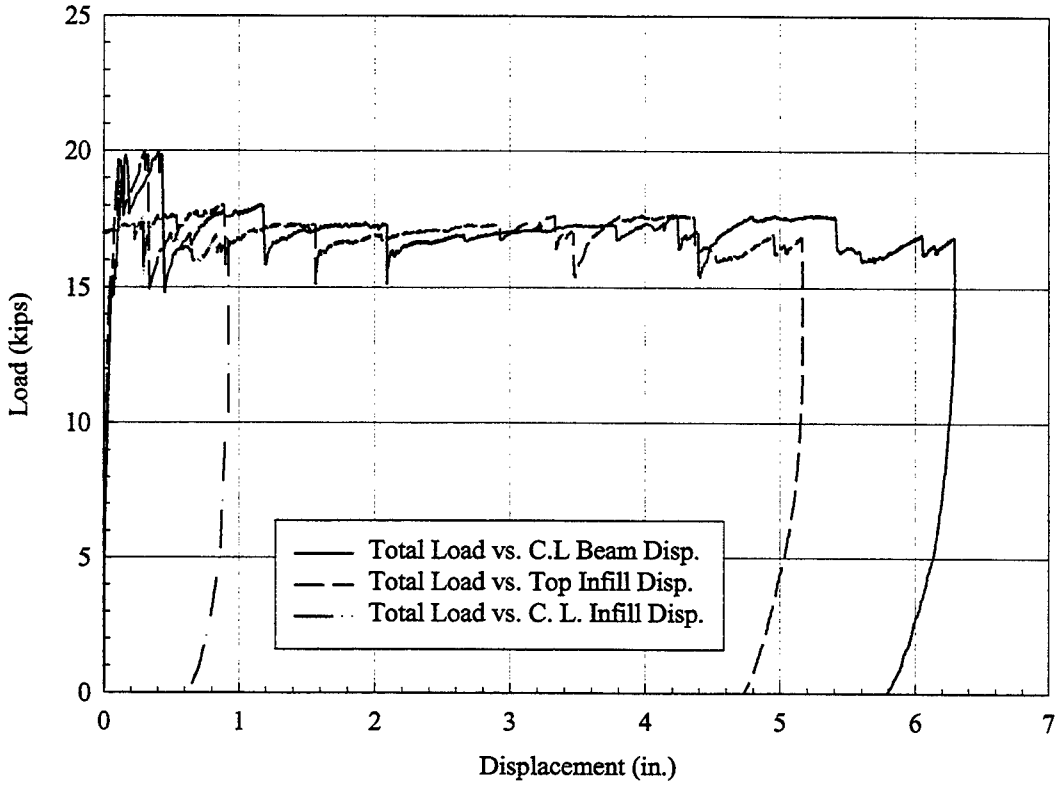

Figure 6.23 Model 3, Single-Bay Brick Infilled Specimen Lateral Displacement of Infill and Frame

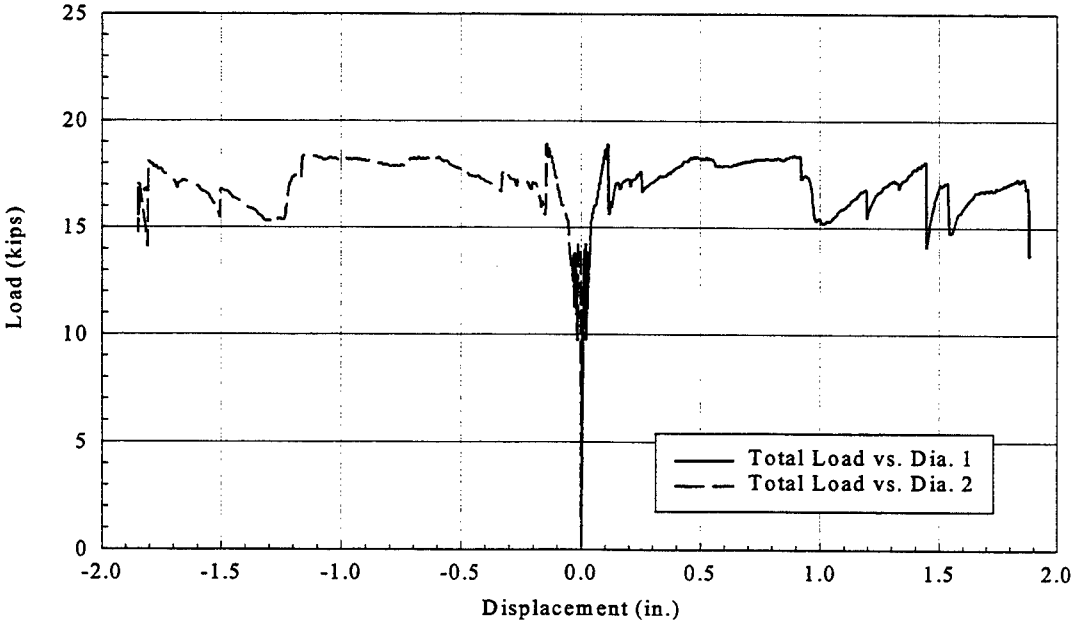

Figure 6.24 Model 3, Single-Bay Brick Infilled Specimen Displacements Across the Diagonals

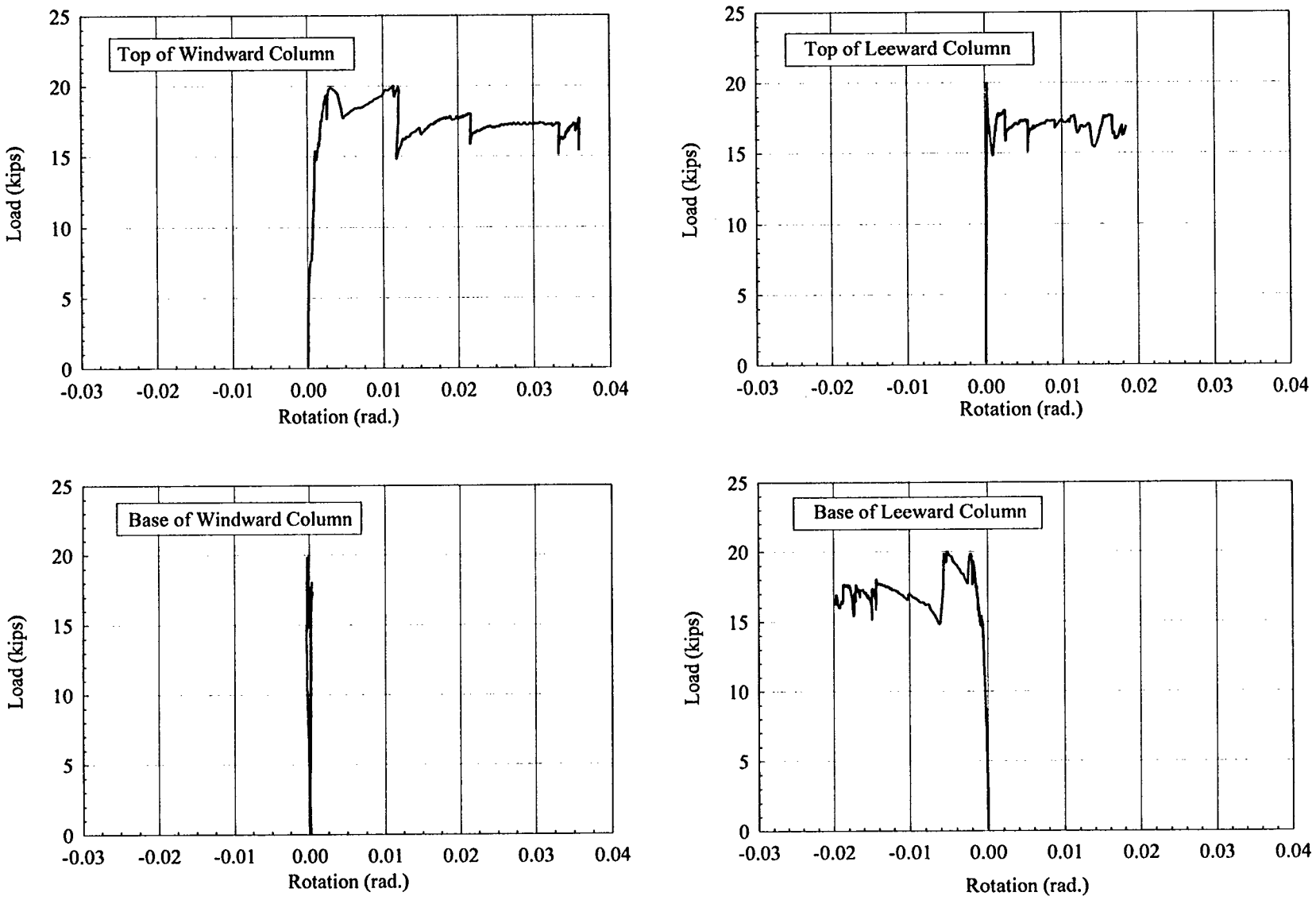

Figure 6.25 Model 3, Single-Bay Brick Infilled Specimen Rotations

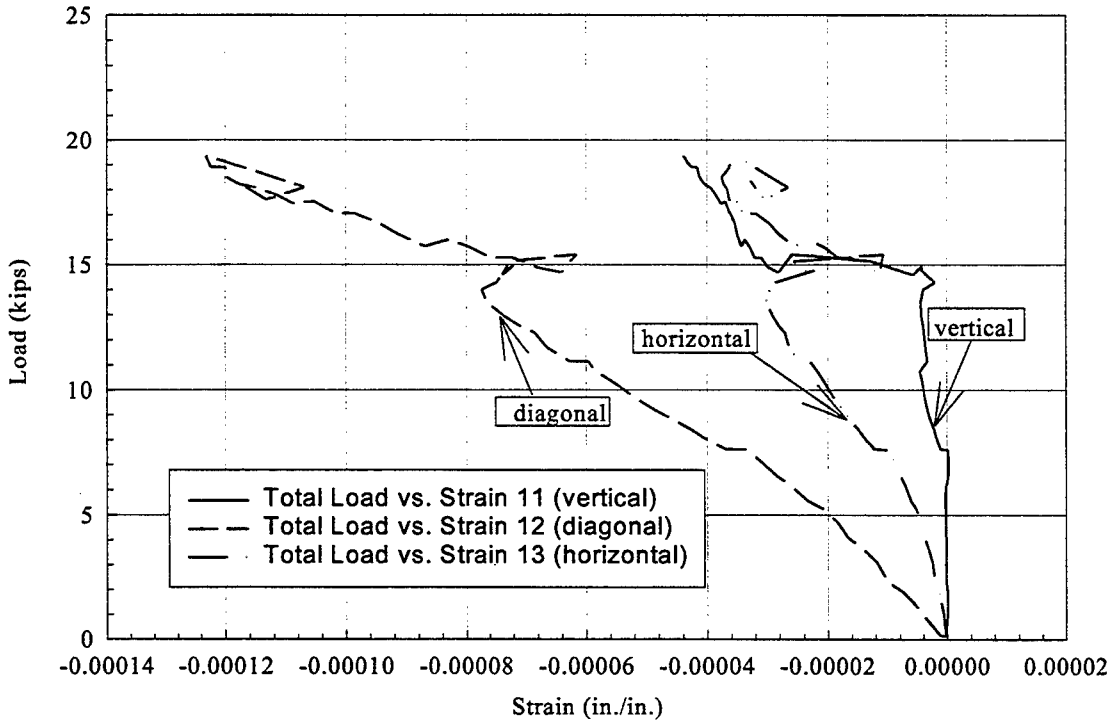

Figure 6.26 Model 3, Single-Bay Brick Infilled Specimen Rosette Gage Strains at Center of Infill

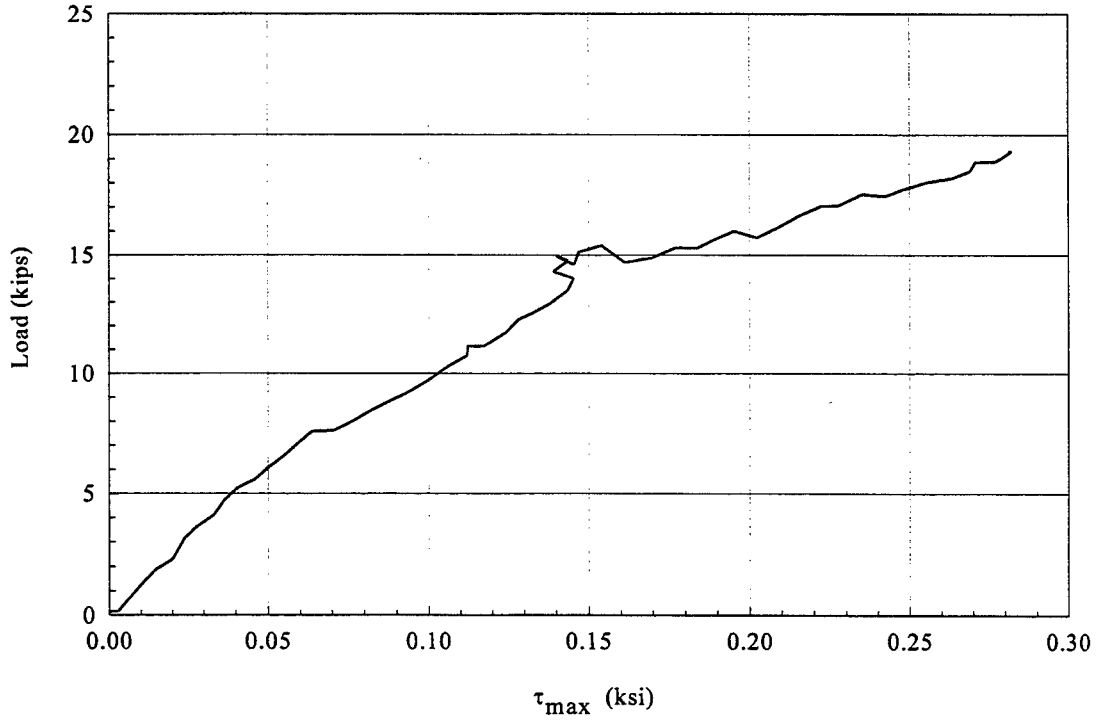

Figure 6.27 Model 3, Single-Bay Brick Infilled Specimen Shear Stress at Center of Infill

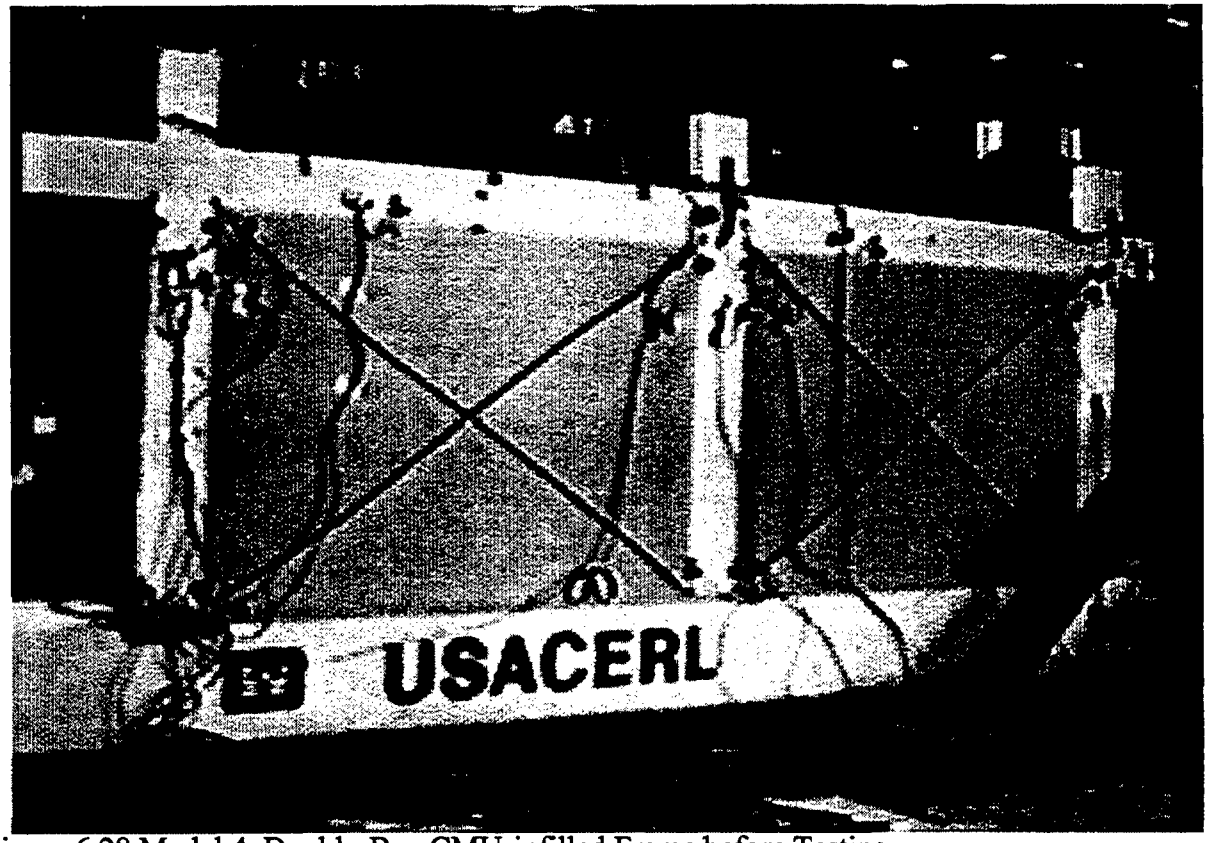

Figure 6.28 Model 4, Double-Bay CMU-infilled Frame before Testing

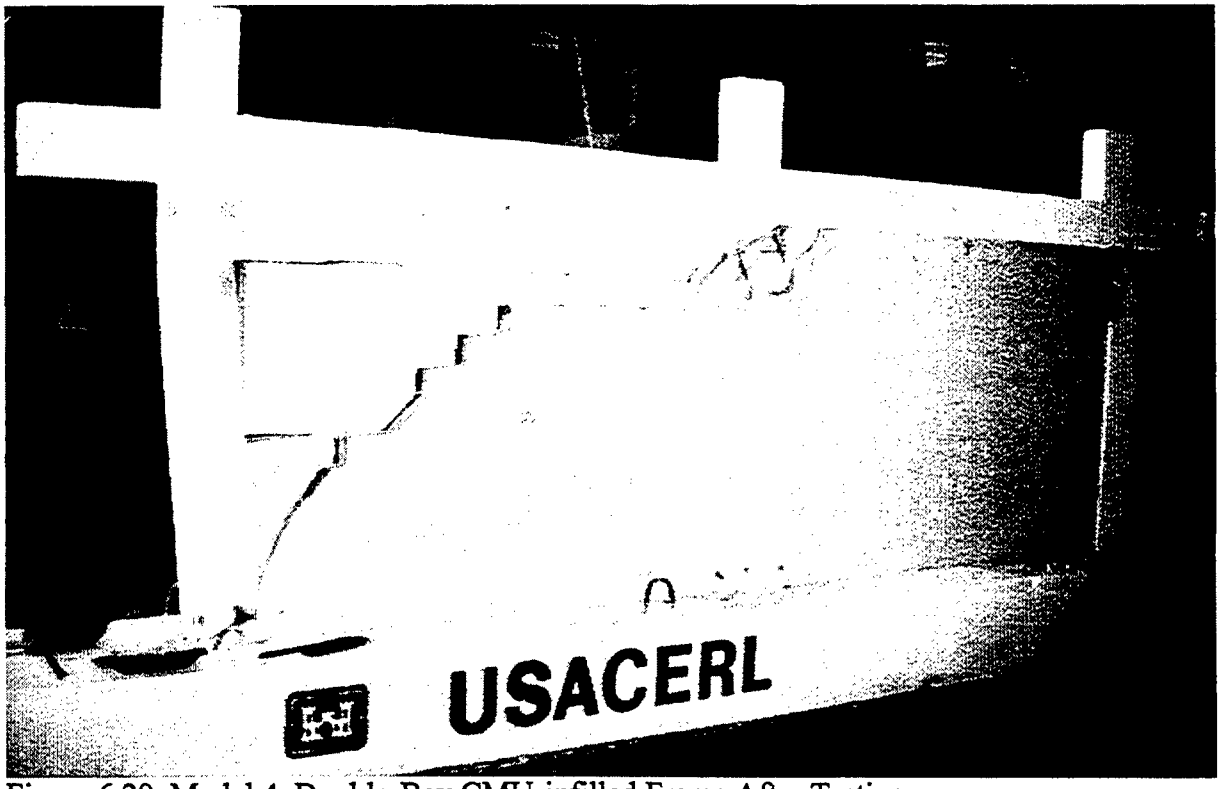

Figure 6.29 Model 4, Double-Bay CMU-infilled Frame After Testing

Figure 6.30 Model 4, Double-Bay CMU-Infilled Frame, Windward, Center, Leeward Columns Failure, From Left to Right

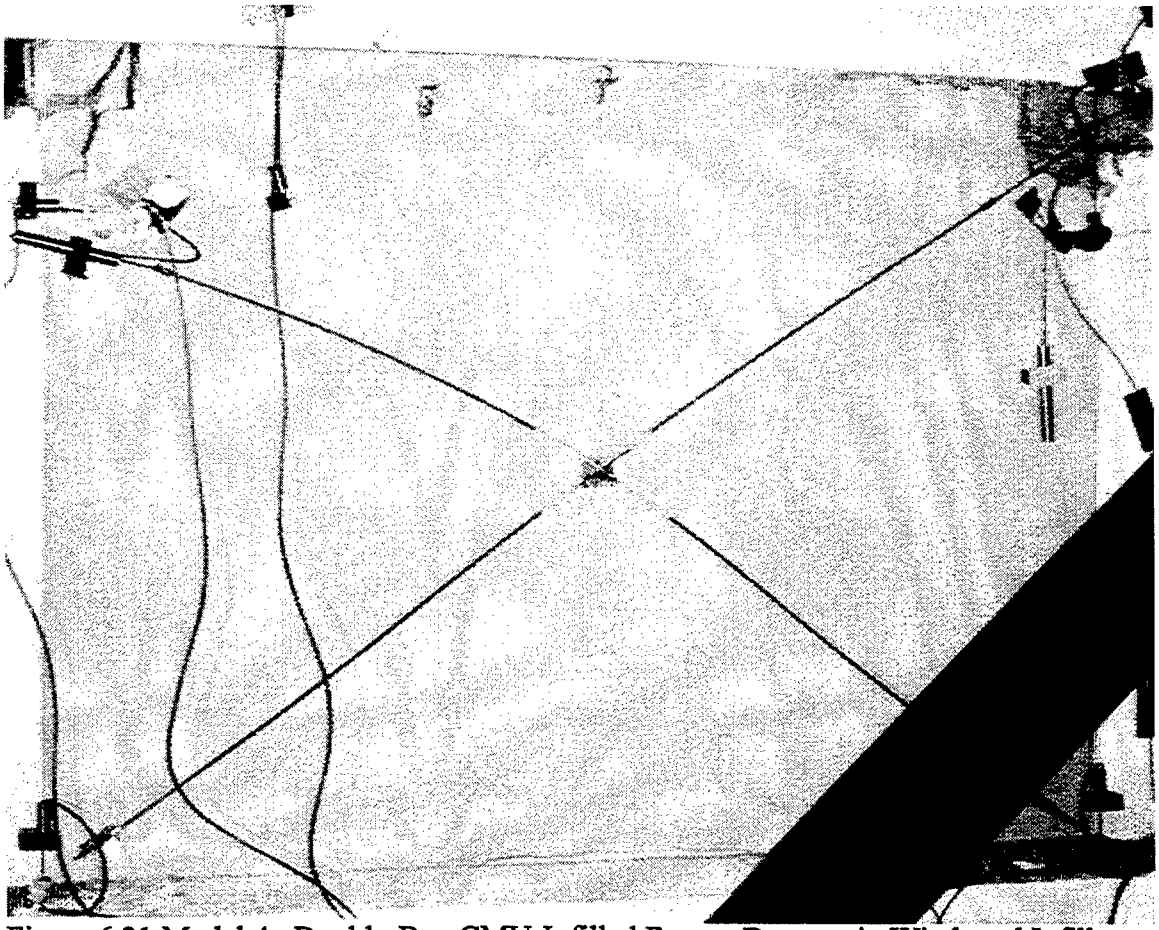

Figure 6.31 Model 4, Double-Bay CMU-Infilled Frame, Damage in Windward Infill

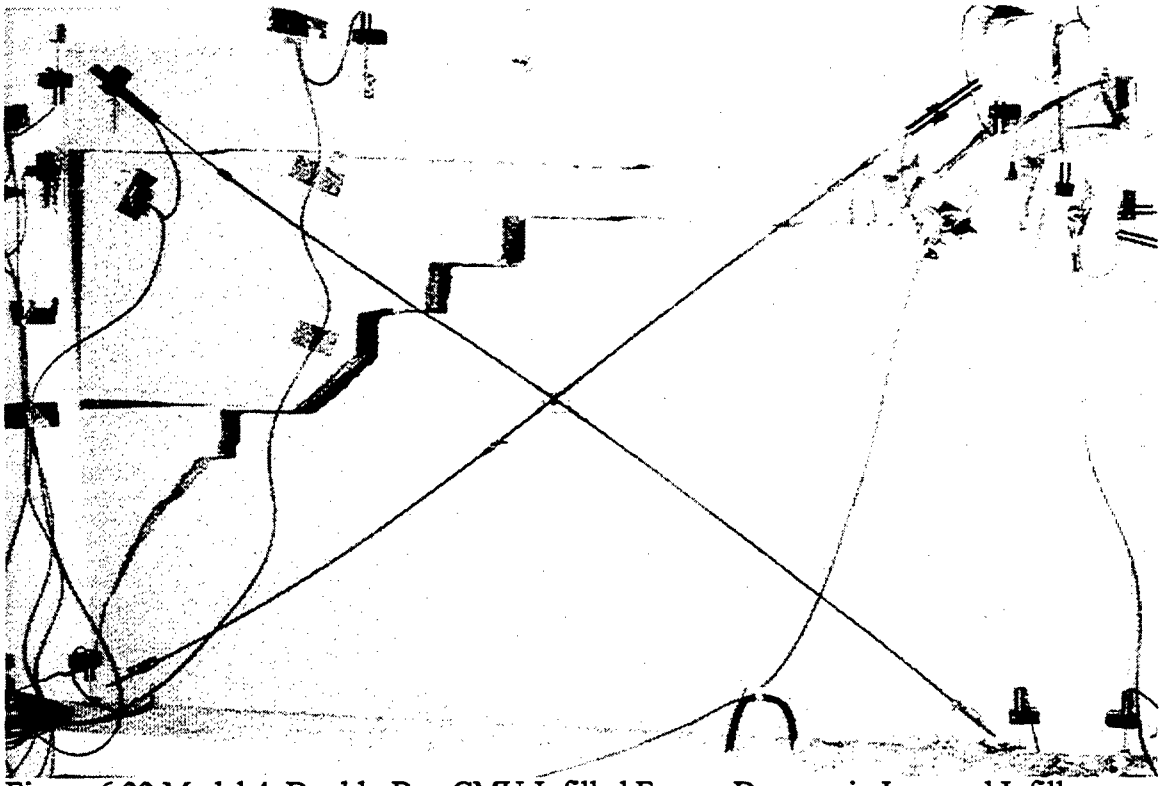

Figure 6.32 Model 4, Double-Bay CMU-Infilled Frame, Damage in Leeward Infill

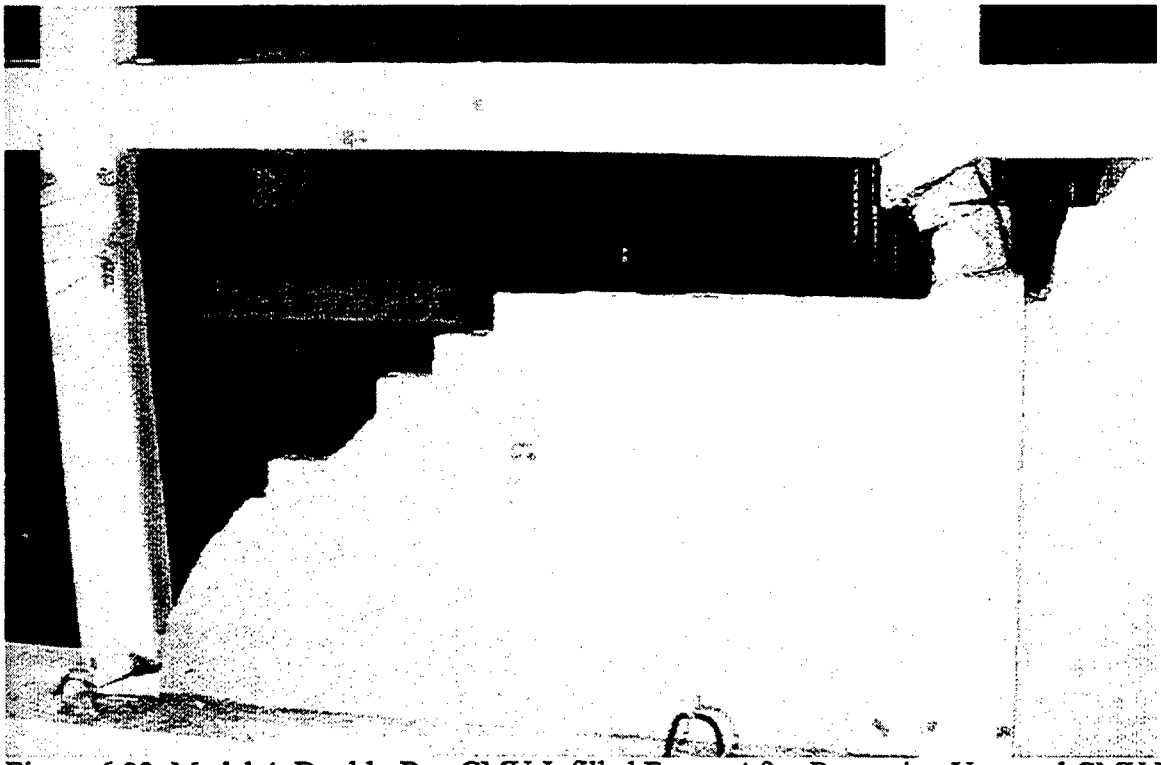

Figure 6.33 Model 4, Double-Bay CMU-Infilled Frame After Removing Unsound CMU Blocks from the Leeward Infill

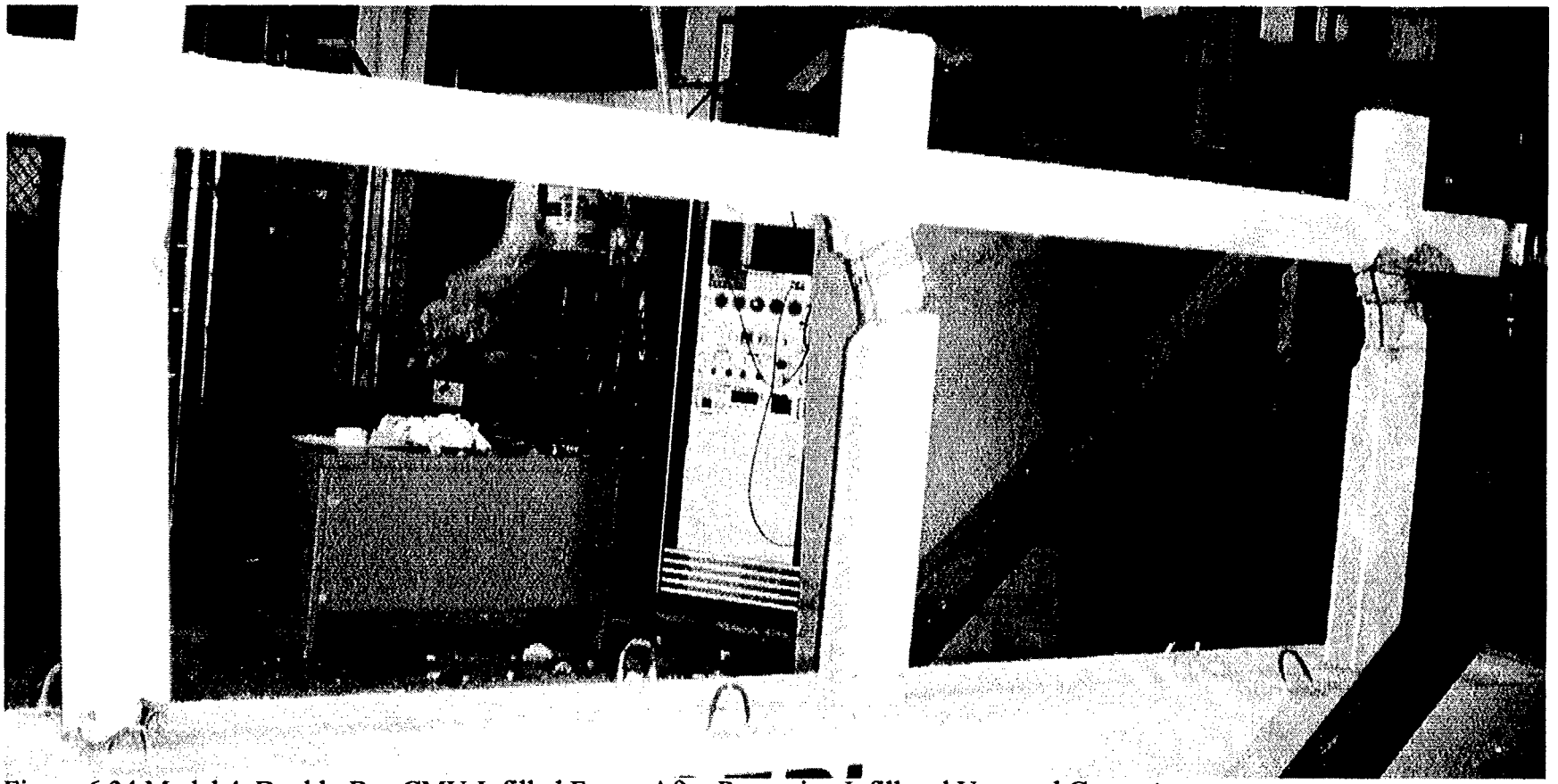

Figure 6.34 Model 4, Double-Bay CMU-Infilled Frame After Removing Infill and Unsound Concrete

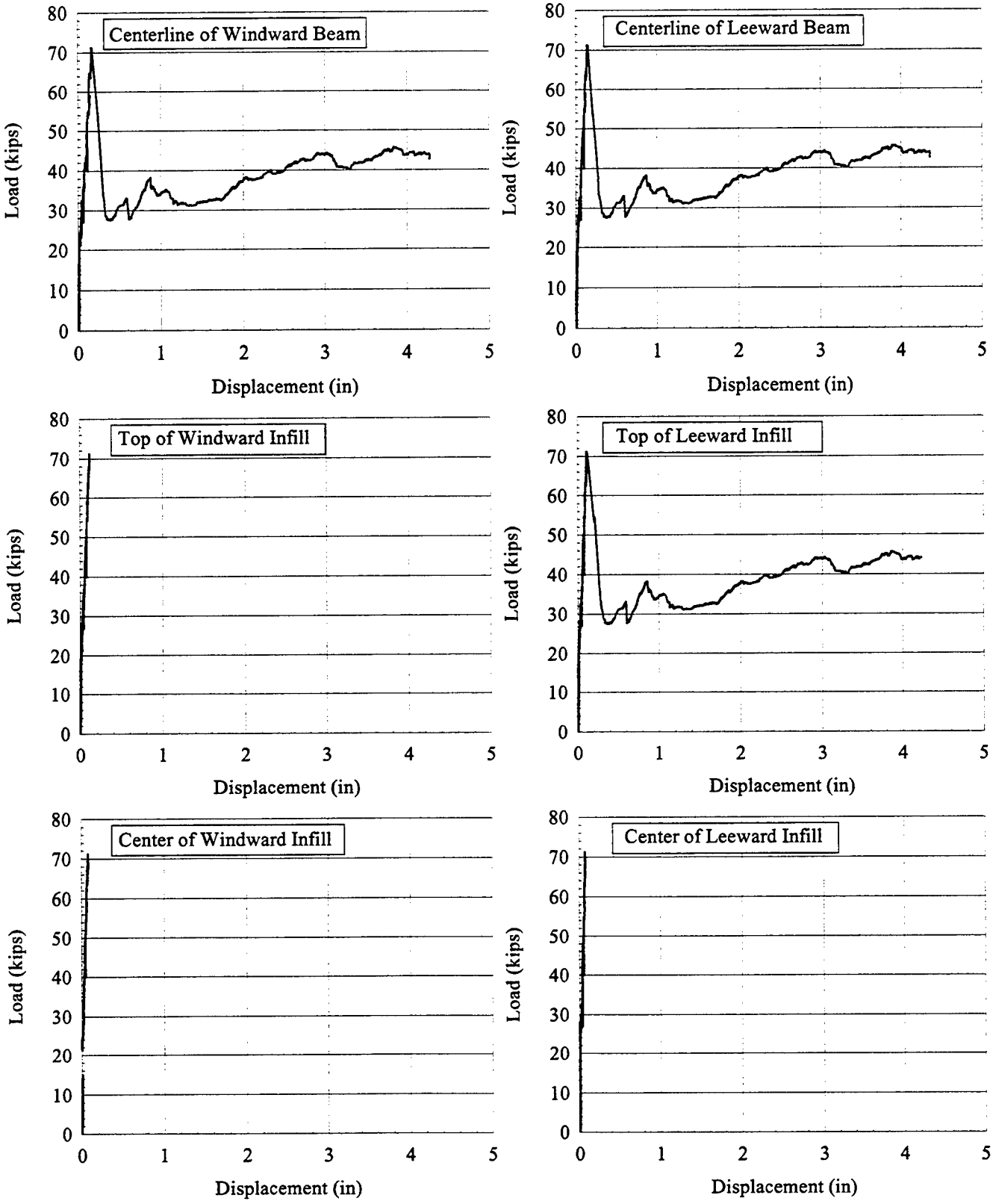

Figure 6.35 Model 4, Double-Bay CMU Infilled Specimen Lateral Displacements

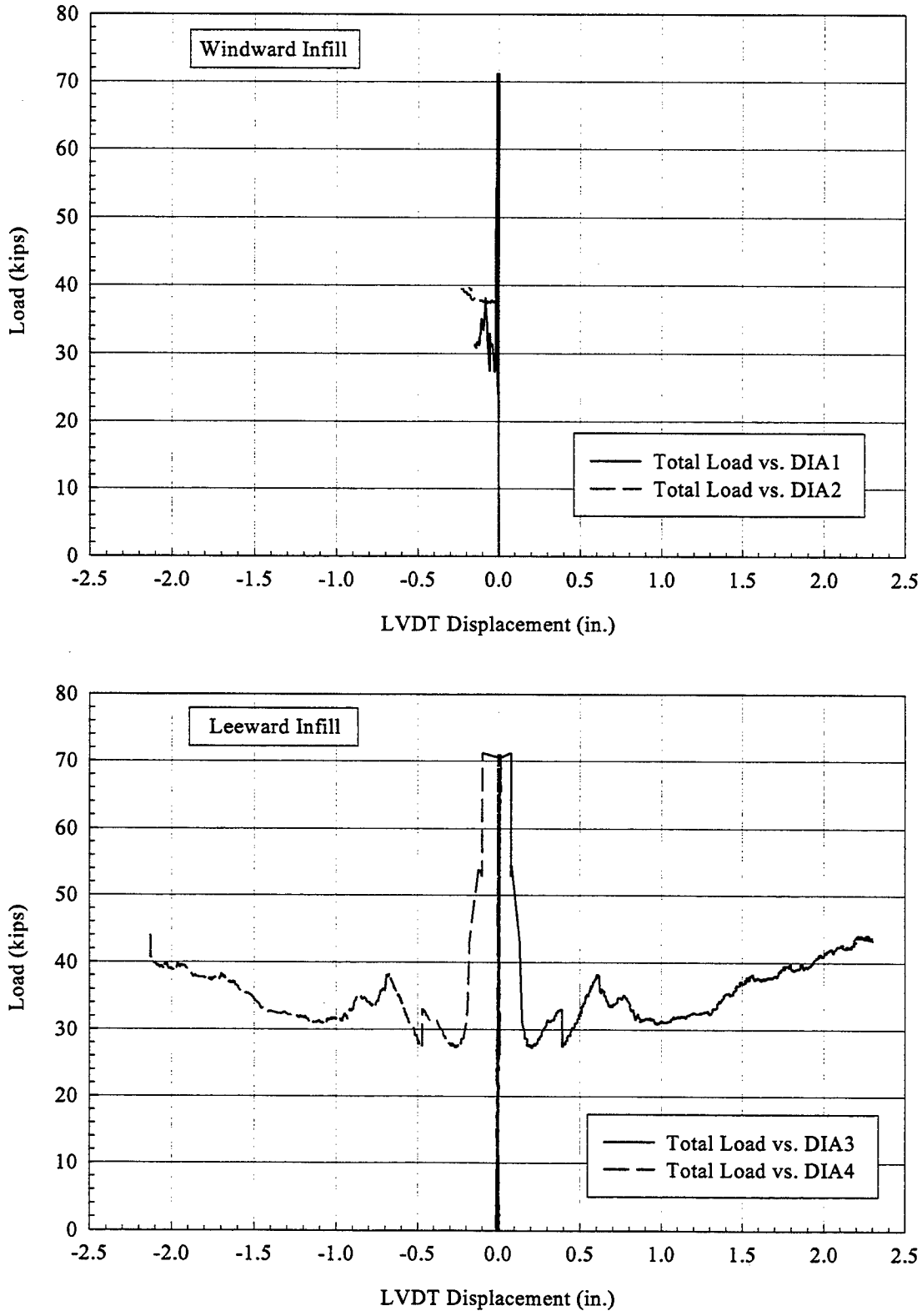

Figure 6.36 Model 4, Double-Bay CMU Infilled Specimen Displacements Along Diagonals

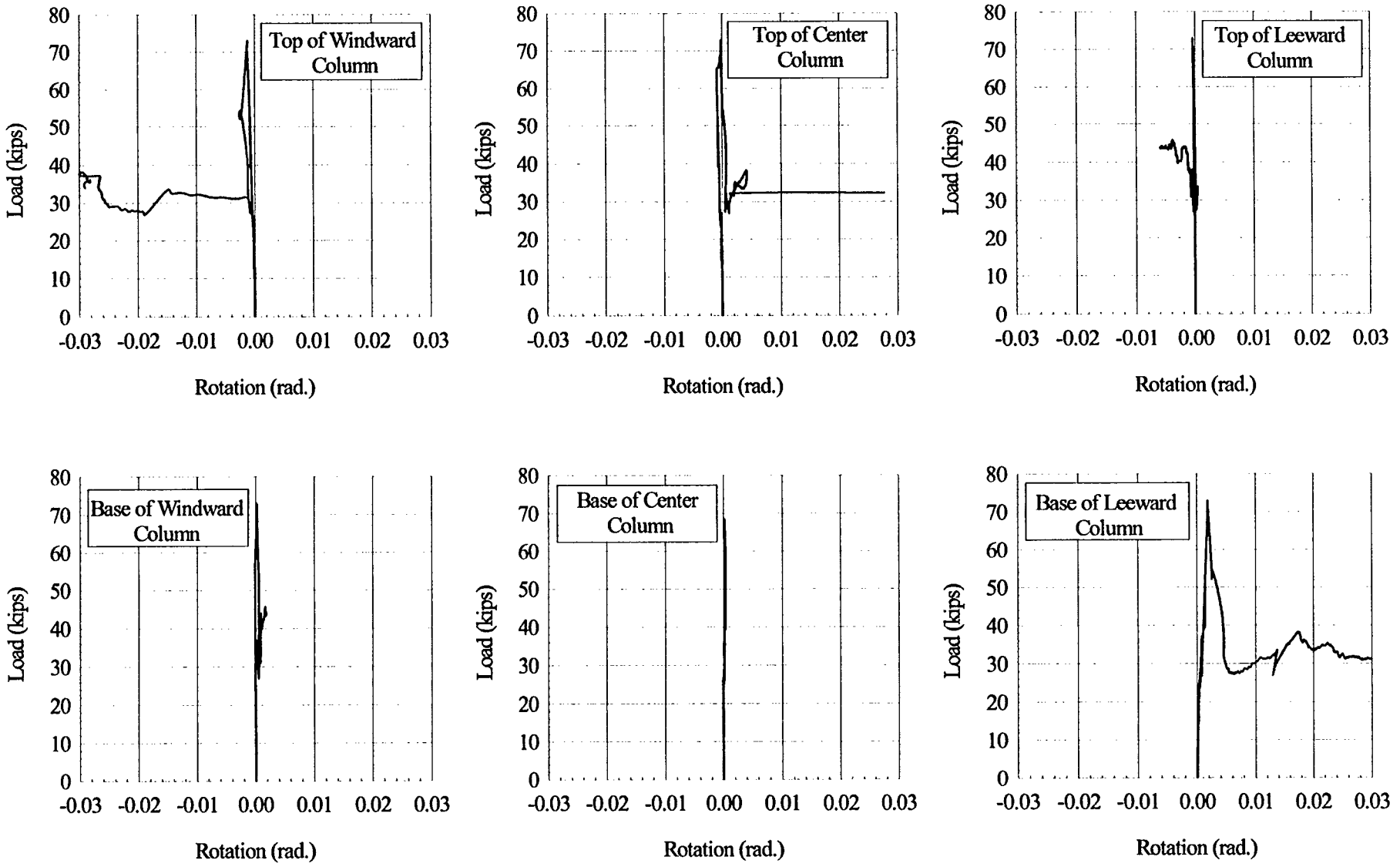

Figure 6.37 Model 4, Double-Bay CMU Infilled Specimen Rotations

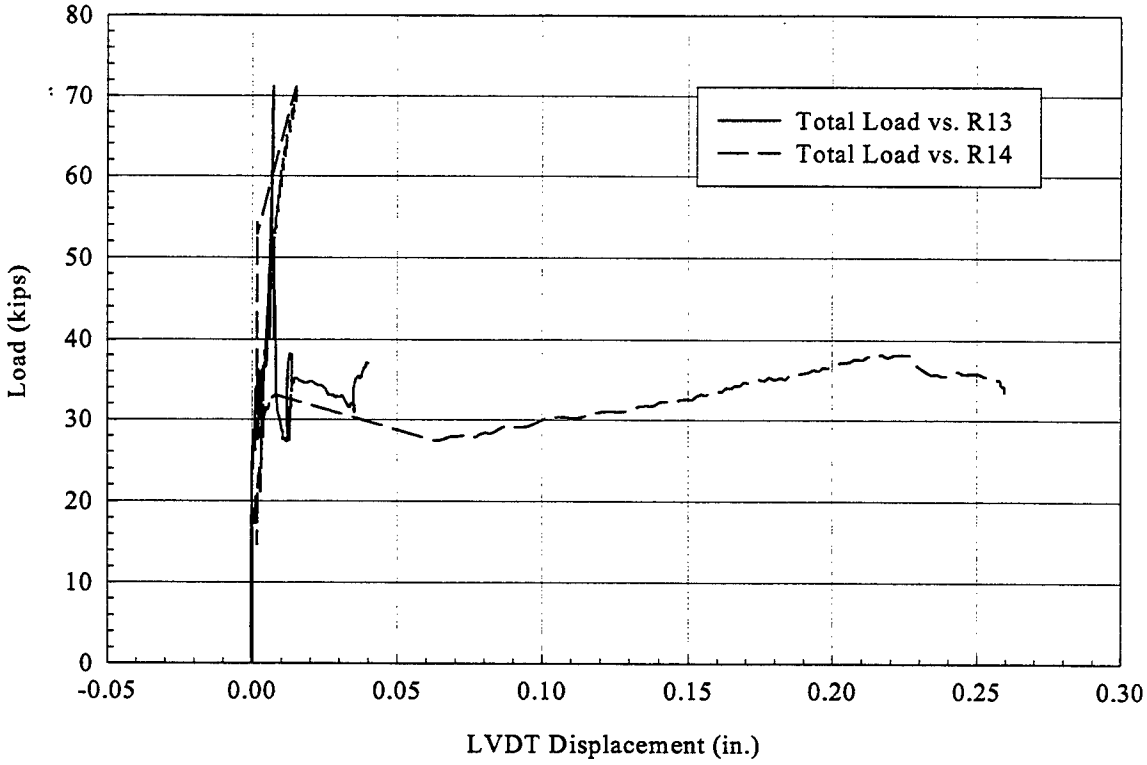

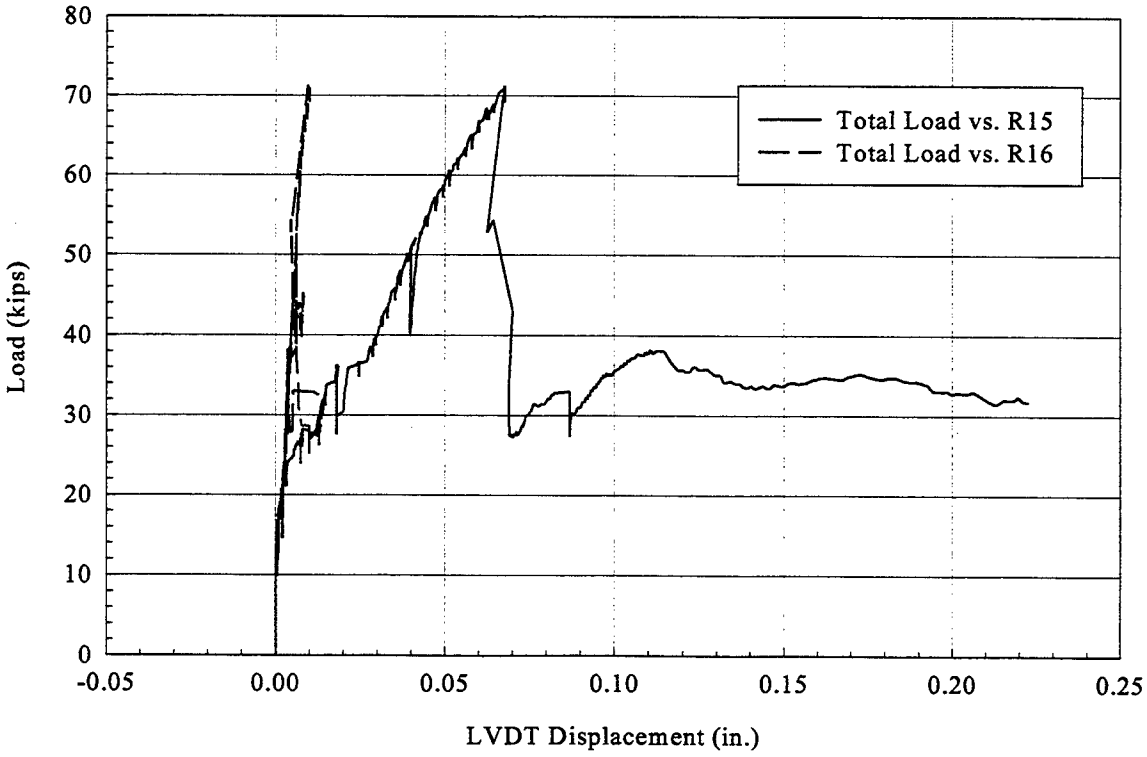

Figure 6.38 Model 4, Double-Bay CMU Infilled Specimen

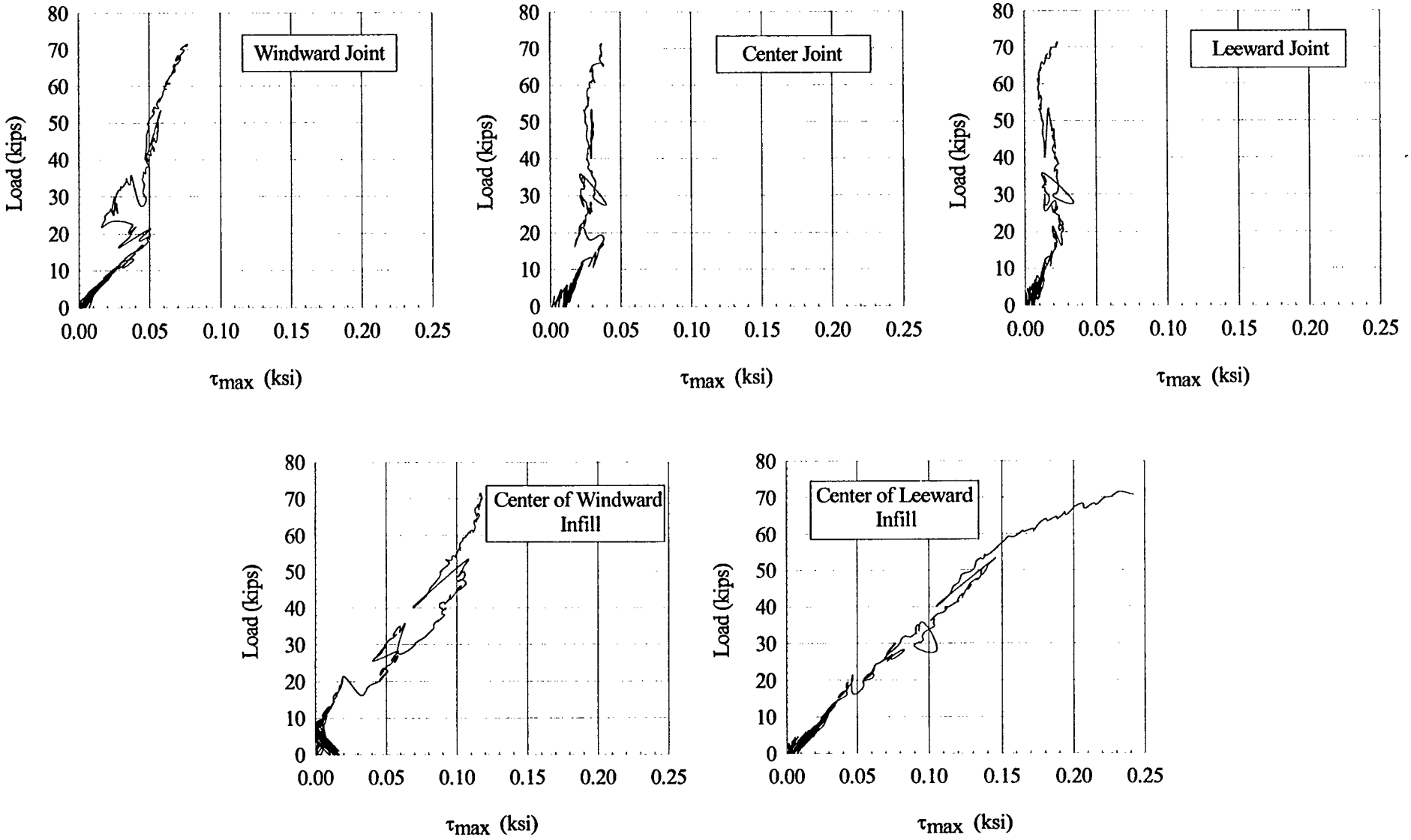

Figure 6.39 Model 4, Double-Bay CMU Infilled Specimen Shear Stress

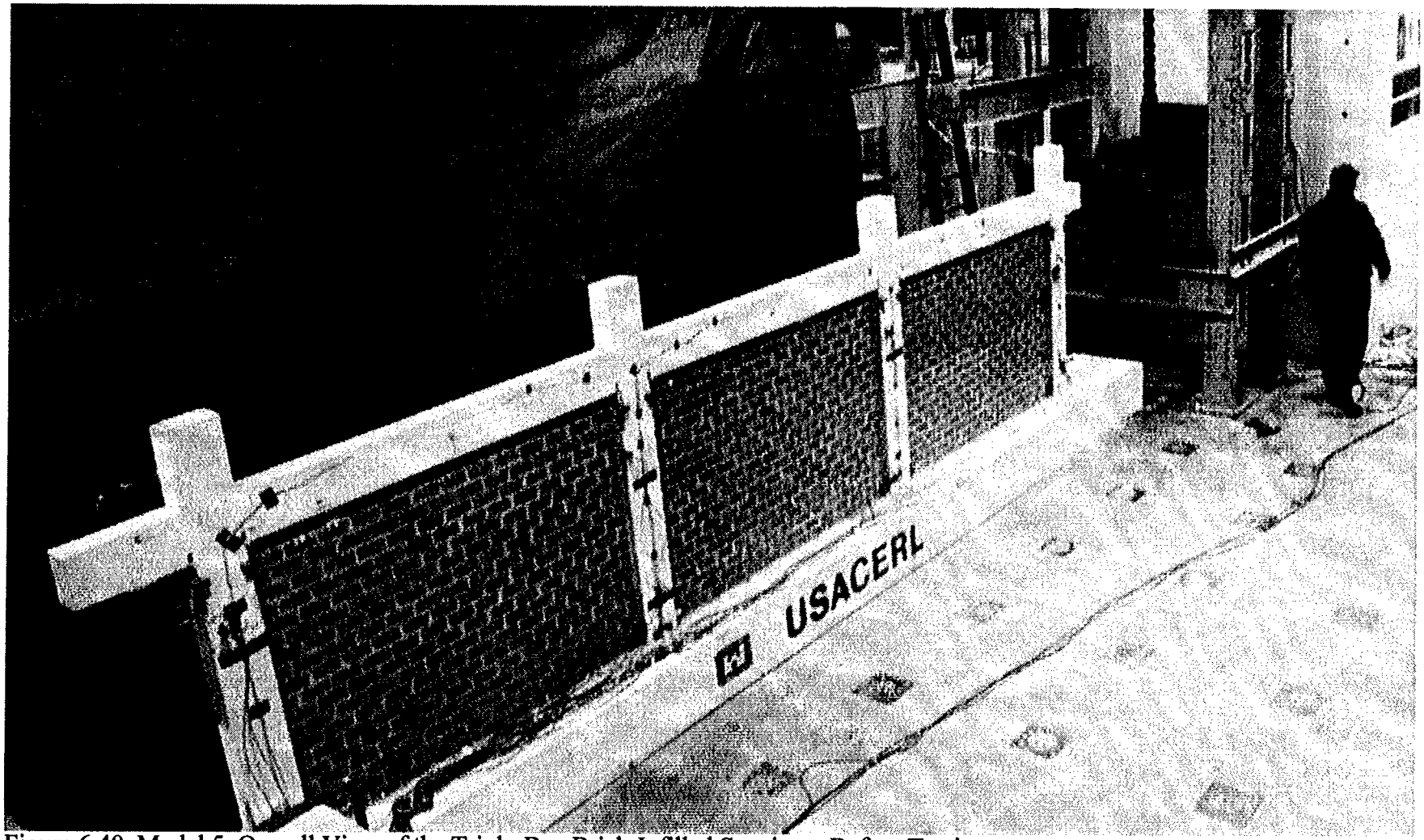

Figure 6.40 Model 5, Overall View of the Triple-Bay Brick-Infilled Specimen Before Testing

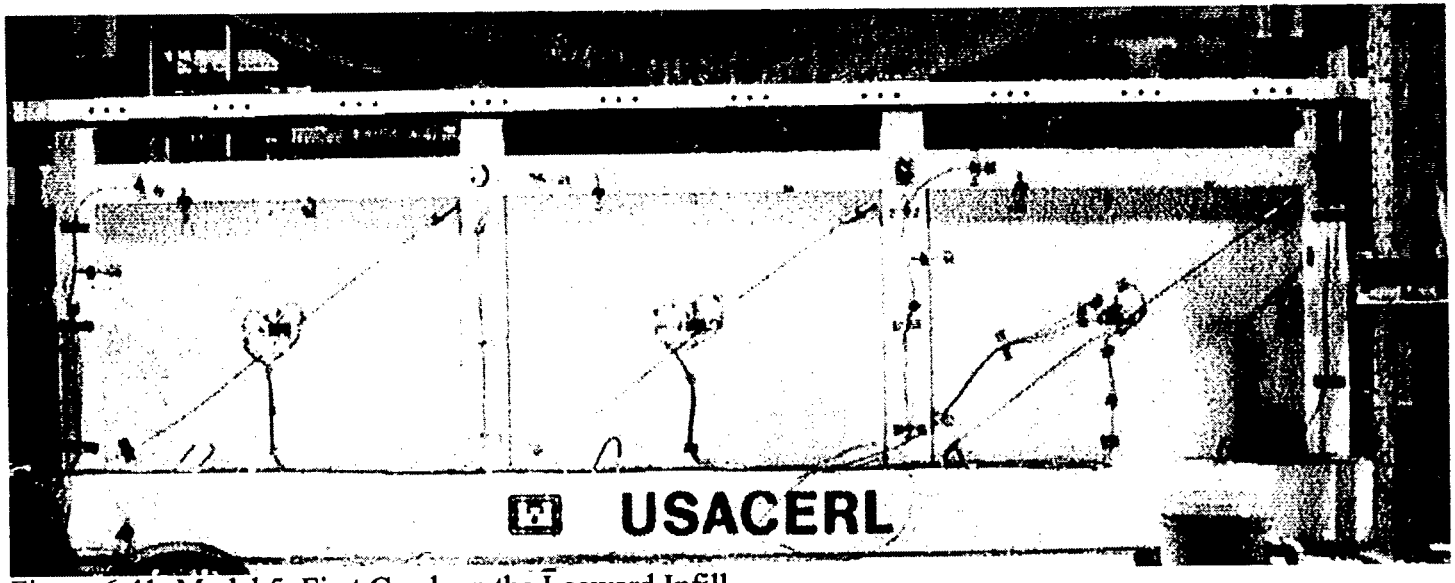

Figure 6.41 Model 5, First Crack on the Leeward Infill

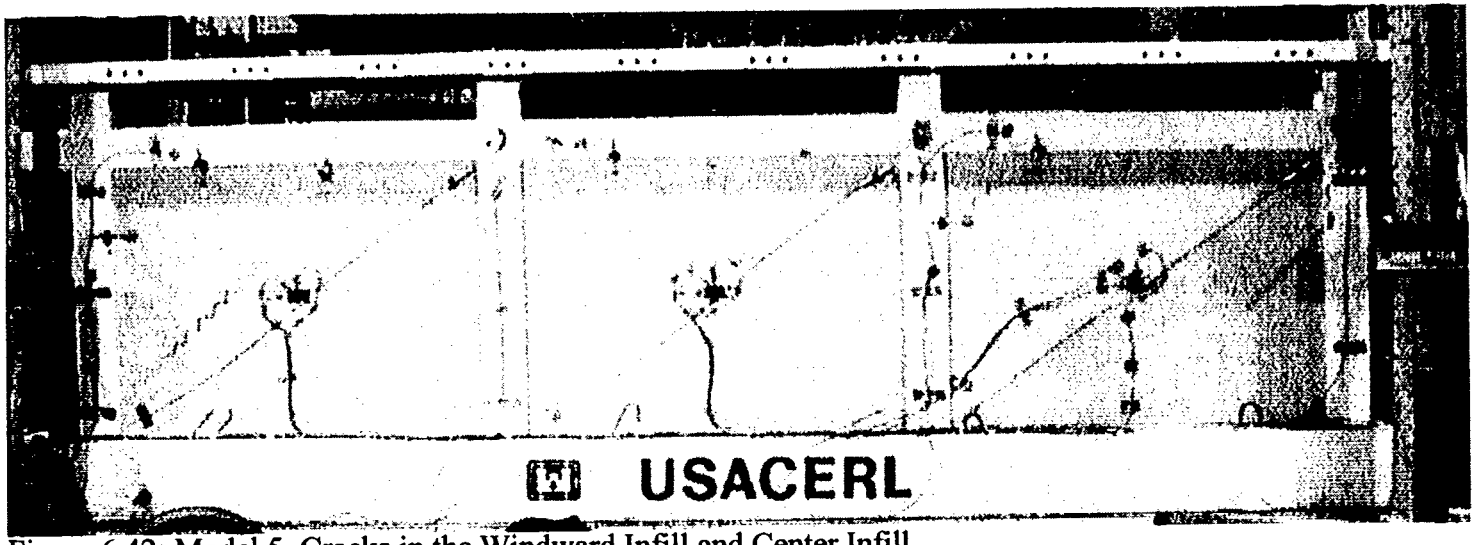

Figure 6.42: Model 5, Cracks in the Windward Infill and Center Infill

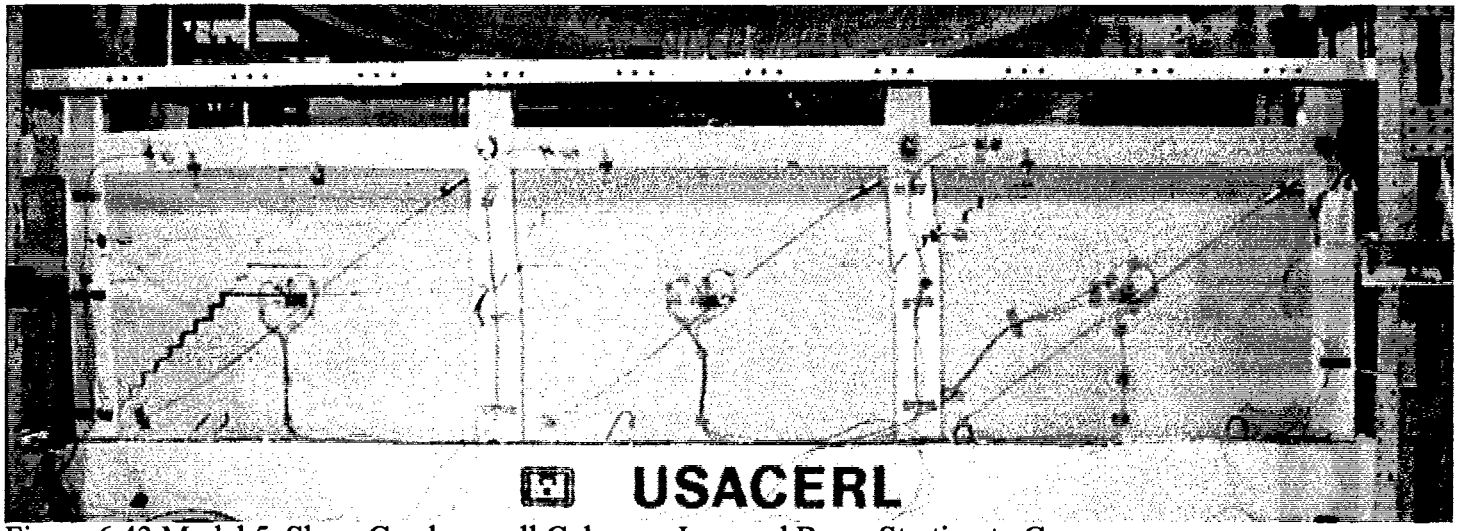

Figure 6.43 Model 5, Shear Cracks on all Columns, Leeward Beam Starting to Curve

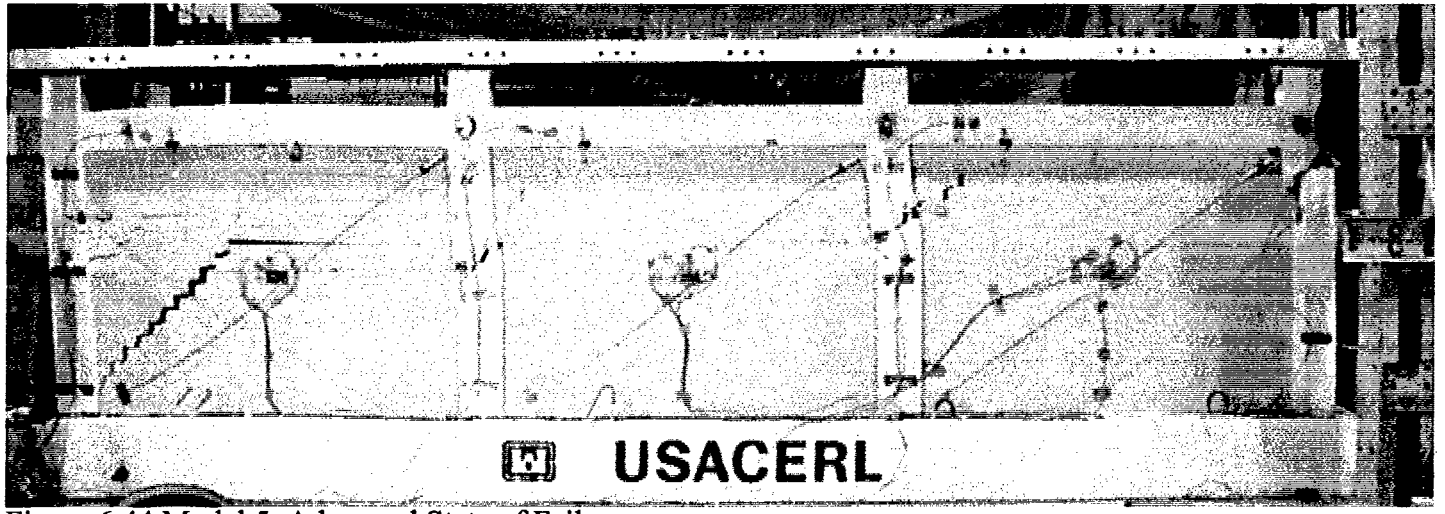

Figure 6.44 Model 5, Advanced State of Failure

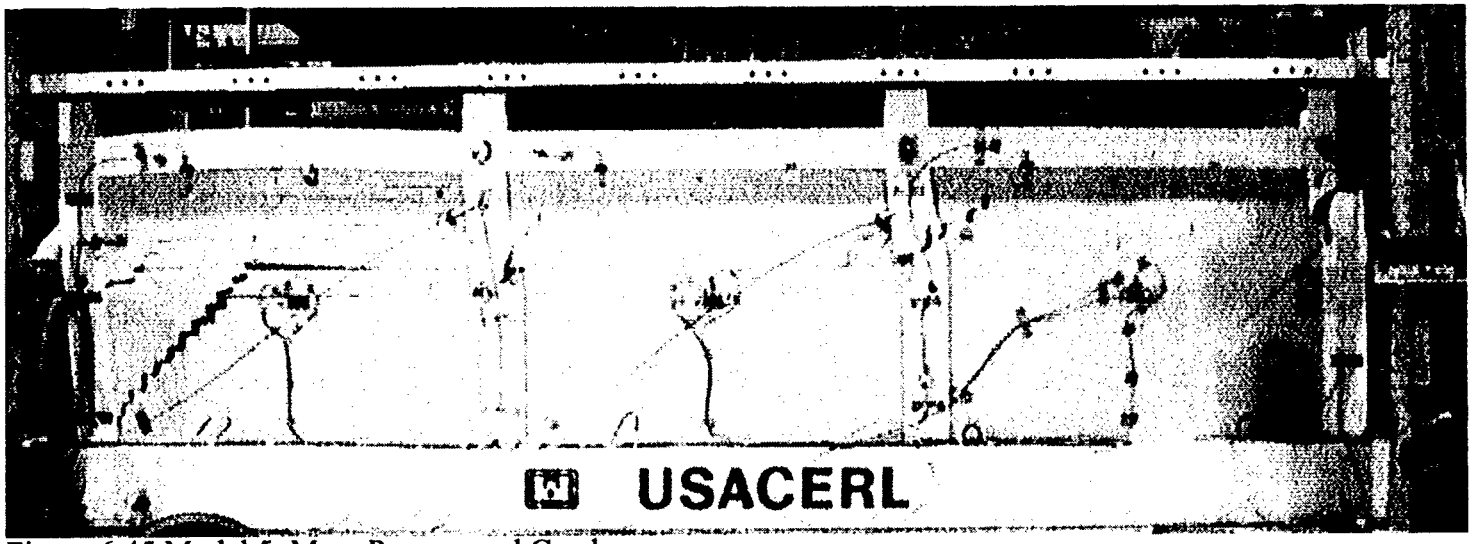

Figure 6.45 Model 5, More Pronounced Cracks

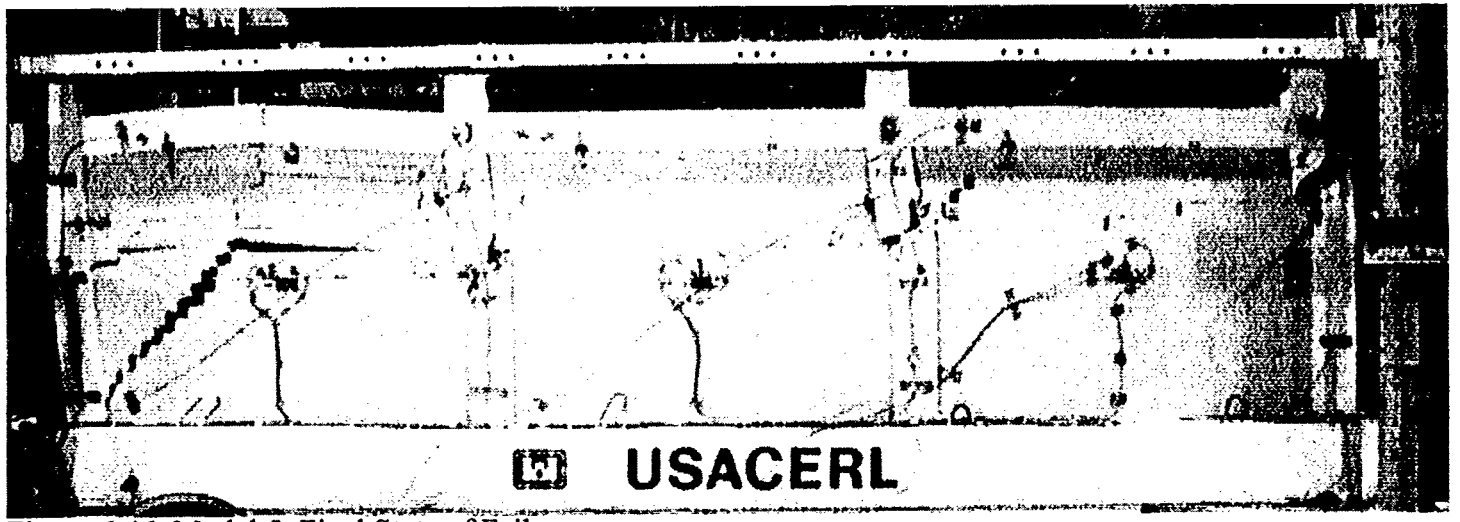

Figure 6.46 Model 5, Final State of Failure

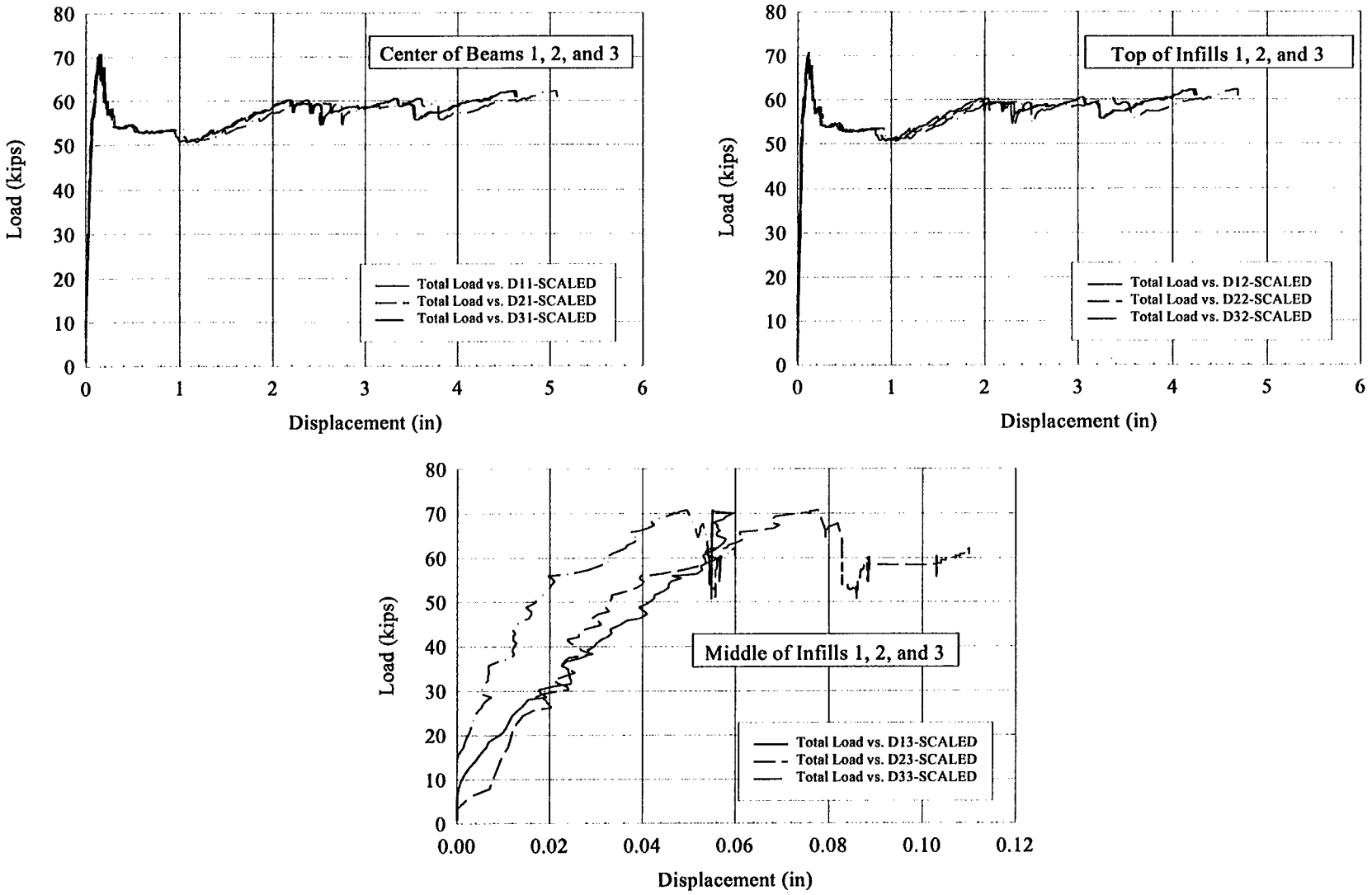

Figure 6.47 Model 5, Triple-Bay Brick Infilled Specimen Lateral Displacements

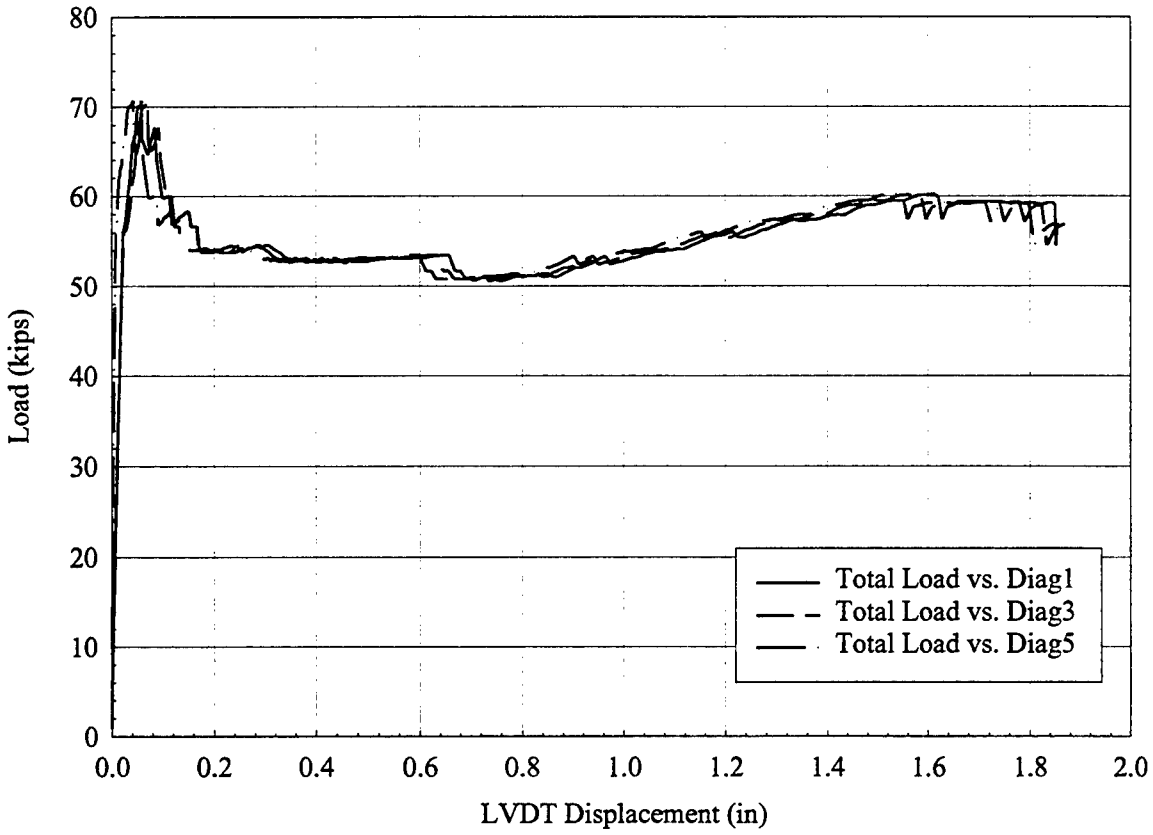

Figure 6.48 Model 5, Triple-Bay Infilled Specimen LVDT Displacements Along Compressive Diagonals 1, 3, and 5

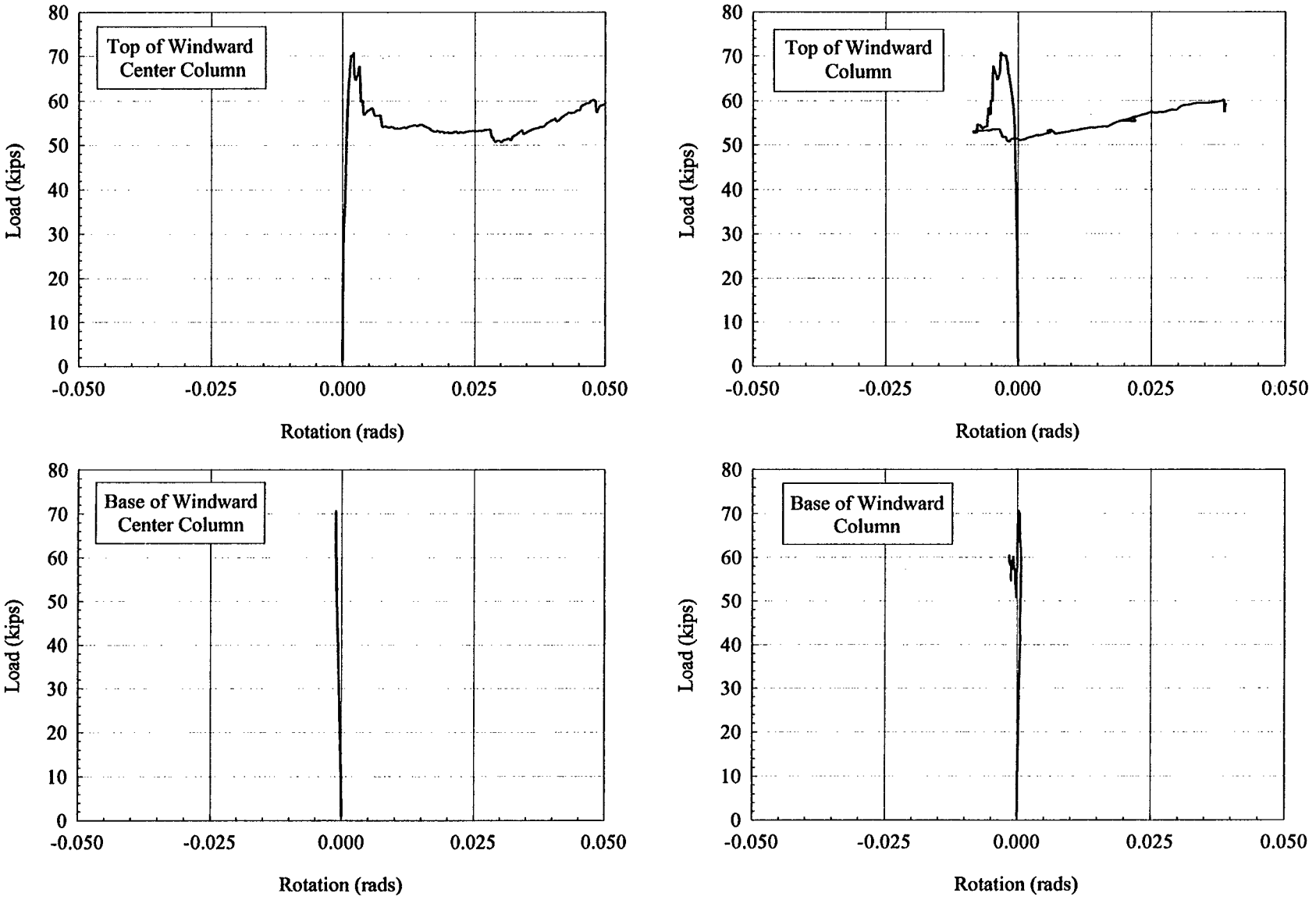

Figure 6.49 Model 5, Triple-Bay Brick Infilled Specimen Rotations

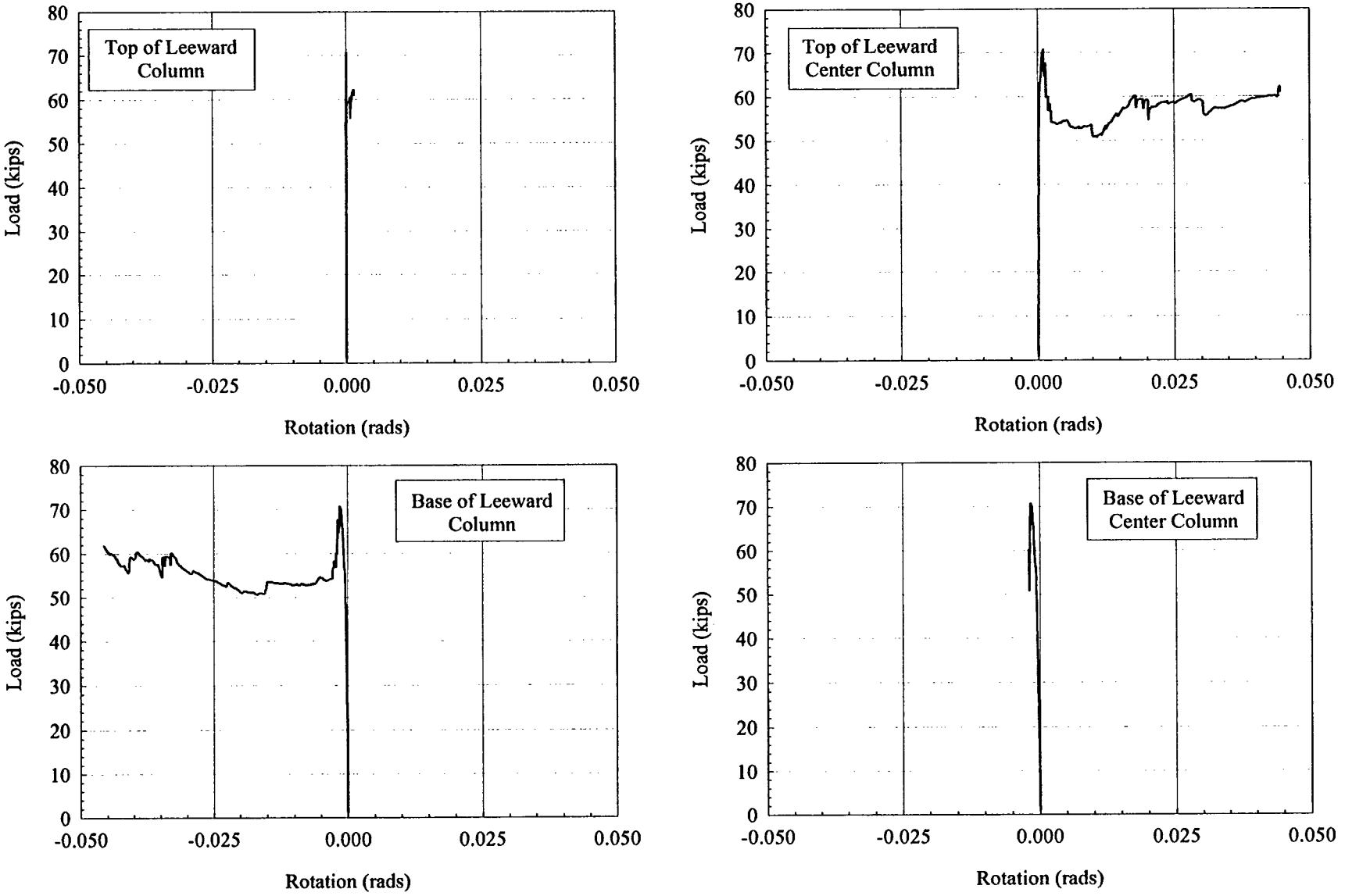

Figure 6.50 Model 5, Triple-Bay Infilled Specimen Rotations

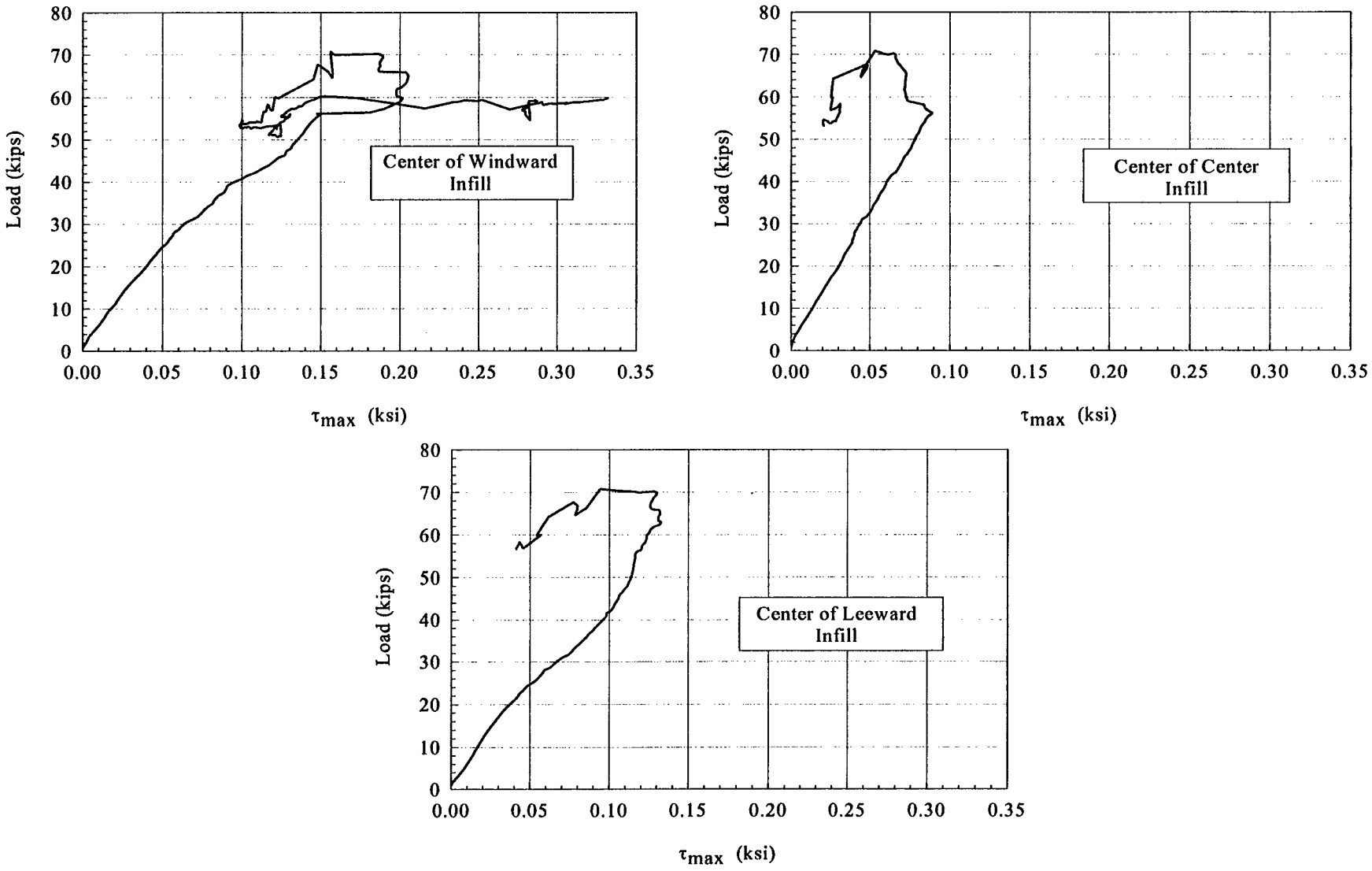

Figure 6.51 Model 5, Triple-Bay Brick Infilled Specimen Shear Stresses

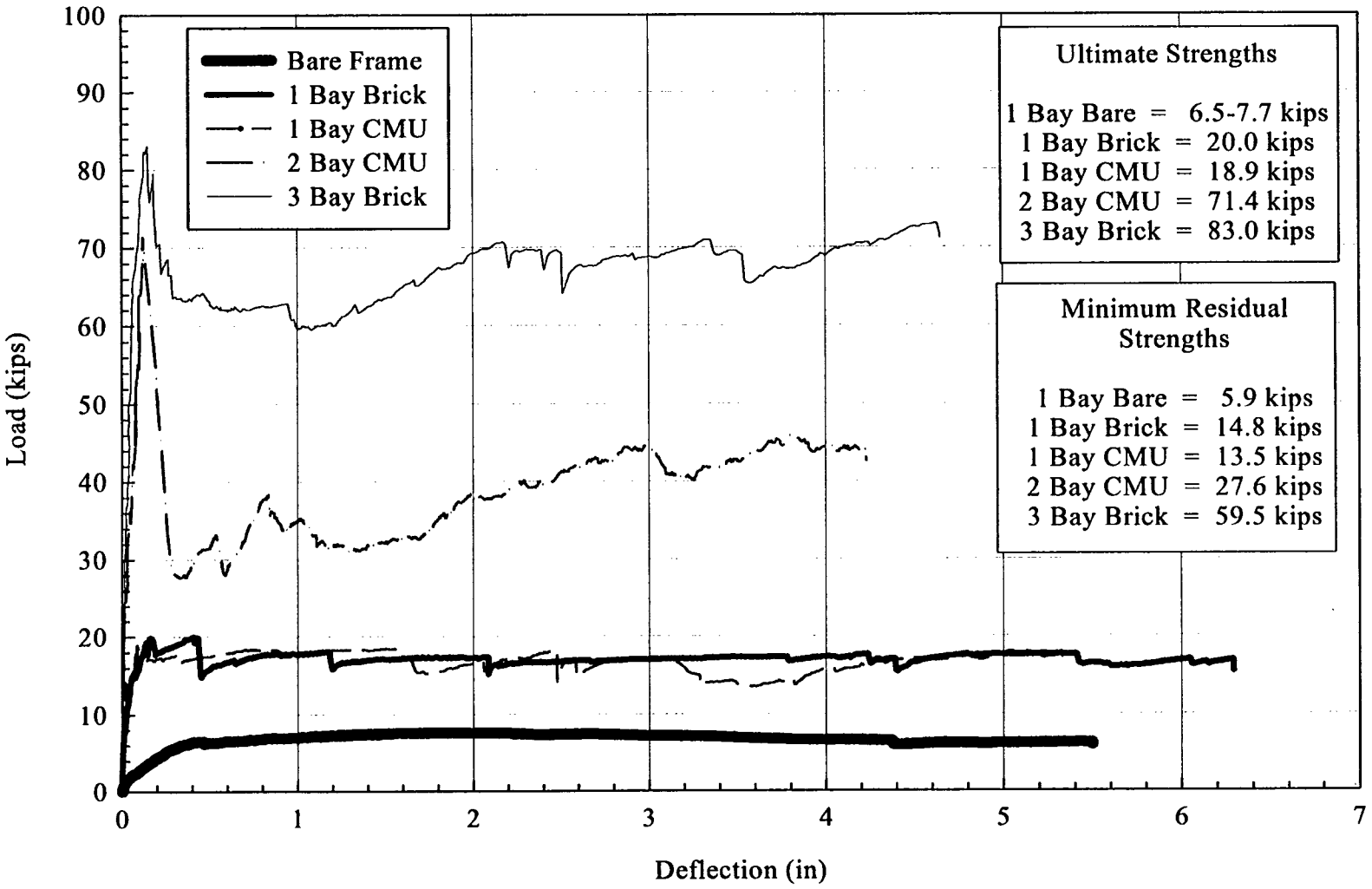

Figure 6.52 Load-Deflection Plot of Infilled Frame Specimens

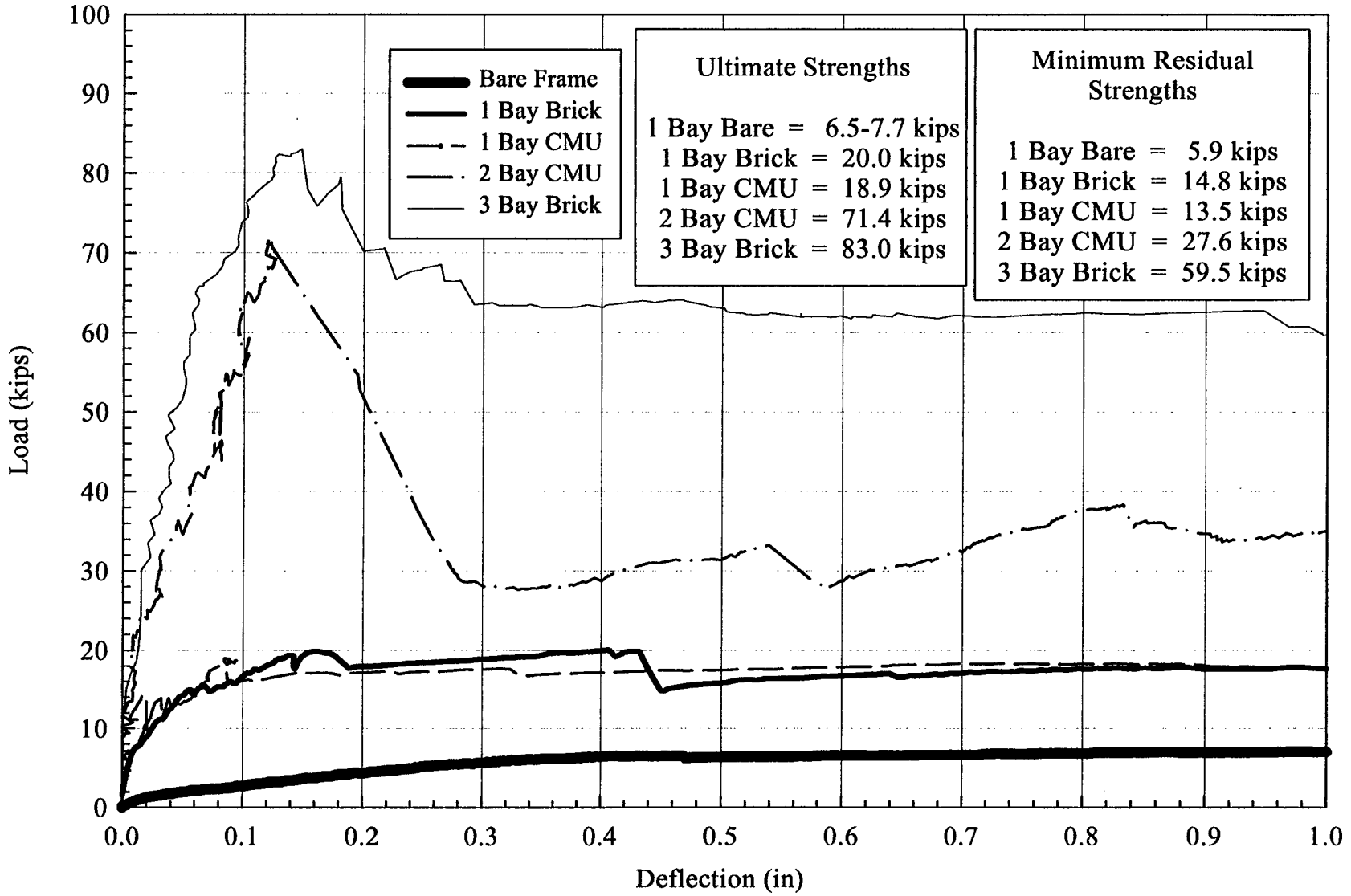

Figure 6.53 Load-Deflection Plot of Infilled Frame Specimens

CHAPTER 7

COMPARISON OF EXPERIMENTAL AND ANALYICAL IDEALIZATION

7.1 Introduction

Results of analytical models proposed by researchers presented in Chapter 4, finite element models described in Chapter 5, and experimental models of reinforced concrete frames with masonry infill described in chapter 6, are compared in this Chapter. The strength and stiffness parameters were used in the comparison of experimental and analytical idealization methods. For strength comparison, four different methods (Table XXV) were used to estimate the loads at first cracking and the ultimate loads of the infilled frame specimen. Two of the methods, Holmes' and Mainstone's, were of the equivalent-strut form. The Liauw and Kwan method is based on energy principles and plastic behavior, whereas ECOEST/PREC-8 is based on the value of diagonal cracking strength of the infill material. For stiffness comparison, several different analytical methods were used to predict the stiffnesses prior to cracking of the infilled frame being tested (Table XXVII). Several equivalent-strut analytical methods were used along with two other approaches based on the shear moduli of the specimen. The equivalent-strut areas were determined according to the specimen geometry and material properties obtained from material tests of the infill frame components.

Non of the four different models predicted the cracking and the ultimate loads accurately The finite element method yielded an acceptable prediction and was a very useful tool in understanding the overall behavior of the models.

7.2 Empirically Fitting Analytical Methods to Experimental Strengths

The experimental first cracking strength did not necessarily correspond to the formation of the first visible cracks in the infill material. The first cracking strength was taken to be a point based on judgment, when the load-deflection curve showed a significant change in stiffness or when sudden displacement was apparent (indicating the formation of imperceptible cracks). During testing, many popping and cracking noises could be heard even when no cracks or fractures were seen. All of the analytical methods overestimated the experimentally determined strengths of the specimens, as shown in Table XXV below. Table XXVI summarizes these results by averaging the strength ratios for each method.

The ratio values of estimated strength to experimental strength at ultimate, summarized in Table XXV, varied significantly. They ranged from 3.0 to 11.3 for Models 2, 2.3 to 6.3 for model 3, 1.5 to 3.9 for Model 4, and 2.5 to 6.5 for Model 5. The ratio values of estimated strength to experimental strength at first cracks also varied significantly. They ranged from 3.5 to 4.4 for Models 2, 2.5 to 2.8 for model 3, 3.3 to 3.5 for Model 4, and near 5.4 for Model 5. It can be concluded from these ratio values of analytically determined strength and experimentally determined strength that all these proposed methods over estimate the strength.

Neither the ECOEST/PREC-8 nor the Mainstone methods accurately predicted the loads at first cracking. Racking tests were performed to determine the diagonal cracking strengths of the infill materials for CMU 2 ft. by 2 ft. specimens where the strength was found to be 225 psi. The diagonal cracking strengths can be taken to be equal to one tenth of the compressive strength of the masonry prisms. The Liauw and Kwan method best estimated the ultimate strengths of the infills, although its predictions were over twice the experimental strengths in three of the four cases.

Table XXV

Comparison of Estimated to Experimental Strengths

Method	Model 2		Model 3		Model 4*		Model 5*	
	Strength (kips)	Est / Exp	Strength (kips)	Est / Exp	Strength (kips)	Est / Exp	Strength (kips)	Est / Exp
Experimental								
First Cracking Strength	14.2	-	14.1	-	24.3	-	29.7	-
Ultimate Strength	18.9	-	20.0	-	71.4	-	83.0	-
ECOEST/PREC-8								
First Cracking Strength	44	3.1	35	2.5	80	3.3	159	5.4
Ultimate Strength	57	3.0	45	2.3	104	1.5	207	2.5
Holmes								
(ultimate strength)	215	11.4	126	6.3	276	3.9	543	6.5
Liauw and Kwan (ultimate strengths)								
1 – Crushing with Column Failure	50	2.6	38	1.9	80	1.1	138	1.7
2 – Crushing with Beam Failure	69	-	52	-	110	-	189	-
3 – Diagonal Crushing	87	-	52	-	114	-	222	-
Mainstone								
First Cracking Strength	62	4.4	40	2.8	85	3.5	161	5.4
Crushing Strength	101	5.3	67	3.4	142	2.0	263	3.2

* For the multiple-bay specimen, the estimated strengths are the product of the strength for a single bay and the number of bays.

Table XXVI

Average of the Estimated to Experimental Strength Ratios

Method	Average
ECOEST/PREC-8	
First Cracking Strength	3.6 ± 1.3
Ultimate Strength	2.3 ± 0.7
Holmes (ultimate strength)	7.0 ± 3.1
Liauw and Kwan (ultimate strengths)	1.8 ± 0.6
Mainstone	
First Cracking Strength	4.0 ± 1.1
Crushing Strength	3.5 ± 1.4

7.3 Empirically Fitting Analytical Methods to Experimental Stiffnesses

The infill-frame stiffnesses were calculated from linear elastic analyses with the equivalent struts serving as pin-connected diagonal compression members bracing the rigidly connected reinforced concrete frames. These stiffnesses are compared to those measured in the experimental testing summarized in Table XXVII.

None of the equivalent-strut methods consistently predicted the experimentally determined stiffnesses. The method of Dawe and Seah best estimated the actual stiffness and provided the most consistent results. Mainstone's method also provided better estimates and his method presently employed in the NEHRP Guidelines for the Seismic Rehabilitation of Buildings [41].

Various constants were introduced in each method so that the estimated stiffness would match the experimental value. The linear elastic analysis previously described was again used to determine the area of the equivalent-strut necessary to match the experimental stiffnesses exactly. Instead of running numerous analyses interactively, data from Table XXVII were used to estimate the area of the strut necessary to make the ratio of estimated stiffness to experimental stiffness equal to 1. These plots are shown in Figure 7.1 and the regressions for each line show

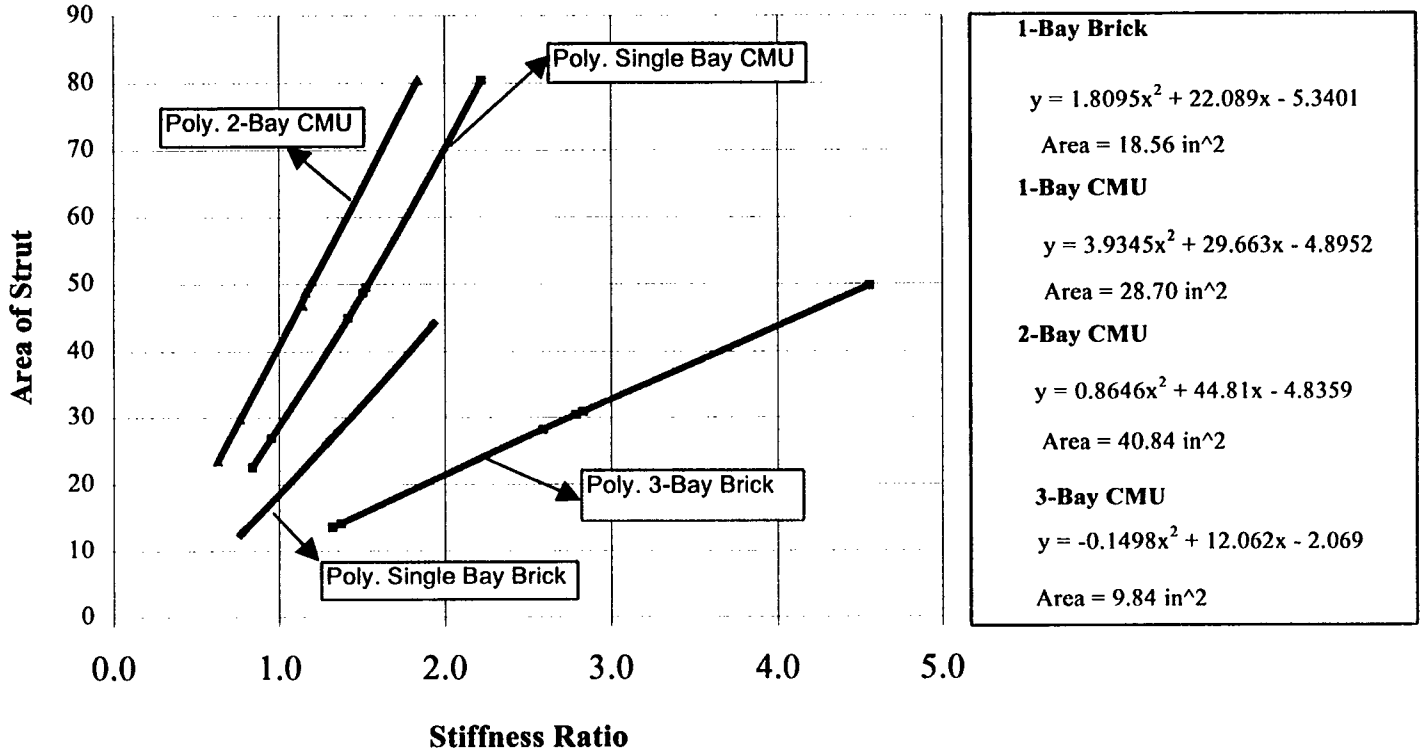

Figure 7.1 Area of Equivalent Strut Versus Ratio of Estimated to Experimental Stiffness

Table XXVII

Comparison of Estimated and Experimental Stiffnesses

Model	Analytical Method	Area of Strut (in^2)	Estimated Stiffness (kip/in)	Ratio of Estimated to Experimental
1-Bay Brick	Experimental Stiffness = 410 kip/in			
	Dawe and Seah	12.6	313	0.76
	Mainstone	13.1	322	0.78
	Durrani	26.1	528	1.29
	SS1	26.8	539	1.31
	SS2	27.9	556	1.36
	Holmes	44.2	794	1.94
	Lefter and Colville	*	1817	4.43
	ECOEST/PREC 8	*	2267	5.53
1-Bay CMU	Experimental Stiffness = 547 kip/in			
	Mainstone	22.6	457	0.83
	Dawe and Seah	26.9	520	0.95
	Durrani	45.0	774	1.42
	SS1	48.7	824	1.51
	SS2	49.5	834	1.52
	Holmes	80.4	1215	2.22
	Lefter and Colville	*	3081	5.63
	ECOEST/PREC 8	*	3926	7.18
2-Bay CMU	Experimental Stiffness = 814 kip/in			
	Mainstone	23.5	662	0.81
	Dawe and Seah	29.7	802	0.99
	Durrani	46.8	1210	1.49
	SS1	48.7	1228	1.51
	SS2	50.4	1268	1.56
	Holmes	80.4	1944	2.39
	Lefter and Colville	*	3962	4.87
	ECOEST/PREC 8	*	4972	6.11
3-Bay Brick	Experimental Stiffness = 923 kips/in			
	Dawe and Seah	13.6	1219	1.32
	Mainstone	14.2	1266	1.37
	Durrani	28.2	2392	2.59
	SS1	30.4	2574	2.79
	SS2	30.9	2611	2.83
	Holmes	49.8	4207	4.56
	Lefter and Colville	*	7806	8.46
	ECOEST/PREC 8	*	9894	10.72

* These are not equivalent-strut methods.

that the estimated areas should be sufficiently accurate. (Equivalent strut areas calculated from the trend lines are for stiffnesses equal to experimental values, at x=1, for each case).

7.4 Comparison of Finite Element Solution to Experimental Data

The finite element analysis results and experimental strengths, displacements, and stiffnesses for Models I, II, IV, and VI are shown in Table XXVIII. It can be clearly seen that the finite element analysis and experimental ultimate loads are very close for each model and they fall all within 8.5%. The finite element analysis underestimates the corresponding displacements for all of the four models, which therefore causes a corresponding discrepancy in the stiffness values at 100% of the ultimate load (Table XXVIII). The predicted FEM stiffness at 50% of the ultimate loads are closer than those at 100% of ultimate. (Table XXVIII).

Looking at the different models 100% of ultimate values, the bare frame model's (I) finite element data were in closest agreement with the experimental data. The displacement value predicted by the finite element was approximately 20% lower than the experimentally determined value of displacement. Obviously, the corresponding difference in the stiffnesses reflects the difference in displacements. The double-bay CMU model, also having close analytical and experimental ultimate load values, has the largest relative gap in displacement values with the predicted over 60% lower than the experimentally determined value. The predicted stiffness values for the single-bay and double-bay CMU models are much greater than the experimental, over 83% and 139%, respectively. The triple-bay brick model also has very close predicted and experimental ultimate loads, but the predicted displacement is approximately 32% lower than the actual experimental. Once again, this causes a corresponding discrepancy in

the stiffness values. The single-bay CMU model also has relatively close analytical and experiment values for ultimate load, but has a finite element displacement over 41% lower than the experimental.

Looking at the different models at 50% of ultimate load, all of the corresponding finite element displacements were within 48% of the experimental. The bare frame and double-bay CMU had finite element displacements underestimating the experimental values, while the single-bay CMU and triple-bay brick had finite element displacements larger than experimental. The corresponding stiffnesses where also closer than for 100% of ultimate with all finite element stiffness values within 81% of experimental.

Table XXVIII

Comparison of Experimental Data and Finite Element Analysis

Model Designation		Description	Load at 50% Of Ultimate (kips)		Corresponding displacement to 50% of Ultimate load (in)		Stiffness At 50% Ultimate (kips/in.)		Ultimate Load (kips)		Corresponding displacement At ultimate load (in)		Stiffness At 100%	
FEA	EXP		FEA	Exp.	FEA	Exp.	FEA	Exp.	FEA	Exp.	FEA	Exp.	FEA	Exp.
I B1O	I	Single-bay bare frame	3.5	3.25	0.109	0.141	32	23	7.0	6.5	0.370	0.467	19	14
II B1F-CMU	II	Single-bay CMU Infilled Frame	10.25	9.45	0.024	0.017	427	547	20.5	18.9	0.050	0.085	410	223
IV B2F-CMU	IV	Double-bay CMU infilled frame	33.5	35.7	0.023	0.044	1475	814	67.0	71.4	0.047	0.120	1425	595
VI B3F-BR	VI	Triple-bay Brick Infilled frame	44.0	41.5	0.052	0.045	853	923	88.0	83.0	0.100	0.148	830	561

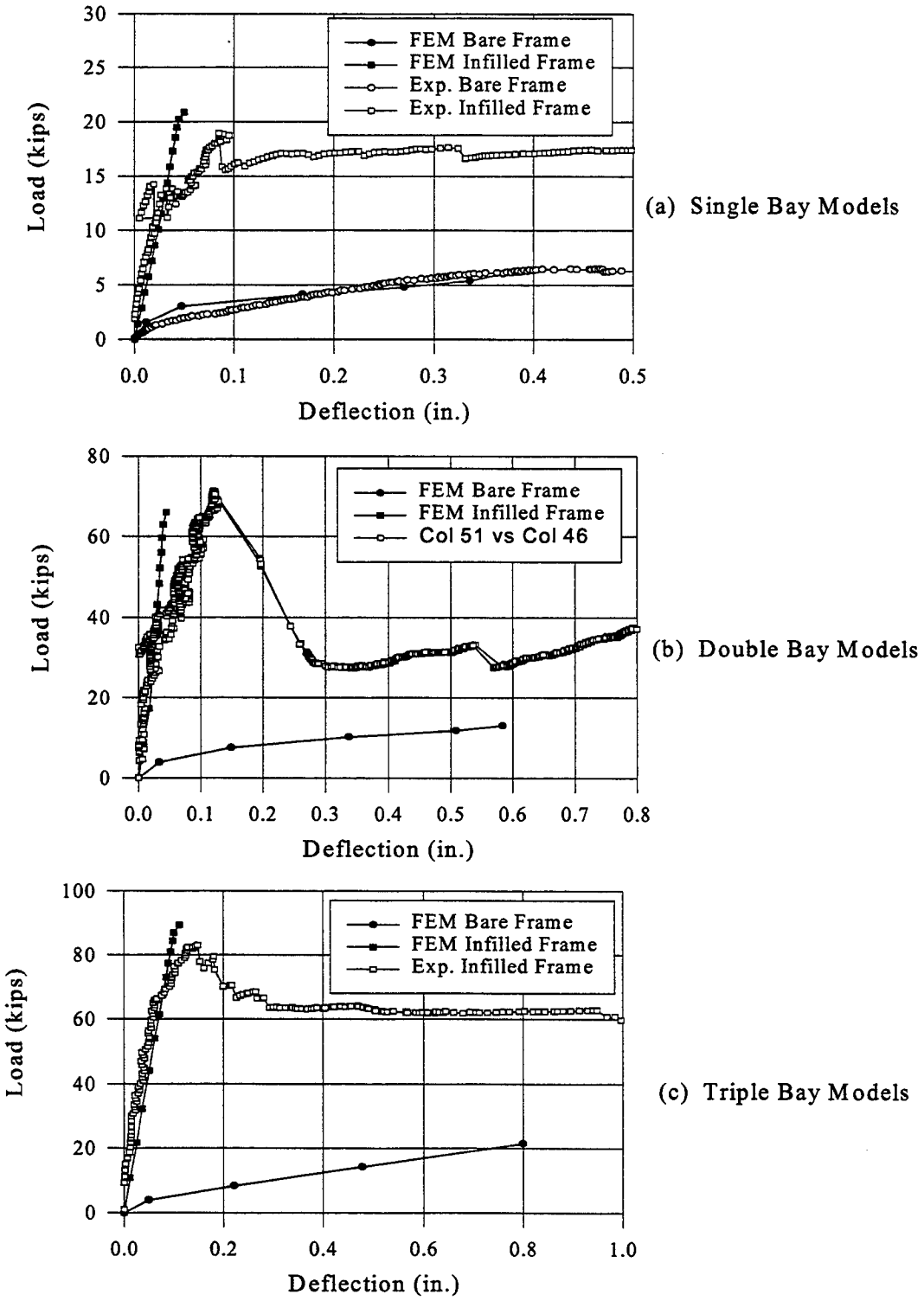

Figure 7.2 Load-Deflection Curves for FEM and Experimental Results

CHAPTER 8

PROPOSED SIMPLIFIED METHOD FOR CAPACITY EVALUATION OF NON-DUCTILE R/C FRAMES INFILLED WITH MASONRY PANELS

8.1 Introduction

Due to the wide variation in experimental and analytical results, it was necessary to develop an analytical method applicable only to the tested models and the structures they represent. This proposed method adopts the equivalent diagonal strut philosophy to predict the behavior of the system. Determination of the diagonal strut width is the key to accurate analysis. This new approach identifies the appropriate width of the strut to reflect the strength and stiffness of structures incorporates new parameters that best reflect the modes of failure of the system. Some basic parameters used in previous studies were also used, and rearranged to reflect the properties of the non-ductile R/C frame with masonry infill. These properties were related based on experimental results, analytical investigations, judgments, and numerical correlation.

Basic dimensions parameters:

H: Height of the infill (inch)

w: Width of the infill (inch)

D: Diagonal length of the infill (inch)

θ : Angle of the diagonal from horizontal

h : Height of the frame, column center-to-center (inch)

L : Length of beam between center of columns (inch)

t : Infill thickness (inch)

Lc1, Lc2: Columns dimensions

Lb1, Lb2: Beams dimensions

Ac, Ab: Cross-section area of columns and beams

Ic, Ib: moment of inertia (in^4)

Basic mechanical properties:

Ei : Young's modulus of the infill (ksi)

Ef: Young's modulus of the frame (ksi)

f'm: prism compressive strength

Fv: shear strength

Kf: stiffness of the frame

ε_col: strain energy from tension column

ε_strut: strain energy from compression in strut

Behavioral properties:

λ Relative stiffness parameter of the infill and frame

R_Str: Compressive/shear strength ratio

w_o: Unadjusted strut width

R_ε: Factor of strain ratio

η: Factor for multiplicity of bays

w: Adjusted strut width

Φ Load distribution factor in trusses

The relative stiffness parameter λ described by Smith (1966) is adopted to describe the contact length between the frame and the infill. However, this parameter is the result of two components, λc and λb, related to the interaction of infill to columns and beams, respectively. The projection of the resultant contact length parameters, λc and λb perpendicular to the diagonal, is defined as the relative stiffness parameter.

The width of the diagonal strut is also adopted from Smith (1966). Smith related the relative stiffness parameter to account for the effect of aspect ratios, as shown in Figure. 8.1.

Figure 8.1 shows that the aspect ratio and λh can be used to determine the value for w/d, for which w can be solved. The value for w/d can also be determined by the following equation for an aspect ratio of 1.38.

$$\frac{w}{d} = 1000 + \frac{0.3827}{\lambda h}$$

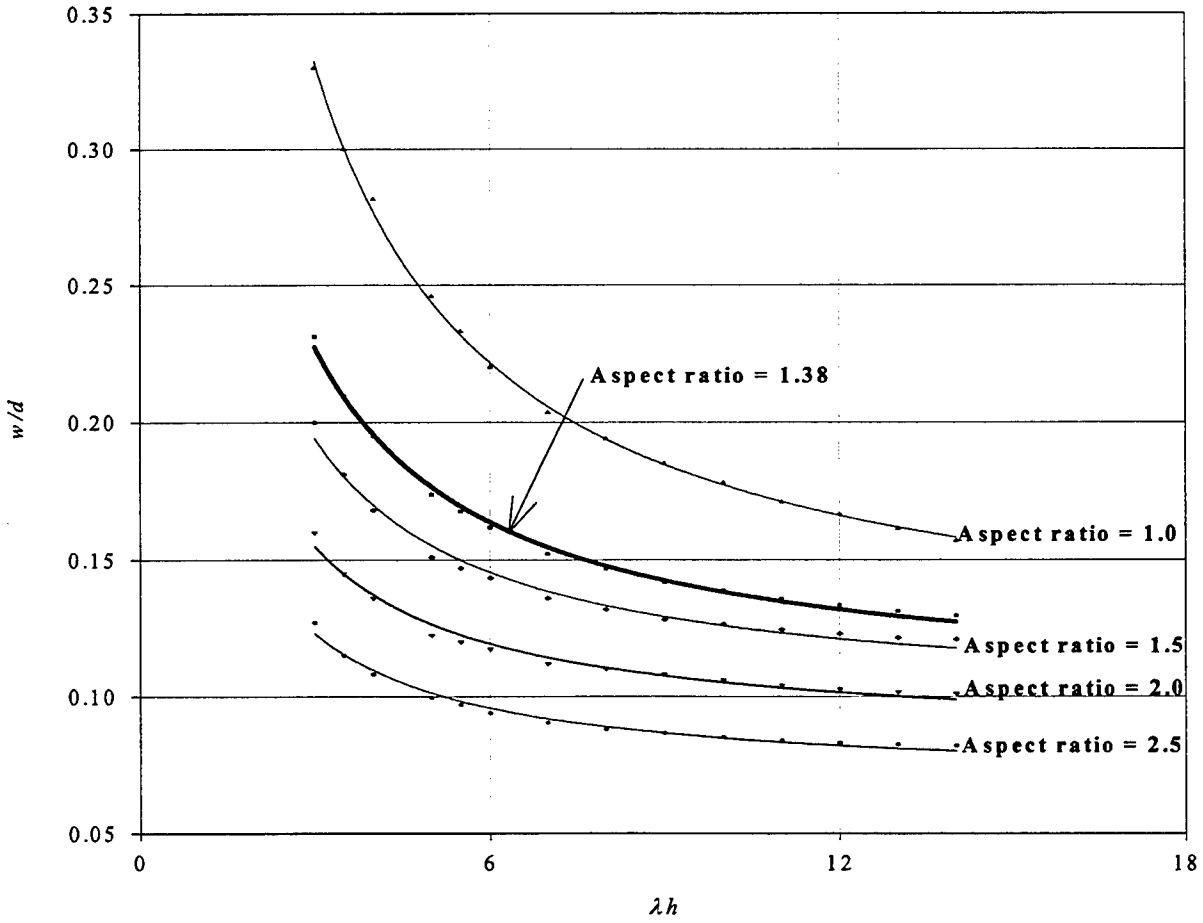

Figure 8.1: w/d as a Function of λh for Different Aspect Ratios

8.2 Adjusted Strut Width

The strut width shall be adjusted to account for:

1. multiplicity of bays factor
2. modes of failure factors
3. non-ductility factors
4. load distribution in trusses factors

8.2.1 Multiplicity of Bays Factor (η)

Analytical methods proposed previously did not account for the effects of the number of bays in their procedures. The hypothesis that the number of bays must be considered in the analytical procedures was obviously accurate from examining the variations of strength and stiffness of tested models. The variation in strength between the models was not linear. As shown in Figure 8.2, the function best describing the variation of strength in terms of bay numbers is:

$$P = 60Ln(x) + 20$$

where x is the number of bays and P is the ultimate load.

Based on this relationship, the multiplicity of bays (bay numbers) factors are listed in Table XXIX. They are calculated for two or more bays as follows:

$$\eta = \frac{\ln(\frac{0.85\ \beta\ f_c^{'} A_b}{P})}{\ln(\frac{0.85\ \beta\ f_c^{'}}{20})}[\frac{1}{x}]$$

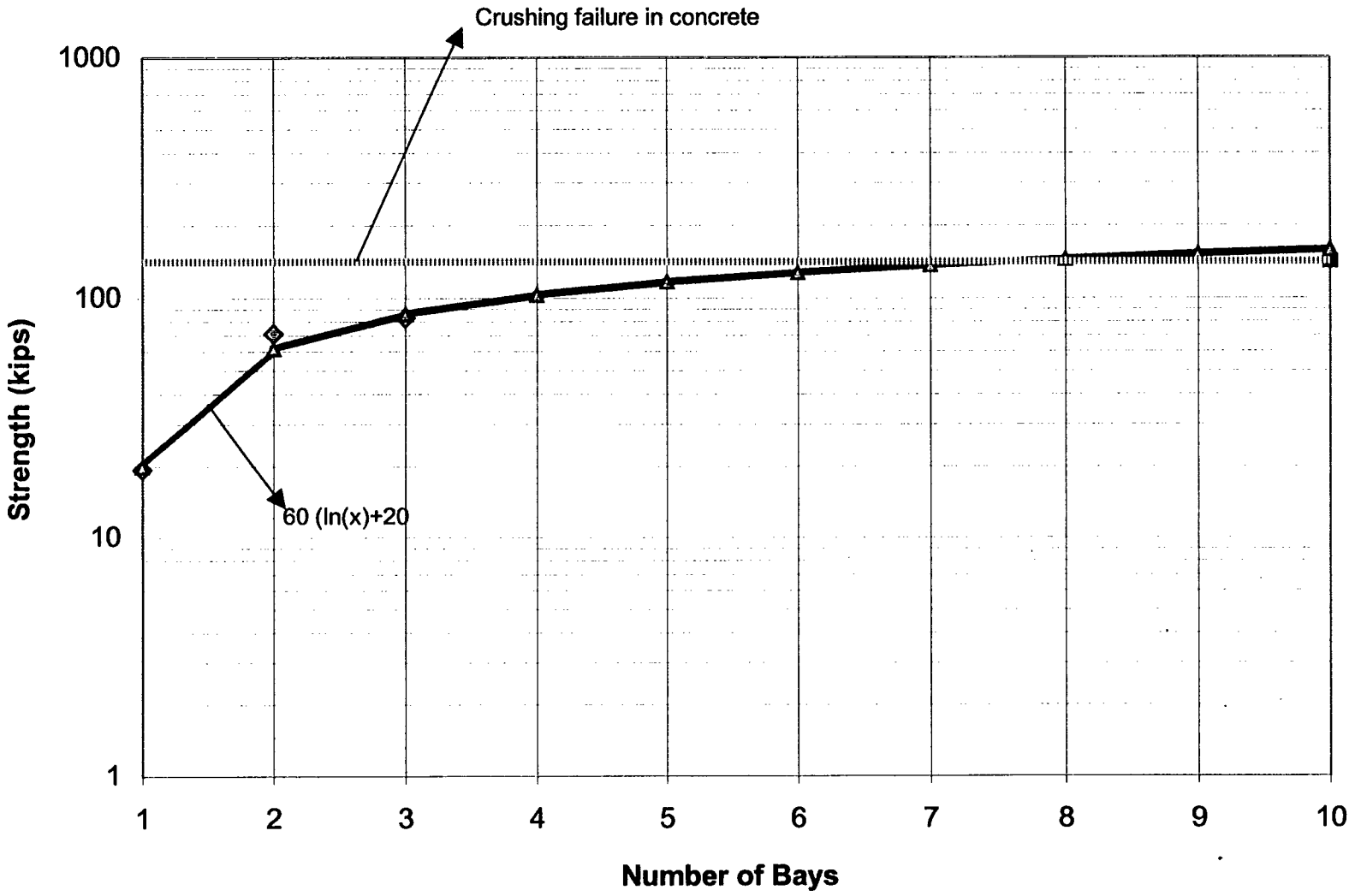

Figure 8.2 Relationship Between Number of Bays and Ultimate Strength

Table XXIX

Bay Factors

Number of Bay	1	2	3	4	5	6	7	8	9 or more
Bay Factor	1.000	1.436	1.278	1.203	1.160	1.131	1.111	1.097	1.000

8.2.2 Modes of Failure Factors

The infill panels of the tested models were observed to fail by one of the three mechanisms, namely:

1. strut formation failure
2. plate formation failure
3. corner crushing failure

Strut formation failure represents a desirable structural behavior since the system reflects a good composite behavior between the infill and the R/C frame. The plate formation failure exhibited the weakest failure mechanism, while the corner crushing failure, surprisingly, exhibited the highest strength. Despite the local crushing of the infill at the panel's corners, significant strength remained in the system. This is attributed to the fact that this failure was not associated with any diagonal cracks and the R/C frame confinement was effective. Factors related to the modes of failure are summarized in Table XXX.

Table XXX

Expected Modes of Failure and Their Factors

	Failure Mechanism Compressive-Shear Ratio Factor Column-Beam Strain Energy Ratio Factor
Model 2*	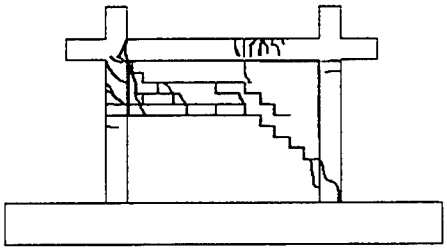 **R_str = 1.0, R_ε = 1.0** Plate Formation Failure
Model 3*	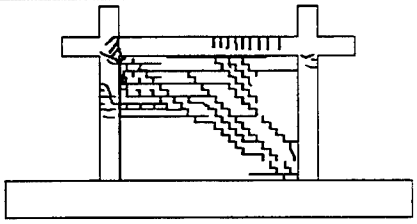 **R_str = 1.05, R_ε = 1.0** Strut Formation Failure
Model 4*	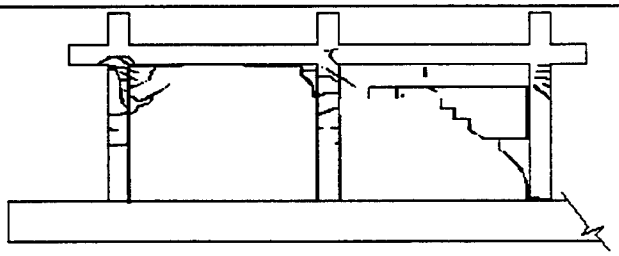 **R_str = 1.0, R_ε = 1.05** Corners Crushing Failure
Model 5*	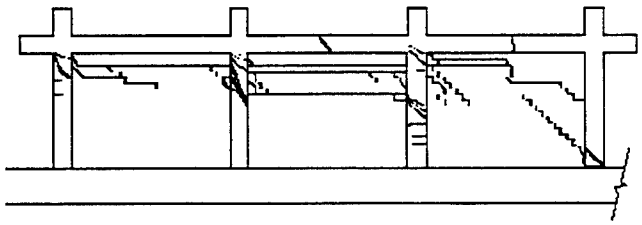 **R_str = 1.0, R_ε = 1.0** Plate Formation Failure

* All Models loaded at the left ends

The question as to why the infill panels fail by forming struts or plates needs further investigation. However, the available data indicates that the modes of failure are driven by compressive and shear strength panels. This observation was based on the brick and CMU panel material properties. The brick panels had a high compressive strength of 3387 psi and a shear strength of 134 psi, while the CMU panels had a lower compressive strength and a higher shear strength. This explains why the single-bay with CMU infill specimen failed by the plate formation mechanism, while the single-story with brick infill specimen failed by the truss formation mechanism. The compressive and shear strength ratio of one panel by itself does not explain why the three-bay brick specimen failed by the plate formation mechanism. The failures caused by strut formations are also limited by the shear resistance of all the infilled panels. Based on these observations, the compressive and shear strength ratio factor is introduced as follows:

$$R\_str = 1.05 \ \ for \ \ \frac{\psi}{v} > 36, \ otherwise \ is \ 1.0$$

where:

$$\psi = \frac{f'm}{wt}$$

$$v = \frac{f}{xHt}$$

Corner crushing failures depend on the strain energy from tension in column and the strain energy from compression in the equivalent diagonal strut. The equations for computing strain energies are described by Smith (1962). The strain energy from tension in the column is:

$$\varepsilon\_col = \frac{h \tan(2\theta)}{Ac\ Ef}$$

Strain energy from compression in the equivalent diagonal strut is:

$$\varepsilon\_strut = \frac{d}{W_0\, t\, Ei \cos(2\theta)}$$

It is estimated that crushing occurs at:

$$\frac{\varepsilon\_strut}{\varepsilon\_col} \geq 3.5 \quad \Rightarrow \textit{crushing}$$

Therefore the strain ratio factors are defined as:

$$R\_\varepsilon = 1.05 \;\; for \frac{\varepsilon\_strut}{\varepsilon\_col} > 3.5 \;\; and \;\; x > 1, \;\; otherwise \;\; is \; equal \; to \; 1.0$$

These factors are used on the unadjustable equivalent strut to obtain the adjustable equivalent strut as follows:

$$w = \phi\eta \, (R\_str) \, (R\_\varepsilon) \, W_0$$

where ϕ is the non-ductility factor = 0.48 for CMU infill and = 0.6 for brick infill.

8.2.3 Load Distribution in Trusses Factor of Multiple-Bay and Multiple-Story Specimens

The Stafford-Smith II method was used to model multiple-bay reinforced concrete frames with masonry infill subjected to a single lateral load applied at the top story. Nine different configurations of multiple bays were evaluated, ranging from a single-bay to a three-story high and three-bay wide frame. For each configuration, the relative resistance each strut provided was determined by dividing the force within each strut by the sum of all the forces in the struts. The resistance provided by each strut was indicated by a percentage of the total resistance in each configuration.

The effects of the infill stiffness were also evaluated by using three different infills with the same reinforced concrete frame sections. The first iteration represented infills of concrete masonry units with the same material properties as the single-bay specimen tested previously. In the Stafford-Smith II method, this infill and frame system had a stiffness parameter of $\lambda h = 3.5$, which is a relatively stiff infill. The second iteration had a more flexible infill with $\lambda h = 3.5$, which is a typical value. The third iteration sought to model the frame system with essentially no infill. Very slight struts were used to determine the distribution of forces within each bay, and these struts provided little resistance.

The stiffer the infill, the greater was the resistance provided by equivalent struts located within a diagonal path originating from the upper windward column down to the base of the leeward column. In contrast, the frames with very slight diagonal struts tended to distribute forces uniformly throughout the structural system. In the frames with typical infills, the amount of resistance provided at each floor level by the sum of the struts at that level was evenly distributed between each floor. This distribution was not evident in the frames with the slight struts.

The lateral resistance provided by the infills worked to significantly reduce the leeward drift as compared to the windward drift. The stiffer the infills the greater in reduction was the windward drift at the top floor. The frames with slight struts had essentially the same amount of leeward drift as windward drift. Moment-curvature and moment-thrust diagrams used in this investigation were developed (Figures 8.3 and 8.4, respectively). The load distribution factors are summarized in Figure 8.5 and Table XXXIII.

Applying this procedure to the four models and using the DRAIN-2DX structural program [11, 25, 43] yielded the equivalent strut widths shown in Table XXXI, and the loads summarized in Table XXXII.

Table XXXI

Equivalent-Strut Width Summary

	Width of Equivalent Strut Based on Proposed Procedure (in)	Width of Equivalent Strut to Satisfy Empirical Loads Using RAIN-2DX (in)	Percentage of Errors
Model 2	7.05	8.16	-15.7%
Model 3	12.65	10.69	15.5%
Model 4	13.67 (Windward) 11.18 (Leeward)	13.54 (Windward) 11.07 (Leeward) 12.3 *	0.95% 0.98%
Model 5	16.5 11.23 9.28	16.7 11.99 9.67 12.9 *	-1.2% -6.7% -4.2%

* Adjusted width not factored for load Distribution

Table XXXII

Load Summary

	Strength of Models Based on Proposed Procedure Using DRAIN-2DX (kips)	Empirical Strength of Models (kips)	Percentage of Errors
Model 2	21.03	18.9	10.1 %
Model 3	17.7	20.0	-13.0 %
Model 4	70.8	71.4	-0.85 %
Model 5	84.7	83.0	+2%

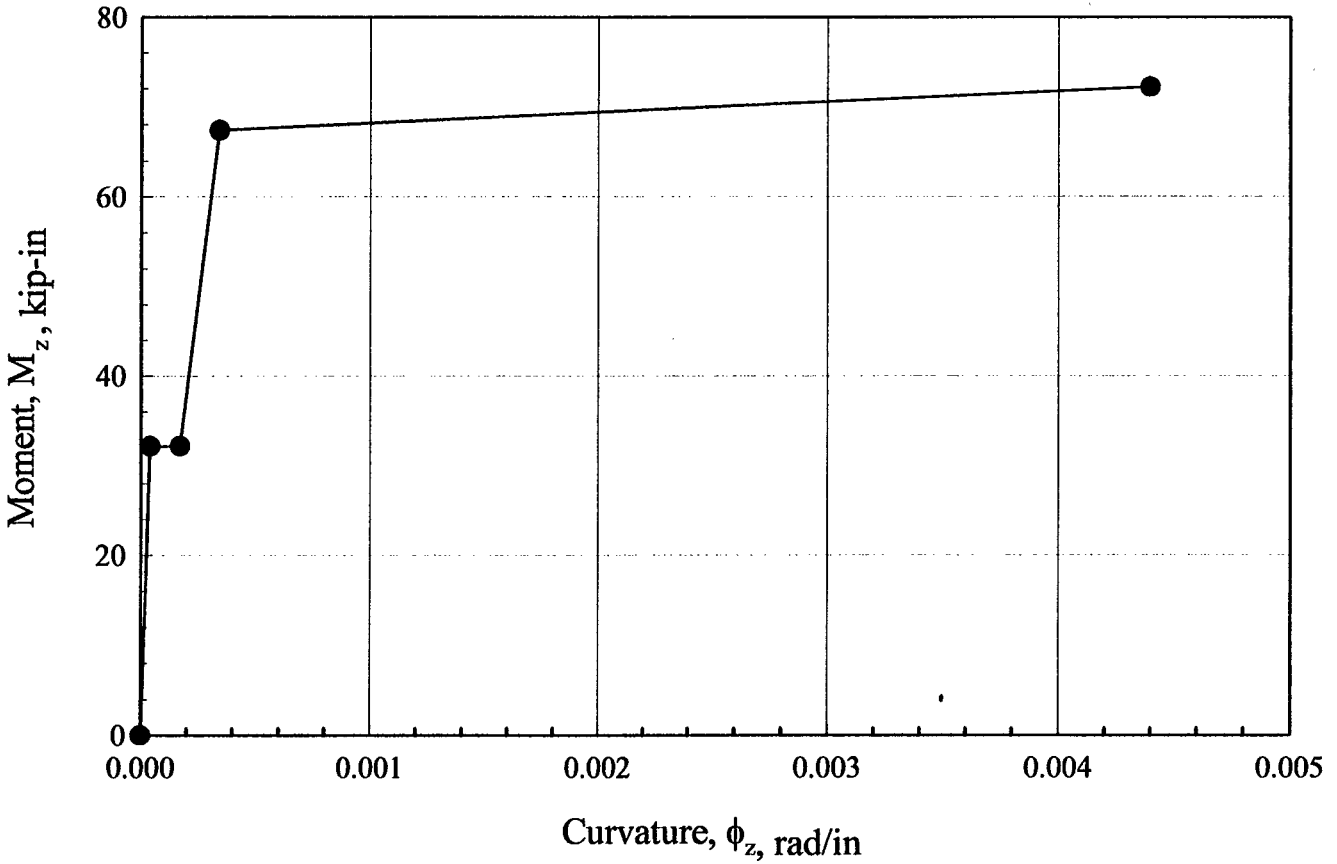

Figure 8.3 Moment-Curvature Diagram for Positive and Negative Column Bending, Bare Single-Bay

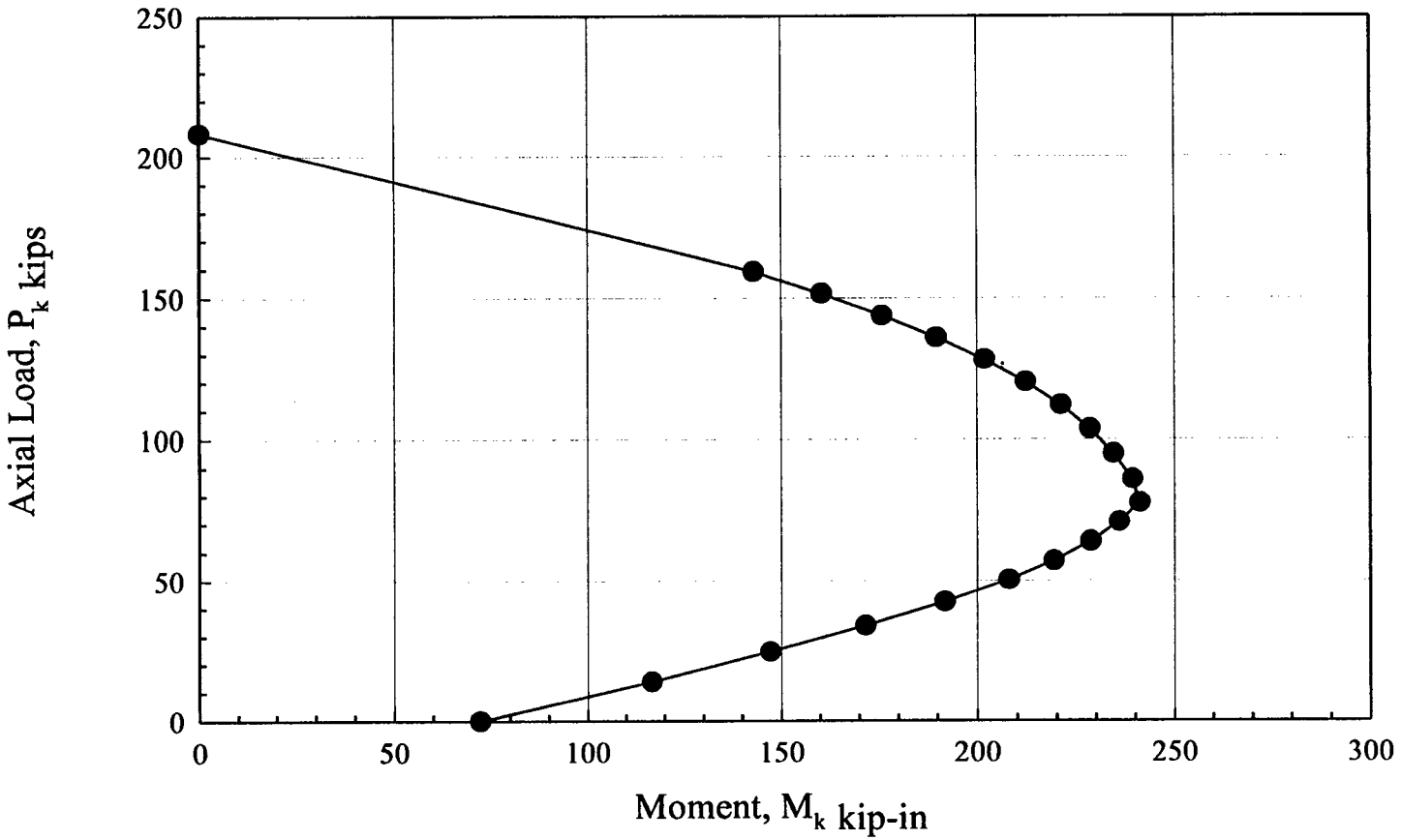

Figure 8.4 Moment-Thrust Diagram for Positive and Negative Bending of Columns, Bare Single-Bay

Table XXXIII

Distribution of Forces in Equivalent Struts*

h = 3.5

	Level	Single-Bay	Double-Bay		Triple-Bay		
			Windward	Leeward	Windward	Center	Leeward
Single-Story	1	100%	55%	45%	44%	31%	25%
Two-Story	2	50%	30%	20%	23%	17%	10%
	1	50%	21%	29%	13%	18%	19%
Three-Story	3	33%	20%	13%	15%	12%	6%
	2	34%	16%	17%	10%	13%	11%
	1	33%	13%	20%	8%	11%	14%

h = 10.5

Single-Story	1	100%	54%	46%	41%	32%	27%
Two-Story	2	50%	29%	21%	22%	17%	12%
	1	50%	22%	28%	14%	17%	19%
Three-Story	3	33%	19%	14%	14%	12%	7%
	2	34%	16%	17%	10%	12%	11%
	1	33%	14%	19%	9%	11%	13%

h >> 10.5

Single-Story	1	100%	50%	50%	34%	33%	33%
Two-Story	2	46%	27%	26%	18%	18%	17%
	1	54%	23%	23%	16%	16%	16%
Three-Story	3	34%	17%	17%	11%	10%	11%
	2	38%	19%	19%	12%	13%	13%
	1	28%	14%	15%	10%	10%	10%

* Strut width is based on SS2 idealized method. Frames were analyzed using SAP90

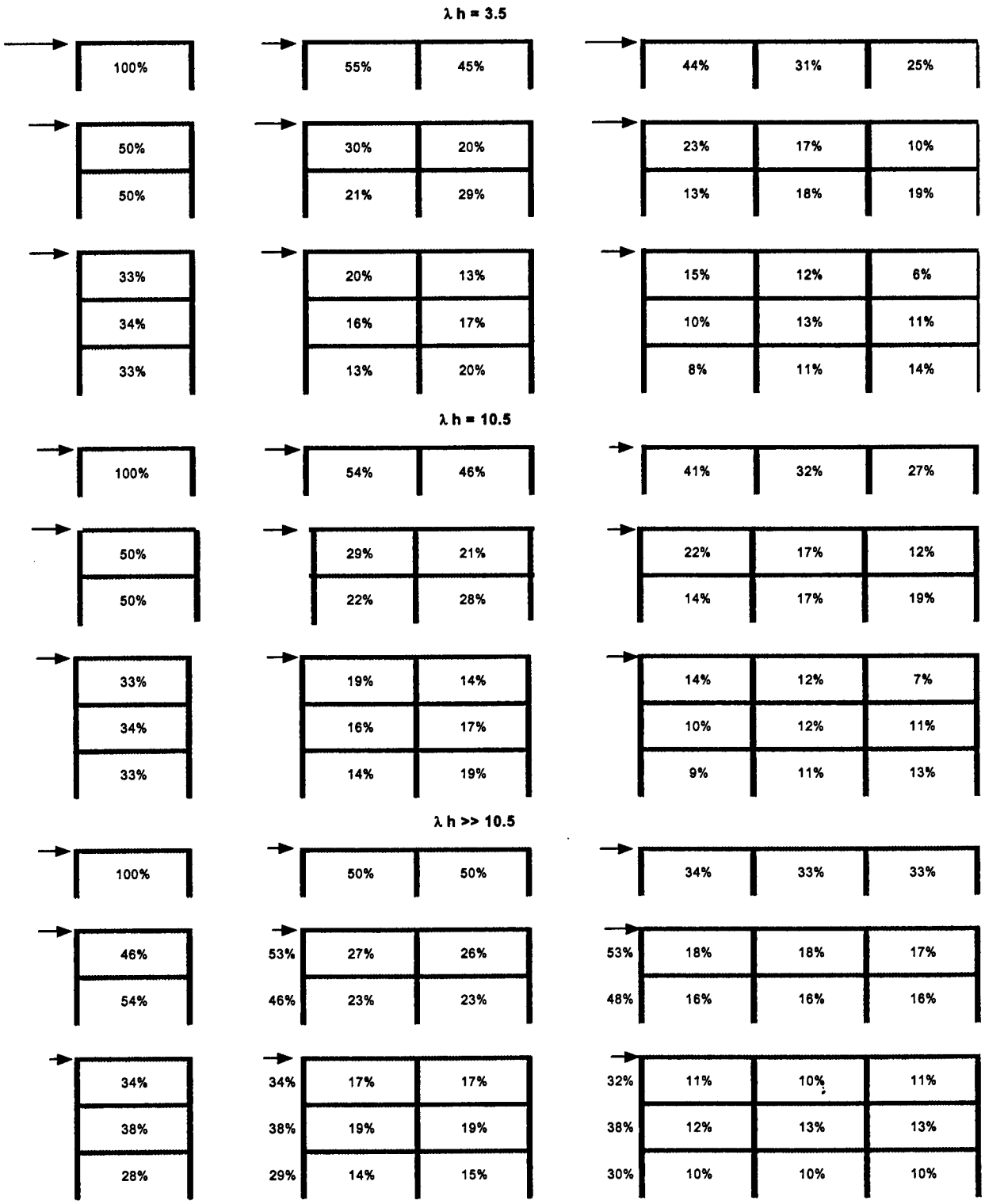

Note: Strut width is based on SS2 method frames were analyzied by SAP90 structural program

Figure 8.5 Distribution of Forces in Equivalent Struts

CHAPTER 9

CONCLUSIONS AND RECOMMENDATIONS FOR FUTURE RESEARCH

9.1 Conclusions

Five half-scale models were fabricated, instrumented, and tested under lateral in-plane loading to failure. These models represent Type 10 of the 15 lateral-load-resisting systems in buildings identified by FEMA. This type of structure is typical in high seismic zones for its economy, however, the non-ductile R/C frames must be distinct from ductile detailing of the R/C frame required by recent building codes. The models consisted of:

1. Single-bay bare frame
2. Single-bay with CMU infill
3. Single-bay with brick infill
4. Double-bay with CMU infill
5. Triple-bay with brick infill

Non-linear finite element analysis were carried out on six models. Three out of these six models were single-bay, double-bay, and triple-bay reinforced concrete frame infilled with masonry. The remaining three models were single-bay, double-bay, and triple-bay reinforced concrete frames without masonry infill.

The following conclusions can be drawn as a result of the study:

1. A new analytical simplified method is proposed in this study, which accounted for all possible failure mechanisms identified during testing. This simplified approach provides less conservative, more cost-effective, and accurate assessment procedures for existing non-ductile infilled frames.

2. The compressive and shear strength ratio was believed to introduce certain failure mechanism types.
3. The relationship in strain energy of columns and strain energy of the equivalent diagonal strut is also believed to impose a failure by corners crushing infill panels. This method is the first to account for the variation of strength in terms of bay multiplicity. The variation in strength is due to the composite behavior of the system as the confinement condition on each infill panel and degree of restraint of neighboring panels varies.
4. The load distribution varies in diagonal struts of frames loaded in plane. The unequal proportion of loads in the diagonal struts has shown that unequal diagonal struts reflect more accurately the behavior of structural systems under considerations. Thus, the new analytical simplified method has accounted for this observation and suggested increasing or decreasing the equivalent diagonal strut to reflect the load distribution in diagonal struts subjected to lateral in-plane load. Prior to cracking, the infill redistributes the stresses in the frame resulting in more displacement and stresses in the windward column than that of the others. After cracking, diagonal struts were developed in the infill, resulting in increasing the overall shear capacity of the infilled frame.
5. All proposed simplified analytical procedures were modified to satisfy the experimental results. Factors were added to the basic equations such that the width of the equivalent-strut yields the measured strength of stiffness intended in the methods. The nonlinear FEA indicated that the infill increases significantly the ultimate load capacity and overall stiffness of the infilled brick and CMU frames.

6. Results from FEA for each model were a useful preliminary guide in evaluating behavior of such complex structures and providing critical indications for locating strain gages and LVDTs.
7. Load-deflection curves for FEA reasonably predicted experimental behavior of specimens in terms of deflection. Ultimate failure load corresponding to each specimen was predicted with accuracy as indicated by change in direction in curves obtained from FEA analysis.

9.2 Recommendations for Future Research

Table XXXIV provides a list of variables that characterize any structural system constructed from frames with masonry infill panels. Combinations of these variables are numerous, and conducting tests to cover all variables is not economical. It is obvious that generalizing the findings based on one set of variables may be misleading.

Due to the stochastic nature of masonry infill, the approach to analyze any combination of variables may agree with other variable combinations in philosophy, but not necessarily in methodology. A complete set of tests to investigate the effect of boundary conditions shall cover at least nine specimens as shown in Figure 9.1. The cost associated with testing a complete set of full or reasonable scales is high. However, comparing the testing costs with the cost of repairing damage of buildings makes further testing economically feasible.

The effect of bay-multiplicity in single-story models was investigated in this study. The effect of bay-multiplicity combined with multiplicity of stories shall be investigated in future research to produce a more refined analytical method with a higher level of accuracy.

Table XXXIV

Major Variables that Characterize Frame Structures with Masonry Infill

Variable	Main Possibilities	USACERL Models
Ductility of reinforced concrete frame	• Ductile • Non-ductile	non-ductile
Scaling of the models	Any	Half or small scale
Infill type	• CMU • Brick	CMU and brick
Frame type	• Steel • Reinforced concrete	Concrete
Mortar	• M • S • N • O	N
Infill reinforcement	• Reinforced • Unreinforced	Unreinfroced
Frame and infill layout	• Integral • Non-integral	Integral
Frame infilled	• Fully • Partially	Fully
Opening in the infill panels	• With/without opening	No opening
Aspect ratio of the infill	Any	1.377
Slenderness ratio	Any	• 19.28 for triple-bay infill brick panels • 13.93 for CMU infill panel
Bays	Any	• Single • Double • Triple
Stories	Any	1
Loading	• Monotonic • Cyclic • Earthquake	Monotonic
Cell grout of masonry units	• Grouted cells • Not grouted • Partially grouted	Not grouted
Direction of loading	• In-plane • Out-of-plane	In-plane
Statistic	• Single data point per one model • Two or more data points per model.	Single data point per model

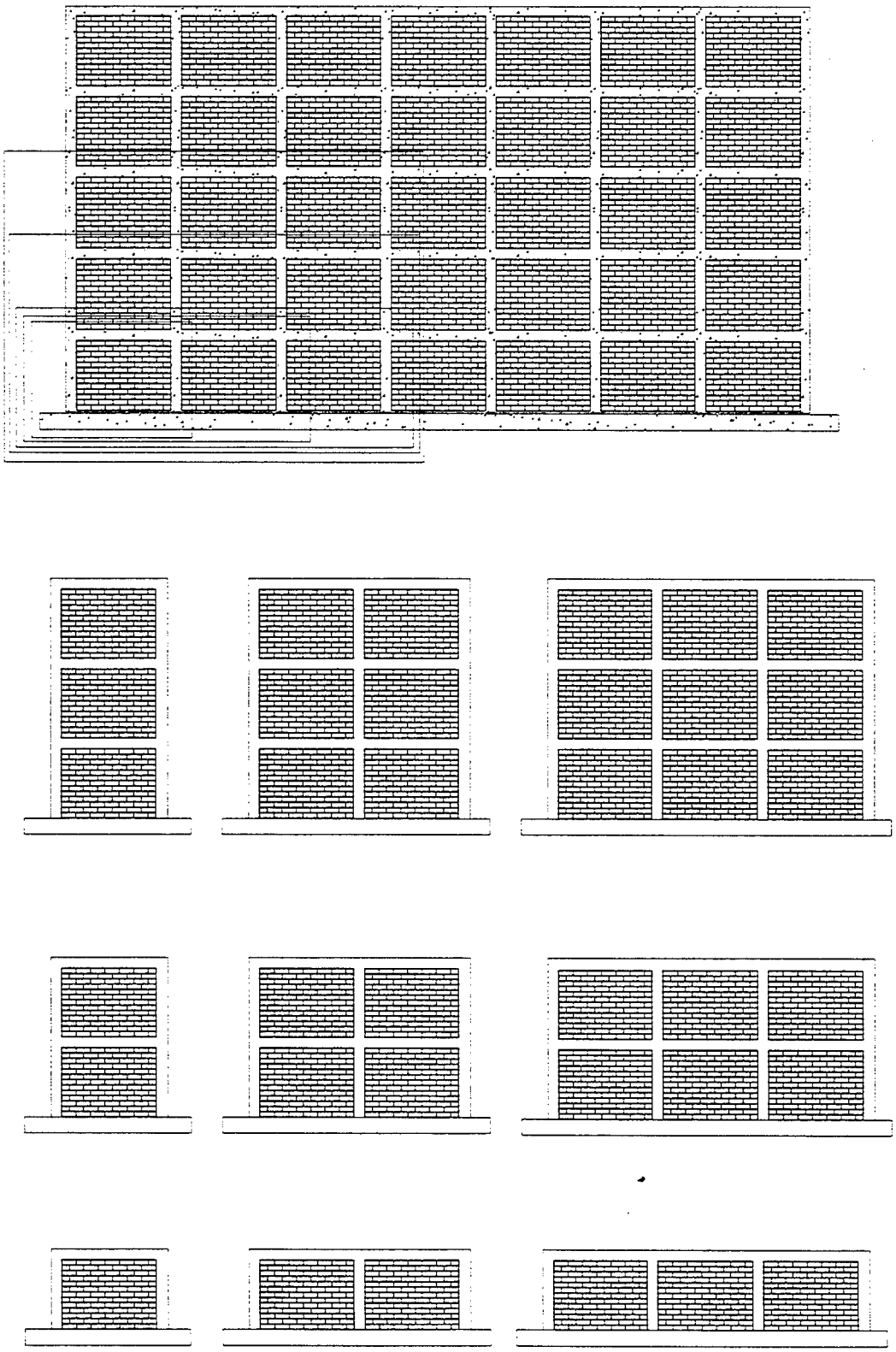

Figure 9.1: Minimum Model Required to Account for all Boundary Conditions

REFERENCES

1. Al-Chaar, G., Sweeney, S., and Brady, P.: Push Over Laboratory Testing of Unreinforced Masonry Infills. Wind and Seismic Effects, NIST SP 904, August 1996.

2. AlGOR Manual, Accupak Reference Manual, Nonlinear Stress and Vibration Analysis, 1996.

3. Allahbadi, R. and Powel, G. H. DRAIN-2DX User Guide.: EERC Report No. 88/06, University of California, Berkeley, 1988.

4. Allen, DeGarrs.: Relaxation Methods in Engineering and Science. McGraw-Hill Book Co., Inc New York, N. Y., 1954, pp. 105-111.

5. Angel, R.: Behavior of Reinforced Concrete Frames with Masonry Infill Walls. Ph.D. Thesis, Department of Civil Engineering, University of Illinois at Urbana-Champaign, 1994.

6. Barura, H.K., and S.K. Mallick.: Behavior of Mortar Infilled Steel Frames Under Lateral Load. Building and Environment, vol. 12, 1977.

7. Bathe, K-J.: Finite Element Procedures. Prentice-Hall, Inc., 1996.

8. Benjamin, J.R., and H.A. Williams.: The Behavior of One-Story Shear Walls. Journal of the Structural Division, Proceedings of the American Society of Civil Engineers, vol. 84, no. ST4, July 1958.

9. Bennett, R.M., R.D. Flanagan, S. Adham, W.L. Fischer, and M.A. Tenbus.: Evaluation and Analysis of the Performance of Masonry Infills During the Northridge Earthquake. Oak Ridge National Laboratory, February 1996.

10. Carter, C. and S.B. Smith.: Structural Behavior of Masonry Infilled Frames Subjected to Racking Loads. Designing, Engineering, and Constructing with Masonry Products F.B. Johnson, ed., 1969, pp 226-233.

11. Charney, F.A.: DrainPro User's Manual, Version 2.00, Advanced Structural Concepts, Inc., Golden, CO.

12. Dawe, J.L., and T.C. Yong.: An Investigation of Factors Influencing the Behavior of Masonry Infill in Steel Frames Subjected to In-Plane Shear. Proceedings of the 7th International Brick Masonry Conference, Brick Development Research Institute, 17-20 Febuary 1985, pp 803-814.

13. Dawe, J.L., and C.K. Seah.: Behavior of Masonry Infilled Steel Frames. Canadian Journal of Civil Engineering, vol. 16, 1989.

14. Despeyroux, J.: The El Asnam Earthquake of 10 October 1980: Characteristics of the Main Shock and Lessons To Be Drawn for Earthquake Engineering. Engineering Structures, vol. 4, July 1982.

15. Dhanasekar, M., and A.W. Page.: The Influence of Brick Masonry Infill Properties on the Behavior of Infilled Frames. Proceedings of the Institute of Civil Engineers, part 2, vol. 81, no. 9061, December 1986.

16. Durrani, A.J., and Y.H. Luo.: Seismic Retrofit of Flat-Slab Buildings With Masonry Infills. Proceedings from the NCEER Workshop on Seismic Response of Masonry Walls, Technical Report NCEER-94-0004 (National Center for Earthquake Engineering Research, 1 March 1994), pp 1-3 – 1-8.

17. El Haddad, M. H.: Finite Element Analysis of Infilled Frames Considering Cracking and Separation Phenomena. Computers & Structures, vol. 41, no. 3, 1991.

18. Fardis, M.N., Editor.: Experimental and Numerical Investigations on the Seismic Response of R.C. Infilled Frames and Recommendations for Code Provisions. European Consortium of Earthquake Shaking Tables and Prenormative Research in Support of Eurocode 8, no. 6 November 1996.

19. Federal Emergency Management Agency.: A Handbook for Seismic Evaluation of Existing Buildings. FEMA-178, June 1989.

20. Fedorkiw, J.P. and M.A. Sozen.: A Lumped-Parameter Model to Simulate the Response of Reinforced Concrete Frames with Filler Walls. Civil Engineering Studies, Structural Research Series No. 338, (University of Illinois, Urbana, June 1968.

21. Fiorato, A.E., M.A. Sozen, and W.L. Gamble.: Behavior of Five-Story Reinforced Concrete Frames with Filler Walls. An Interim Report to the Department of Defense, Office of the Secretary of the Army, Office of Civil Defense, University of Illinois, Urbana, January 1968.

22. Fiorato, A.E., M.A. Sozen, and W.L. Gamble.: An Investigation of the Interaction of Reinforced Concrete Frames with Masonry Filler Walls. Civil Engineering Studies, Structural Research Series No. 370 (University of Illinois, Urbana, November 1970).

23. Holmes, M.: Steel Frames with Brickwork and Concrete Infilling. Proceedings of the Institution of Civil Engineers, vol. 19, no. 6501 (August 1961).

24. Holmes, M.: Combined Loading on Infilled Frames. Proceedings of the Institutions of Civil Engineers, vol. 25, no. 6621, May 1963.

25. Kanaan, A. E. and Powel, G. H.: DRAIN-2DX. EERC Report No. 73-6 and 3-22, University of California, Berkeley, 1988.

26. King, G. J.W., and P.C. Pandey.: The Analysis of Infilled Frames Using Finite Elements. Proceedings of the Institution of Civil Engineers, part 2, vol. 65, no. 8145, December 1978.

27. Klingner, R. E., and V.V. Bertero.: Earthquake Resistance of Infilled Frames. Journal of the Structural Division, Proceedings of the American Society of Civil Engineers, vol. 104, no. ST6, June 1978.

28. Klingner, R.E., and V.V. Bertero.: Infilled Frames in Earthquake-Resistant Construction. Report EERC 76-32, University of California, Berkeley, California, December 1976.

29. Langenbach, Randolph.: Earthquakes: A New Look at Cracked Masonry. Civil Engineering, November 1992.

30. Lefter, J., and J. Colville.: Reinforcing Existing Building to Resist Earthquake Forces. Proceedings of CENTO Symposium on Earthquake Engineering and Engineering Seismology, University of Ankara, Turkey, 18-20 November 1974.

31. Leuchars, J.M., and J.C. Scrivener.: Masonry Infill Panels Subjected to Cyclic In-Plane Loading. Bulletin of the New Zealand National Society for Earthquake Engineering, vol. 9, no. 2, 1973.

32. Liauw, T.C. and K.H. Kwan.: Nonlinear Analysis of Multistory Infilled Frames. Proceedings of the Institution of Civil Engineers, Part 2, no. 73, pp. 441-454, 1982.

33. Lofti, H.R., and P.B. Shing.: An Appraisal of Smeared Crack Models for Masonry Shear Wall Analysis. Computers and Structures, vol. 41, no. 3, 1991.

34. Lotfi H.R., and P.B. Shing.: Interface Model Applied to Fracture of Masonry Structures. Journal of Structural Engineering, vol. 120, no. 1, January 1994.

35. Mainstone, R.J.: On the Stiffness and Strengths of Infilled Frames. Proceedings of the Institution of Civil Engineers, supplement (iv), paper 7360 S, 1971.

36. Mallick, D.V., and R.P. Garg.: Effects of Openings on the Lateral Stiffness of Infilled Frames. Proceedings of the Institution of Civil Engineers, vol. 49, no. 7371, June 1971.

37. Mehrabi, A.B., P.B. Shing, M.P. Schuller, and J.L. Noland.: Performance of Masonry-Infilled Reinforced Concrete Frames Under In-Plane Lateral Load. Department of Civil, Environmental, and Architectural Engineering, University of Colorado at Boulder, Structural Engineering and Structural Mechanics Research Series, Report CU/SR, 1996.

38. Mehrabi, A.B., and P.B. Shing.: Finite Element Modeling of Masonry-Infilled Reinforced Concrete Frames. Journal of Structural Engineering, vol. 123, no. 5 May 1997.

39. Mehrabi, P.B., Shing, and M.P. Schullar.: Experimental Evaluation of Masonry-Infilled RC Frames. Journal of Structural Engineering, vol. 122, no. 3, 1996.

40. Mosalam, K.M., R.N. White, and P. Gergely.: Static Response of Infilled Frames Using Quasi-Static Experimentation. Journal of Structural Engineering, vol. 123, no. 11, November 1997.

41. NEHRP Guidelines for the Seismic Rehabilitation of Buildings. Federal Emergency Management Agency 273 [FEMA], August 1996, chapters 7 and C7.

42. Polyakov, S.V.: On the Interactions Between Masonry Filler Walls and Enclosing Frame When Loaded in the Plane of the Wall. (English translation by G.L. Cairns, 1963) Translations in Earthquake Engineering Research Institute, Moscow, Russia 1956.

43. Prakash, V., G.H. Powell, and S. Campbell.: DRAIN-2DX Base Program Description and User Guide, Version 1.10, Department of Civil Engineering, University of California, Berkeley, November 1993.

44. Reinhorn, A.M., A. Madan, R.E. Valles, Y. Reichmann, and J.B. Mander.: Modelling of Masonry Infill Panels for Structural Analysis, Report No. NCEER-95-0018 National Center for Earthquake Engineering Research, State University of New York at Buffalo, 8 December 1995.

45. Riddington, J. R.: The Influence of Initial Gaps on Infilled Frame Behavior. Proceedings of the Institution of Civil Engineers, part 2, vol. 77, paper 8767, September 1984.

46. Riddington, J.R., and S.B. Smith.:Analysis of Infilled Frames Subject to Racking With Design Recommendations. The Structural Engineer, vol. 55, no. 6, June 1977.

47. Sabnis, Gajanan M., Harris, Harry G., White, Richard N., Mirza, M. Saeed.: Structural Modeling and Experimental Techniques. Prentice-Hall, INC., Englewood Cliffs, N.J. 1983.

48. Saneinejad, A., and B. Hobbs.: Inelastic Design of Infilled Frames. Journal of Structural Engineering, vol. 121, no. 4, April 1995.

49. Smith, B. S.: Lateral Stiffness of Infilled Frames. Journal of the Structural Division, Proceedings of American Society of Civil Engineers, vol. 88, no. 3355, December 1962.

50. Smith, B.S.: Behavior of Square Infilled Frames. Journal of the Structural Division, Proceedings of American Society of Civil Engineers, vol. 92, no. ST1, February 1966.

51. Smith, B.S., and C. Carter.: A Method of Analysis for Infilled Frames. Proceedings of the Institution of Civil Engineers, vol. 44, paper 7218, 1969.

52. Smolira, M.: Analysis of Infilled Shear Walls. Proceedings of the Institution of Civil Engineers, part 2, vol. 55, paper 7672, December 1973.

53. Sweeney, S., Al-Chaar, G.: Strength of Concrete Frames With Masonry Infill. Wind and Seismic Effects Proceeding of the 27th Joint Meeting, Technical Memorandum of PWRI No. 3387, May1995.

54. Thomas, R.D., and R.E. Klingner.: Behavior of Infilled Frames. Limit States Design of Masonry – TMS Draft Report, chapter 4.

55. Yettram, A.L., and M.J.S. Hirst.: The Collapse Load for Square Concrete Infill Panels. Building Science, vol. 7, 1972.

56. Yorulmaz, M., and M.A. Sozen.: Behavior of Single-Story Reinforced Concrete Frames with Filler Walls. Civil Engineering Studies Research Series No. 337, University of Illinois, Urbana, May 1968.

Appendix A

Supportive Figures in Experimental Analysis

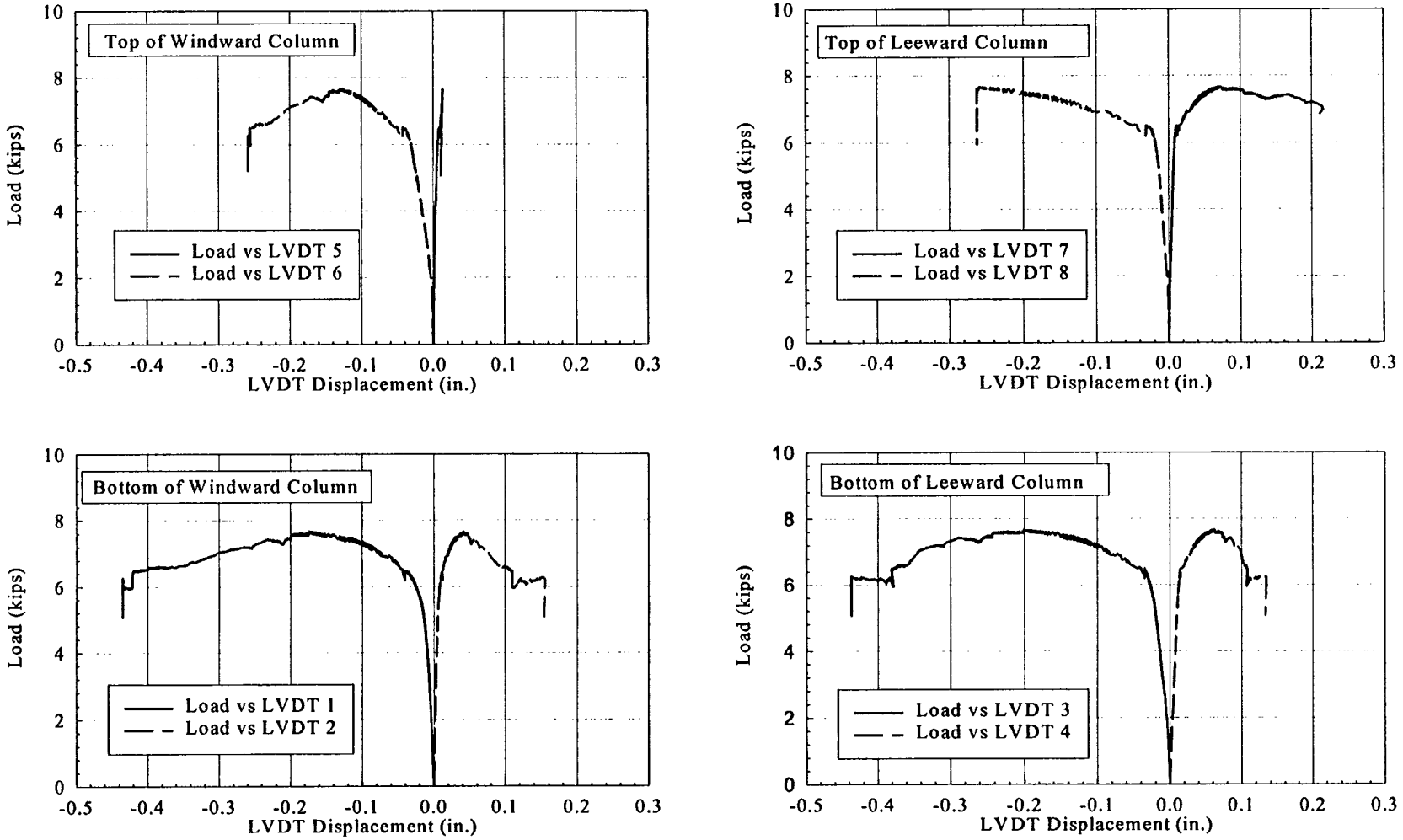

Figure A.1 Model 1, Single-Bay Bare Frame Specimen LVDT Displacements

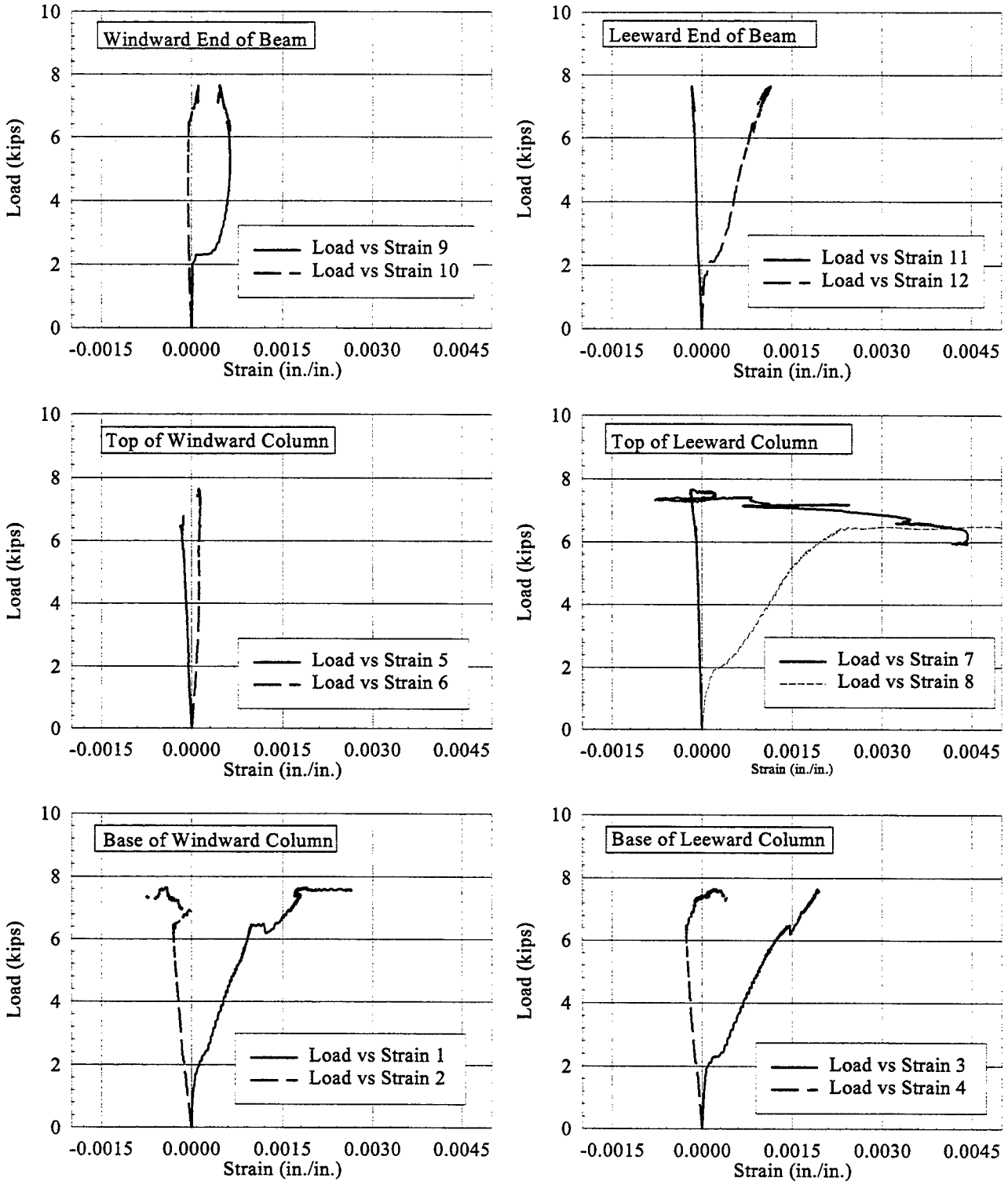

Figure A.2 Model 1, Single-Bay Bare Frame Specimen Strains

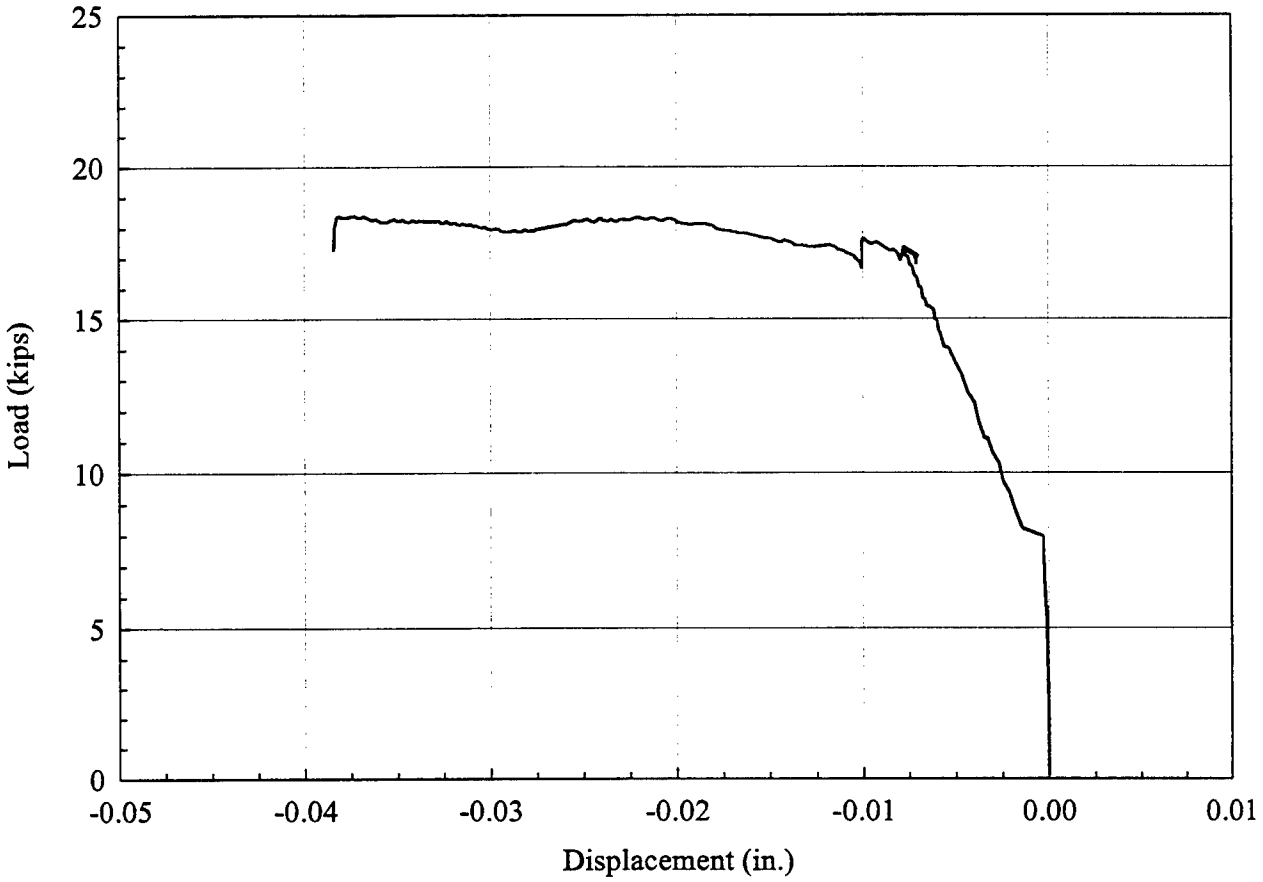

Figure A.3 Model 2, Single-Bay CMU Infilled Specimen Gap Between Infill and Leeward Column

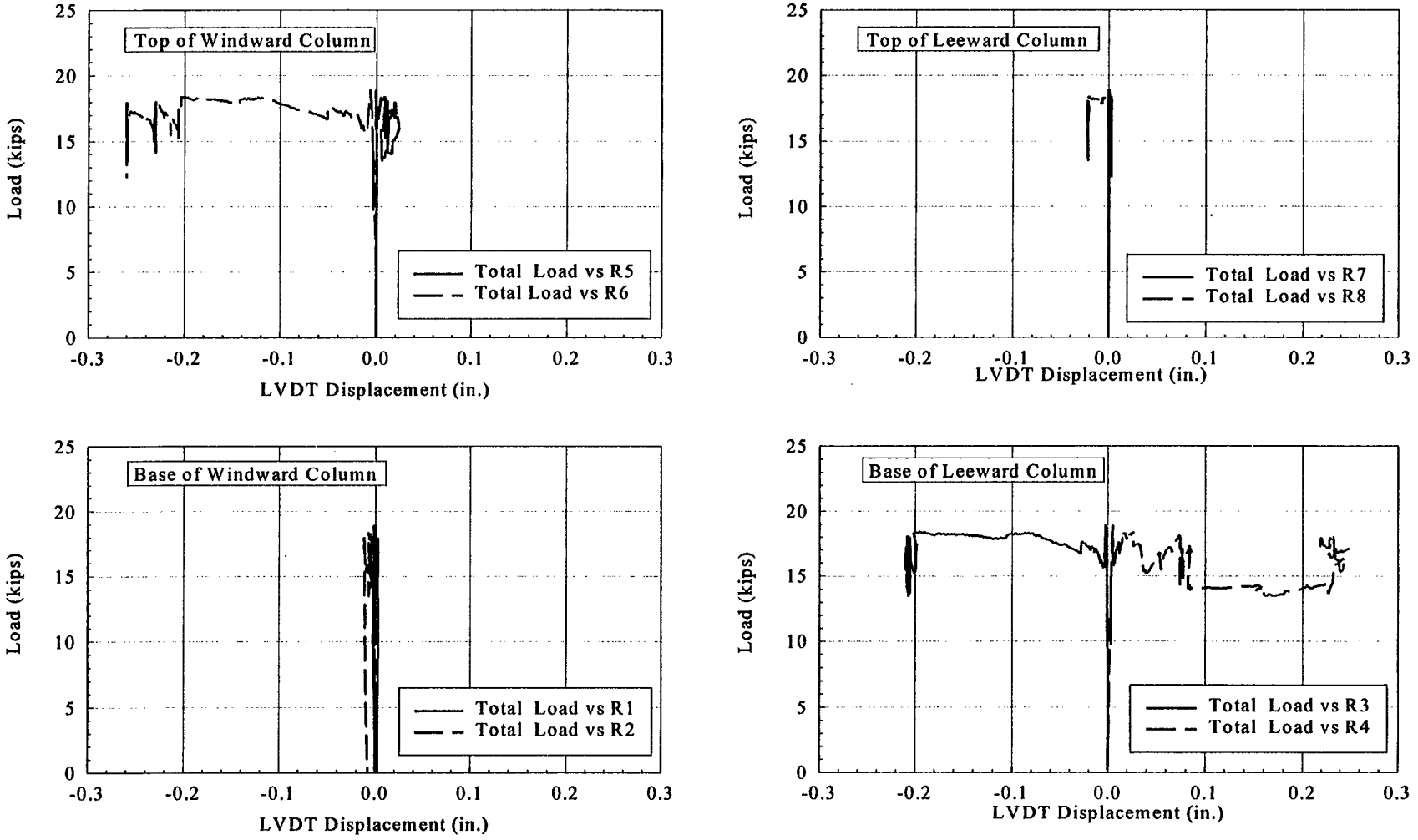

Figure A.4 Model 2, Single-Bay CMU Infilled Specimen LVDT Displacements

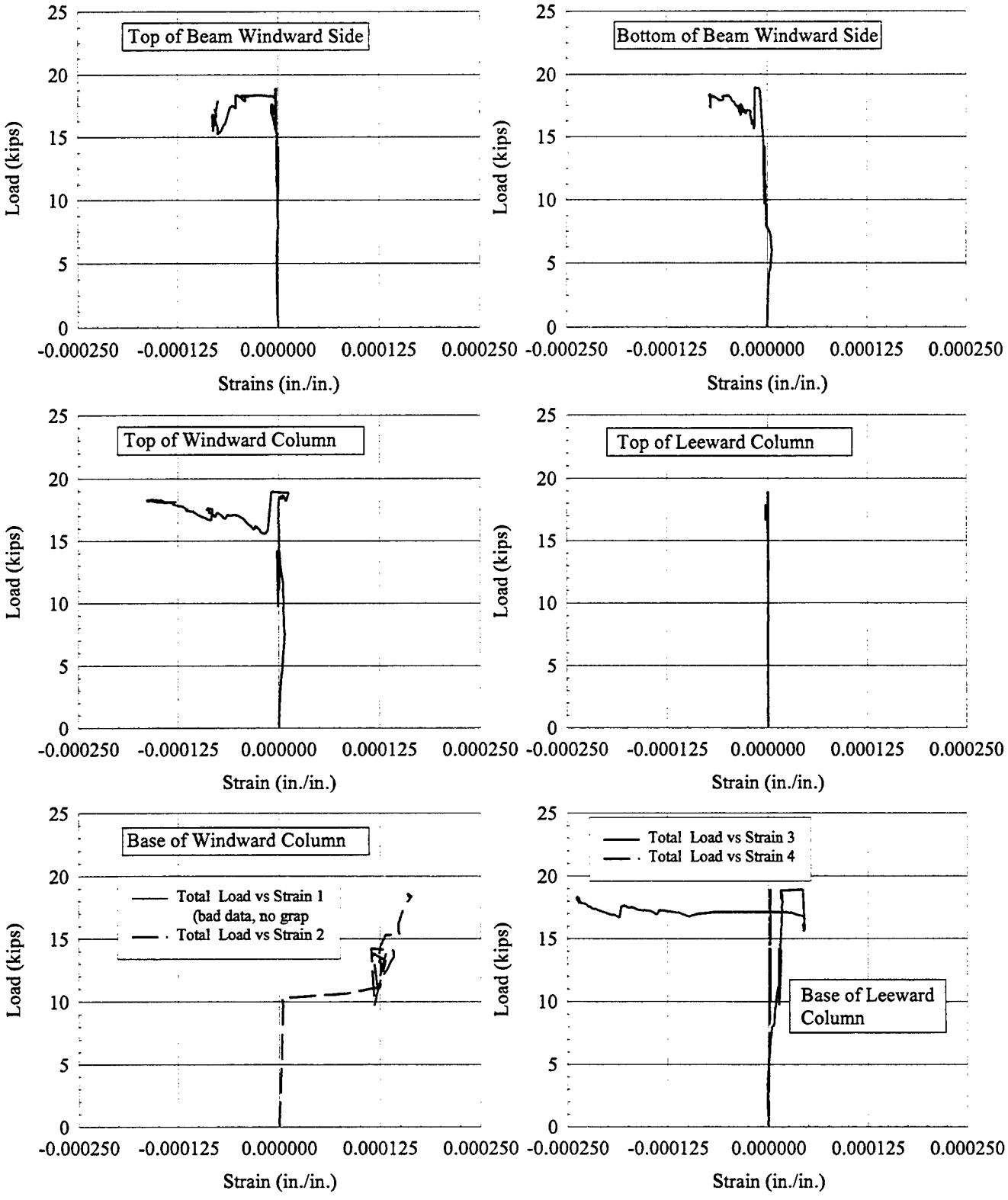

Figure A.5 Model 2, Single-Bay CMU Infilled Specimen Strains

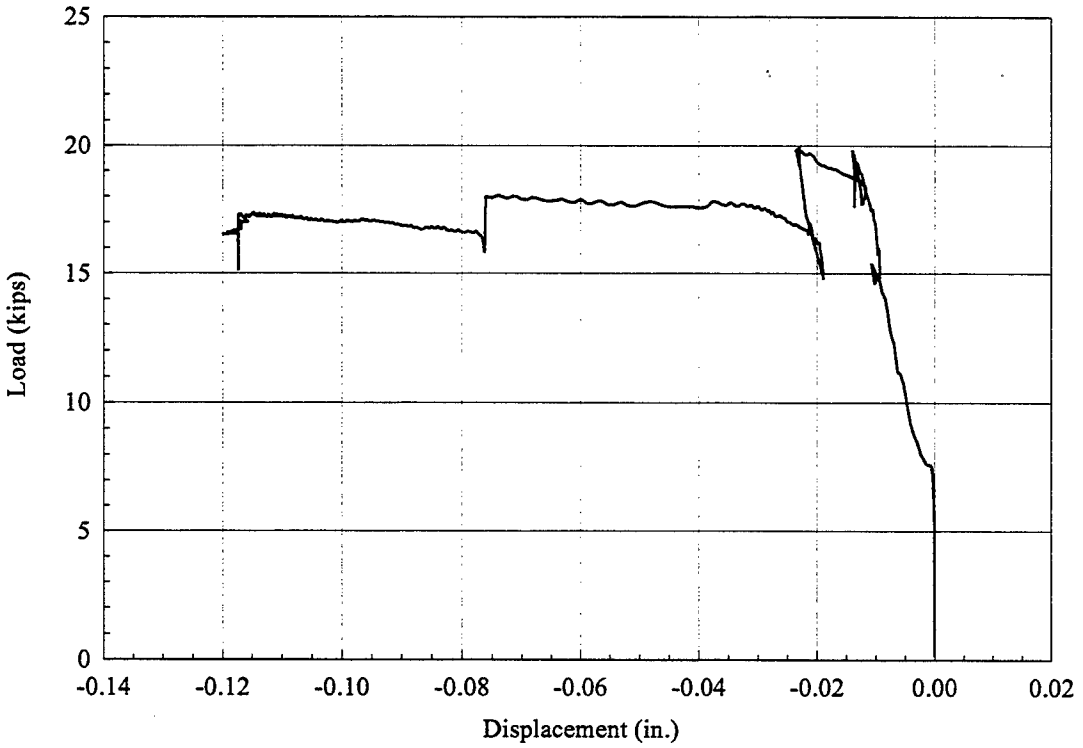

Figure A.6 Model 3, Single-Bay Brick Infilled Specimen Gap Between Infill and Leeward Column

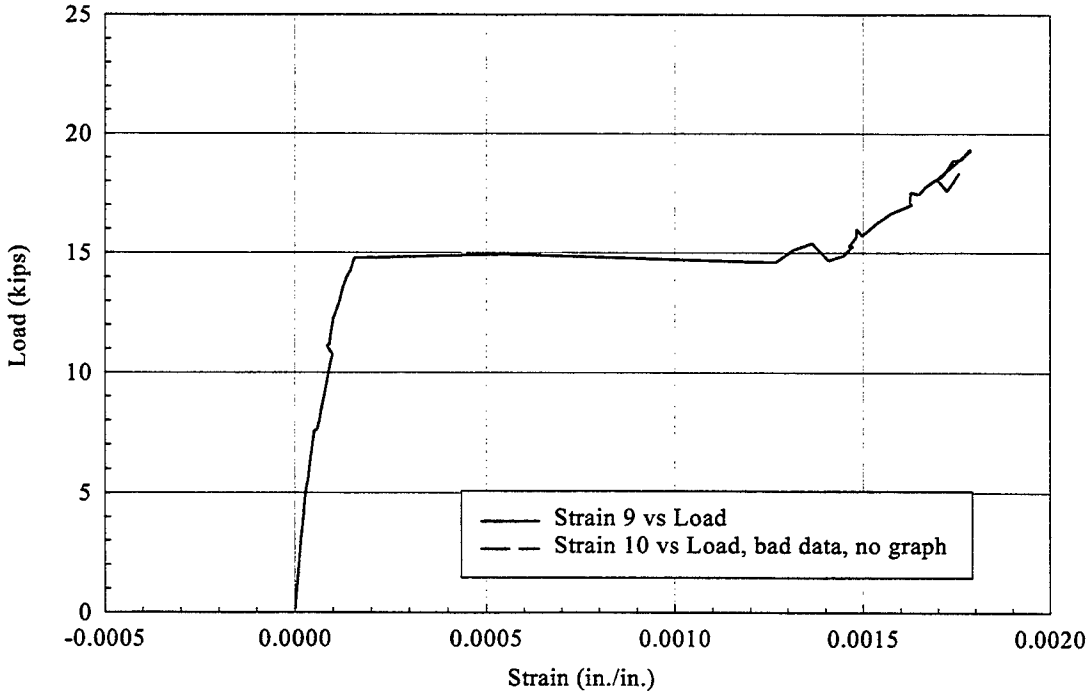

Figure A.7 Model 3, Single-Bay Brick Infilled Specimen Surface Strains at Base of Columns

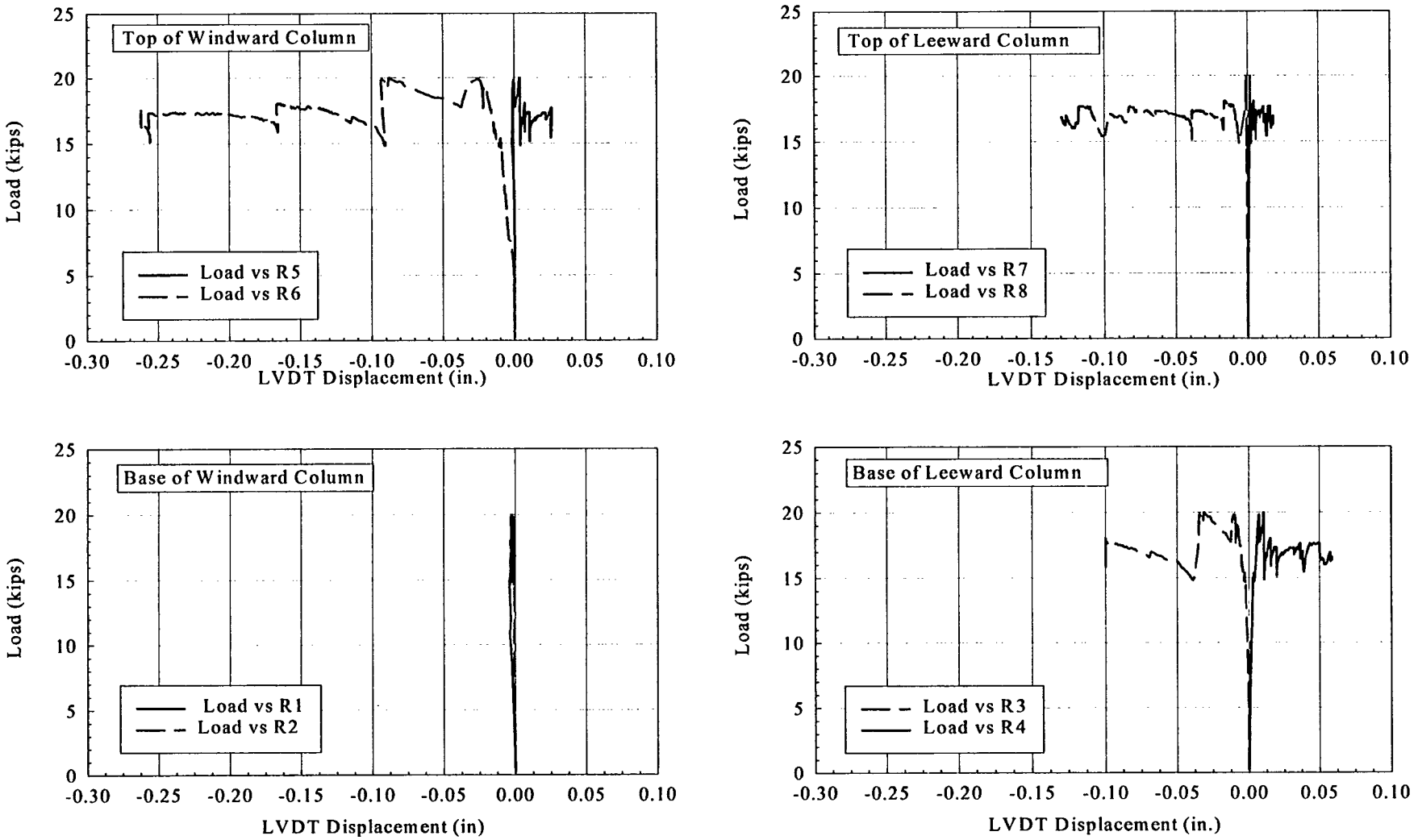

Figure A.8 Model 3, Single-Bay Brick Infilled Specimen LVDT Displacements

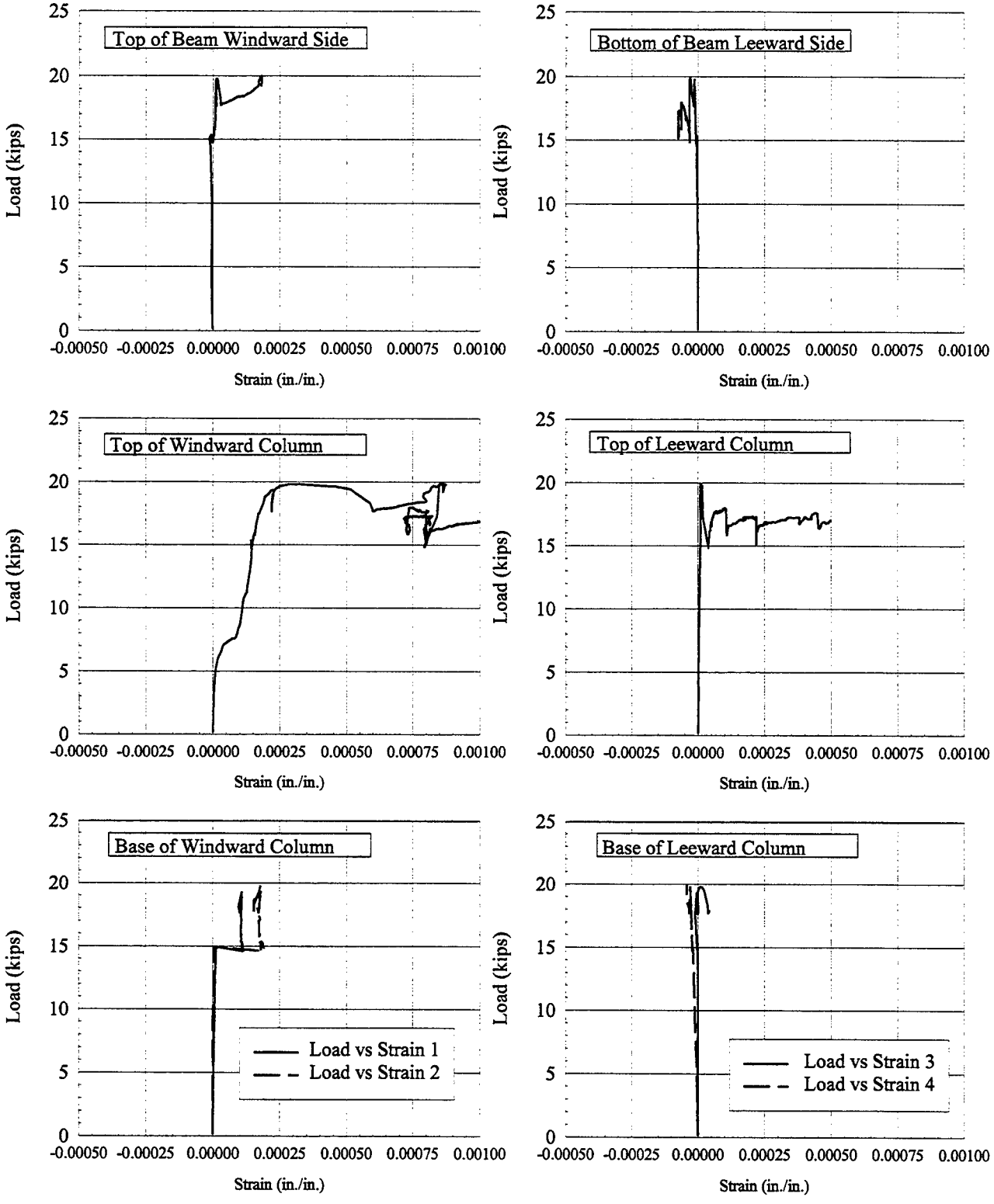

Figure A.9 Model 3, Single-Bay Infilled Specimen Strains

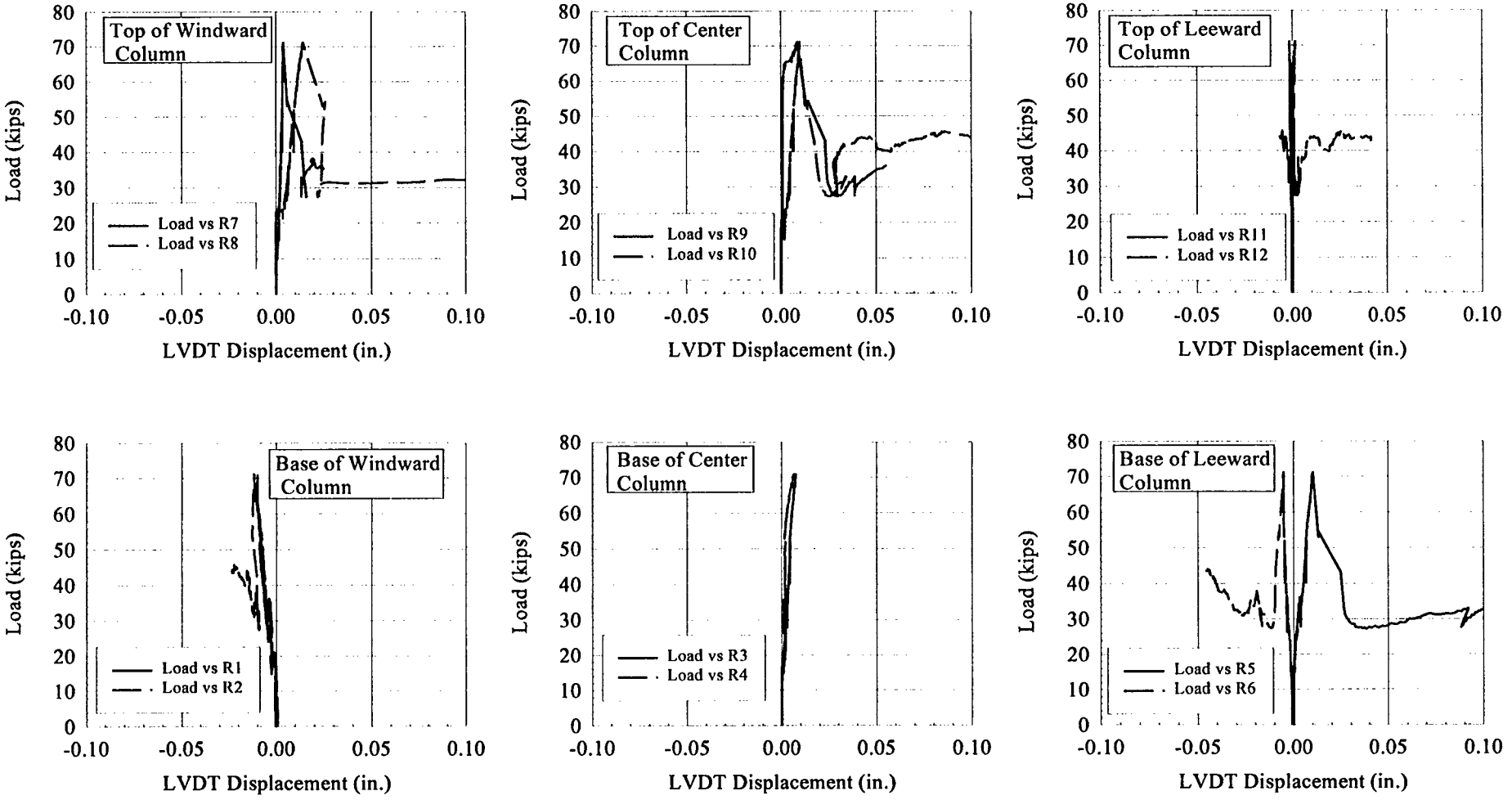

Figure A.10 Model 4, Double-Bay CMU Infilled Specimen LVDT Displacements

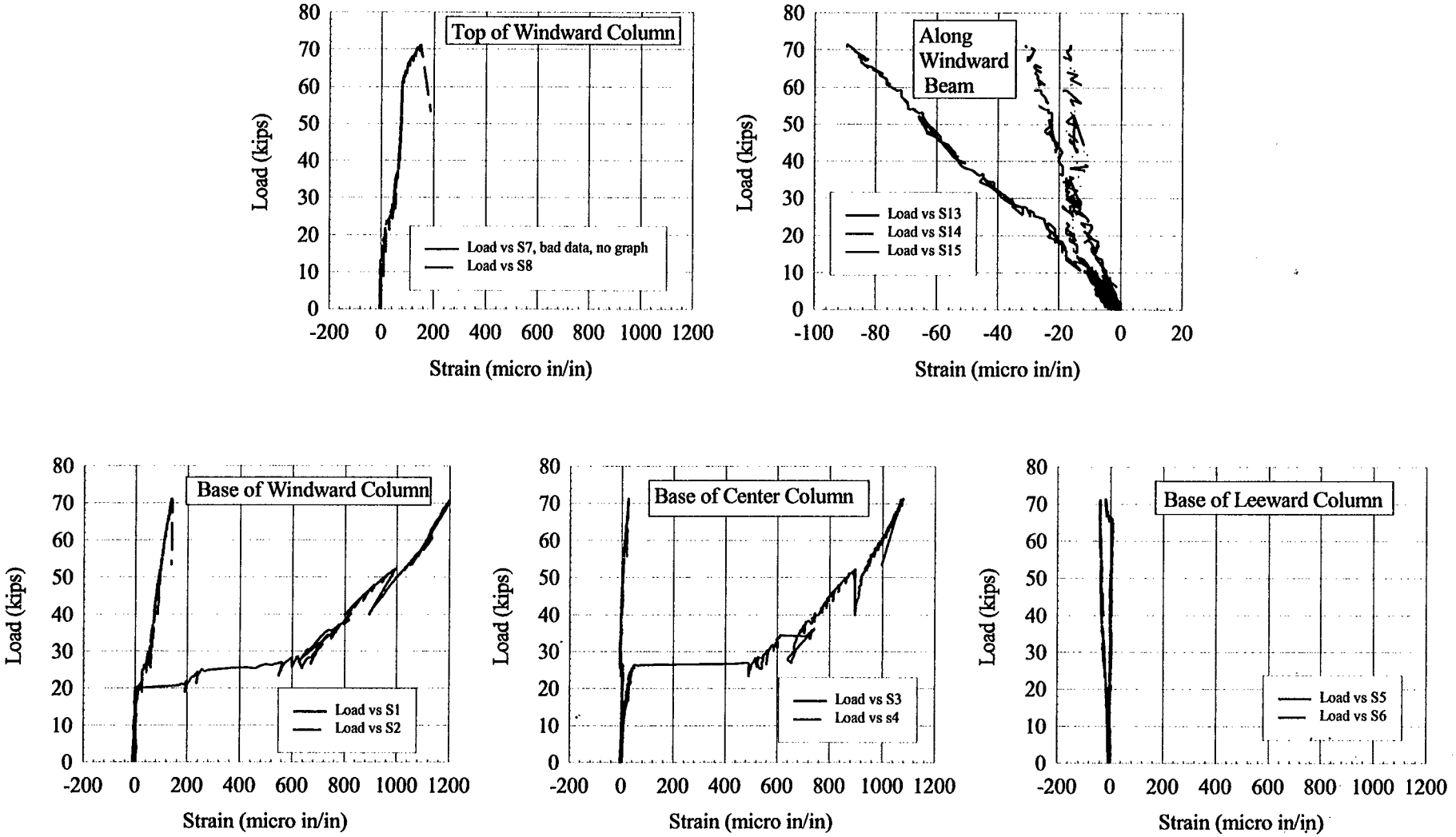

Figure A.11 Model 4, Double-Bay CMU Infilled Specimen Strains

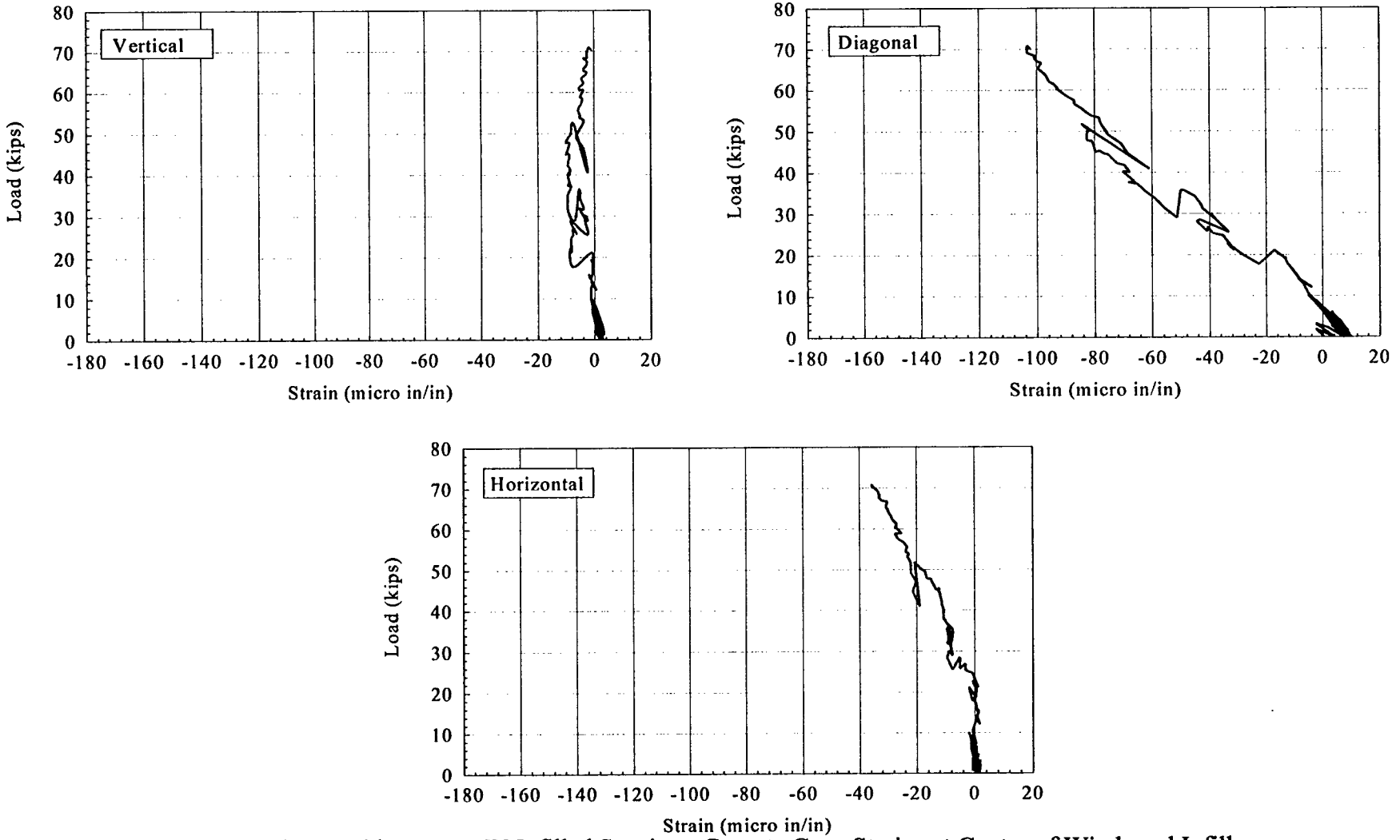

Figure A.12 Model 4, Double-Bay CMU Infilled Specimen Rosette Gage Strains at Center of Windward Infill

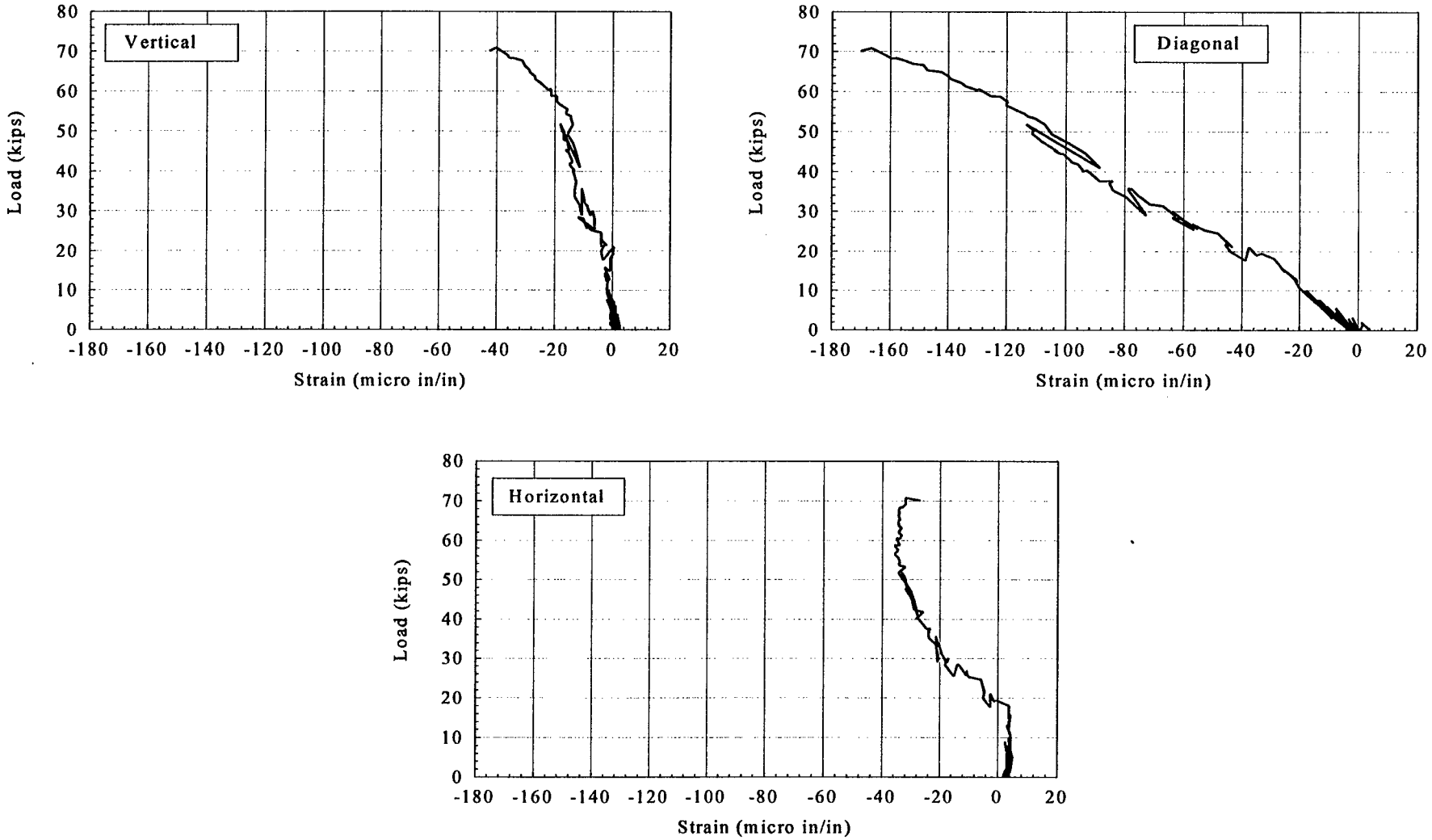

Figure A.13 Model 4, Double-Bay CMU Infilled Specimen Rosette Gage Strains at Center of Leeward Infill

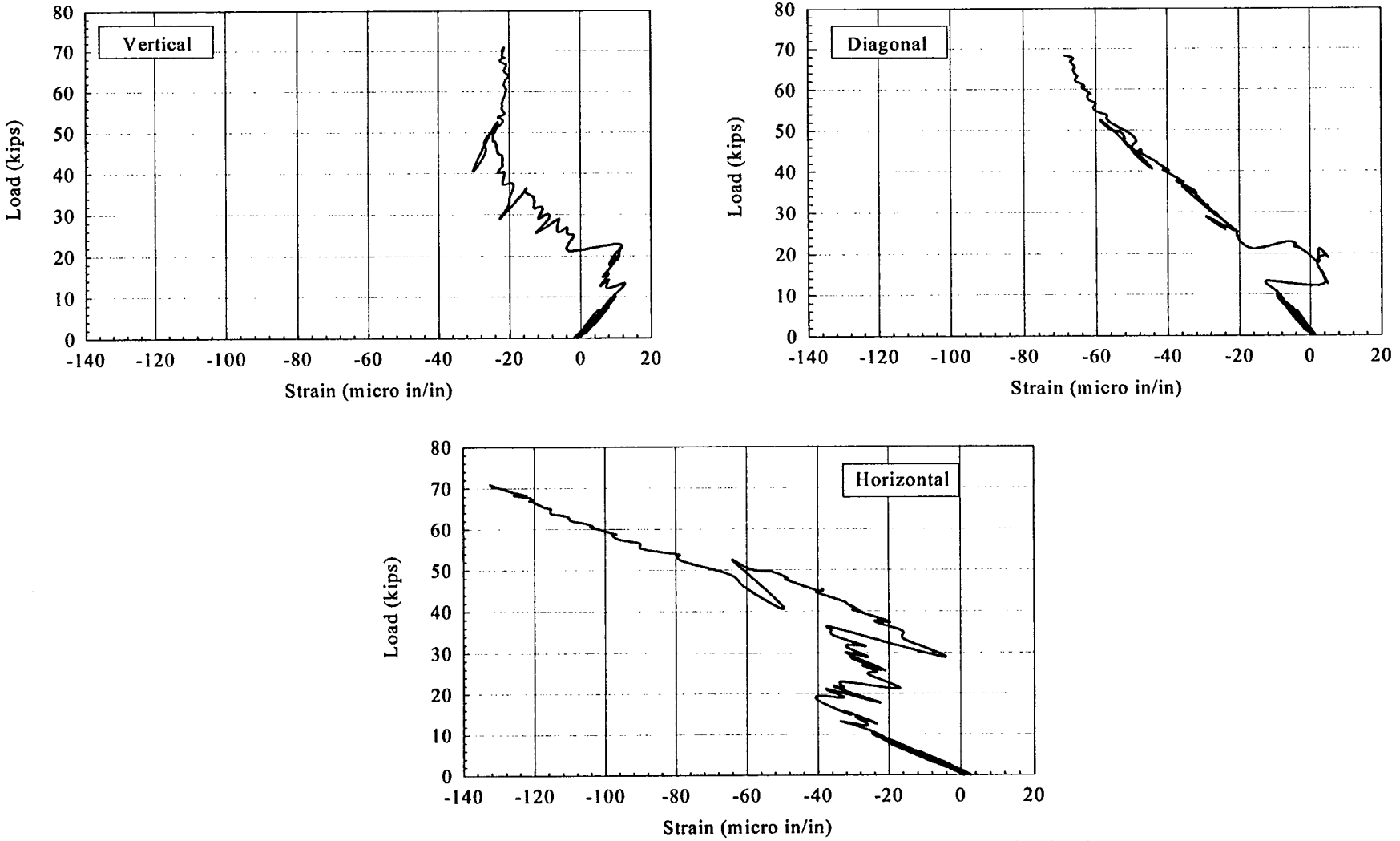

Figure A.14 Model 4, Double-Bay CMU Infilled Specimen Rosette Gage Strains at Windard Joint

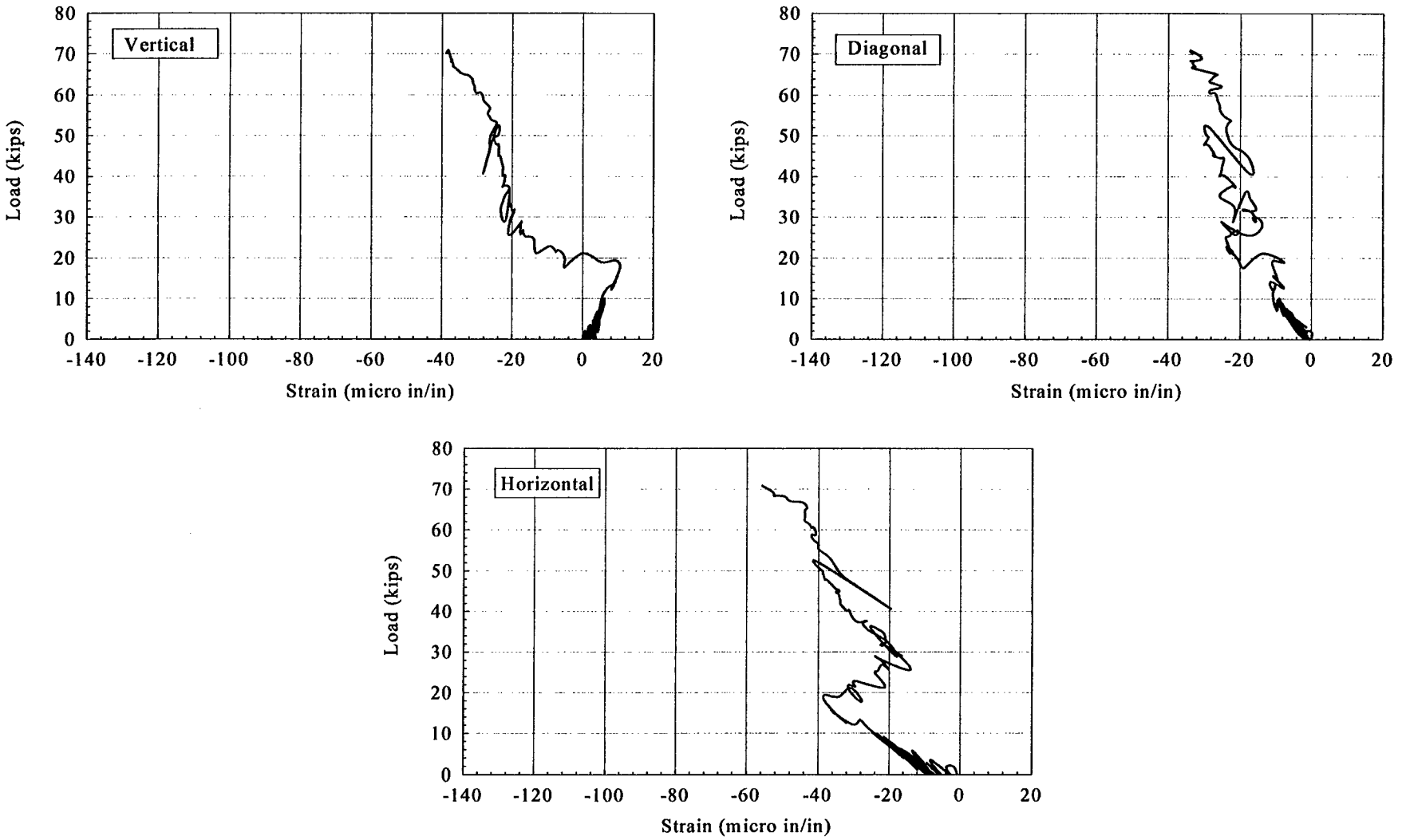

Figure A.15 Model 4, Double-Bay CMU Infilled Specimen Rosette Gage Strains at Center Joint

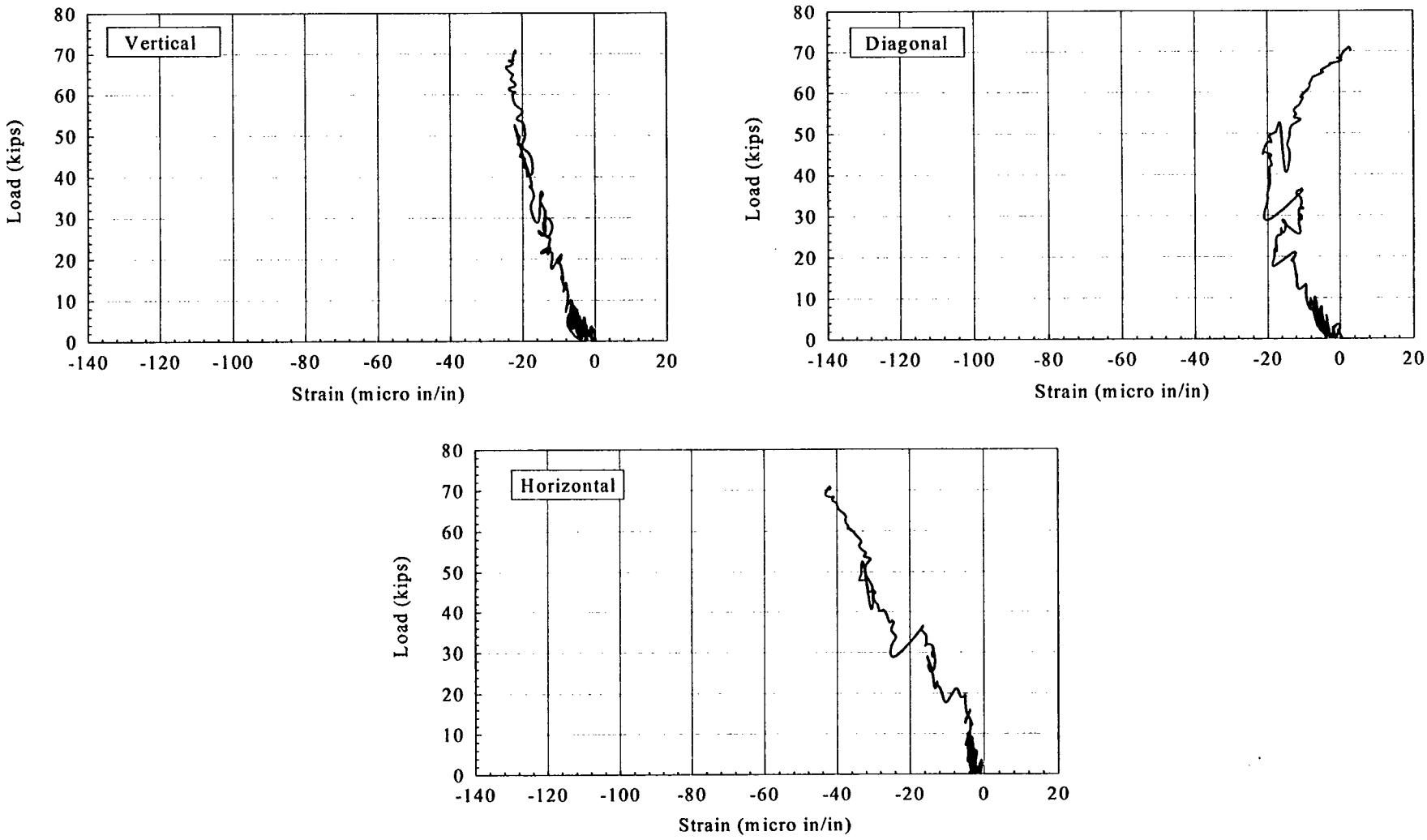

Figure A.16 Model 4, Double-Bay CMU Infilled Specimen Rosette Gage Strains at Leeward Joint

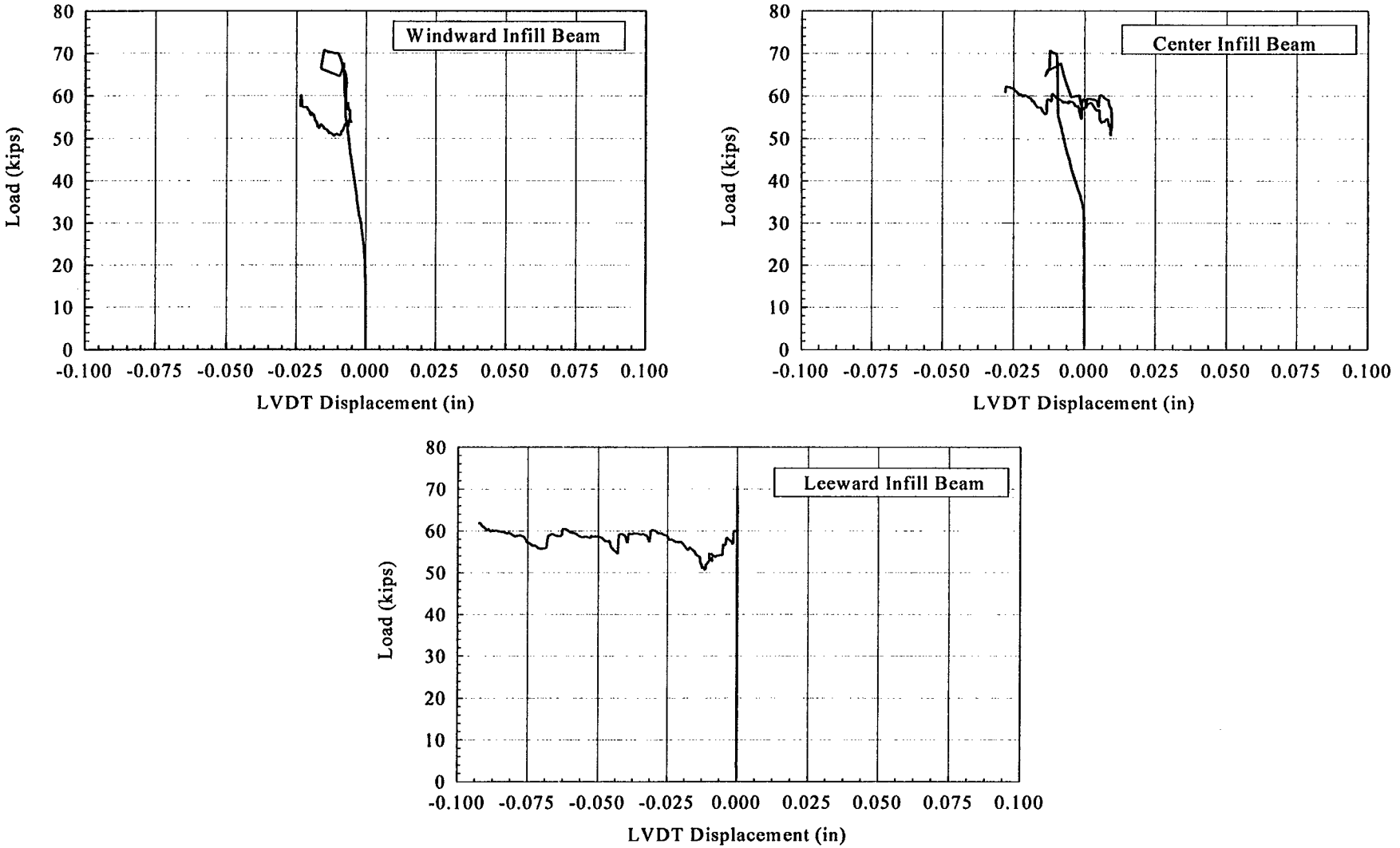

Figure A.17 Model 5, Triple-Bay Infilled Specimen Gap Between Infill and Beam

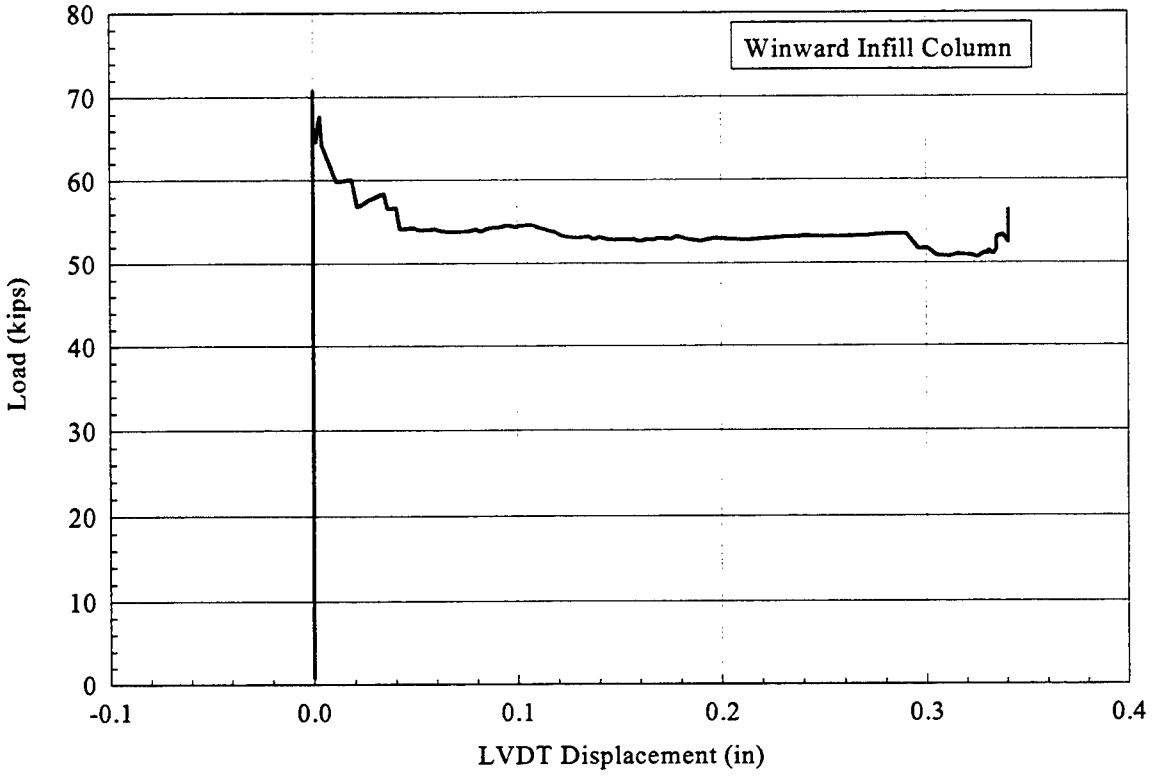

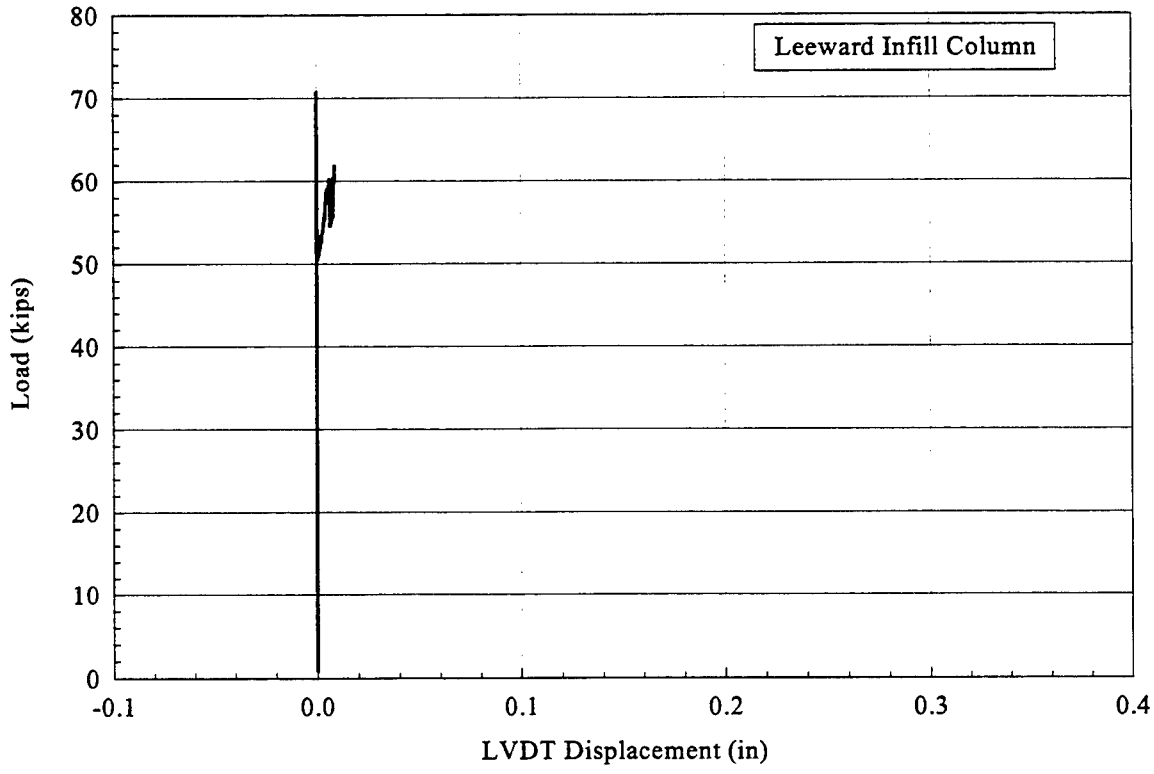

Figure A.18 Model 5, Triple-Bay Brick Infilled Specimen Gap Between the Infill and Column

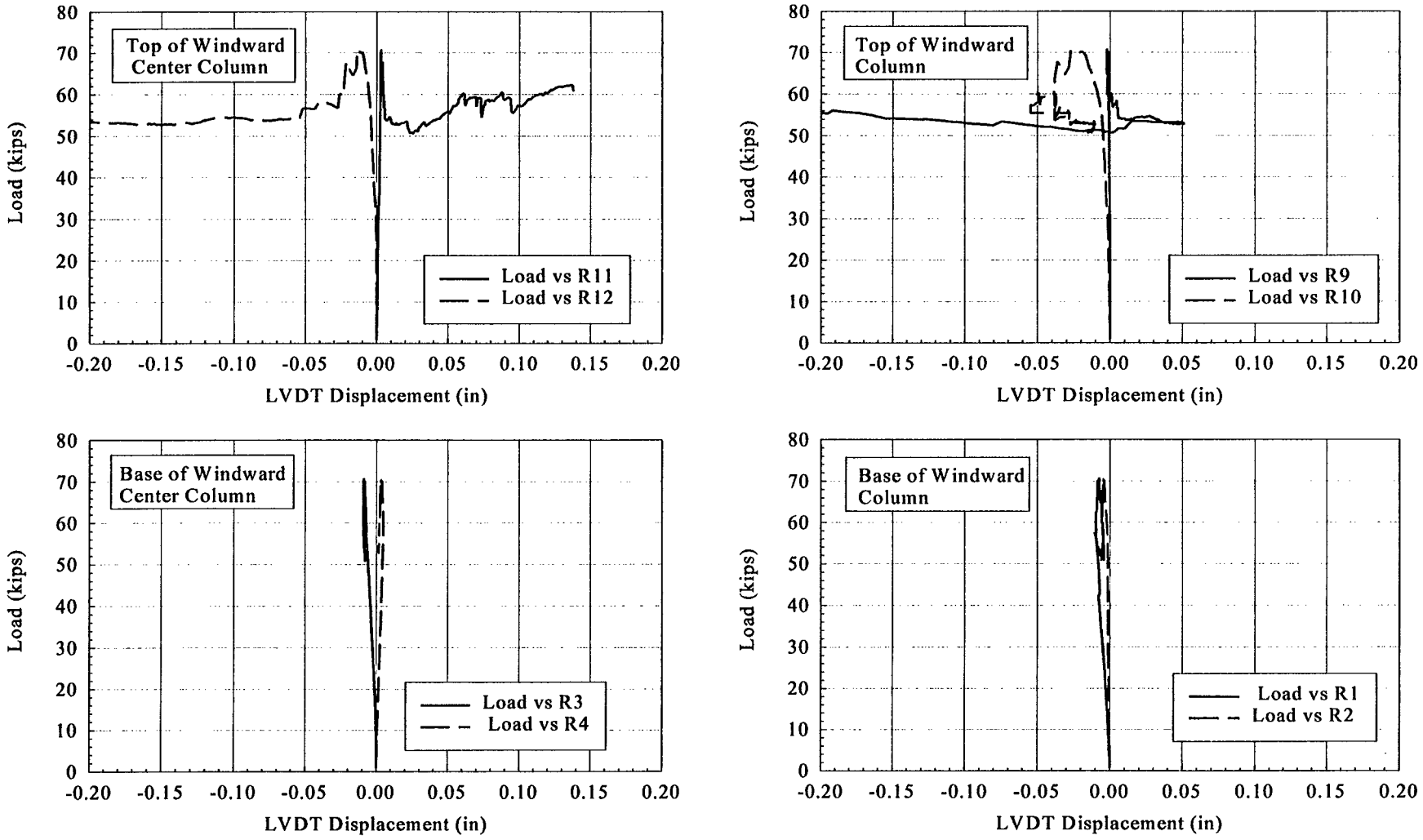

Figure A.19 Model 5, Triple-Bay Brick Infilled Specimen LVDT Displacements

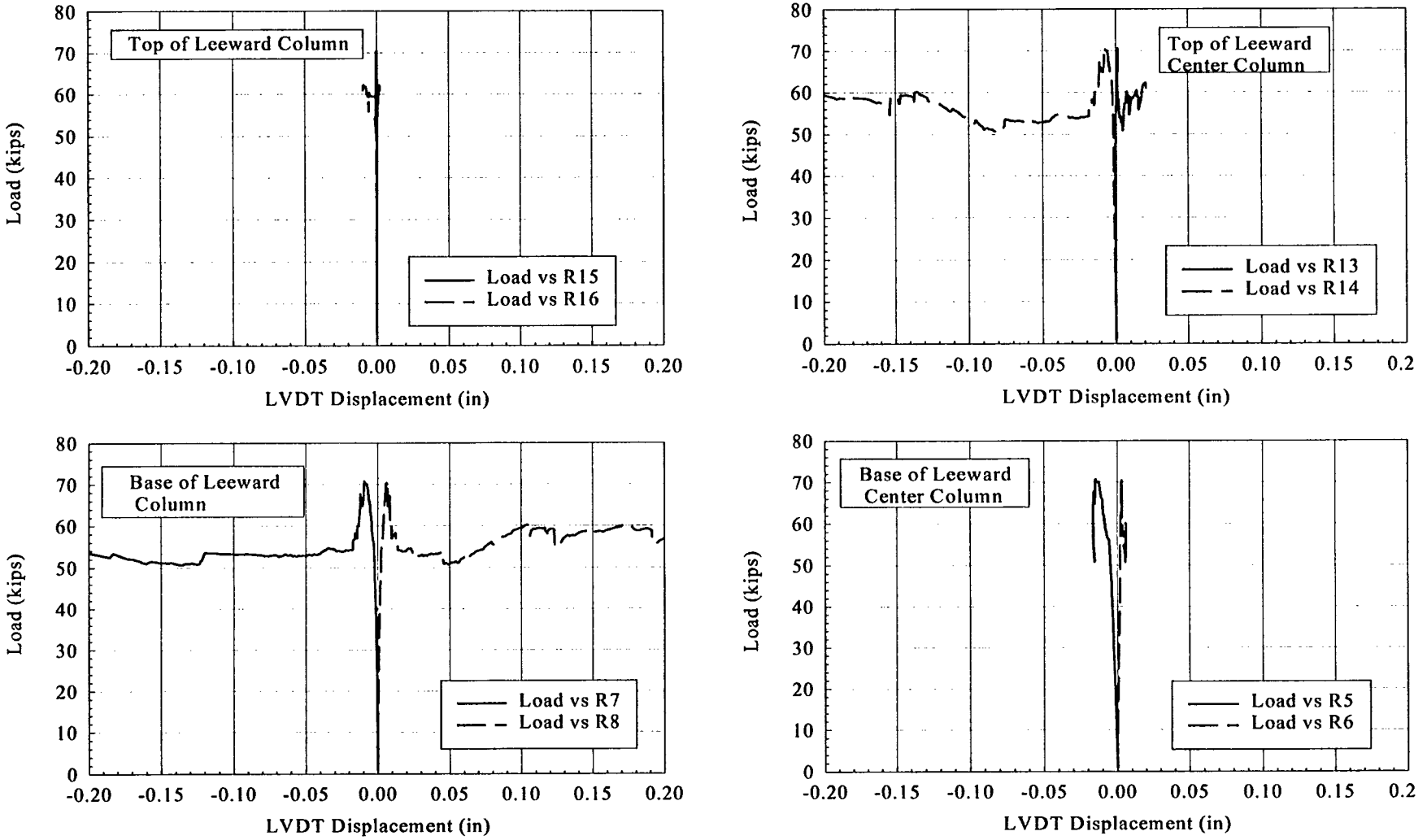

Figure A.20 Model 5, Triple-Bay Brick Infilled Specimen LVDT Displacements

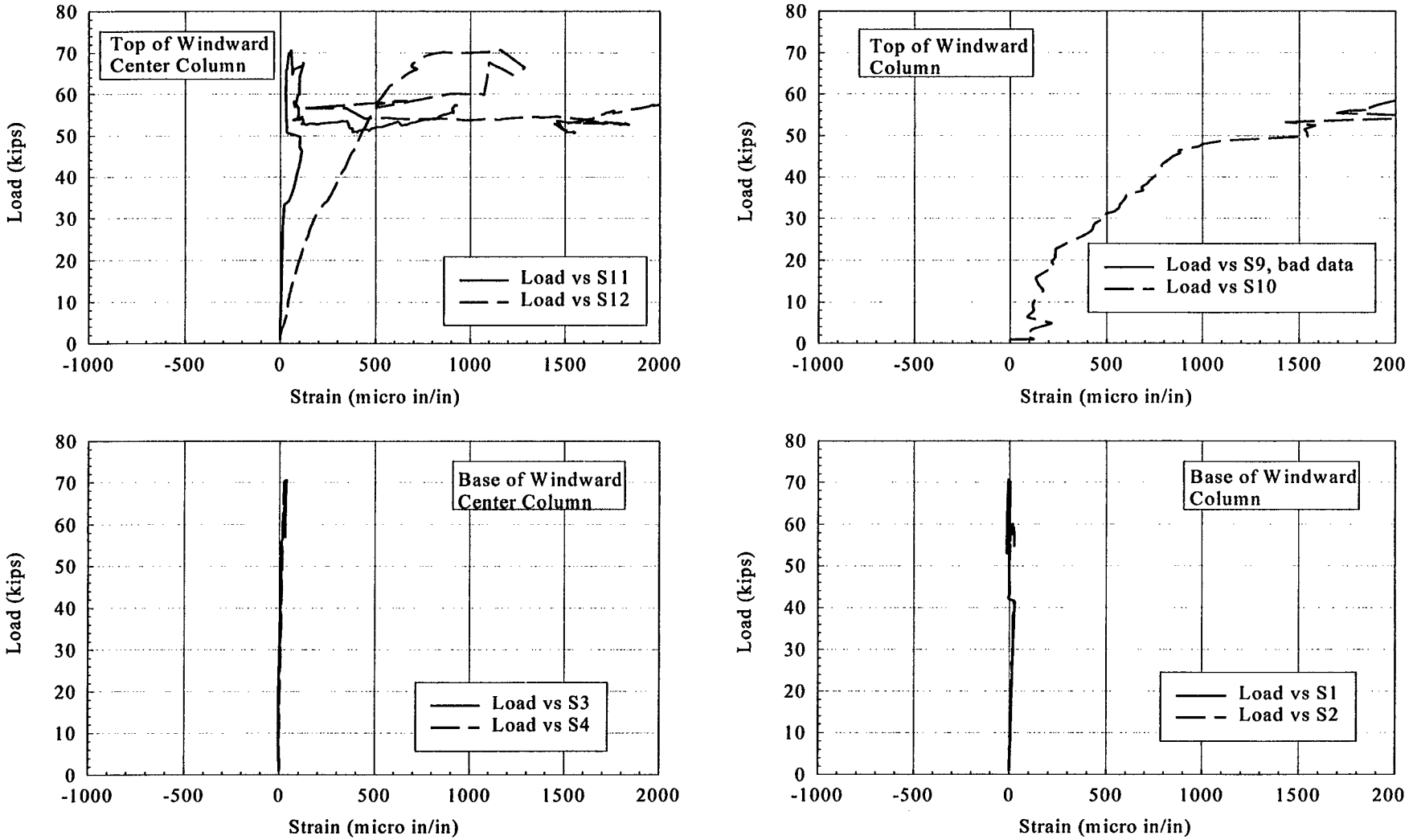

Figure A.21 Model 5, Triple-Bay Brick Infilled Specimen Strains

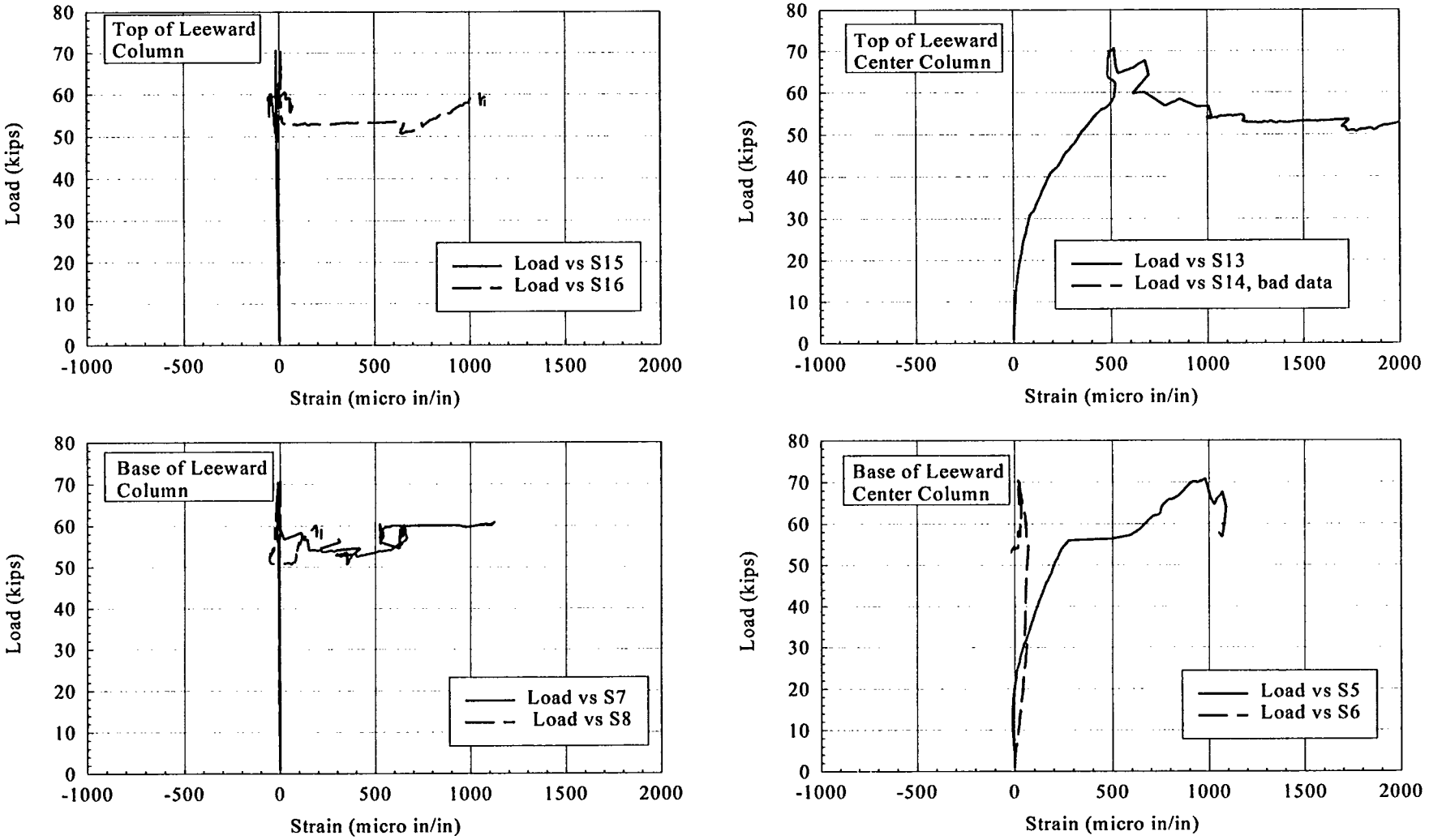

Figure A.22 Model 5, Triple-Bay Brick Infilled Specimen Strains

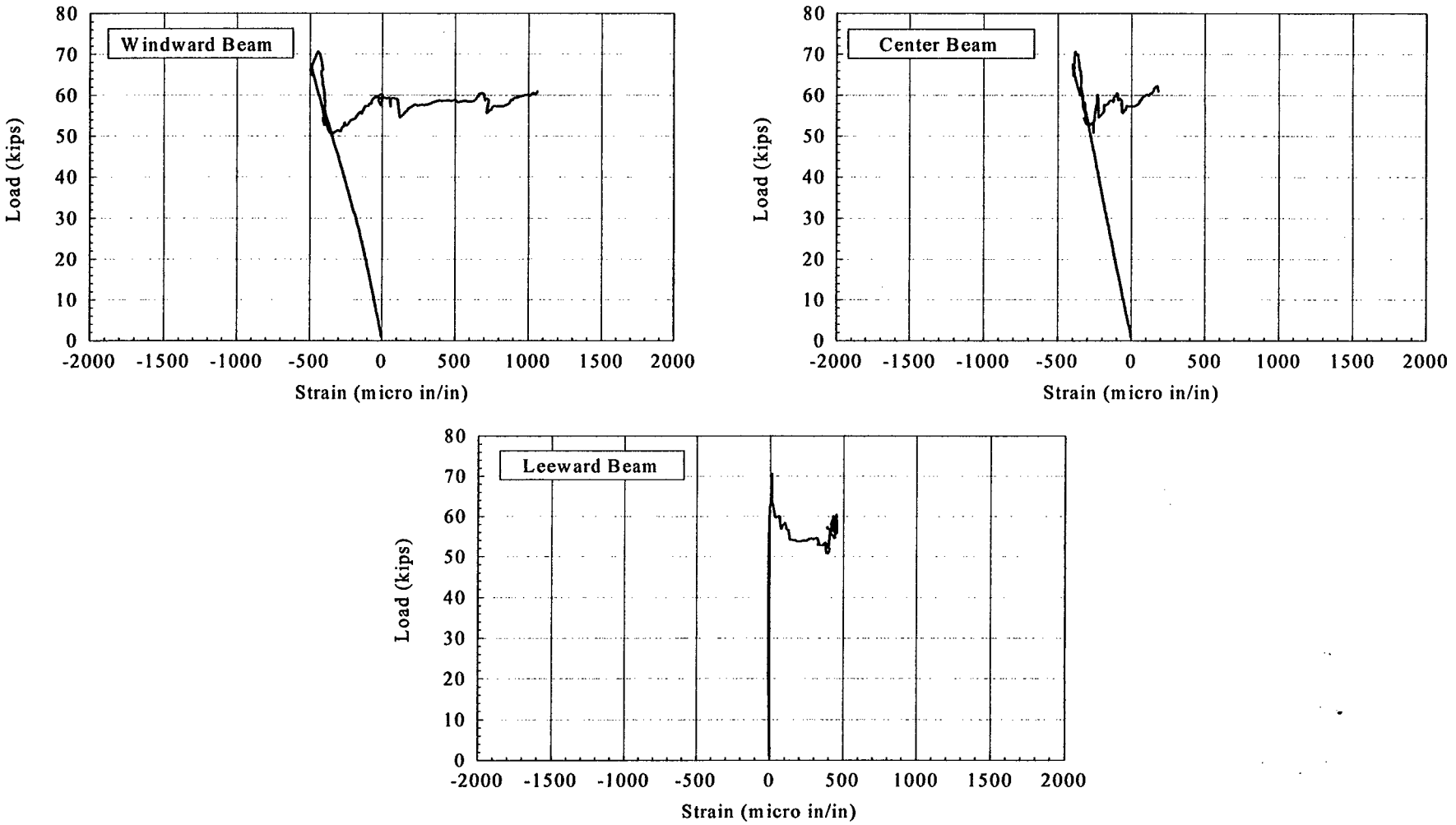

Figure A.23 Model 5, Triple-Bay Brick Infilled Specimen Strains on Windward Side of Beams

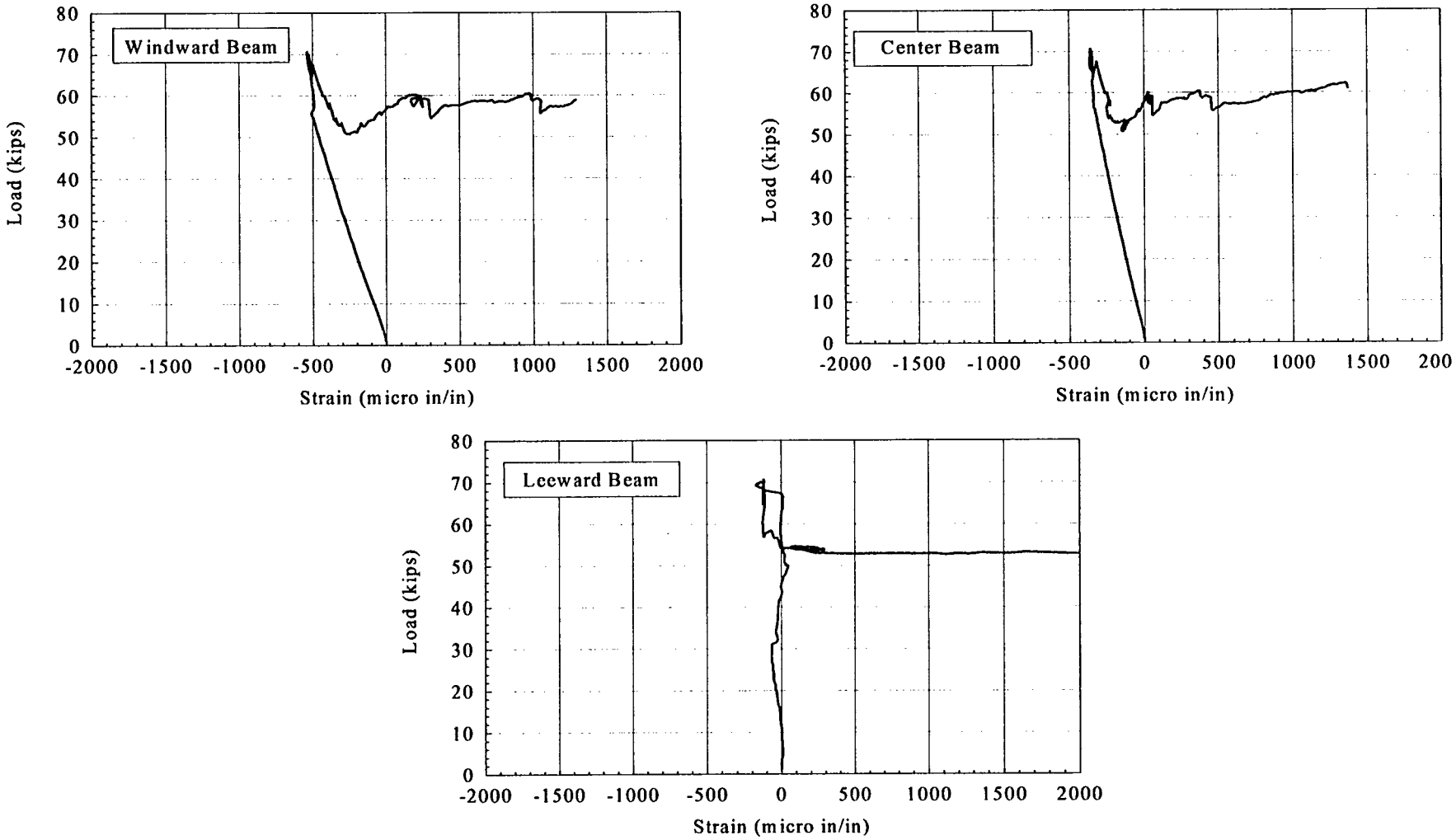

Figure A.24 Model 5, Triple-Bay Brick Infilled Specimen Strains on Center of Beams

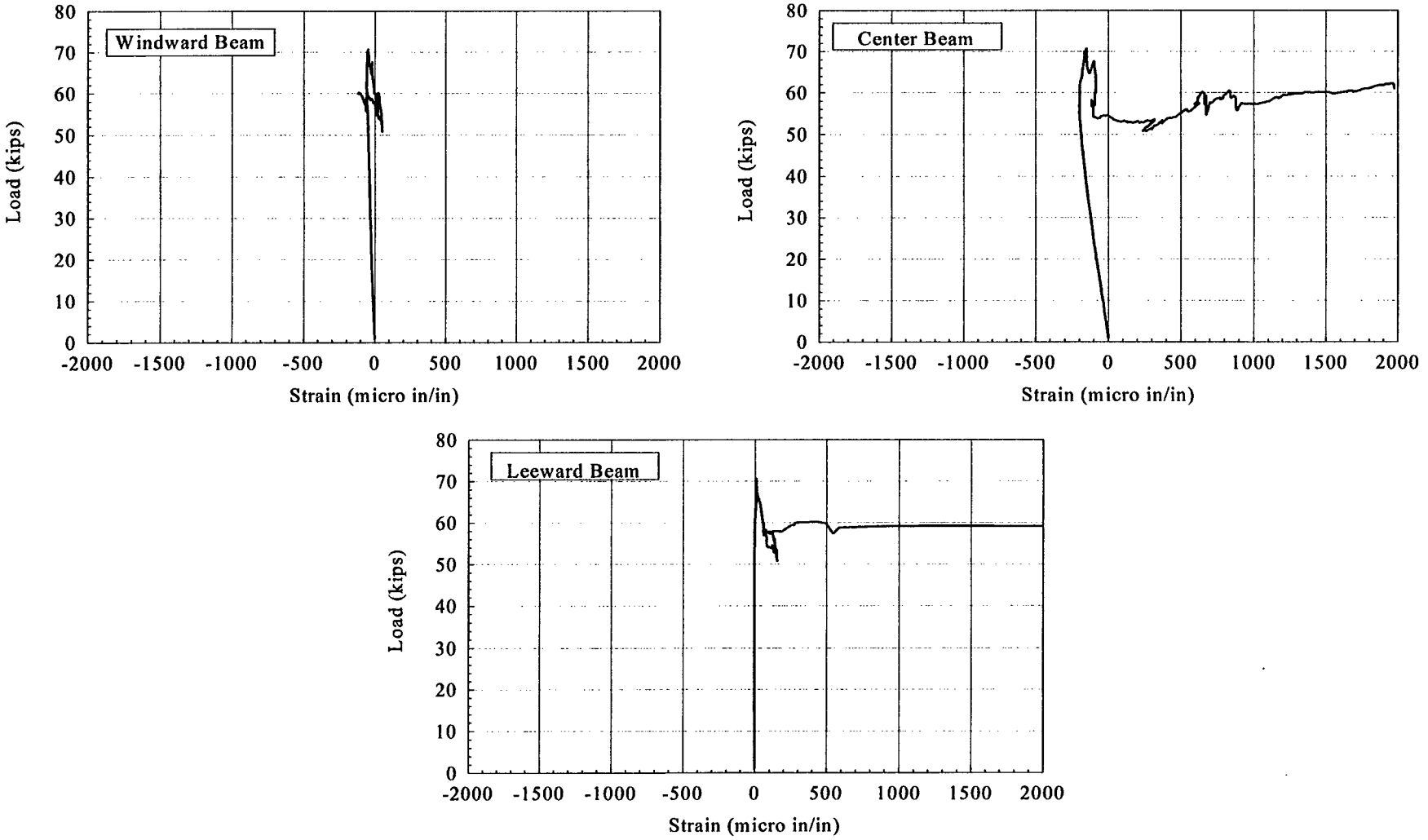

Figure A.25 Model 5, Triple-Bay Brick Infilled Specimen Strains on Leeward Side of Beams

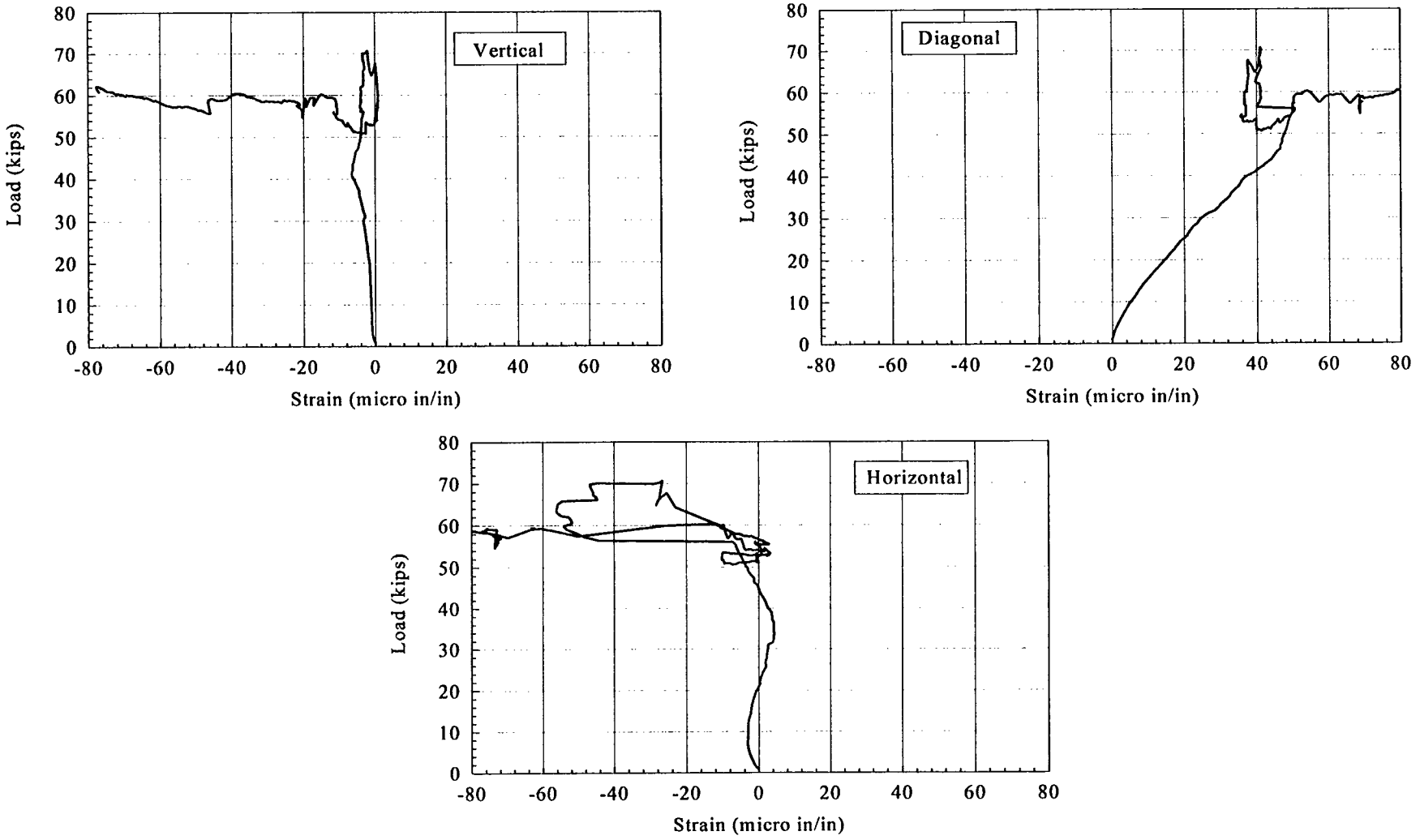

Figure A.26 Model 5, Triple-Bay Brick Infilled Specimen Rosette Gage Strains on Center of Windward Infill

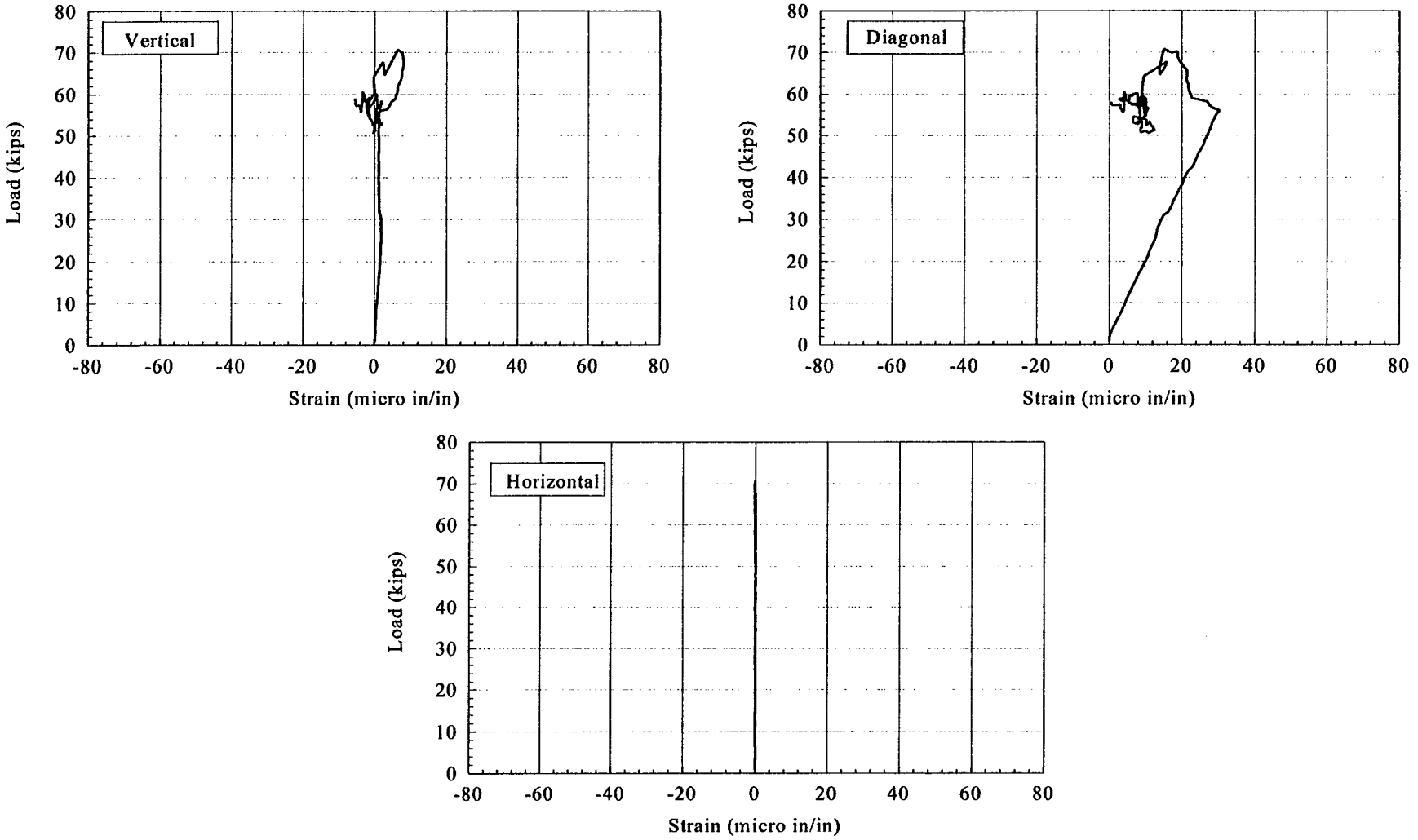

Figure A.27 Model 5, Triple-Bay Brick Infilled Specimen Rosette Gage Strains on Center of Center Infill

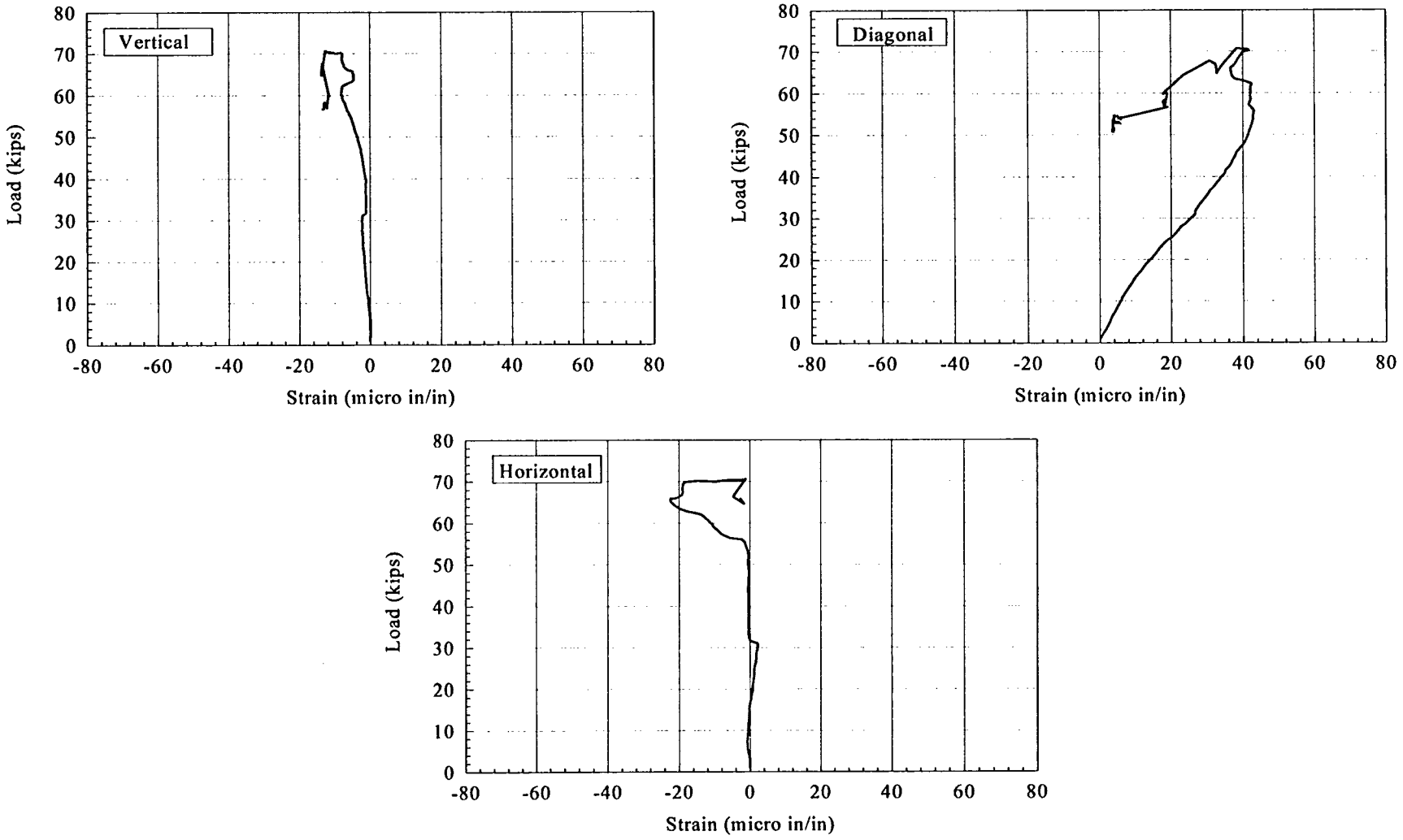

Figure A.28 Model 5, Triple-Bay Brick Infilled Specimen Rosette Gage Strains on Center of Leeward Infill

Appendix B

Proposed Idealized Analytical Method Applied on Experimental Models

Proposed Idealized Method
Single-Bay Infilled with Concrete Masonry Wall

The height of the infill:	$H := 52.25$	in
The width of the infill:	$W := 72$	in
The height of the column:	$h := 56.125$	in
Length of the beam:	$L := 80$	in
Diagonal length of the infill panel:	$d := \sqrt{W^2 + H^2}$	in
	$d = 88.96$	in
Effective thickness of the infill:	$t := 2.71$	in
Angle of diagonal to horizontal:	$\theta := \operatorname{atan}\left(\frac{H}{W}\right)$	
	$\theta = 0.628$	Ra
Column's dimensions:	$Lc1 := 8$	in
	$Lc2 := 5$	in
Cross-sectional area of the column:	$Ac := Lc1 \cdot Lc2$	
	$Ac = 40$	in^2
Moment of inertia of the column:	$Ic := \frac{Lc2 \cdot Lc1^3}{12}$	
	$Ic = 213.3$	in^4
Beam's dimensions:	$Lb1 := 7.75$	in
	$Lb2 := 5$	in
Moment of inertia of the beam:	$Ib := \frac{Lb2 \cdot Lb1^3}{12}$	
	$Ib = 194$	in^4
Elastic modulus of the frame:	$Ef := 4210$	ksi
Elastic modulus of infill panel:	$Ei := 1531$	ksi

Relative stiffness parameter of infill and frame:

$$\lambda c := \sqrt[4]{\frac{Ei \cdot t \cdot \sin(2 \cdot \theta)}{4 \cdot Ef \cdot Ic \cdot h}} \qquad \lambda c = 0.067$$

$$\lambda b := \sqrt[4]{\frac{Ei \cdot t \cdot \sin(2 \cdot \theta)}{4 \cdot Ef \cdot Ib \cdot h}} \qquad \lambda c = 0.067$$

$$\lambda := \left(\sqrt{\lambda c^2 + \lambda b^2}\right) \cdot \cos\left(\theta - \frac{\pi}{4}\right) \qquad \lambda = 0.094$$

The unadjusted width of diagonal strut:

$\lambda \cdot h = 5.276$

$$wo := if\left[\lambda \cdot h < 13, \left[0.0005(\lambda \cdot h)^2 - 0.0143(\lambda \cdot h) + 0.2534\right] \cdot d, (-0.0013\lambda \cdot h + 0.167) \cdot d\right]$$

$wo = 17.1$

Bay factor for number of bays:

$x := 1$

$\eta := 1.0$

Modes of failure factors:

Prism and shear strength ratio factor:

Prism strength: $fm := 3387$ $\qquad \psi := \frac{fm}{W \cdot t}$

Shear strength: $fv := 134$ $\qquad v := \frac{fv}{x \cdot H \cdot t}$

$\frac{\psi}{v} = 18.3 \quad < \quad 36$

$R\_str := 1.00$

Strain energy from tension in the windward column:

$$\varepsilon\_col := \frac{h \cdot \tan(2 \cdot \theta)}{Ac \cdot Ef}$$

$\varepsilon\_col = 0.001$ in/k

Strain energy from compression in equivalent strut:

$$\varepsilon\_strut := \frac{d}{wo \cdot t \cdot Ei \cdot \cos(2 \cdot \theta)}$$

$\varepsilon\_strut = 0.00405$ in/k

$$\frac{\varepsilon\_strut}{\varepsilon\_col} = 3.965$$

Strain factor: if x > or equal 2

and: $\frac{\varepsilon\_strut}{\varepsilon\_col} = 3.965$ > 3.5

$R\_\varepsilon := 1.05$ Otherwise $R\_\varepsilon := 1.0$

$R\_\varepsilon := 1.00$

The adjusted width of diagonal strut:

$w := 0.48 \cdot \eta \cdot wo \cdot R\_str \cdot R\_\varepsilon$

$w = 8.2$ in

Single-Bay Infilled with Brick Masonry Wall
Proposed Idealized Method

The height of the infill: $H := 52.25$ in

The width of the infill: $W := 72$ in

The height of the column: $h := 56.125$ in

Length of the beam: $L := 80$ in

Diagonal length of the infill panel: $d := \sqrt{W^2 + H^2}$ in

$d = 88.96$ in

Effective thickness of the infill: $t := 1.49$ in

Angle of diagonal to horizontal: $\theta := \operatorname{atan}\left(\frac{H}{W}\right)$

$\theta = 0.628$ Rad

Column's dimensions: $Lc1 := 8$ in

$Lc2 := 5$ in

Beam's dimensions: $Lb1 := 7.75$ in

$Lb2 := 5$ in

Cross-sectional area of the column: $Ac := Lc1 \cdot Lc2$

$Ac = 40$ in^2

Cross-sectional area of the beam: $Ab := Lb1 \cdot Lb2$

$Ab = 38.75$ in^2

Moment of inertia of the column: $Ic := \frac{Lc2 \cdot Lc1^3}{12}$

$Ic = 213.3$ in^4

Beam's dimensions:

$Lb1 := 7.75$ in

$Lb2 := 5$ in

Moment of inertia of the beam: $Ib := \frac{Lb2 \cdot Lb1^3}{12}$

$Ib = 194$ in^4

Elastic modulus of the frame: $Ef := 4260$ ksi

y factor for number of bays:

Number of bays: $x := 1$

$\eta := 1.0$

odes of failure factors:

Prism and shear strength ratio factor:

Prism strength: $fm := 3387$ $\psi := \frac{fm}{W \cdot t}$

Shear strength: $fv := 134$ $\nu := \frac{fv}{x \cdot H \cdot t}$

$\frac{\psi}{\nu} = 18.3$ < 36

$R\_str := 1.05$

Strain energy from tension in the windward column:

$\varepsilon\_col := \frac{h \cdot \tan(2 \cdot \theta)}{Ac \cdot Ef}$

$\varepsilon\_col = 0.001$

Strain energy from compression in equivalent strut:

$\varepsilon\_strut := \frac{d}{wo \cdot t \cdot Ei \cdot \cos(2}$

$\varepsilon\_strut = 0.00348$

$\frac{\varepsilon\_strut}{\varepsilon\_col} = 3.441$

rain factor: if x > or equal 2

and: $\frac{\varepsilon\_strut}{\varepsilon\_col} = 3.441$ > 3.5

$R\_\varepsilon := 1.05$ Otherwise $R\_\varepsilon = 1.0$

$$\varepsilon\_col := \frac{h \cdot \tan(2 \cdot \theta)}{Ac \cdot Ef}$$

$\varepsilon\_col = 0.001$ in/k

Strain energy from compression in equivalent strut:

$$\varepsilon\_strut := \frac{d}{wo \cdot t \cdot Ei \cdot \cos(2 \cdot \theta)}$$

$\varepsilon\_strut = 0.00348$ in/k

$$\frac{\varepsilon\_strut}{\varepsilon\_col} = 3.441$$

Strain factor: if x > or equal 2

and: $\frac{\varepsilon\_strut}{\varepsilon\_col} = 3.441$ > 3.5

$R\_\varepsilon := 1.05$ Otherwise $R\_\varepsilon := 1.05$

$R\_\varepsilon := 1.0$

The adjusted width of diagonal strut:

$w := 0.6 \cdot \eta \cdot wo \cdot R\_str \cdot R\_\varepsilon$

$w = 10.7$ in

Proposed Idealized Method
Double-Bay Infilled with CMU

The height of the infill:	$H := 52.25$	in
The width of the infill:	$W := 72$	in
The height of the column:	$h := 56.125$	in
Length of the beam:	$L := 80$	in
Diagonal length of the infill panel:	$d := \sqrt{W^2 + H^2}$	in
	$d =$	in
Effective thickness of the infill:	$t := 2.71$	in
Angle of diagonal to horizontal:	$\theta := \operatorname{atan}\left(\frac{H}{W}\right)$	
	$\theta =$	Rad
Column's dimensions:	$Lc1 := 8$	in
	$Lc2 := 5$	in
Cross-sectional area of the column:	$Ac := Lc1 \cdot Lc2$	
	$Ac =$	in^2
Moment of inertia of the column:	$Ic := \frac{Lc2 \cdot Lc1^3}{12}$	
	$Ic =$	in^4
Beam's dimensions:	$Lb1 := 7.75$	in
	$Lb2 := 5$	in
Moment of inertia of the beam:	$Ib := \frac{Lb2 \cdot Lb1^3}{12}$	
	$Ib =$	in^4
Elastic modulus of the frame:	$Ef := 4210$	ksi
Elastic modulus of infill panel:	$Ei := 1531$	ksi

Relative stiffness parameter of infill and frame:

$$\lambda c := \sqrt[4]{\frac{Ei \cdot t \cdot \sin(2 \cdot \theta)}{4 \cdot Ef \cdot Ic \cdot h}} \qquad \lambda c = 0.067$$

$$\lambda b := \sqrt[4]{\frac{Ei \cdot t \cdot \sin(2 \cdot \theta)}{4 \cdot Ef \cdot Ib \cdot h}} \qquad \lambda c = 0.067$$

$$\lambda := \left(\sqrt{\lambda c^2 + \lambda b^2}\right) \cdot \cos\left(\theta - \frac{\pi}{4}\right) \qquad \lambda = 0.094$$

The unadjusted width of diagonal strut:

$\lambda \cdot h = 5.276$

$wo := if\left[\lambda \cdot h < 13, \left[0.0005(\lambda \cdot h)^2 - 0.0143(\lambda \cdot h) + 0.2534\right] \cdot d, (-0.0013\lambda \cdot h + 0.167) \cdot d\right]$

$wo = 17.1$

Bay factor for number of bays:

$x := 2$

$\eta := 1.435$

Modes of failure factors

Prism and shear strength ratio factor:

Prism strength: $fm := 3387$ $\qquad \psi := \frac{fm}{W \cdot t}$

Shear strength: $fv := 134$ $\qquad v := \frac{fv}{x \cdot H \cdot t}$

$\frac{\psi}{v} = 36.7 \quad < \quad 36$

$R\_str := 1.00$

Strain energy from tension in the windward column:

$$\varepsilon\_col := \frac{h \cdot \tan(2 \cdot \theta)}{Ac \cdot Ef}$$

$\varepsilon\_col = 0.001$ in/k

$$\frac{\varepsilon\_strut}{\varepsilon\_col} = 3.965$$

Strain factor: if x > or equal 2

and: $\frac{\varepsilon\_strut}{\varepsilon\_col} = 3.965$ > 3.5

$R\_\varepsilon := 1.05$

Otherwise: $R\_\varepsilon := 1.05$

The adjusted width of diagonal strut:

$w := 0.48 \cdot \eta \cdot wo \cdot R\_str \cdot R\_\varepsilon$

$w = 12.3$ in

Proposed Idealized Method
Triple-Bay Infilled with Masonry Brick Wall

The height of the infill:	$H := 52.25$	in
The width of the infill:	$W := 72$	in
The height of the column:	$h := 56.125$	in
Length of the beam:	$L := 80$	in
Diagonal length of the infill panel :	$d := \sqrt{W^2 + H^2}$	in
	$d = 88.96$	in
Effective thickness of the infill:	$t := 1.68$	in
Angle of diagonal to horizontal:	$\theta := \operatorname{atan}\left(\frac{H}{W}\right)$	
	$\theta = 0.628$	Rad
Column's dimensions:	$Lc1 := 8$	in
	$Lc2 := 5$	in
Beam's dimensions:	$Lb1 := 7.75$	in
	$Lb2 := 5$	in
Cross-sectional area of the column:	$Ac := Lc1 \cdot Lc2$	
	$Ac = 40$	in^2
Cross-sectional area of the beam:	$Ab := Lb1 \cdot Lb2$	
	$Ab = 38.75$	in^2
Moment of inertia of the column:	$Ic := \frac{Lc2 \cdot Lc1^3}{12}$	
	$Ic = 213.3$	in^4
Beam's dimensions:	$Lb1 := 7.75$	in
	$Lb2 := 5$	in
Moment of inertia of the beam:	$Ib := \frac{Lb2 \cdot Lb1^3}{12}$	
	$Ib = 194$	in^4
Elastic modulus of the frame:	$Ef := 4260$	ksi
Elastic modulus of infill panel:	$Ei := 3277$	ksi

Concrete compressive strength $fc := 4943$ psi

Relative stiffness parameter of infill and frame:

$$\lambda c := \sqrt[4]{\frac{Ei \cdot t \cdot \sin(2 \cdot \theta)}{4 \cdot Ef \cdot Ic \cdot h}} \qquad \lambda c = 0.071$$

$$\lambda b := \sqrt[4]{\frac{Ei \cdot t \cdot \sin(2 \cdot \theta)}{4 \cdot Ef \cdot Ib \cdot h}} \qquad \lambda c = 0.071$$

$$\lambda := \left(\sqrt{\lambda c^2 + \lambda b^2}\right) \cdot \cos\left(\theta - \frac{\pi}{4}\right) \qquad \lambda = 0.101$$

The unadjusted width of diagonal strut:

$\lambda \cdot h = 5.646$

$$wo := if\left[\lambda \cdot h < 13, \left[0.0005(\lambda \cdot h)^2 - 0.0143(\lambda \cdot h) + 0.2534\right] \cdot d, (-0.0013\lambda \cdot h + 0.167) \cdot d\right]$$

$wo = 16.8$

Bay factor for number of bays:

Number of bays: $x := 1$

$\eta := 1.2774$

Modes of failure factors:

Prism and shear strength ratio factor:

Prism strength: $fm := 3387$ $\psi := \frac{fm}{W \cdot t}$

Shear strength: $fv := 134$ $v := \frac{fv}{x \cdot H \cdot t}$

$\frac{\psi}{v} = 18.3 \quad < \quad 36$

$R\_str := 1.00$

Strain energy from tension in the windward column:

$$\varepsilon\_col := \frac{h \cdot \tan(2 \cdot \theta)}{Ac \cdot Ef}$$

$\varepsilon\_col = 0.001$ in/k

Strain energy from compression in equivalent strut:

$$\varepsilon\_strut := \frac{d}{wo \cdot t \cdot Ei \cdot \cos(2 \cdot \theta)}$$

$\varepsilon\_strut = 0.00311$ in/k

$$\frac{\varepsilon\_strut}{\varepsilon\_col} = 3.076$$

Strain factor: if x > or equal 2

and: $\frac{\varepsilon\_strut}{\varepsilon\_col} = 3.076$ > 3.5

$R\_\varepsilon := 1.05$ Otherwise $R\_\varepsilon := 1.0$

$R\_\varepsilon := 1.0$

The adjusted width of diagonal strut:

$w := 0.6 \cdot \eta \cdot wo \cdot R\_str \cdot R\_\varepsilon$

$w = 12.9$ in

$A\_strut := w \cdot t$

$A\_strut = 21.6$

Dr. Ghassan Al-Chaar was born on December 19, 1955 in Boussan Village of Sweda State in Syria. He attended elementary school in Boussan Village, middle school in Sweda City and high school in Abin Al-Ameed, Damascus.

After high school, Dr. Al-Chaar completed a two-year program at the Technical Health Institution in Damascus, majoring in Anesthesia. For two years he led the elected Student Board of Directors at the Technical Health Institution through the National Organization of Syrian Students.

Dr. Al-Chaar came to the United States in 1979. He completed his BS in Civil Engineering in the University of Illinois at Chicago in 1985, MS in Structural Engineering in 1987, MS in Geotechncial Engineering in 1996, Ph.D. in Structural Engineering in 1998.

Dr. Al-Chaar has worked for Sargent and Lundy and for Bechtel North America Power. In 1989 he joined the U.S. Army Corps of Engineers. He is currently a member of the Seismic and Structural Engineering Group, Construction Engineering Research Laboratories, in Champaign, Illinois. He has conducted research in the areas of seismic engineering, masonry, and lifelines.

Dr. Al-Chaar assisted in developing an evaluation procedure to determine the seismic vulnerability of Airport Traffic Control Towers owned by the Federal Aviation Administration. He also, has led a research work unit to study the dynamic behavior of reinforced concrete frames with masonry infill. This research was aimed toward developing design criteria for repairing and strengthening masonry infilled reinforced concrete frames subjected to earthquake loading.

Dr. Al-Chaar has also conducted research on lifelines to characterize their seismic response and develop vulnerability assessment criteria. He identifying buried pipeline parameters related to system vulnerability and developing a generalized method to relate these parameters to the seismic vulnerability assessment of existing systems on military installation.

For five months Dr. Al-Chaar served as a volunteer member of the U.S. Army Corps of Engineers recovery operation in the Southwest Asia Gulf War. While with the Kuwait Emergency Recovery Office, he assessed damage of 23 structures and provided methods for their restoration. He performed damage assessment of structures after natural disaster such as earthquakes, floods, and hurricanes. He also assessed structural damage from expansive soil and wood decay.

Summary of Publications

1. Al-Chaar G.: Condition Assessment of Structures Damaged from Drought/Rain Cycles. ASCE Infrastructure Condition Assessment Conference, 1997.

2. Al-Chaar G.: Structural Damage Evaluation and Repair of Al-Shuwake Immigration Building. Rehabilitation of Damaged Buildings, Sick Building Syndrome Proceeding, 1992.

3. Al-Chaar G.: Structural Evaluation Procedures for Heavy Wood Truss Structures. USACERL Technical Report 98/89, July 1998.

4. Al-Chaar G.:Case Study: Structural Evaluation of Aircraft Hangars in Corpus Christi Army Depot, Texas. USACERL Technical Report.

5. Al-Chaar G.: Case Study: Structural Evaluation of Heavy Wood Trusses in Corpus Christi Army Depot, Texas. USACERL Technical Report.

6. Al-Chaar G., Fernandez G., Angel R.: Rapid Seismic Assessment of Buried Pipelines. 1995 Corps of Engineers Structural Conference.

7. Al-Chaar G., Fernandez G., Brady P.: Seismic Assessment of Buried Pipelines. ASCE 4th U.S. Conference on Lifelines Earthquake Engineering.

8. Al-Chaar G., R. Angel, D. Abram.: Dynamic Testing of Unreinforced Masonry Infills. ASCE, Structures Congress XII.

9. Al-Chaar G., R. Angel, Sweeney S.: Strength Evaluation of Externally Repaired Double-T Beams. 1995 Corps of Engineers Structural Conference.

10. Al-Chaar G., Sweeney S., Angel R.: Seismic Evaluation Software Package for Steel Structure. University of Bahrain, 1996 Conference UNISCO, ASCE & ACI.

11. Al-Chaar G., Sweeney S., Brady P.: Push Over Laboratory Testing of Unreinforced Masonry Infills. Wind and Seismic Effects, 28th Meeting.

12. Al-Chaar G., Sweeney S., Brady P.: Dynamic Testing of R/C Frame with Unreinforced Masonry Infill.

13. Al-Chaar, G. Husein H.: Masonry Bearing and Shear Walls Retrofitted with Overlay Composite Material. USACERL Technical Report 98/86, July 1998

14. Angel R., Al-Chaar G.: Testing and Evaluation of Out-of-Plane Strength of Unreinforced Masonry Infill:. Proceeding on :Structures Under Shock and Impact Conference , SUSI 98. It is organized by the Wessex Institute of Technology in the UK and by the Aristotle University of Thessaloniki.

15. Angel R., Al-Chaar G., Sweeney S.: Out-of-Plane Strength Evaluation of Damaged URM Infill Panels. 1995 Corps of Engineers Structural Conference.

16. Angel R., Al-Chaar G., Sweeney S.: Discussion of Effects of Structural Properties on the Out-of-Plane Behavior of URM Infill Panels. 1995 Corps of Engineers Structural Conference.

17. Brady P., Pazagardi S.,Al-Chaar G.: Development of an Improved Seismic Analysis Procedures. ASCE, Structural Engineering In Natural Hazards Mitigation,1993.

18. Brady P., Sweeney S., Al-Chaar G.,Hayes J.: Seismic Vulnerability Assessment of Selected Facilities at Three SAC Air Force Bases in California. USACERL Technical Report, July 1991.

19. Fernandez, G., Al-Chaar, G. Brady. P.: Estimate of Maximum Strains Induced in Buried Pipelines by Dynamic Loading. ASCE 4th U.S. Conference on Lifelines Earthquake Engineering.

20. Issa M, Al-Chaar G.: Structural Evaluation Procedure for Heavy Wood Truss Structures. USACERL Technical Report 98/89, July 1998.

21. Sweeney S., Al-Chaar G.: Strength of Concrete Frames with Masonry Infill. 1995 Corps of Engineers Structural Conference.

22. Sweeney S., Al-Chaar G.: Strength of Concrete Frames with Masonry Infill. UJNR 27th Joint Meeting, May, 1995.

Distribution

Chief of Engineers
ATTN: CEMP-ET (2)

Defense Tech Info Center 22304
ATTN: DTIC-O (2)